Publications of the Astronomical Society of the Pacific, 128:082001 (86pp), 2016 August doi:10.1088/1538-3873/128/966/082001

Hot Subluminous Stars*

U. Heber
Dr. Remeis-Sternwarte & ECAP, Astronomical Institute, University of Erlangen-Nürnberg, Sternwartstr. 7, D-96049 Bamberg, Germany
Received 2015 December 25; accepted 2016 April 19; published 2016 July 12

Abstract

Hot subluminous stars of spectral type B and O are core helium-burning stars at the blue end of the horizontal branch or have evolved even beyond that stage. Most hot subdwarf stars are chemically highly peculiar and provide a laboratory to study diffusion processes that cause these anomalies. The most obvious anomaly lies with helium, which may be a trace element in the atmosphere of some stars (sdB, sdO) while it may be the dominant species in others (He-sdB, He-sdO). Strikingly, the distribution in the Hertzsprung–Russell diagram of He-rich versus He-poor hot subdwarf stars of the globular clusters ω Cen and NGC 2808 differ from that of their field counterparts. The metal-abundance patterns of hot subdwarfs are typically characterized by strong deficiencies of some lighter elements as well as large enrichments of heavy elements. A large fraction of sdB stars are found in close binaries with white dwarf or very low-mass main sequence companions, which must have gone through a common-envelope (CE) phase of evolution. Because the binaries are detached they provide a clean-cut laboratory to study this important but yet poorly understood phase of stellar evolution. Hot subdwarf binaries with sufficiently massive white dwarf companions are viable candidate progenitors of type Ia supernovae both in the double degenerate as well as in the single degenerate scenario as helium donors for double detonation supernovae. The hyper-velocity He-sdO star US 708 may be the surviving donor of such a double detonation supernova. Substellar companions to sdB stars have also been found. For HW Vir systems the companion mass distribution extends from the stellar into the brown dwarf regime. A giant planet to the acoustic-mode pulsator V391 Peg was the first discovery of a planet that survived the red giant evolution of its host star. Evidence for Earth-size planets to two pulsating sdB stars have been reported and circumbinary giant planets or brown dwarfs have been found around HW Vir systems from eclipse timings. The high incidence of circumbinary substellar objects suggests that most of the planets are formed from the remaining CE material (second generation planets). Several types of pulsating star have been discovered among hot subdwarf stars, the most common are the gravity-mode sdB pulsators (V1093 Her) and their hotter siblings, the *p*-mode pulsating V361 Hya stars. Another class of multi-periodic pulsating hot subdwarfs has been found in the globular cluster ω Cen that is unmatched by any field star. Asteroseismology has advanced enormously thanks to the high-precision *Kepler* photometry and allowed stellar rotation rates to be determined, the interior structure of gravity-mode pulsators to be probed and stellar ages to be estimated. Rotation rates turned out to be unexpectedly slow calling for very efficient angular momentum loss on the red giant branch or during the helium core flash. The convective cores were found to be larger than predicted by standard stellar evolution models requiring very efficient angular momentum transport on the red giant branch. The masses of hot subdwarf stars, both single or in binaries, are the key to understand the stars' evolution. A few pulsating sdB stars in eclipsing binaries have been found that allow both techniques to be applied for mass determination. The results, though few, are in good agreement with predictions from binary population synthesis calculations. New classes of binaries, hosting so-called extremely low mass (ELM) white dwarfs ($M < 0.3\,M_{\odot}$), have recently been discovered, filling a gap in the mosaic of binary stellar evolution. Like most sdB stars the ELM white dwarfs are the stripped cores of red giants, the known companions are either white dwarfs, neutron stars (pulsars) or F- or A-type main sequence stars ("EL CVn" stars). In the near future, the

* Subdwarf O/B stars and extremely low mass white dwarfs: atmospheric parameters and abundances, formation and evolution, binaries, planetary companions, pulsation, and kinematics.

Gaia mission will provide high-precision astrometry for a large sample of subdwarf stars to disentangle the different stellar populations in the field and to compare the field subdwarf population with the globular clusters' hot subdwarfs. New fast-moving subdwarfs will allow the mass of the Galactic dark matter halo to be constrained and additional unbound hyper-velocity stars may be discovered.

Key words: binaries: close – stars: abundances – stars: evolution – stars: oscillations – subdwarfs – white dwarfs

Online material: color figures

1. Introduction

The hot subluminous stars of B and O-type (sdB, sdO) represent several late stages in the evolution of low-mass stars. In the Hertzsprung–Russell diagram they can be found between the main sequence and the white-dwarf sequence (see Figure 1). The discovery of subluminous blue stars at high Galactic latitudes dates back to the 1950s after exploitation of the Humason & Zwicky (1947) photometric survey of the North Galactic Pole and Hyades regions (e.g., Luyten 1953; Greenstein 1956; Münch 1958). The number of known objects remained small until the 1980s when the Palomar-Green survey (PG, Green et al. 1986) of the northern Galactic hemisphere was published (see Greenstein 1987; Lynas-Gray 2004, for overviews of early developments). Several other photometric surveys followed, e.g., the Kitt Peak-Downes survey of the Galactic plane (KPD, Downes 1986) and the Edinburgh-Cape Survey (EC, Stobie et al. 1997b) for the southern sky, as well as objective prism surveys, e.g., Byurakan surveys (FBS, SBS, Mickaelian et al. 2007), the Hamburg Quasar Survey (HS, Hagen et al. 1995) for the northern and the Hamburg ESO survey (HE, Wisotzki et al. 1996) for the southern sky. The Sloan Digital Sky survey has doubled the number of known hot subdwarfs within a few years and the *Galaxy Evolution Explorer* (*GALEX*) all-sky survey extended the list further.

Most of the B-type subdwarfs were identified as helium burning stars of about half a solar mass at the blue end of the horizontal branch, the so-called Extreme Horizontal Branch (EHB, Heber 1986). In contrast to the normal horizontal branch (HB) stars, the hydrogen envelope is too thin ($M_{\rm env} < 0.01\,M_{\odot}$) to sustain hydrogen shell burning. Hence, subluminous B stars are the stripped cores of red giants, which managed to ignite helium while retaining just a little bit of hydrogen as their envelope.

Maxted et al. (2001) found two-thirds of all sdBs to be in detached binary systems with short periods from hours to days and their companion stars to be mostly white dwarfs. More recent investigations indicate that half of the sdBs reside in such close binaries (Napiwotzki et al. 2004; Copperwheat et al. 2011), still a very high fraction. Their orbital separations are only a few solar radii. Since the sdB stars have evolved from red giants, much larger in size than the present binary orbit, the progenitor system must have undergone a common-envelope (CE) phase, during which the orbit shrank when the companion was engulfed in the red giant's envelope. Finally, the common envelope is ejected and a tight, detached binary system remains. The evolution through CE ejection is crucial to an understanding of various types of binaries, including X-ray binaries, double neutron stars, double white dwarfs and sdB binaries. However, CE formation and evolution is poorly understood because of the complexity of the physics involved (for a review see Ivanova et al. 2013). Among the various types of post-CE systems, the sdB binaries provide an important laboratory for studying CE evolution. Because the systems are non-interacting, the properties of the components can be derived in more detail, with higher precision, and selection effects are less severe than for interacting systems such as cataclysmic variables (Pretorius et al. 2007). Hence, sdB stars form an important piece in the puzzle of CE evolution.

Many sdB binaries host unseen white dwarf companions and sdBs with neutron star or black hole partners are predicted to exist. Such systems join the zoo of compact binary systems and play a role as progenitors of the cosmologically important type Ia supernovae (SNe Ia) and other transient phenomena via mergers driven by gravitational wave radiation. Because of their short periods the orbital gravitational wave emission may be strong enough to be detectable by future space-based missions. An extensive review of the formation and evolution of compact binary star systems has been published recently by Postnov & Yungelson (2014).

However, besides degenerate companions, main-sequence stars and brown dwarfs have been discovered to orbit sdB stars. Binary population synthesis has identified several possible channels for the formation of hot subdwarfs, both in binaries as well as single stars that involve Roche lobe overflow (RLOF), CE ejection and gravitational wave-driven mergers of helium white dwarfs. A CE phase does not necessarily lead to an envelope ejection but may also result in a core merger, e.g., for a sub-stellar companion. Single hot subdwarf stars have been suggested to result from mergers of two helium white dwarfs (Han et al. 2002, 2003) but may also form via internal instabilities and mixing processes in the envelope of the progenitor.

Though sdBs and sdOs occupy neighboring regions in the Hertzsprung–Russell diagram, they are quite different both with respect to their chemical compositions and evolutionary status. The atmospheres of sdBs are mostly helium poor, their

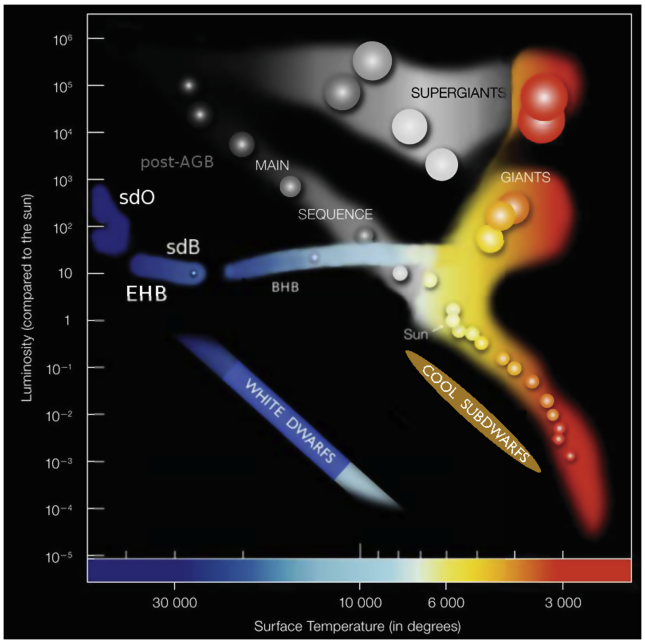

Figure 1. Hertzsprung–Russell diagram highlighting the position of the extreme horizontal branch (EHB) populated by subluminous B stars and located between he upper main sequence and the white dwarf sequence. The EHB is separated from the blue horizontal branch (BHB). The location of subluminous O stars as well as stars having evolved from the asymptotic giant branch is shown for comparison. From Heber (2009); copyright ARA&A; reproduced with permission.

(A color version of this figure is available in the online journal.)

helium abundances might be as low as a thousandth of the solar value or less. Subluminous O stars, on the other hand, show a variety of helium abundances, ranging from a hundredth of the solar content to pure helium atmospheres (He-sdO). Therefore, a direct evolutionary link between these two types of stars has always been considered questionable. It is not clear how diffusion, which is thought to be responsible for the helium deficiency of sdBs, should turn them into helium rich objects when an EHB star evolves to higher effective temperatures after core helium burning has ceased. Because of their low binary frequency He-sdO stars are thought to have formed by a merger of two helium white dwarfs or in isolation via internal mixing in the hot flasher scenario (Miller Bertolami et al. 2008).

Asteroseismology has become an important tool to study the internal structure of hot subluminous stars, because several classes of pulsating star have been discovered among them. Their light variations are multi-periodic, many showing a multitude of acoustic and/or gravity modes. The analysis of their light curves using sophisticated models allowed the internal structure, mass, and rotation of several sdB pulsators to be probed and ages to be estimated. Although amplitude variations are frequently encountered, some stars show modes that are sufficiently stable for years and allow a search for periodic light travel time variations caused by planetary companions. Indeed, a giant planet companion of the pulsator V391 Pegasi has been discovered (Silvotti et al. 2007) and several circumbinary planets followed in recent years.

Because they are UV-bright and relatively luminous, hot subdwarf stars have been used as UV-light sources to probe the interstellar medium (ISM) out to ≈1 kpc or more from the Galactic plane for all components of the ISM (e.g., Bluhm et al. 1999; Lehner & Howk 2004; Linsky et al. 2006; Tumlinson 2006; Jenkins 2013) as well as to constrain the distances and chemical composition to high velocity interstellar clouds (e.g., Wakker 2001; Smoker et al. 2004; Hernandez et al. 2013). The ultraviolet upturn phenomenon in elliptical galaxies is suspected to be caused by EHB stars. Binary population models have recently been found to be a promising explanation of this this phenomenon as well. First results suggest that the UV upturn may not be an age indicator as previously assumed (Han et al. 2010b).

A broad review of hot subluminous stars has been given by Heber (2009). The field is flourishing thanks to many new observational opportunities provided by the *Kepler* and *GALEX* satellites, and the Sloan Digital Sky Survey (SDSS) to name a few and it is timely to report on recent progress. In this paper I shall address the atmospheric properties, abundance patterns, rotation, and magnetic fields of hot subdwarf stars in Section 2. Section 3 deals with the formation and evolution of hot subdwarfs, followed in Section 4 by a brief discussion of hot subdwarfs in stellar clusters. The progress made in understanding binary stars from observations are reported in Section 5. Substellar companions to sdB binaries are introduced in Section 6 and a brief account of the recent developments in asteroseismology follows in Section 7. A tight relation between binary subdwarf stars and the new classes of binaries, hosting low-mass helium-core objects (also called extremely low mass (ELM) white dwarfs) is suggested. Such objects are also found as companions to early-type main-sequence stars (EL CVn variables), reported in Section 8. The kinematics of hot subdwarf stars and a unique hyper-velocity star (HVS) are discussed in Section 9.

A summary and some conclusions are presented at the end of the paper. A comprehensive overview of the progress in this field of research can be found in the proceedings of the fourth, fifth, and sixth meetings on hot subdwarf stars and related objects (Han et al. 2010a; Kilkenny et al. 2012; van Grootel et al. 2014a).

2. Atmospheric Properties and Chemical Composition of Hot Subdwarf Stars

Because of their peculiar spectra the hot subluminous stars cannot be classified in the MK spectral classification scheme. Therefore, Drilling et al. (2013) introduced three additional

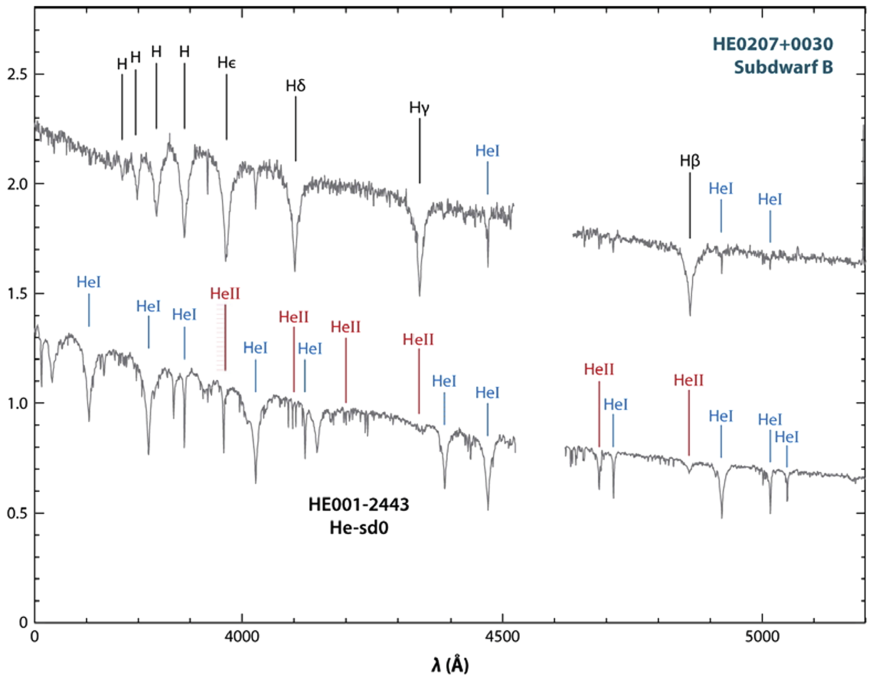

Figure 2. Spectra of typical sdB and He-sdO stars (Napiwotzki 2008). Important lines of hydrogen and helium are indicated. Helium lines are weak in sdB stars. Balmer lines are absent in He-sdOs, but note that every hydrogen Balmer line is blended with a He II Pickering line. From Heber (2009); copyright ARA&A; reproduced with permission.
(A color version of this figure is available in the online journal.)

luminosity classes and added helium classes (0–40) as a third dimension to the MK scheme. Additional sequences were identified with respect to the carbon and nitrogen line spectra.

A less detailed classification has become common practice, though. According to their helium line spectra hot subdwarf stars are grouped into sdB, sdOB, sdO, He-sdB and He-sdO. This scheme is not well defined. The classes sdOB and sdB are often merged into sdB, although sdOB stars are characterized by the presence of He II 4686 Å, which becomes strong in sdO stars (see Figure 2). An extension of this nomenclature is proposed by Kilkenny et al. (2010) for pulsating hot subdwarf stars.

About 10% of the hot subluminous stars have helium-dominated spectra (Green et al. 1986) and come in two flavors, the He-sdBs and the He-sdOs. The term He-sdB is inconsistent as the He II 4686 Å line is weakly present, but He I lines dominate. Nevertheless the term is useful to distinguish them from the He-sdO stars, in which He II lines prevail. Spectral classification is based on medium-resolution (≈2 Å) spectra and, therefore, of limited value to study the chemical composition of stars beyond the helium-to-hydrogen ratio.

Hence quantitative spectral analyses are necessary to provide us with detailed information on atmospheric parameters (effective temperature, gravity, and helium abundances, see Sections 2.2 and 2.3). The chemical composition of sdB and sdO stars are reviewed in Sections 2.4 and 2.5.

It is a general consensus that the helium-deficiency of the atmospheres of most sdB stars as well as of many (mostly helium poor) sdO stars is caused by diffusion processes as first proposed by Greenstein (1967). Therefore, we briefly revisit the diffusion theory in Section 2.6. In addition, the surface rotation can be studied from high-resolution spectra (Section 2.7), while spectropolarimetry or Zeeman splittings of spectral lines provide information on the magnetic fields of hot subdwarf stars (Section 2.8).

2.1. Model Atmospheres

The first attempt to model the spectrum of a hot subdwarf (an He-sdO) star was carried out by Münch (1958). Pioneering work by Mihalas (1965) and the Unsöld school followed thereafter by Tomley (1970 three sdO stars) and Richter (1971) for the sdO HD 49798. Models for sdB stars were constructed by Sargent & Searle (1966), and Baschek & Norris (1970) demonstrating that sdB stars are helium deficient.

For the O-type subdwarfs is became clear that departures from local thermodynamic equilibrium (LTE) are significant (Kudritzki 1979). The complete linearization method pioneered by Auer & Mihalas (1969) marked a milestone and allowed Kudritzki (1976), Kudritzki & Simon (1978) and Giddings (1981) to carry out the first non-LTE (NLTE) analyses of sdO

stars. A breakthrough was achieved by the invention of the accelerated lambda iteration technique using approximate lambda operators (Werner & Husfeld 1985; Werner 1986) which allowed more detailed model atoms to be implemented in computations of non-LTE model atmospheres. This technique was applied to He-sdO stars, e.g., by Dreizler et al. (1990) and Dreizler (1993).

2.2. Atmospheric Parameters

Thanks to the efforts of several research teams, atmospheric parameters have become available for many hundreds of hot subdwarfs, which allow the distribution of stars in the $T_{\rm eff}$–log g parameter space to be investigated. It has to be taken into account that results may differ systematically because of different model atmospheres used (LTE versus NLTE; treatment of line blanketing, see Jeffery et al. (2012) for a detailed discussion), different observational material (spectral resolution, wavelength coverage, normalization procedure[1]) and analysis strategy (choice of spectral lines, fitting procedure). Hence it would be timely to compare the results of different published analyses. Few such attempts have been made (e.g., Latour et al. 2014b), though.

2.2.1. Results from Major Surveys

We shall consider five major projects which studied samples of hot subdwarf stars recently. The only study that makes use of high-resolution spectra (spectral resolution better than 0.4 Å) is the sample drawn from the ESO/SPY-survey (Napiwotzki et al. 2001a). We regard this sample as a benchmark because the spectra also allowed the abundances of many chemical elements to be determined (see Section 2.4). Furthermore, the results of three studies at intermediate (1–5 Å) and one at low resolution (≈8.7 Å) will be discussed and compared. Altogether, effective temperatures, surface gravities and helium abundances have become available for many hundreds of hot subdwarf stars in the field. The largest project is the Arizona-Montréal Spectroscopic Program (Green et al. 2008; Fontaine et al. 2014). Because the stars are drawn from different surveys they might represent different stellar populations. The *GALEX* sample and those drawn mostly from the PG (Green et al. 1986) and EC (Stobie et al. 1997b) surveys have relatively bright average magnitudes, whereas the ESO/SPY sample includes fainter and, therefore, on average more distant stars. The Hamburg quasar survey extends the sample of hot subdwarfs deeper by another magnitude. The SDSS survey will extend the distribution in depth reaching out into the halo.

The ESO/SPY survey—the benchmark sample. The ESO Supernova Ia Progenitor Survey (Napiwotzki et al. 2001a) obtained high-resolution optical spectra of more than 1000 white dwarf candidates, containing some 140 previously misclassified hot subdwarfs of various types. The targets were largely drawn from the Hamburg-ESO survey (Wisotzki et al. 1996) which was a wide-angle survey for bright quasars ($12.5 < B < 17.5$ mag) in the southern hemisphere, based on objective prism plates taken with the ESO Schmidt telescope over an effective area of ≈1000 square degrees. Observations were obtained at the ESO Very Large Telescope with the UV-Visual Echelle Spectrograph (UVES) at a spectral resolution of 0.36 Å or better. Wavelength coverage of 3300–6650 Å was achieved, with gaps at 4500–4600 Å and 5600–5700 Å.

The sample of sdB stars was analyzed by Lisker et al. (2005) using metal-line blanketed LTE models of solar composition and the LINFOR program for spectrum synthesis (Heber et al. 1999, 2000). The spectra of the subluminous O stars from that sample were originally analyzed by Stroeer et al. (2007) using NLTE models of hydrogen/helium composition calculated with the TMAP package (Werner & Dreizler 1999; Rauch & Deetjen 2003; Werner et al. 2003b).[2] A more sophisticated analysis of the same data using NLTE models of H/He/C or H/He/N composition also calculated with the TMAP package was carried out by Hirsch (2009), see also Heber & Hirsch (2010) for a brief account.

The Arizona-Montréal Spectroscopic Program. The largest sample of hot subdwarfs presently under investigation is the Arizona-Montréal Spectroscopic Program (Fontaine et al. 2014), which targets mostly bright stars including many from the PG survey. It is based on low-resolution spectra (≈8.7 Å) covering the spectral range from the Balmer jump to 6800 Å, taken over more than a decade with the Bok 2.3 m telescope of the Steward Observatory Kitt Peak Station. The data set is characterized by its high signal-to-noise ratio (S/N) (typically above 200) and its homogeneity, surpassing any other sample. Fontaine et al. (2014) give a brief account of effective temperatures, gravities and helium abundances for 320 of the 421 stars that make up the sample (see Figure 3). The team uses TLUSTY and SYNSPEC (Hubeny 1988; Hubeny & Lanz 1995) to construct grids of non-LTE model atmospheres and to synthesize optical spectra (Brassard et al. 2010), which are then matched to the observed spectra to extract effective temperatures, surface gravities and helium abundances.

The PG and EC Surveys. This study was restricted to PG and EC stars classified as B-type subdwarfs; O-types were excluded. Observations of the northern targets were obtained with the IDS at the 2.5 m Isaac Newton Telescope on La Palma at a resolution of ≈1.5 Å. Southern targets were observed with the grating spectrograph mounted on the 1.9 m telescope at the South African Astronomical Observatory at a resolution of better than 1 Å. This sample of sdB stars has been analyzed using the same metal-line blanketed LTE models used for the samples from the ESO/SPY and Hamburg Quasar Survey

[1] Németh et al. (2012) extensively discuss the effect arising from different instrumentation and spectral resolution.

[2] http://www.uni-tuebingen.de/de/41621

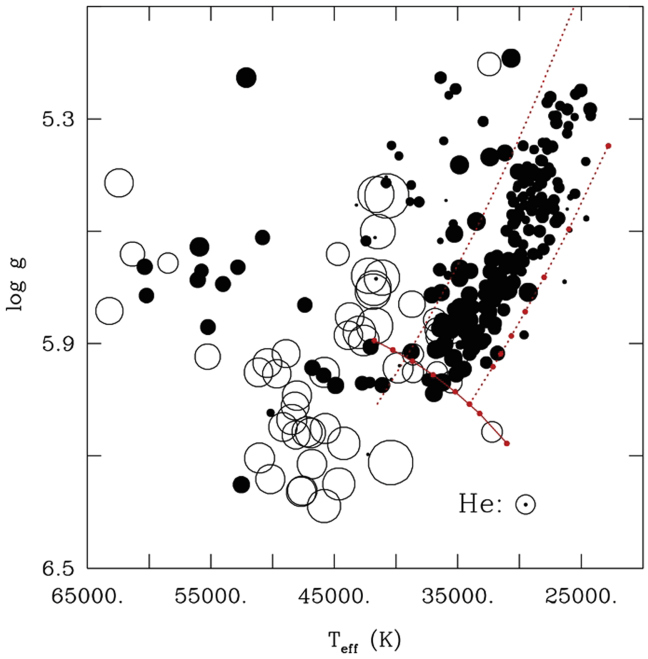

Figure 3. The distribution of hot subdwarfs stars from the Arizona-Montréal Spectroscopic Program (Green et al. 2008; Fontaine et al. 2014) is depicted in the log g–$T_{\rm eff}$ plane. The size of a given circle is a logarithmic measure of the helium abundance relative to that of hydrogen (the solar He abundance is indicated by the symbol in the lower right corner). He-poor and He-rich stars are represented by filled and open circles, respectively. Also shown are the zero-age helium main-sequence (ZAHEMS, full drawn), as well as zero-age extreme horizontal branch (ZAEHB) and the terminal-age extreme horizontal branch (TAEHB, dotted lines) for a core mass of 0.47 $M_{\odot}$ and a metallicity of $Z = 0.02$. From Latour et al. (2014c); copyright ApJ; reproduced with permission.

(A color version of this figure is available in the online journal.)

(HQS) surveys (Maxted et al. 2001; Morales-Rueda et al. 2003; Copperwheat et al. 2011). The sample comprises about 150 subluminous B stars.

The HQS—the deepest sample. The HQS, an objective prism survey (spectral resolution of 45 Å FWHM at H_{γ} covering the magnitude range $13\overset{\rm m}{.}5 \leqslant B \leqslant 18\overset{\rm m}{.}5$) was carried out, starting in 1980, with the 80 cm Schmidt telescope at the German-Spanish Astronomical Center on Calar Alto, Spain (Hagen et al. 1995). Although it aimed primarily at finding quasars, it is also a very rich source of faint blue stars. Spectroscopic follow-up of visually selected candidates of hot stars at the Calar Alto observatory mostly with the TWIN Spectrograph at the 3.5 m telescope resulted in a sample of 400 faint blue stars (Heber et al. 1991). Half of them turned out to be hot white dwarfs (e.g., Dreizler et al. 1995; Heber et al. 1996; Homeier et al. 1998) and PG 1159 stars (e.g., Dreizler et al. 1994, 1996), whereas the other half were classified as hot subdwarfs of B- and O-type. A sample of 107 sdB stars has been analyzed by Edelmann et al. (2003) using the same metal line-blanketed LTE atmospheres as in Heber et al. (2000) and another 58 O-type subdwarfs were analyzed using TMAP non-LTE model atmospheres by Lemke et al. (1997) and Stroeer (2004).

The GALEX sample—the brightest one. The *GALEX* all-sky survey provides ultraviolet photometry in two bands, the FUV (≈154 nm) and NUV (≈232 nm), as described by Morrissey et al. (2007). Because the hot subdwarfs are the dominant population of UV-bright sources at high Galactic latitudes they should be easy to find in large numbers in the *GALEX* data base, provided the white dwarf contamination can be eliminated, e.g., by making use of reduced proper motions. Most previous surveys were limited to high Galactic latitudes, whereas the *GALEX* survey covers all Galactic latitudes, making it an important tool to study the hot subdwarf population in or near the Galactic plane, a region yet poorly explored with respect to hot subdwarf stars and white dwarfs (but see Verbeek et al. 2013, 2014).

Vennes et al. (2011b) identified 280 hot subluminous stars among the bright *GALEX* sources (NUV < 14 mag) based on UV, optical, and IR color indices, with about 120 hot subdwarfs previously uncovered. Even among the brightest stars ($V < 12$ mag) two were uncataloged and nine previously unstudied. Németh et al. (2012) presented a homogeneously modeled sample of 124 sdB and 42 sdO stars from the *GALEX* survey and determined non-LTE atmospheric parameters by considering H, He and CNO opacities in their computations using TLUSTY/SYNSPEC (Hubeny & Lanz 1995).

2.2.2. *Effective Temperatures and Surface Gravities from Major Samples in Comparison*

Besides systematic differences in the quantitative spectral analyses, the samples suffer from different selection biases. Therefore, it is worthwhile to compare the distribution of parameters derived by the different projects. In Section 4 we shall also compare with the sample of hot subdwarfs in the globular cluster ω Cen.

The $T_{\rm eff}$–log g diagram resulting from the Arizona-Montréal Spectroscopic Program is shown in Figure 3, while Figure 4 (a)–(d) display it for the samples drawn from the ESO/SPY, *GALEX*, HQS and PG & EC samples, respectively.

Németh et al. (2012) found that sdB stars concentrate in two groups in the $T_{\rm eff}$–log g and $T_{\rm eff}$–He diagrams suggesting two typical H envelopes with different masses and compositions. However, this clustering is not seen in the full set of sdB stars (see Figure 5). There is a clear gap between He-sdO and He-weak sdO stars in the $T_{\rm eff}$–He diagram and a clustering of He-sdO stars in the temperature range from ≈40,000 to ≈47,000 K (see Figures 3–5).

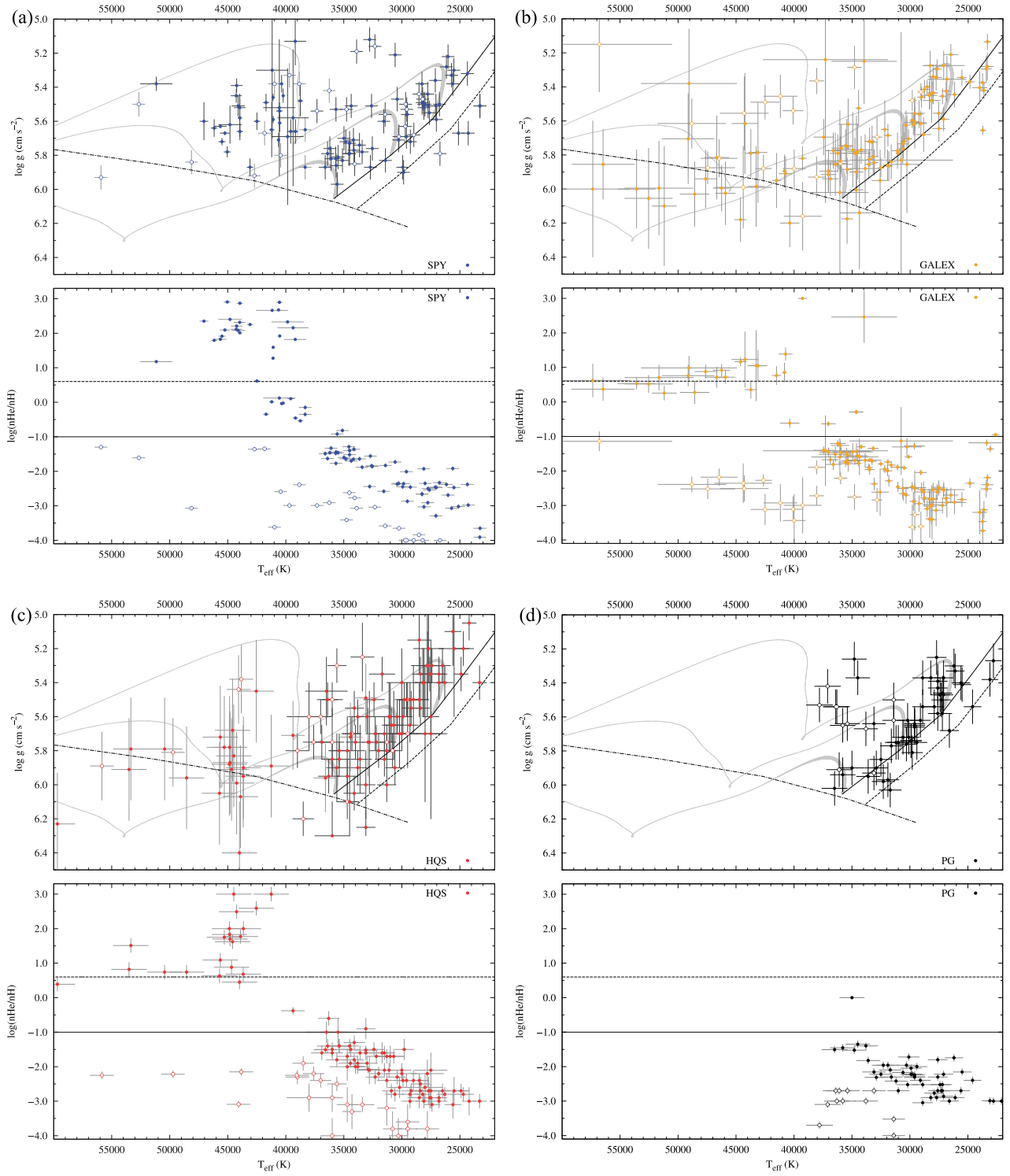

Figure 4. Distribution of hot subdwarf stars in the $T_{\rm eff}$–log g plane (upper panels) and of the helium abundances vs. $T_{\rm eff}$ (lower panels) for hot subdwarf stars (a) from the ESO/SPY sample; (b) from the *GALEX* sample; (c) from the HQS sample; and (d) from the sample drawn from the PG and EC surveys. The location of the ZAEHB is shown for two masses (0.45 $M_{\odot}$, dotted, and 0.5 $M_{\odot}$, full drawn). Evolutionary tracks for three envelope masses (0.000 $M_{\odot}$, 0.001 $M_{\odot}$, and 0.005 $M_{\odot}$, from left to right) by Han et al. (2002) are shown as dark gray lines. Linewidths are proportional to evolutionary timescales. The helium main sequence is shown as a dashed-dotted line. Lower panels: distribution of the helium abundances vs. $T_{\rm eff}$. The solar helium abundance is shown as a dotted horizontal line. From P. Németh (2016, private communication).

(A color version of this figure is available in the online journal.)

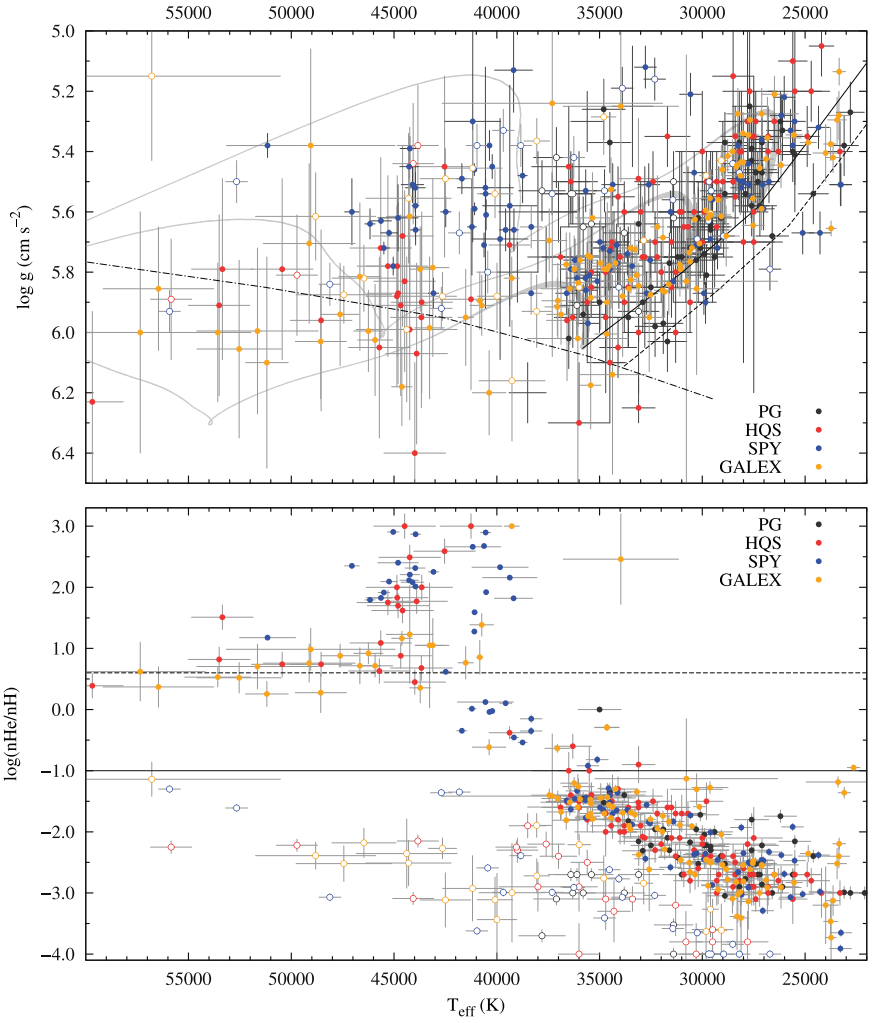

Figure 5. Same as Figure 4 but combining all samples shown in Figure 4(a)–(d). From P. Németh (2016, private communication). (A color version of this figure is available in the online journal.)

The most intriguing difference between the various $T_{\rm eff}$, $\log g$ diagrams is the distribution of the He-sdO stars. The Arizona-Montréal Spectroscopic Program finds a large population of high-gravity He-sdO stars with $\log g$ from 6.0 to 6.4; that is, they seem to lie below the helium main sequence. Their number even exceeds the number of He-sdOs of lower gravity ($\log g < 6$), which are on or above the He main sequence. A few such high-gravity He-sdOs are also found in the *GALEX* sample. However, their uncertainties are such that most of them are still consistent with an He-main sequence nature. The $T_{\rm eff}$, $\log g$ diagram of the ESO/SPY sample does not show He-sdOs located at gravities larger than 6.0. However, it is worth noting that Stroeer et al. (2007) in their early analysis of the ESO/SPY sdO sample found several sdO stars having gravities below the helium main sequence (see Figure 6 of Stroeer et al. 2007). The reanalysis using NLTE models that include carbon or nitrogen line blanketing by Hirsch (2009) resulted in atmospheric parameters that differ significantly from those of Stroeer et al. (2007), who used NLTE models that were composed of hydrogen and helium only. In particular, the gravities turned out, on average, to be lower than the ones previously derived. A very steep correlation between surface gravity and effective temperature has to be acknowledged leading to large systematic uncertainties for the He-sdOs.[3] The reason for these difference between the samples is still obscure.

Another riddle is, that the rather large spread in gravities among the He-sdO stars can hardly be explained by

[3] A significant source of systematic uncertainty comes from helium line broadening theory. Unfortunately sophisticated line broadening tables are not available, in particular for many He I transitions. The tables of Beauchamp et al. (1997) for white dwarfs need to be adapted to the physical conditions in the atmospheres of hot subdwarf stars.

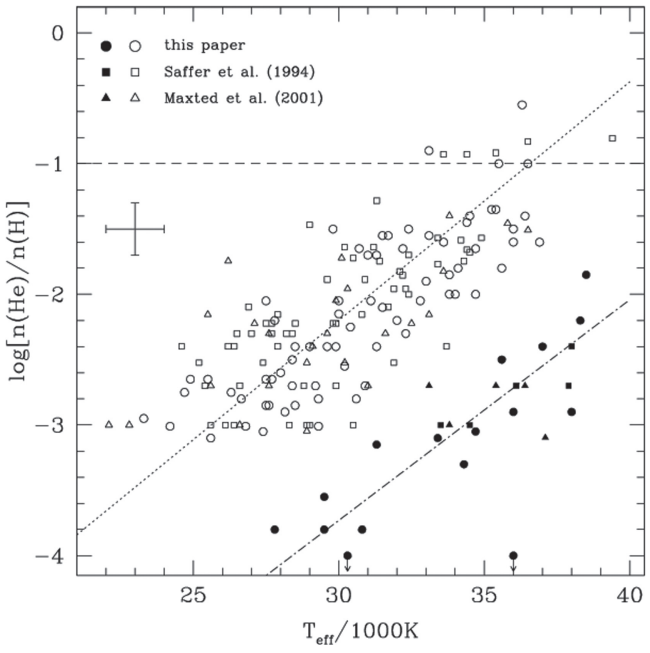

Figure 6. Plot of the helium abundance vs. effective temperature from Edelmann et al. (2003), Saffer et al. (1994), and Maxted et al. (2001) The dotted line indicates the linear regression for the bulk of the sdB stars (open symbols) and the dashed–dotted line shows the linear regression for the minority sdB stars (filled symbols). The dashed horizontal line denotes the solar helium abundance. From Edelmann et al. (2003); copyright A&A; reproduced with permission.

evolutionary models (neither in the hot flasher nor the merger scenario, see Section 3).

2.3. Helium Abundances

Besides the effective temperature and surface gravity, the helium abundance is an atmospheric parameter that has an important impact on the temperature–density stratification of the atmosphere, in particular for helium rich stars.

SdB star helium abundances tend to increase with increasing effective temperature, *as first reported* by Edelmann et al. (2003) for the first time. Moreover two clearly defined sequences stand out—a minority of stars follows a trend at a significantly lower helium abundance than the majority of stars (see Figure 6). These trends appear in all samples as can be seen from Figure 2 of Fontaine et al. (2014) and Figure 4(a)–(d). Some He-sdOs from the ESO/SPY sample have very high helium abundances (up to $n_{\rm He}/n_{\rm H} = 1000$) much larger than any star in the *GALEX* sample, for instance. However, this may be due to the high spectral resolution of the ESO/SPY (UVES) data, which allows small distortions of the He II Pickering lines by very weak hydrogen Balmer lines to be detected, which cannot be detected at the lower spectral resolution of the *GALEX* data. Hence some of the *GALEX* helium abundances may have to be considered as lower limits only.

The existence of these trends in helium abundance has been confirmed by recent studies but still awaits an explanation (see O'Toole 2008; Fontaine et al. 2014 for detailed discussions of this issue).

2.3.1. The ^{3}He Isotopic Anomaly

Another spectroscopic anomaly in sdB stars, which was first reported by Heber (1987), is related to the ^{3}He isotope. The ^{3}He isotope can easily be identified in high resolution spectra, because the isotopic shifts with respect to the ^{4}He isotope vary from line to line. While some lines like ^{3}He I, 5876 Å are shifted only slightly (0.04 Å) toward redder wavelengths, the shifts of ^{3}He I, 4922 Å and ^{3}He I, 6678 Å are significant (0.33 and 0.50 Å, respectively). The observed helium lines are blends of lines arising from ^{3}He and ^{4}He isotopes. Hence the observed line shifts increase with increasing ^{3}He/^{4}He ratio. In a few sdB stars, ^{3}He was found to be strongly enriched and has almost completely replaced the ^{4}He isotope, e.g., for SB 290 (Heber 1987; Geier et al. 2013a). It is generally believed that diffusion is causing this anomaly. By now eight sdB stars are known to show this anomaly, which cluster on the EHB in a narrow temperature regime from $T_{\rm eff} = 27{,}000$ to $31{,}000$ K (Geier et al. 2013a). The ^{3}He isotopic anomaly has also been observed among blue horizontal branch (BHB) stars (Hartoog 1979) as well as chemically peculiar B-type main sequence stars (Sargent & Jugaku 1961; Maza et al. 2014), although at lower temperatures.

2.4. The Chemical Composition of sdB Stars

Concerning elements heavier than helium, information from optical spectra of sdB stars is quite comprehensive for carbon, nitrogen, magnesium, silicon, sulfur, and to a lesser extent for iron, because those elements show prominent lines in the optical. Ultraviolet spectra gave access to the iron group and trans-iron elements, which have been detected in optical spectra in exceptional cases only. Since the spectra of hydrogen-rich subdwarfs differ considerably from those of hydrogen-poor ones, we shall discuss them separately starting with the hydrogen-rich ones.

The vast majority of subluminous B stars are hydrogen-rich and populate the EHB from ≈20,000 K to the helium main-sequence. Their anomalous chemical composition is due to atmospheric diffusion. A very small group (termed He-sdB) is helium-rich, with helium abundances ranging from solar to almost pure helium. Naslim et al. (2013) subdivided the helium rich sdB stars into extreme and intermediate He-sdBs drawing a

line at (n(He)/n(H) = 4). The subclass of intermediate He-sdB stars (n(He)/n(H) < 4) are of particular interest, because they are regarded as transition objects which might link the evolution of helium-poor sdB stars to that of helium-rich sdO stars or vice versa (for a review see Jeffery et al. 2012) and shall be discussed separately (Section 2.4.1).

Optical Spectroscopy. High-resolution optical spectra, *mainly* from the ESO/SPY project, have been used to determine the abundance pattern. Early analyses (e.g., Edelmann et al. 1999, 2001, 2006; Heber et al. 2000; Napiwotzki et al. 2001b; Heber & Edelmann 2004) have now been extended to more than 100 stars and to elemental abundances of up to 24 different ions per star (Geier 2013). This large progress became possible thanks to the excellent spectra from the ESO/SPY project that contributed two thirds of the sample (Geier et al. 2008a). To do this in an efficient way Geier (2013) designed a semi-automatic analysis pipeline to fit synthetic spectra computed from LTE models to a standard set of spectral lines.

Despite the large star-to-star variations, some similarities became obvious (see Figure 7). Unlike for helium, no trends with effective temperatures can be found.[4] It has to be noted that for several elements in many stars only upper limits could be derived, which means that the star-to-star scatter for some elements might be larger than it appears in Figure 7.

Carbon and nitrogen show very different distributions (see Figure 7) although radiative levitation is predicted to be very similar for C and N (as well as O, Unglaub & Bues 2001) irrespective of the assumed mass loss rates (see also Chayer et al. 2009). While the nitrogen abundance is slightly subsolar throughout the entire temperature range, the abundance of carbon varies by orders of magnitudes from star to star ranging from strongly subsolar to slightly super-solar. Oxygen is depleted on average by 1…2 dex, i.e., the scatter is less extreme than for C but not as small as for N.

Németh et al. (2012) determined C, N, and O abundances for sdB and sdO stars and find a positive correlation of C and N with helium abundance, when combining both sdB and sdO stars (see Figure 9 of Németh et al. 2012, see also Section 4).

Magnesium and iron show little scatter (like nitrogen), Mg being subsolar by one order of magnitude on average while Fe has almost solar abundance. It is conspicuous that the intermediate mass elements like Si, Al, and S are depleted, Si showing a particularly large star-to-star scatter. All the heavier elements (K to Co) are enriched with respect to solar. Titanium and Vanadium are found in at least half (Ti) or one third (V) of the sample, both strongly enhanced by +2 dex and +3 dex, respectively. Scandium and Chromium are detected in a few stars, only, and strongly enriched.

[4] Note that in a few cases such as Ar II the trends appeared likely to be caused by NLTE effects unaccounted for.

Ultraviolet spectroscopy. Spectral analyses of FUV and UV spectra offer a plethora of spectral lines from the same ions as observed in the optical, but are much more sensitive to the elemental abundance, that is detection limits are at a much lower abundance level. In addition spectral lines from elements can be detected that are not represented in the optical. However, spectral analyses of UV spectra are available for a few stars only. They corroborate the findings (see Figure 8) from optical studies, extend them for elements that have upper limits from optical analyses (e.g., Cr), and add a lot of information on heavier elements (e.g., Ni), and trans-iron group elements such as Cu, Zn, Ga, Ge, Sn, Zn, and Pb (see Figure 8; Chayer et al. 2006; O'Toole & Heber 2006; Blanchette et al. 2008).

In general, all elements beyond Ar are enriched with the notable exception of iron. The enhancements vary from star to star but increase with increasing effective temperatures to as much as a factor of 1000 (see Figure 8). Whether a star is pulsating or not does not appear to matter; that is, no correlation of the stellar abundance pattern with pulsation type has been found (O'Toole & Heber 2006; Blanchette et al. 2008).

Chayer et al. (2006) analyzed far-UV spectra of 18 sdB stars taken with the *FUSE* satellite in the temperature range from 24,000 to 34,000 K and derived abundances of germanium, zirconium, and lead, almost all of them being enriched by 0.5–3 dex relative to solar. It is worth noting that lead is present in large quantities in many sdB stars.

Lead and lead isotopes. The presence of lead in the UV spectra of many sdB stars, whether helium poor or helium rich, opens an interesting opportunity to study neutron-capture nucleosynthesis. Lead is effectively the terminal product of the *s*-processing and therefore one of the most important elements in stellar nucleosynthesis modeling. Due to the lack of Pb spectral features in the cool metal-poor stars, it is hard to measure reliable abundances (Sneden et al. 2008). The significant overabundances of lead in sdB atmospheres are due to diffusion, which acts like an amplifier and enriches otherwise non-detectable trace elements in the atmosphere, where their spectral features can then be analyzed. A much better indicator for nucleosynthesis processes than the abundance of lead is the mixture of the lead isotopes. Stellar nucleosynthesis models predict different isotope mixtures depending on which of the neutron capture processes is dominant, as well as the metallicity of the source stars. O'Toole & Heber (2007) have already been able to detect the individual lead isotope lines in very high resolution *Hubble Space Telescope* (*HST*)-STIS spectra thanks to the very slow rotation of the stars. In the two stars studied, the lead isotope ratio is consistent with the solar system value.

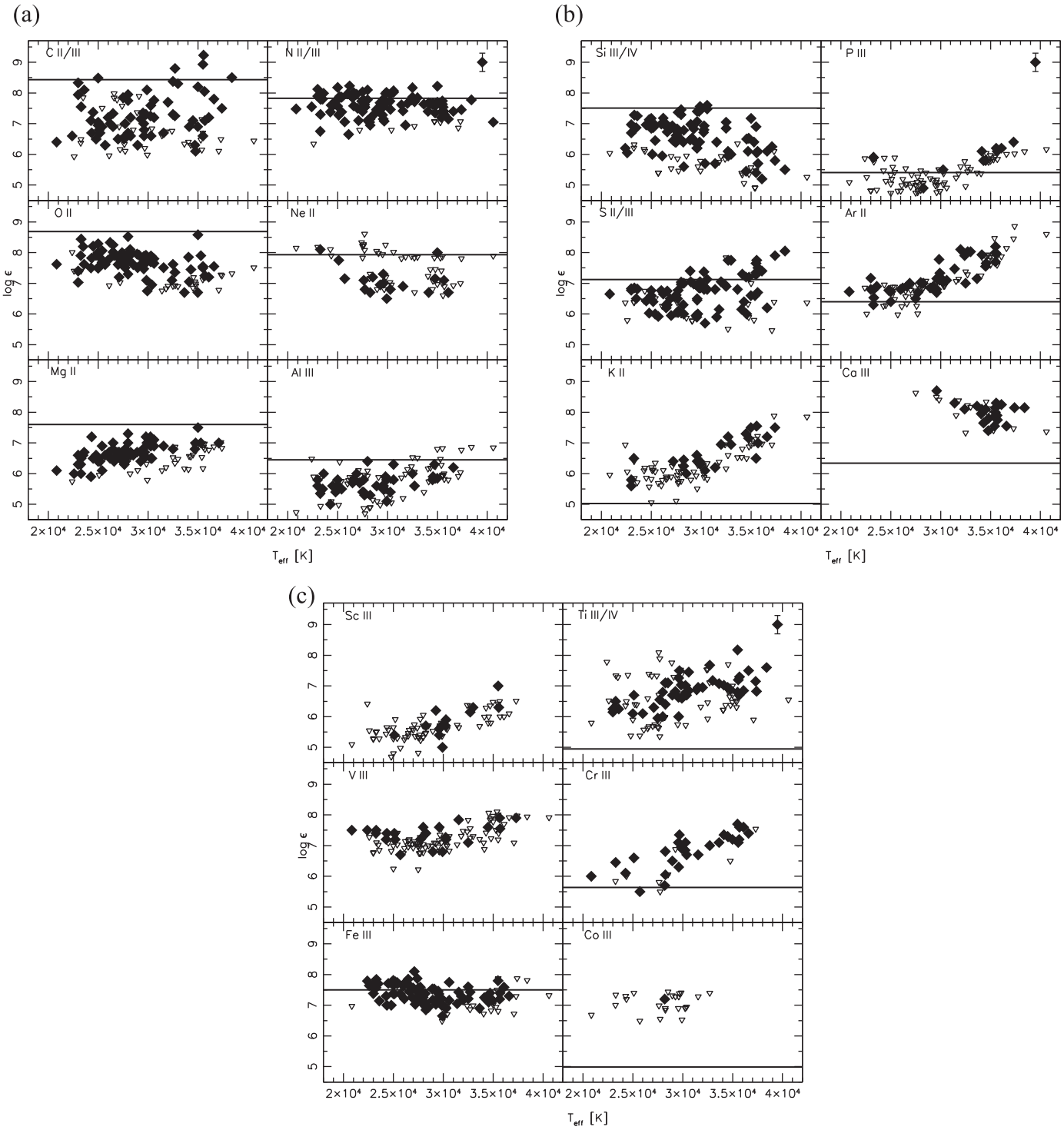

Figure 7. Elemental abundances of sdB stars plotted against effective temperature. The filled diamonds mark measured abundances while the open triangles mark upper limits. Typical error bars are given in the upper right corner. The solid horizontal lines mark solar abundances (Asplund et al. 2009). (a) Carbon to aluminum. (b) Silicon to calcium, and (c) Scandium to cobalt. From Geier (2013); copyright A&A; reproduced with permission.

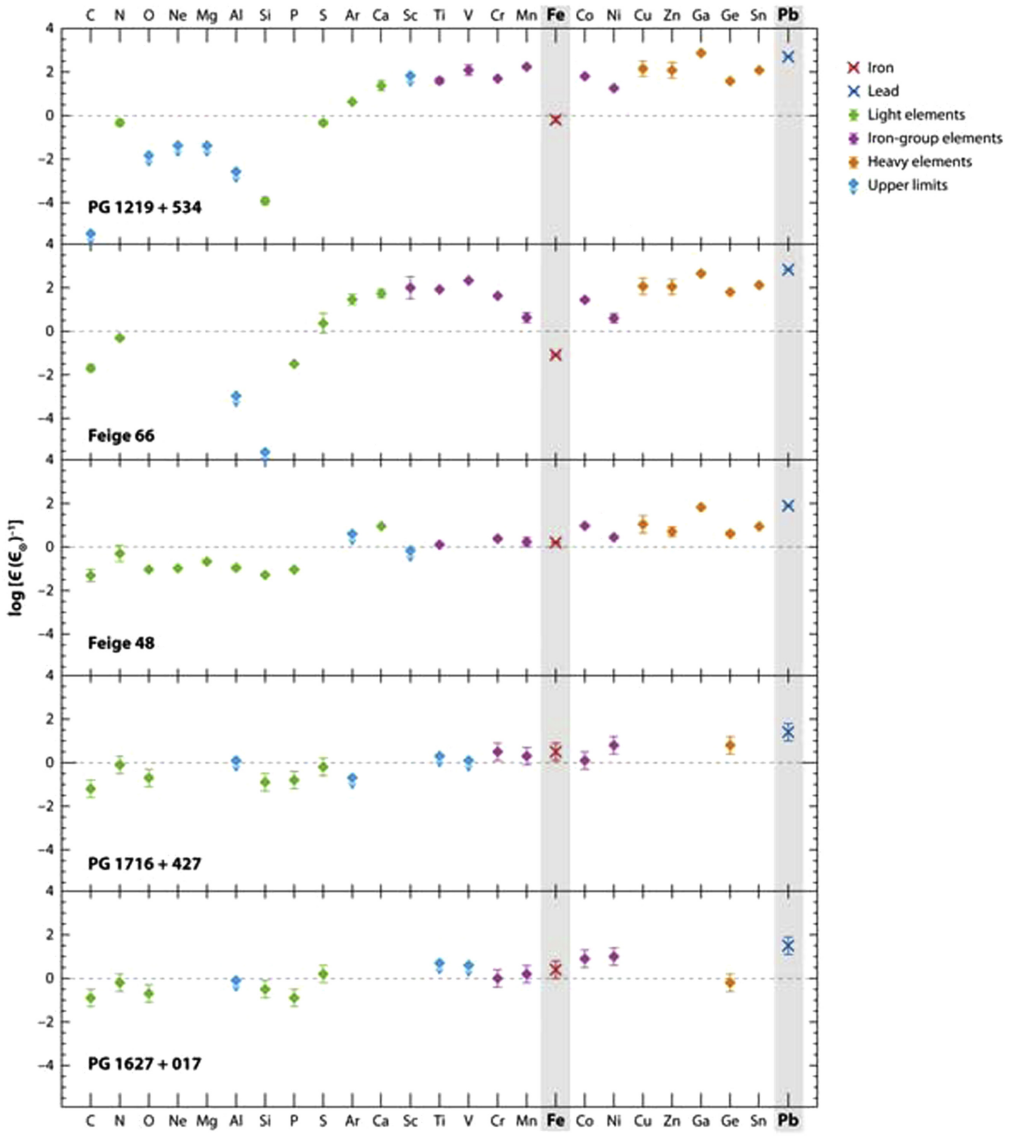

Figure 8. Abundances derived for three sdB stars from UV spectra measured with *HST*-STIS (top three panels, from O'Toole & Heber 2006) and derived from far-UV spectra measured with *FUSE* (Blanchette et al. 2008). The stars are arranged with decreasing $T_{\rm eff}$ from top to bottom. PG 1219+534 ($T_{\rm eff}$ = 33,500 K) and Feige 48 ($T_{\rm eff}$ = 29,500 K) are rapid *p*-mode pulsators of the V361 Hya type, while PG1716+427 ($T_{\rm eff}$ = 27,400 K) and PG 1627+017 ($T_{\rm eff}$ = 22,800 K) are slow *g*-mode pulsators of V1093 Her type, and Feige 66 is a constant star of $T_{\rm eff}$ = 34,000 K, very similar to PG 1219+534. Light elements are marked by green symbols, the iron group elements in magenta, iron by red crosses, and lead by blue crosses. Upper limits are given by cyan symbols. N is almost solar irrespective of the $T_{\rm eff}$ of the star. Fe also changes little (around the solar value) whereas most other elements show large differences from star to star, while lead is found to be strongly overabundant irrespective of $T_{\rm eff}$. The overall enrichment of heavy elements in the hot stars (≈2 dex) is much larger than the mild one in the cooler stars. From Heber (2009); copyright ARA&A; reproduced with permission.

(A color version of this figure is available in the online journal.)

2.4.1. Intermediate He-sdB Stars: The Transition Population

Naslim et al. (2010, 2011, 2012, 2013) derived abundances for He-sdB stars from high-resolution optical spectra using line-blanketed LTE models of Behara & Jeffery (2006; see Figure 9). The resulting abundance pattern is shown in Figure 10. The enrichment of some trans-iron elements is compelling. They are much larger than that of the normal sdB stars of similar temperature.

Three stars are particularly interesting. The intermediate[5] He-sdB LS IV−14°116 may be the most remarkable and actually a unique object up to now. It is distinct from any other hot subdwarf, not only by the presence of Ge III, Sr II, Y III and Zr IV in its optical spectrum (see Figure 9), but it shows a kind of oscillations that has not been seen in any other pulsating hot

[5] An illustrative account of the properties of this enigmatic star and the history of discovery can be found in Jeffery et al. (2015b).

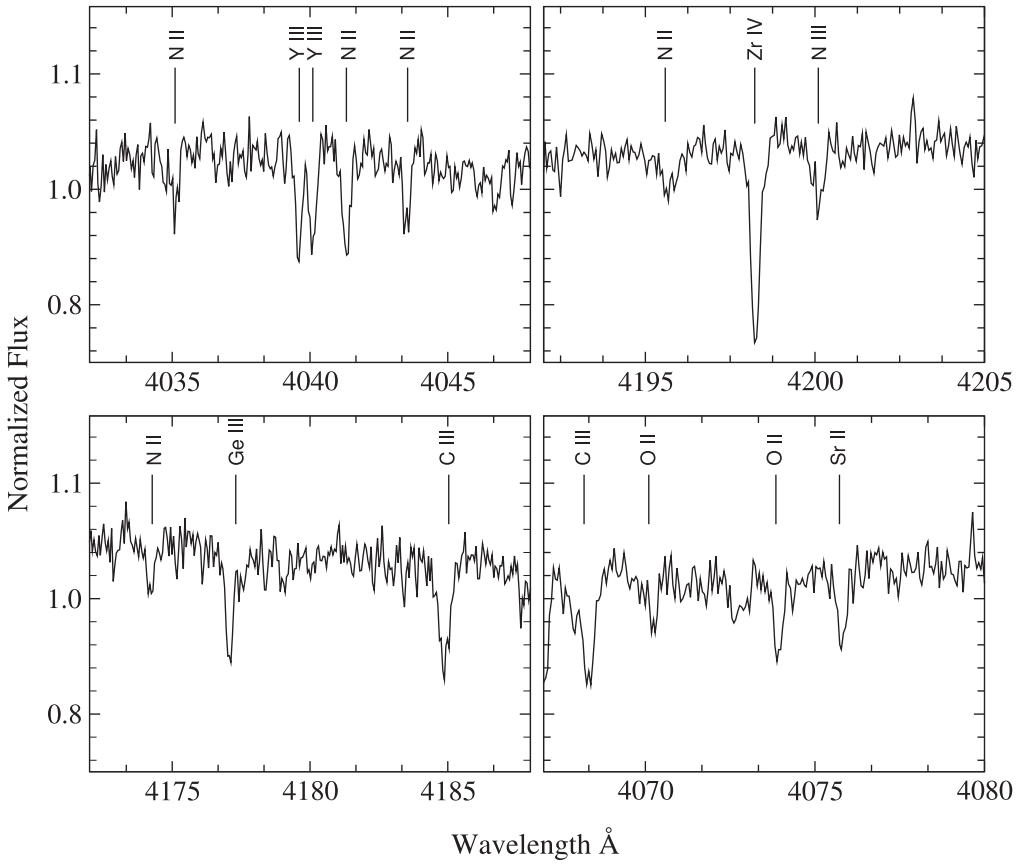

Figure 9. Y III, Zr IV, Sr II and Ge III lines in LS IV−14°116. From Naslim et al. (2011); copyright MNRAS; reproduced with permission.

subdwarf (Ahmad & Jeffery 2005). Last but not least, LS IV −14°116 was found recently to have kinematics typical of the Galactic halo population (Randall et al. 2015).

While Ge and Zr have been found in the FUV and UV spectra of many sdB stars (O'Toole 2004; Chayer et al. 2006), they have not been seen in optical spectra. This is because the overabundances of these elements in LS IV−14°116 is up to 4 orders of magnitude in the line-forming region of the photosphere, much higher than in the hydrogen-rich sdB stars. The He-sdB HE 2359−2844 also shows zirconium and yttrium abundances similar to those of LS IV−14°116 (Naslim et al. 2013). One hypothesis invoked was that a strong magnetic field may be responsible. FORS2 spectro-polarimetry of LS IV−14° 116, however, ruled out a mean longitudinal magnetic field of more than 300 G (Randall et al. 2015).

Lead has been detected in the FUV and UV spectra of many hydrogen-rich sdBs but never have any lines been found in optical spectra until Naslim et al. (2013) found two He-sdBs, HE 2359–2844 and HE 1256–2738, to show absorption lines due to triply ionized lead (Pb IV) in the optical spectrum. From these lines, the atmospheric abundance of lead was found to be nearly 10,000 times solar, that is 10–100 times higher than that previously measured in normal hot-subdwarf atmospheres.

The strong chemical peculiarities, in particular for the heavy metals, as seen in the atmospheres of some sdB stars, e.g., LS IV−14°116, suggest that some diffusion process may have led to clouds of high concentration in the line-forming region.

2.5. The Chemical Composition of Subluminous O Stars

Most of the hydrogen-rich sdO stars have been identified as the progeny of the normal sdB stars (hydrogen-rich EHB stars). Hence core helium burning has ceased, but helium continues to burn in a shell surrounding the C/O core. These stars have evolved off the EHB to high effective temperature and are destined to end up on the white dwarf graveyard.

Among the apparently brightest sdO stars, several belong to the luminous subclass (e.g., Heber & Hunger 1987), share properties with some central stars of planetary nebulae and DAO white dwarfs (Napiwotzki 1999; Gianninas et al. 2010), and are, therefore, likely evolving from the asymptotic giant branch (AGB). This subclass shall not be discussed here (for a review see Werner et al. 2003a) with the exception of BD+28° 4211, which is one of the brightest sdO stars, actually the first

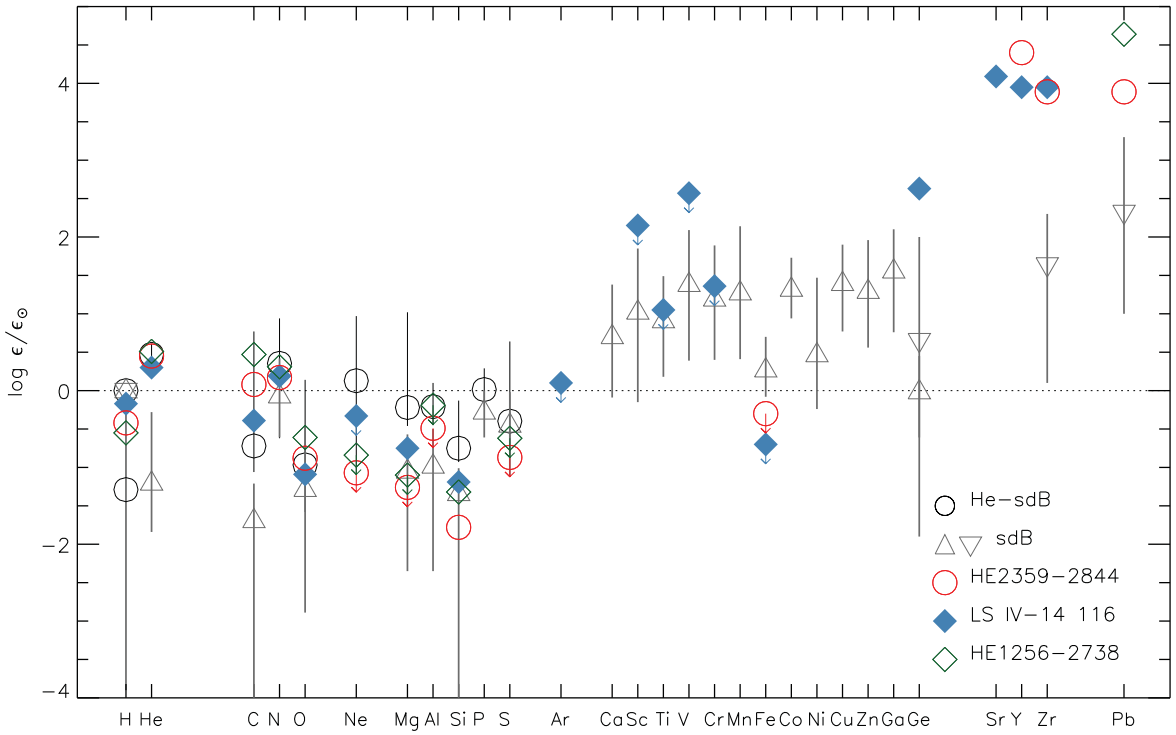

Figure 10. Surface abundances of the zirconium star LS IV−14 116 and the lead stars HE 2359−2844 and HE 1256–2738 relative to solar values. Mean abundances and ranges for other helium-rich subdwarfs and normal subdwarfs are also shown. This is an enhanced version of Figure 5 in Jeffery et al. (2015b), provided by C. S. Jeffery (2015, private communication).
(A color version of this figure is available in the online journal.)

classified as such (Macrae et al. 1951; Greenstein 1952) and, therefore, warrants a closer inspection here.

2.5.1. BD+28°4211 and the "Balmer Line Problem"

BD+28°4211 is frequently observed as a flux standard star, because its spectrum is simple at first glance. However, at high spectral resolution emission lines of highly ionized carbon, nitrogen, and oxygen in its optical spectrum (Herbig 1999) point to a very high temperature and strong NLTE effects. Its atmospheric parameters come close to that of DAO stars except for its somewhat lower gravity ($\log g = 6.2$). LS V+46°21, the central star of the planetary nebula Sh 2–216 ($T_{\rm eff} = 95{,}000$ K, $\log g = 6.9$, Rauch et al. 2007) comes close to BD+28°4211 in the ($T_{\rm eff}$–$\log g$) plane (see Figure 2 of Napiwotzki 1999). Hence, it is tempting to identify BD+28°4211 as a post-AGB star although no nebula has been detected.

Indeed, the star challenged quantitative spectral analyses. In early attempts to model the optical spectrum, using NLTE model atmospheres, Napiwotzki (1992, 1993) came across a problem with the Balmer lines. The observed Balmer lines could not be simultaneously reproduced with a unique set of fundamental parameters ($\log g$—$T_{\rm eff}$). Individual lines needed different temperatures in order to be matched properly. The higher lines of the series require higher temperatures. The Hα line requires $T_{\rm eff} \simeq 50{,}000$ K while a much higher temperature (85,000 K) was necessary to match Hϵ. The helium ionization equilibrium, a very sensitive temperature indicator, required a high temperature (82,000 K), in agreement with the high Balmer lines.

Subsequent spectroscopic analyses of very hot central stars of planetary nebulae and DAO white dwarfs showed that this "Balmer line problem" is often encountered for such stars hotter than $T_{\rm eff} \gtrsim 50{,}000$ K (Gianninas et al. 2010).

Although the modeling of spectra became more sophisticated by including line blanketing effects (Dreizler & Werner 1993) and ion-dynamical effects on the Stark broadening of hydrogen and singly ionized helium lines (Napiwotzki & Rauch 1994) the problem persisted. Werner (1996) suggested that the Balmer line problem in the case of BD+28°4211 can be solved when surface cooling by photon escape from the Stark wings of CNO lines is accounted for. However, even with the most elaborate NLTE model atmospheres the Balmer lines of BD+28°4211 cannot be matched simultaneously with the same parameter set (Latour et al. 2015). In their analysis of 29 DAO stars Gianninas et al. (2010) found a correlation between higher metallic abundances and instances of the Balmer-line problem. This hints at a "missing opacity

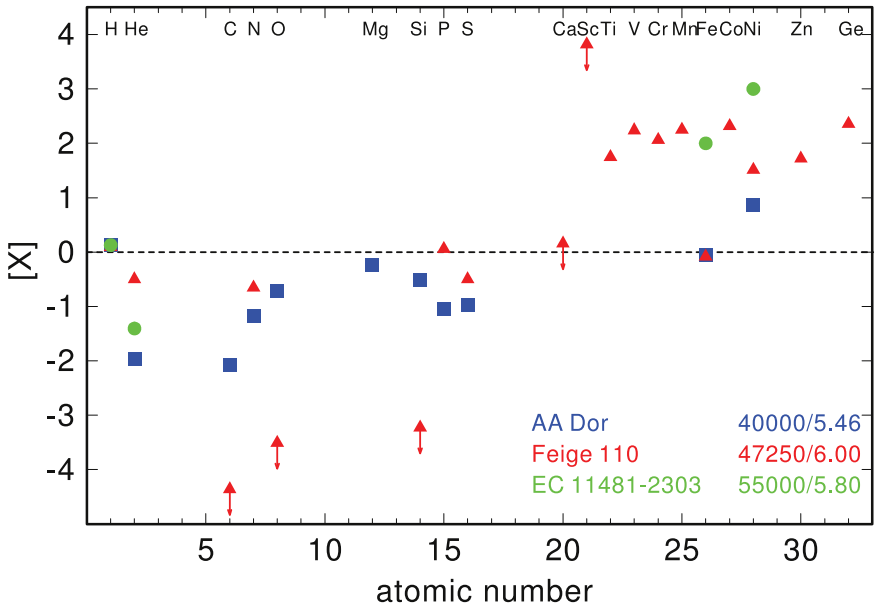

Figure 11. Comparison of the photospheric abundances relative to the solar values (arrows indicate upper limits) determined for the three OB-type subdwarfs AA Dor (Klepp & Rauch 2011), EC 11481−2303 (Rauch et al. 2010), and Feige 110 (Rauch et al. 2014). Their $T_{\rm eff}$ and log g are shown in the legend. From Rauch et al. (2014); copyright A&A; reproduced with permission.
(A color version of this figure is available in the online journal.)

problem." Indeed, the knowledge of atomic data for highly ionized metals of interest is quite incomplete. To account for missing opacity Latour et al. (2015) arbitrarily increased the metal abundances by a factor of ten[6] and successfully managed to overcome the Balmer line problem for BD+28°4211. The missing opacity, though, has still to be identified (see also Section 2.5).

2.5.2. The Helium-poor sdO Stars Feige 110, AA Dor, and EC 11481–2303

Among the helium-poor sdO stars three stars have been studied in great detail from far-UV spectra taken with the *FUSE* satellite, Feige 110, AA Dor, and EC 11481−2303 (Rauch et al. 2010, 2014; Klepp & Rauch 2011). The results are summarized in Figure 11. The star-to-star scatter is large as is the case for the sdB stars. The lighter elements (C to S) are mostly subsolar (−2 dex) to solar, except for C, O, and Si, which are strongly depleted in Feige 110. Iron is solar in Feige 110 and AA Dor but strongly enriched in EC 11481−2303. Comparing the resulting patterns to that of the cooler siblings shown in Figure 8 reveals striking similarities. Most remarkable is the strong enrichment of iron-group and trans-iron elements in both sdB and sdO stars. The enhancement of heavy metals increases with increasing temperature but the overall abundance indicate that the diffusion processes act in a similar way over a wide range of temperature, from 23,000 K (PG 1627+047, Figure 8) to 55,000 K (EC 11481−2303, Figure 11), although the degree of ionization changes and the luminosities increase, which should have a strong influence on radiative levitation and the strength of stellar winds.

The metal abundance pattern of BD+28 4211 (determined from HST and FUSE spectra by Latour et al. 2013), however, does not fit into this scheme, because its heavy metal abundances are on average subsolar (see Figure 8 of Latour et al. 2013). However, the star is far hotter (82,000 K), of higher gravity (log g = 6.2), solar helium content, and possibly a post-AGB star, and may therefore not be comparable to the other helium-poor sdO stars.

2.5.3. He-sdO Stars

For He-sdO stars most of the abundance information on carbon and nitrogen came from the sample drawn from the ESO/SPY project.

In Figure 12 the He, C, and N abundances of the 33 He-sdO stars from SPY are plotted, sorted by descending carbon mass fraction (Hirsch 2009). While the variation in the helium abundance is very small, a bimodal distribution of carbon abundances is clearly seen: either the star has enhanced carbon abundances above the solar value, or carbon is strongly depleted. Nitrogen is super-solar for two thirds of the stars (enriched by a factor 3–10 with respect to the Sun). While four

[6] This work-around has also been used by O'Toole & Heber (2006) to self-consistently match Balmer lines and helium ionization equilibrium in sdOB star spectra.

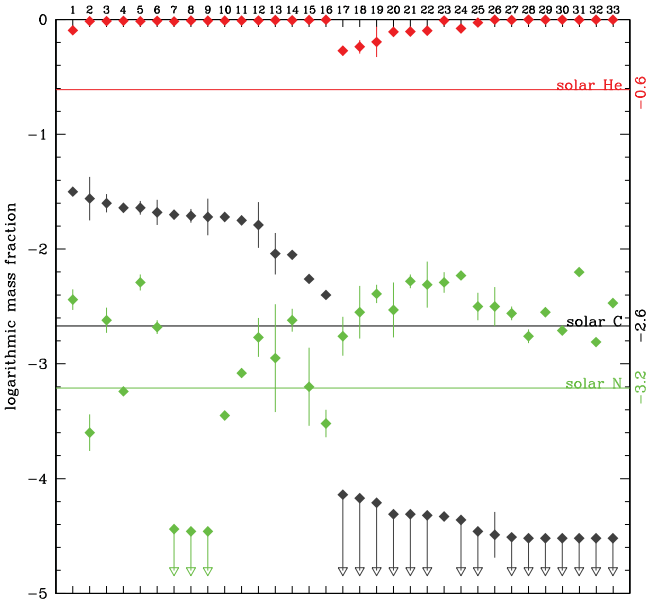

Figure 12. Abundances of He-sdO stars from the ESO/SPY project in logarithmic mass fractions of the programme stars, sorted by descending carbon abundance. Red is the helium, gray is the carbon, and green is the nitrogen mass fraction. The solar values are marked by the horizontal lines. Objects, for which only an upper limit is available are marked by an arrow pointing down. For the sake of brevity the stars listed in Table 1 of the appendix are idenfied with their running number. From Hirsch (2009).
(A color version of this figure is available in the online journal.)

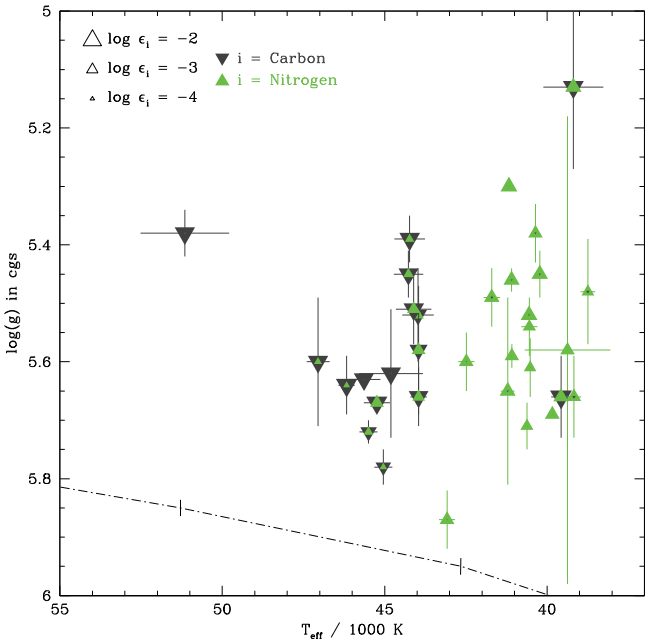

Figure 13. $T_{\rm eff}$–log g diagram for the He-sdO stars from the ESO/SPY sample. The logarithmic mass fractions of carbon (dark gray) and nitrogen (green) are coded in the symbols' sizes. The dashed–dotted line marks the zero-age helium main-sequence. From Heber & Hirsch (2010); copyright AIPC; reproduced with permission.
(A color version of this figure is available in the online journal.)

stars have solar nitrogen three others are mildly depleted in nitrogen, and another three strongly depleted by more than a factor of 15.

The distribution of the He-sdOs from ESO/SPY in the $T_{\rm eff}$–log g plane is shown in Figure 13. The bimodality of the distribution becomes obvious immediately: with only two exceptions, all carbon dominated objects ($\log \beta_{\rm C} > \log \beta_{\rm N}$) are found at the hotter end of the distribution, i.e., $T_{\rm eff} > 43{,}900$ K. Nitrogen is present in nearly all objects, and no correlation between nitrogen abundance and effective temperature becomes obvious. Also no correlation between surface gravity and abundances can be drawn from Figure 13. These results pose important constraints on evolutionary scenarios as shall be discussed in Sections 3.3 and 3.4.

2.6. Diffusion Theory

The abundance anomalies of sdB stars and some sdO stars are caused by atomic diffusion processes in the stellar envelope. In a simplistic model the elemental abundances are set by a balance between gravitational settling and radiative levitation, because the radiative acceleration depends on the elemental abundances through the incidence and strength of their spectral lines. Saturation of the spectral lines limits the radiation pressure which eventually allows an equilibrium elemental abundance to be reached. This is usually established on timescales that are short compared to the evolutionary time.

For helium atoms and ions the radiative support is rather small due to a scarceness of lines in the appropriate spectral range (UV), where the radiation flux is highest. Hence, helium should be depleted to very low abundances, on timescales much shorter than the evolutionary one. Actually, the equilibrium helium abundance is predicted to be lower by two orders of magnitude than the average observed helium abundance. At such low abundances no helium lines should be observable at all in optical spectra of sdB stars. On the other hand, radiative acceleration for ions, which have a plethora of UV lines, may be so large that the equilibrium abundance ends up super-solar.

2.6.1. Slowing Down Diffusion: Mass Loss

Because the predictions for helium from simplistic models failed to match the observed abundances, additional processes were considered in order to slow down the diffusion process and support the chemical elements against gravitational settling. First, a radiatively driven stellar wind has been suggested (Fontaine & Chayer 1997; Unglaub & Bues 2001) which may explain the observed helium abundances if the mass loss rate is of the order 10^{-13}–$10^{-14}\,M_{\odot}\,{\rm yr}^{-1}$. The radiation driven wind theory was used by Vink & Cassisi (2002) to

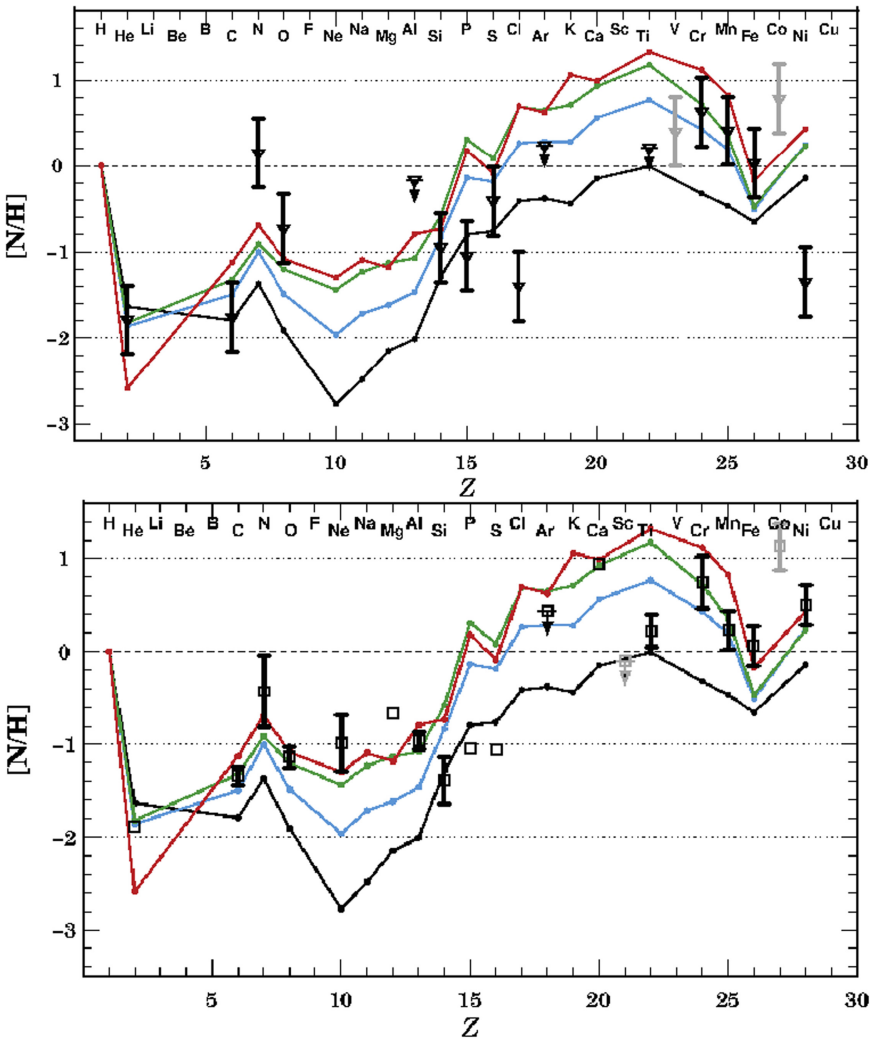

Figure 14. Comparison of the observed abundance pattern of the sdB stars PG 0101+039 (Blanchette et al. 2008, top) and Feige 48 (O'Toole & Heber 2006, bottom) with prediction by diffusion models with turbulence of Michaud et al. (2011) after 25 Myr for models with original metallicities of $Z_0 = 0.0001$ (black), 0.001 (cyan), 0.004 (green), and 0.02 (red), respectively. Cobalt (gray symbol) was not included in the diffusion model due to the lack of atomic data. This is a modified version of Figures 5 and 13 of Michaud et al. (2011).
(A color version of this figure is available in the online journal.)

derive analytical formulae to estimate the mass-loss rates of hot horizontal-branch and sdB stars, assuming that the wind plasma behaves as a single fluid. However, Unglaub (2008) demonstrated that the densities are so low that the metals do not share their momentum with the hydrogen and helium ions through collisions, i.e., the wind will fractionate and becomes metallic.

2.6.2. Slowing Down Diffusion: Turbulence

Diffusion is taking place not only in the atmosphere of sdB stars, but also in subphotospheric layers, where it plays a vital role in order to drive pulsations via an opacity bump created by iron-group elements (see Section 7). A prerequisite is sufficient radiative levitation of those elements in the appropriate layers. Mass loss would weaken the opacity bump and pulsations would stop once the mass loss exceeds a certain critical limit. Hu et al. (2011) found that the mass-loss rates required to match the observed He abundances are not consistent with observed pulsations. Weak turbulent mixing of the outer $10^{-6}\,M_{\odot}$ could also explain the He abundances while still allowing pulsation modes to be driven. A major caveat of the turbulence scenario is that it is not supported by a physical model. Hu et al. (2011) speculated that thermohaline mixing could play a role if a mean molecular weight inversion occurs. Michaud et al. (2008, 2011) adopted the turbulence model and carried out detailed diffusion calculations for metals in blue horizontal-branch stars and hot subluminous stars. They reproduce moderately well the

surface abundances of normal sdB stars (see Figure 14). Diffusion calculations for the trans-iron elements with excessive overabundances have, however, not been possible yet due to the lack of atomic data.

2.7. Surface Rotation

Projected rotation velocities can be derived from high-resolution spectra along with the elemental abundances. Thermal broadening is the main limiting factor for stars as hot as sdB stars. Because the thermal velocity scales inversely with the square root of the atomic mass, it is advisable to make use of metal lines rather than of the helium and hydrogen lines. Unfortunately, metal lines are scarce in the optical spectra of many sdB stars, in particular in the hotter ones. The detection limit in most published studies is $v_{\rm rot} \sin i \approx 5\,{\rm km\,s^{-1}}$. However, processes other than rotation may lead to additional line broadening, in particular, pulsations and magnetic fields. No indication for magnetic line broadening has been found yet in any sdB star. Pulsations cause the shape of the line profiles in the disk-integrated spectra to change with time (e.g., Telting et al. 2008). The pulsation periods of the V361 Hya stars are mostly shorter than the integration times of the spectral observations leading to a smearing of the lines that can easily be mistaken for rotation (see Heber et al. 1999; Kuassivi et al. 2005, for an example). Indeed, substantial line broadening due to pulsational smearing has been found in several rapidly pulsating sdB stars.

Asteroseismology provides another option to determine rotational velocities, if the rotation splitting of pulsation frequencies can be measured. This technique is able to measure rotation rates too slow to be detectable from spectral line fitting. Reed et al. (2014), for instance, detected a rotation period as low as 88 ± 8 days for a g-mode pulsator in the *Kepler* field (see Section 7.3.2).

2.7.1. Close Binaries and Synchronous Rotation

Tidal interaction plays a crucial role in binary stars and exoplanets. In particular the tidal synchronization times are important, but present estimates are quite uncertain, especially for stars with radiative envelopes such as sdB stars.

In the case of single-lined close binary sdB stars the analysis of radial velocity (RV) curves allows us to determine minimum masses from the mass function (see Section 5). While the mass of an sdB star can be reasonably well estimated, the mass of the unseen companion cannot be determined unless the system is eclipsing. However, there is a way to determine the inclination angle if the rotation velocity and the stellar radius are known. The latter can be calculated from surface gravity and mass. Spectroscopically the rotation velocity can be determined only in projection to the line of sight. In a tight binary, however, rotation may be tidally locked to the orbit. In such a case, the inclination results from the orbital period, the stellar radius, and the projected rotational velocity. Therefore, Geier et al. (2010b)

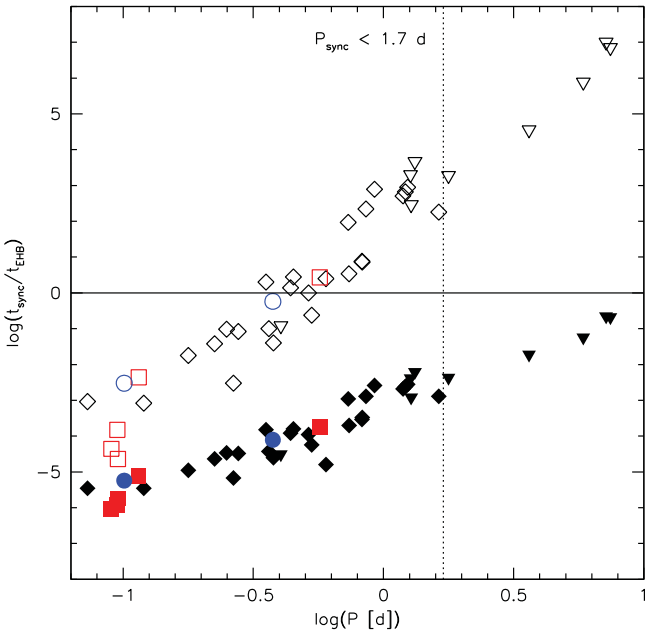

Figure 15. The observed orbital period is plotted against the synchronization times calculated with the theory of Zahn (1977, open symbols), and by that of Tassoul & Tassoul (1992, filled symbols), both in units of the average lifetime on the EHB (10^8 years; Dorman et al. 1993). The solid horizontal line marks the border between synchronization within the EHB lifetime and synchronization times longer than the EHB lifetime. The squares mark sdB binaries, where the primaries have been proven to be synchronized by light curve analysis of eclipsing or ellipsoidal variable systems. The circles mark binaries where synchronization could be shown by asteroseismology. The systems marked with diamonds could be solved consistently under the assumption of synchronization, while the systems marked with triangles rotate faster than synchronized. From Geier et al. (2010b); copyright A&A; reproduced with permission.
(A color version of this figure is available in the online journal.)

embarked on a study to determine the distribution of projected rotational velocities of a sample of 31 close sdB binaries by measuring the broadening of unblended metal lines and derived companion masses. Surprisingly in as many as eight cases (including the well known system KPD 1930+2752) the companion mass may exceed $0.9\,M_{\odot}$, four of which even exceed the Chandrasekhar limit; they may be neutron stars or even black holes. The distribution of the inclinations of the systems with low mass companions appears to be consistent with expectations. A lack of high inclinations for the massive systems signals a warning that the assumption of tidally locked rotation may be incorrect. This could be a matter of stellar age. If the EHB star is too young, synchronization might not yet have been reached. Taking this into account two objects, PG 1743+477 and, in particular, HE 0532-4503 remained whose companions may have masses close to or above the Chandrasekhar limit. However, no X-rays have been detected from both of them using *Swift*/XRT (Mereghetti et al. 2011a) nor has radio emission from HE 0532−4503 been discovered (Coenen et al. 2011), see also Sections 5.4.1 and 5.4.3.

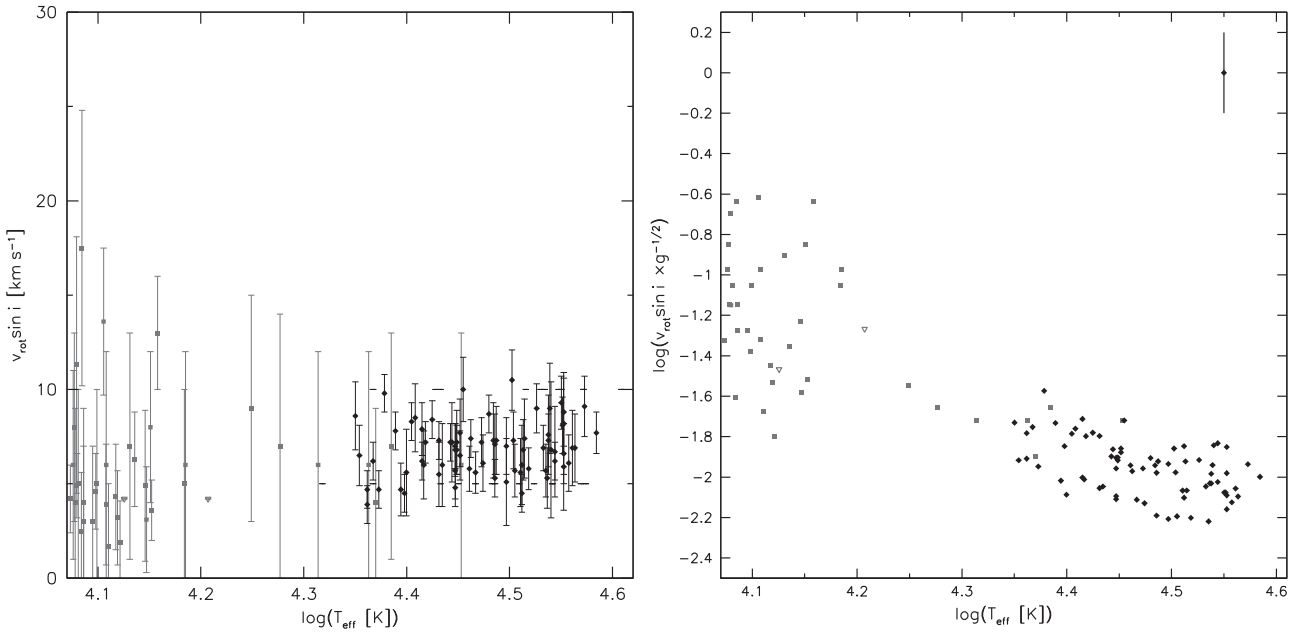

Figure 16. Left hand panel: projected rotational velocity plotted against effective temperature. Right hand panel: $v_{\rm rot} \sin i \times g^{-1/2}$, a proxy for the angular momentum, plotted against effective temperature. The gray squares mark BHB and some sdB stars taken from Peterson et al. (1995), Behr (2003a, 2003b), Kinman et al. (2000), and Recio-Blanco et al. (2002). Upper limits are marked with gray triangles. The black diamonds mark the sdBs from the sample of Geier & Heber (2012). The vertical line marks the jump temperature of 11,500 K. Typical uncertainties for the sdBs are given in the upper right corner. These are modified versions of Figures 6 and 7 in Geier & Heber (2012), provided by S. Geier (2015, private communication).

However, the assumption of tidal locking may not be correct. Because the envelopes of hot subdwarf stars are radiative, the spin-up by tidal forces is inefficient and very difficult to model. The results from rivalling theoretical concepts of tidal interaction (Zahn 1977; Tassoul & Tassoul 1992) differ enormously (see Figure 15). A detailed discussion of the synchronization of sdB+dM binaries through coupling via dynamical tides can be found in Pablo et al. (2012). In the least efficient case (Zahn 1977) tidal synchronization should be established within the evolutionary lifetime of an sdB star (10^8 years) for all systems with periods of less than half a day.

Rotation velocities can be derived via asteroseismology by making use of the frequency splitting of pulsation modes (see Section 7). Hence pulsating sdBs in binaries provide an important testbed. Observational tests were scarce and lead to contradictory conclusions. In the case of the pulsating sdB binary Feige 48, for instance, Van Grootel et al. (2008) derived a spin period of 9.028 ± 0.480 hr from the light curve, remarkably similar to the system's orbital period of 9.024 ± 0.072 hr, from RV variations. Hence, Feige 48 rotates as a solid body in a tidally locked system. On the other hand Pablo et al. (2012) studied the *Kepler* light curves of two pulsating subdwarf B stars in close binaries with dM companions of orbital periods (9 hr) similar to that of Feige 48 and measured the rotational splitting of the pulsation frequencies. Both systems have several triplet spacings, which imply rotation periods of 10.3 and 7.4 days, respectively, indicating the sdB components rotate too slowly for synchronous rotation, because the orbital periods are much shorter.

We shall revisit stellar rotation in the context of asteroseismology in Section 7 in the light of new *Kepler* measurements.

2.7.2. Single sdB Stars and BHB Stars

Projected rotation velocities for single sdB stars[7] were determined from high resolution spectra by Geier & Heber (2012). All stars in their sample have low projected rotational velocities ($v_{\rm rot} \sin i < 10\,{\rm km\,s^{-1}}$). The distribution of projected rotational velocities is consistent with an average rotation of $8\,{\rm km\,s^{-1}}$ for the sample.

It is tempting to compare the rotational properties of sdB stars to those of the BHB stars, because the hot subdwarf stars form the extension of the horizontal branch. In Figure 16 rotation velocities of BHB stars from literature are compared to those of sdB stars from Geier & Heber (2012). BHBs with diffusion-dominated atmospheres are slow rotators as well (Behr 2003a). As can be seen from Figure 16 the sdB sequence extends the BHB trend to higher temperatures. The $v_{\rm rot} \sin i$ values remain at the same level as observed in hot BHB stars.

[7] Subluminous B stars in binaries were also considered single if the separations of the components are so wide that tidal interaction can be neglected, that is their orbital periods exceed 1.2 days (Geier et al. 2010b).

Because BHB stars have larger radii than sdB stars it is important to compare their angular momenta. The quantity $v_{\rm rot} \sin i \times g^{-1/2}$ is a proxy for the angular momentum and a comparison of the BHB and sdB stars is shown in the right hand panel of Figure 16. The transition between BHB and EHB stars is smooth. Since the progenitors of the EHB stars lost more envelope material on the red giant branch (RGB), the EHB stars are expected to have lower angular momenta than the BHB stars. This is consistent with the trend seen in Figure 16. Hence single sdB stars as well as sdB stars in wide binaries are related to BHB stars in terms of surface rotation and angular momentum evolution. This is remarkable because in the case of the binaries, a transfer of mass and angular momentum is likely to have occurred.

SB 290 and EC 22081–1916—the exceptions to the rule. Despite the evidence presented above, that sdB stars are slow rotators unless they are spun-up by tidal forces from a close companion, two apparently single sdB stars, SB 290 (Geier et al. 2013b) and EC 22081–1916 (Geier et al. 2011a), have been found to be rapidly rotating, indicating that both stars may be the result of He-WD mergers.

While SB 290 is located on the EHB band and considered consistent with a He-WD merger by Geier et al. (2013b), EC 22081–1916 is of lower gravity and, hence, higher luminosity, suggesting that the hydrogen envelope may be unusually thick. This, however, would be at variance with the He-WD merger scenario, but consistent with a common envelope merger of a low-mass, possibly substellar object with a red-giant core.

2.8. Magnetic Fields of Hot Subdwarfs: sdBs versus He-sdOs

Strong magnetic fields can be easily detected in high resolution spectra due to Zeeman splitting or corresponding broadening of the lines. Magnetic line broadening can be distinguished from rotational broadening because the former scales with the square of the wavelength of the lines. Although many sdB stars have been studied at high spectral resolution, none have been found to show magnetic broadening or splitting. Spectropolarimetry allows weaker fields to be measured. Indeed, the presence of magnetic fields at the 1 kG level had been concluded for a handful of sdB stars (O'Toole et al. 2005b) from their spectrophotometric observations with FORS@ESO-VLT, although close to the instrumental detection limit. Landstreet et al. (2012) reanalyzed the same data set using an improved wavelength calibration and showed that the detection was an instrumental artefact. The reanalysis resulted in upper limits to the magnetic field strength of a few hundred Gauss. Recently, Randall et al. (2015) derived an upper limit of 300 G for the intermediate He-sdB LS IV−14°116. Claims for the existence of magnetic fields in Feige 66, HD 76431 and the pulsating sdB Balloon 090100001 have also been shown to be spurious (Petit et al. 2012; Savanov et al. 2013).

More recently, though, Zeeman triplets in an He-sdO star were reported by Heber et al. (2013), which was serendipitously discovered in the search for targets for the Massive Unseen Companions to Hot Faint Underluminous Stars from SDSS (MUCHFUSS) project in the SDSS spectral data base by B. Gänsicke. In the same project two additional He-sdO stars were found to show similar splittings indicating the presence of magnetic fields of about 500 kG (Németh 2016, private communication). Because the population of He-sdO stars has been much less extensively studied, these discoveries indicate that the magnetic properties of the He-sdO population is substantially different from that of the sdB stars. Magnetic He-sdO stars might be progenitors of strongly magnetic white dwarfs (>1 MG) if the magnetic flux is conserved during the contraction of the He-sdO to the white dwarf state (see Ferrario et al. 2015 for a recent review on magnetic white dwarfs).

3. Formation and Evolution of Hot Subdwarf Stars

The main difficulty to explain the formation of EHB stars is the large amount of mass lost prior to or at the start of core helium burning. In order to resolve the puzzle of the origin and evolution of sdB and sdO stars and the potential linkage between both classes of stars, several scenarios have been developed.

Binary evolution through mass transfer and CE ejection must be important for sdB stars because of the high percentage of close binaries with periods of less than ten days. The merger of two helium white dwarfs is another vital option to explain the origin of single hot subdwarfs. Alternatively, the origin of hot subdwarf stars could be intrinsic to the star; that is, internal processes may decrease the hydrogen content of the envelope, e.g., through delaying the core helium flash (the so called hot-flasher scenario, see Section 3.3), during which surface hydrogen is burnt after mixing into deeper layers. Finally it cannot be taken for granted that sdB stars are core helium-burning objects. There is observational evidence that some sdB stars have masses too low to ignite core helium burning (Heber et al. 2003). We shall come back to this class of star in Section 8.

3.1. Canonical HB and Post-HB Evolution

Horizontal-branch stars are in the core helium-burning phase of evolution following the red-giant branch (RGB). The ignition of helium burning takes place under electron-degenerate conditions for stars of $\leqslant 2.3\,M_{\odot}$ leading to the helium core flash. The distribution of stars along the HB can be explained by a constant core mass of slightly less than half a solar mass and a spread in envelope and thus total mass. The smaller the envelope the bluer the star ending at the theoretical

helium main-sequence when the envelope mass is zero. The core mass is fixed at the onset of the core helium flash at the tip of the RGB and depends only slightly on metallicity and helium abundance (Sweigart 1987). Accordingly the core mass is restricted to a narrow range from 0.46 to 0.5 $M_{\odot}$. The post-EHB evolution proceeds toward higher temperatures until the white-dwarf cooling track is reached and gravity increases. Hence the star will avoid the AGB stage.

Only very few calculations have been able to follow stellar evolution through the violent helium core flash. Most HB models were calculated by starting new sequences on the HB, where the initial structure is taken from that of a red-giant progenitor, but the core composition on the ZAHB has to be adjusted to account for the modest carbon production during the flash (see Sweigart 1997a, 1997b). Widely used models (e.g., Dorman et al. 1993) are calculated in such an approximate way, but have been shown to be reliable, because recent full evolutionary models following the star from the ZAMS through the helium core-flash to the ZAHB (e.g., Serenelli & Weiss 2005) differ only slightly from the approximate ones. More recent two and three-dimensional models of the evolution of a star through a helium core flash also confirm that the structure of the star is not significantly altered, because convection plays an important role in establishing hydrostatic equilibrium, but show that overshooting, indeed, occurs (Mocák et al. 2008, 2009). The MESA[8] code allows to consistently evolve stellar models through the He core flash (Paxton et al. 2011).

Post-EHB evolution has been computed by many groups, e.g., Dorman et al. (1993), Han et al. (2003), and Hu et al. (2008) and evolutionary timescales are found to be shorter by an order of magnitude than the EHB lifetime. The post-EHB tracks nicely connect the (helium-deficient) sdB stars on or near the EHB band to the helium-deficient sdO stars.

However, the formation of EHB stars remains unexplained by canonical models, because there is no straight-forward way for a single red giant to remove all of its envelope.

3.2. Helium mixing on the Red Giant Branch

Sweigart (1997a, 1997b) presented a series of non-canonical models to explain the formation of BHB and EHB stars. Besides the hot flasher scenario, which will be discussed in the next section, he investigated helium mixing on the red giant branch by assuming that the outer convective envelope can penetrate into the hydrogen burning shell and that some helium is mixed into the stellar envelope. Evolutionary sequences were calculated assuming different penetration depth. The most important consequence of helium mixing is that the luminosity of the tip of the RGB increases, which causes stronger mass loss. A caveat of the helium-mixing scenario is that the physical mechanism that causes the mixing remains obscure.[9] Sweigart (1997b) conjectured that rapid rotation may be responsible and a spread in rotation rates may explain the distribution of stars along the horizontal branch. This scenario has recently been revived by Tailo et al. (2015) to explain EHB and blue hook stars in globular cluster, who suggest that rapid rotation of second generation stars may result from the star-forming history and the early dynamics of very massive globular clusters, such as ω Cen (see Section 4).

3.3. The Hot-flasher Scenario

Low-mass stars undergo the helium core flash at the tip of the red giant branch. However, Castellani & Castellani (1993) showed that, if sufficient mass is lost on the RGB, the star can depart from the RGB and experience the helium core flash while descending the hot white-dwarf cooling track. The remnants of these "hot flashers" (e.g., Brown et al. 2001; D'Cruz et al. 1996) are found to lie close to the helium main-sequence, i.e., at the very hot end on the EHB.

The "hot flasher" phase bears a striking similarity to the late helium shell flashes that produce "born-again AGB stars" (Iben 1984). As in the born-again scenario, the high luminosity ($L_{\rm He} \sim 10^{10}\,L_{\odot}$) during the flash generates a convection zone, which might engulf the H-rich envelope (Sweigart 1997a, 1997b). Hence, hydrogen might be mixed into hotter layers and be burnt there leading to a He-enriched surface. Cassisi et al. (2003), Lanz et al. (2004), and Miller Bertolami et al. (2008) showed that the outcome of a hot flasher depends on the evolutionary phase during which it occurs (Lanz et al. 2004, see also Figure 17):

(i) *Early hot flasher:* if the helium core flash occurs early after departure from the RGB, i.e., during the evolution at constant luminosity, hot subdwarf stars with standard H/He envelopes result.
(ii) *Late hot flasher (shallow mixing):* mixing is found to occur only when the star has already embarked on the white-dwarf cooling track. If the flash occurs early on that track, mixing is shallow and the atmosphere of the resulting hot subdwarf is somewhat enriched in helium and nitrogen due to convective dilution of the envelope.
(iii) *Late hot flasher (deep mixing):* deep mixing, however, occurs in late hot flashers in which the H-rich envelope is engulfed and burnt in the convective zone generated by the primary helium core flash leading to strong enrichment of He, C, and N.

[8] Modules for Experiments in Stellar Astrophysics.

[9] The core-envelope coupling of red giants must be much stronger than predicted by theory to explain the results of *Kepler* light curve analyses (Aerts 2015, see Section 7.6.1), which could also lead to helium mixing.

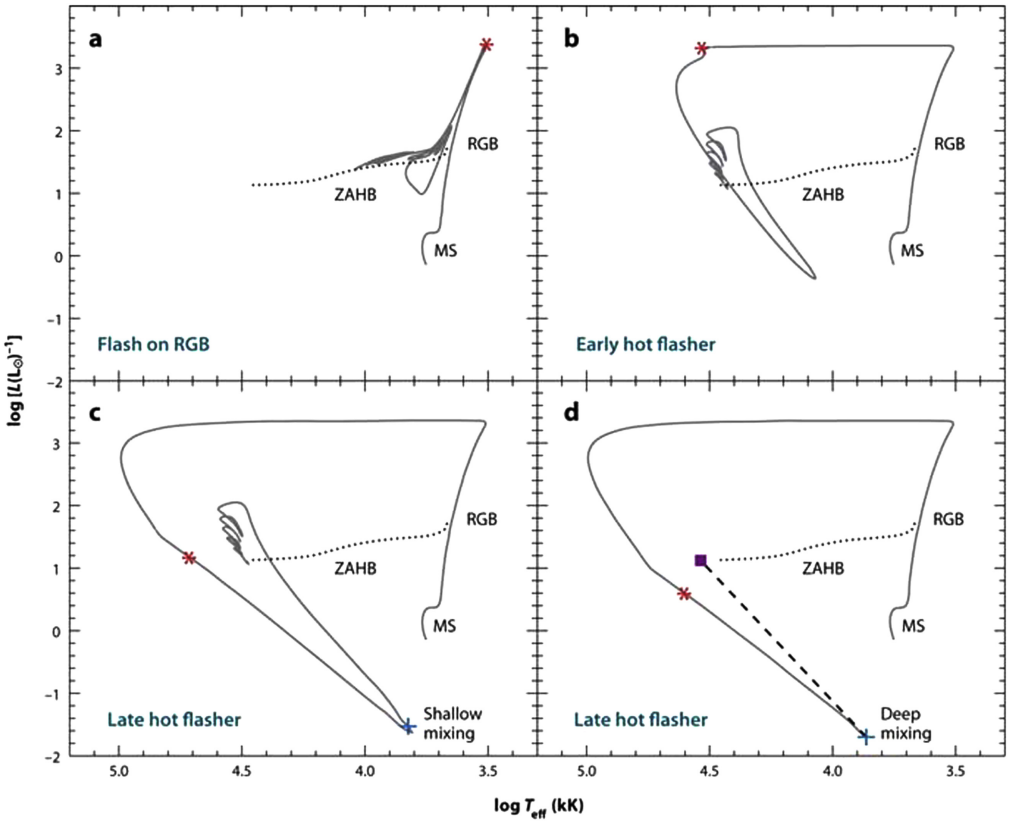

Figure 17. Evolution of a solar metallicity star from the main sequence through the helium flash to the zero-age horizontal-branch (ZAHB, dotted curve) for different amounts of mass loss on the red-giant branch (Lanz et al. 2004). Flash mixing did not occur for the canonical sequences in panel (a) and in an early hot flasher (b). For sufficiently large mass loss, a star evolves off the RGB to high effective temperatures before igniting helium as either an early or late hot flasher. The peak of the helium flash is indicated by an asterisk. The flash convection zone reached the hydrogen envelope at the plus sign along the tracks in panels (c) and (d). These panels illustrate the two types of flash mixing: shallow mixing in which the hydrogen envelope is mixed only with the convective shell in the outer part of the core and deep mixing in which the hydrogen envelope is mixed all the way into the site of the flash. The model calculations in panel (d) were stopped at the onset of deep mixing, and a ZAHB model (solid square) was then computed assuming a helium- and carbon-rich envelope composition. The evolution during this phase is shown schematically by the dashed line. From Heber (2009); copyright ARA&A; reproduced with permission.
(A color version of this figure is available in the online journal.)

3.3.1. The Rapid Evolution of the Exciting Star of the Stingray Nebula

Late thermal pulses proceed on timescale so short that stellar evolution may be observed in "real time." This has been witnessed for three post-AGB stars (FG Sge, V 605 Aql, and Sakurai's object V4334 Sgr) during the last century (see van Winckel 2003 for a review).

The central star of the Stingray nebula might be an exciting new such case. Parthasarathy et al. (1995) first discovered a rapid increase in effective temperature and a drop of luminosity, far too fast for canonical post-AGB evolution. From a detailed quantitative spectral analysis Reindl et al. (2014) found that from 1988 to 2002 the central star has steadily increased in effective temperature from 38 to 60 kK while contracting; that is, the surface gravity increased during this period of time from $\log g = 4.8$ to 6.0 (see Figure 18). By the year 2002 its evolution reversed into cooling down to 55 kK in 2006. Unlike e.g., in Sakurai's object, which showed a dramatic change in chemical composition in only a few months time (H decreasing while Li and *s*-process elements were increasing) no such change of the (nearly) solar composition of the surface of the Stingray's central star has yet been observed. Furthermore, Reindl et al. (2014) showed that the Stingray's central star is a low mass star, consistent with a post-EHB or post-RGB nature (see Figure 18). However its speed of evolution is much too fast for canonical post-EHB or post-RGB evolution suggesting that the star has just suffered from a late shell flash. Although no evidence for binarity has yet been found, Reindl et al. (2014) proposed that binary common envelope evolution might lead to a remnant that has not yet re-established thermal equilibrium after the CE ejection. Continued monitoring will show whether the star is evolving back to the RGB or heading toward the white dwarf graveyard and whether a companion exists.

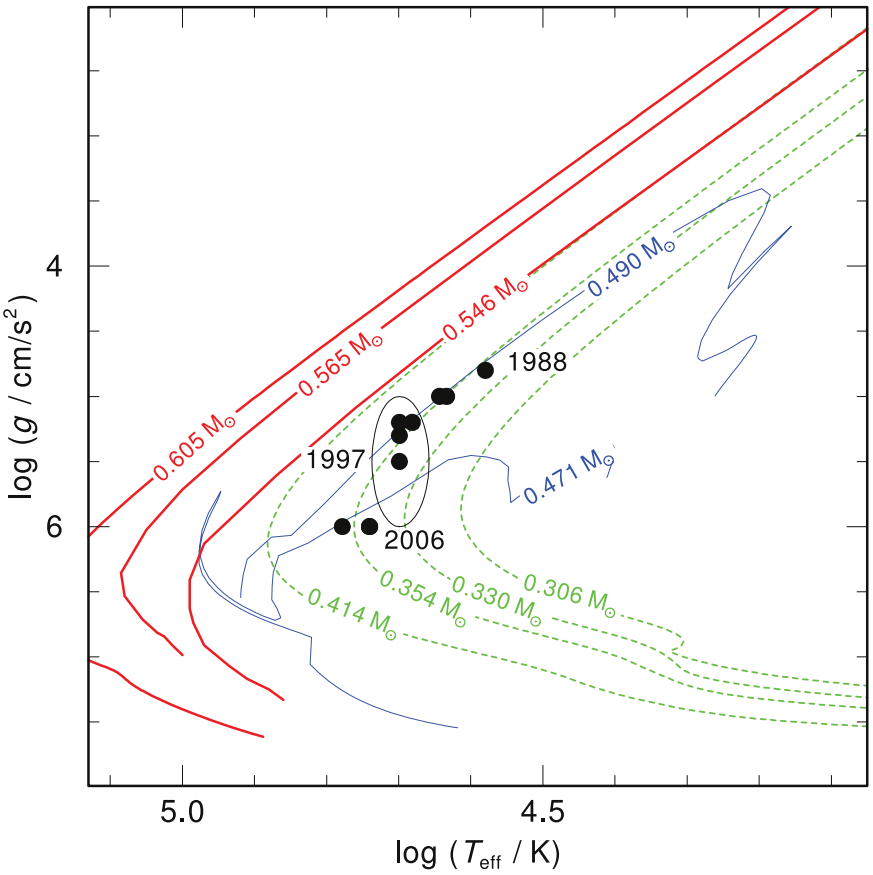

Figure 18. Evolution of the central star of the Stingray nebula (black dots) in the log $T_{\rm eff}$, log g plane compared to post-AGB (red, thick) by Bloecker (1995), post-EHB (blue, thin) by Dorman et al. (1993), and post-RGB (green, dashed) evolutionary tracks by Hall et al. (2013). The tracks are labeled with stellar masses. The ellipse indicates the errors of $T_{\rm eff}$ and log g in 1997. From Reindl et al. (2014); copyright A&A; reproduced with permission.
(A color version of this figure is available in the online journal.)

3.4. Close-binary Evolution

The high fraction of sdB stars in close binaries implies that they are formed by binary-interaction processes. The three main formation channels that have been proposed to produce sdB stars are CE evolution (Paczynski 1976), RLOF evolution and a white-dwarf merger (Webbink 1984). A detailed description of the binary evolution forming hot subdwarf stars can be found in Han et al. (2002, 2003).

In the CE formation model, the sdB progenitor fills its Roche lobe near the tip of the RGB. If the mass transfer rate is sufficiently high the companion star will not be able to accrete all the matter. In consequence a common envelope is formed. Due to friction with the gas the two components will spiral in until enough orbital energy is transferred to the common envelope to eject it. The remaining core of the red giant will become the sdB star. Because the CE phase is short the companion will remain almost unchanged. If the companion is a main-sequence star (MS) the resulting close binary is an sdB + MS with a period between 0.1 and 10 days. Eventually the main -sequence star will evolve into a red giant. When it fills its Roche lobe, a second CE ejection phase occurs resulting in a close sdB + WD binary, because the red giant fills its Roche lobe before the tip of the RGB is reached.

In the RLOF channel no common envelope will form because the mass transfer is dynamically stable and the companion slowly accretes the matter. The red giant loses its entire envelope during RLOF to become an sdB star in a long-period binary with a main-sequence component. Han et al. (2003) predicted that the orbital periods of such systems should be in the range 10–500 days. This is at odds with the period distribution of sdB+MS systems, recently found to have periods ranging from 700 to 1300 days (see Section 5). This discrepancy triggered new binary population synthesis calculations based on Han's models (Chen et al. 2013) which included a more sophisticated treatment of angular-momentum loss and also considered atmospheric RLOF. Periods up to 1100 days result from solar-composition

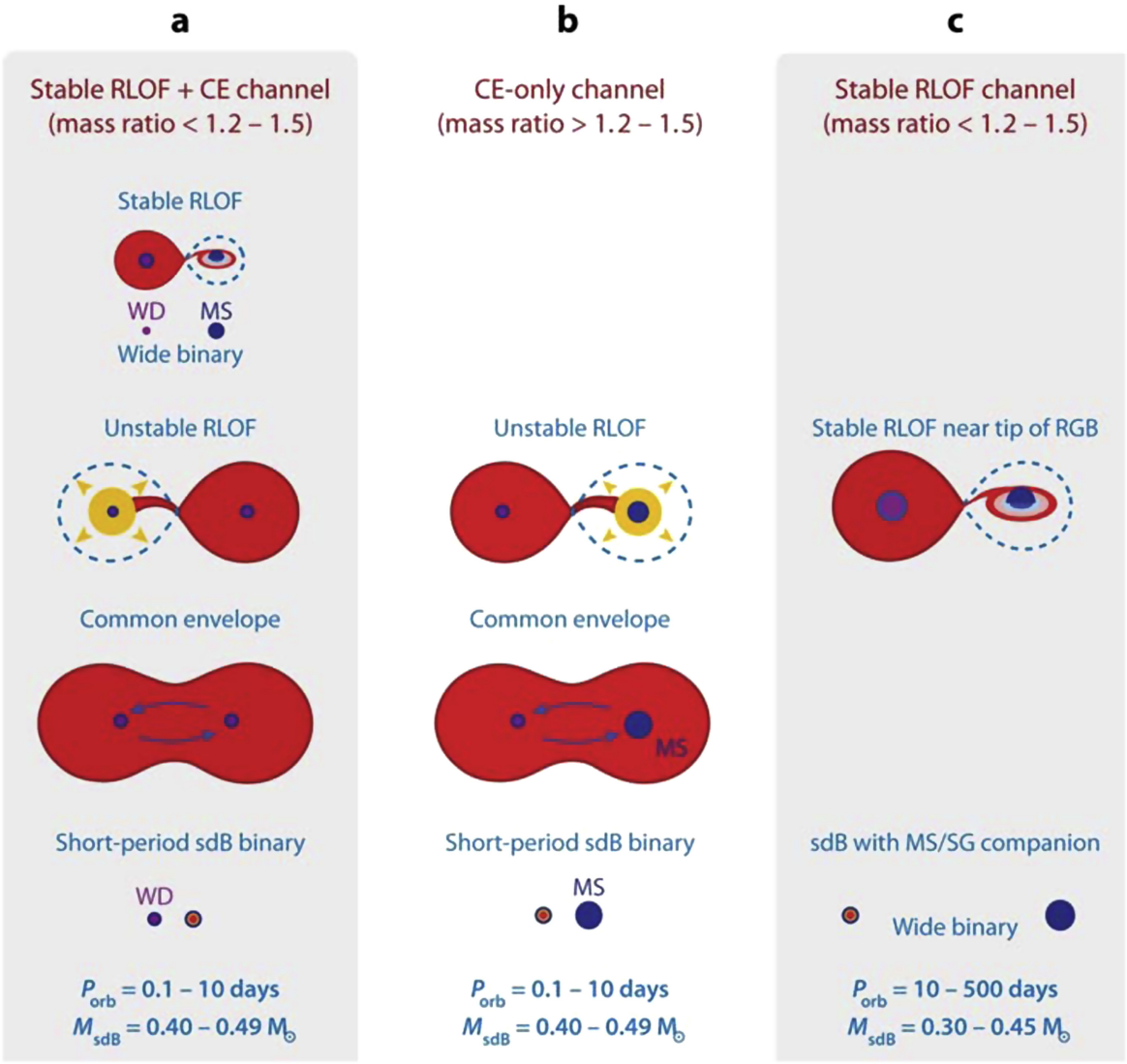

Figure 19. Some formation channels of sdB stars in close binaries (Podsiadlowski et al. 2008). The evolution of the system proceeds from top to bottom. (a) For small initial mass ratios ($q < 1.2$–1.5), two phases of mass transfer occur. The first Roche-lobe overflow (RLOF) is stable, whereas the second one is unstable, leading to the ejection of the common envelope (CE). The resulting binary consists of an sdB star and a white dwarf (WD) in a short-period orbit. (b) For initial mass ratios larger than 1.2–1.5 the first mass-transfer phase is unstable and the common envelope is ejected, producing an sdB star with a non-degenerate (mostly a main sequence star, MS) companion. (c) For low initial mass ratios the sdB star may also form in the first stable RLOF, resulting in a wide, long-period sdB binary with a non-degenerate companion, a main sequence or subgiant star. From Heber (2009) modified by M. Schindewolf; copyright ARA&A; reproduced with permission.
(A color version of this figure is available in the online journal.)

models. In addition, sdB models predict periods up to 1200 days, if atmospheric RLOF is included, close to what has been observed.

Binary population models do not predict a second phase of stable RLOF as contributing to the sdB population. After a RLOF phase, a common envelope phase can occur when the companion evolves to giant structures and fills its Roche lobe. When the envelope of the red giant has been transferred, a close sdB + WD binary emerges with an orbital period between 0.1 and 10 days (see Figure 19).

The physics of the common envelopes is still poorly known despite hydrodynamical simulations (e.g., Passy et al. 2012a; Ricker & Taam 2012). Binary population syntheses of post common envelope binaries still struggle to explain observation. New investigations by e.g., Davis et al. (2010) and Toonen & Nelemans (2013) are aimed at explaining the white dwarf binaries, while those of Clausen et al. (2012) focused on sdB binaries.

Double-core CE evolution is a special case of common envelope evolution where both stars have expanded to giant-type structures by the onset of CE formation. When the

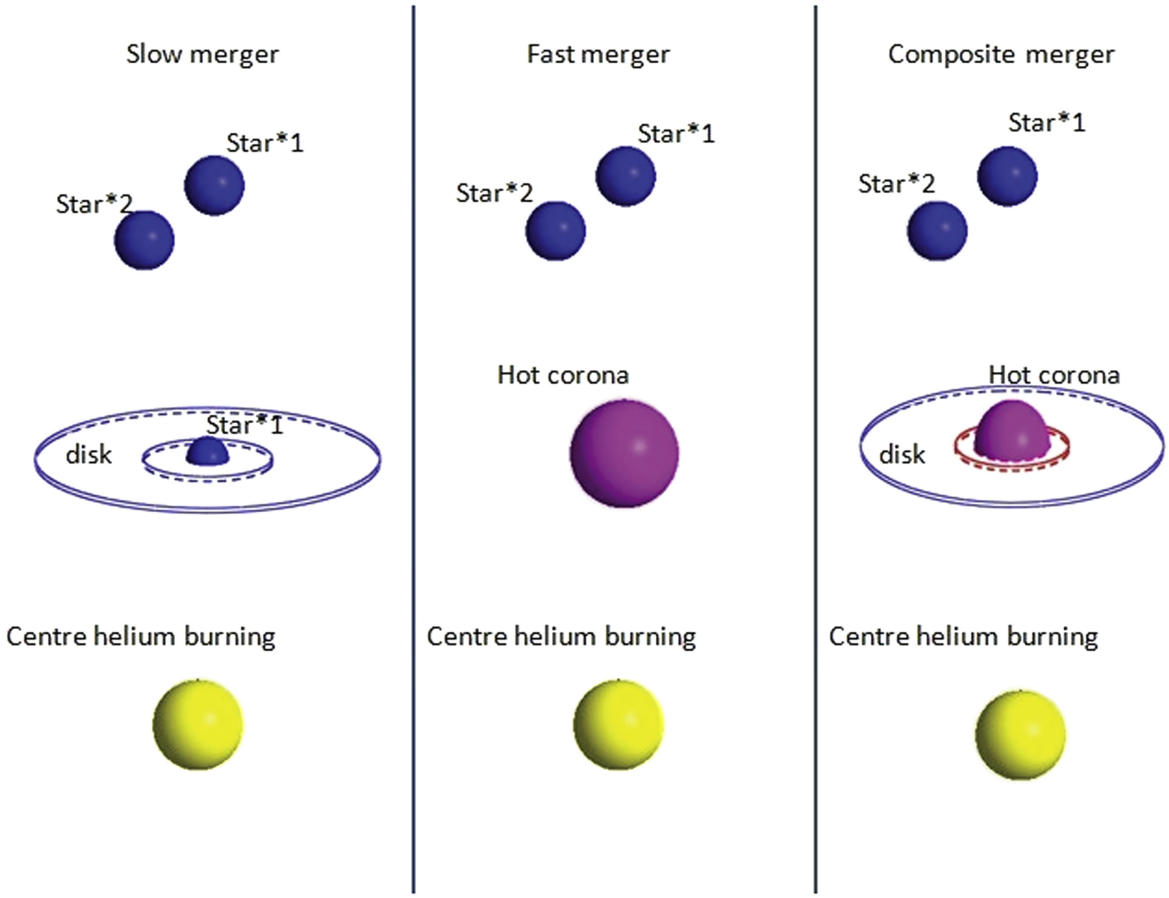

Figure 20. Schematic of three possible ways in which two helium white dwarfs might merge. From Zhang & Jeffery (2012b); copyright PASP; reproduced with permission.
(A color version of this figure is available in the online journal.)

envelope is ejected both cores emerge; that is, a binary composed of two hot subdwarf stars is formed. The binary He-sdB PG 1544+488 (Şener & Jeffery 2014) might be an example of double-core CE evolution (Justham et al. 2011).

Hot subdwarf stars and CE planetary nebulae. About a fifth of all planetary nebula are understood to form by CE ejection (Ivanova et al. 2013). Most of the central stars of those nebulae are likely to be in their post-AGB phase of evolution. A few systems have been suggested as possible post-RGB objects. However, Hall et al. (2013) studied the formation of planetary nebulae arising from RGB CE ejection, and concluded that none of the suggested planetary nebulae can be unambiguously identified as a post-RGB system. The best candidate is the central star of EGB 5, because it has been identified as a close sdB binary (Geier et al. 2011b). However, additional observations are required to clarify whether the nebula is actually associated with the sdB and not an unrelated H II region in the ISM as has been found for the apparently single sdB star PHL 932 (Frew et al. 2010).

CE nebulae will be visible for only a few 10^4 years, before they disperse. Because of their long evolutionary lifetimes only a very small fraction of the sdB stars will be young enough for their CE nebulae to be detectable. Hence, large samples of sdB stars need to be inspected to eventually discover a post-RGB nebulae associated with an sdB star.

3.4.1. Helium White Dwarf Mergers

White dwarf mergers are promising processes to explain the formation of several classes of peculiar stars, e.g., R CrB stars, extreme helium stars and last but not least the single hot subdwarf stars. The focus of hydrodynamical modeling, though, lies with mergers leading to SNe Ia (e.g., Dan et al. 2014).

The merger of helium white dwarfs has been suggested to explain the origin of the hot subdwarf stars (Webbink 1984). Indeed, some He white dwarf binaries are promising candidates to form single sdB stars when they will merge. Arguably the best known candidate is CSS 41177, an eclipsing system

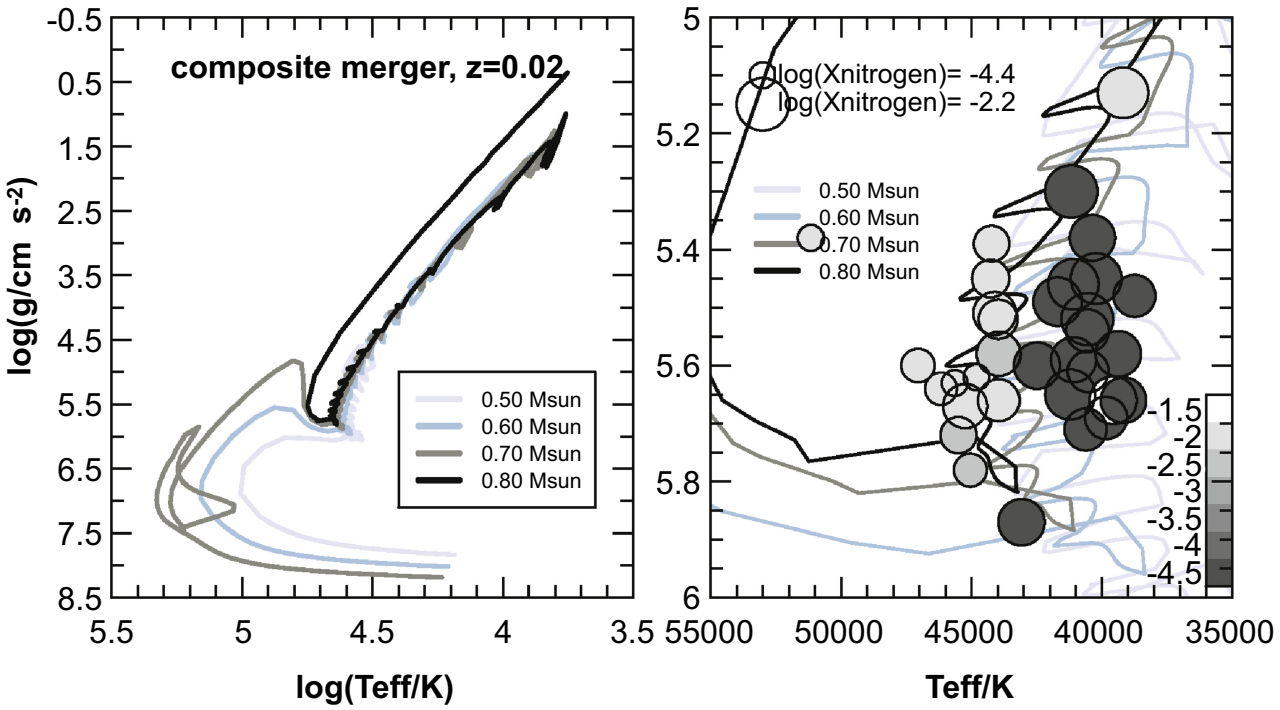

Figure 21. Left Panel: evolutionary tracks for different masses on the gravity–temperature diagram for the composite merger. Right panel: enlarged area of left panel. The tracks plotted from gray to dark have different masses ranging from 0.5 to 0.8 $M_{\odot}$. The circle symbols show the He-sdO stars from Hirsch (2009). Gray to dark symbols depict the abundance of carbon (log β_C) decreasing from −1.5 to −4.5. The abundance of nitrogen is shown by the size of the symbol. From Zhang & Jeffery (2012b); copyright ASPC; reproduced with permission.
(A color version of this figure is available in the online journal.)

(orbital period $P = 2.78$ hr) consisting of two He white dwarfs of $M_1 = 0.38 \pm 0.02\,M_{\odot}$ and $M_2 = 0.32 \pm 0.01\,M_{\odot}$ that will merge in 1.14 ± 0.05 Gyr due to gravitational wave radiation (Bours et al. 2014).

Zhang & Jeffery (2012a) computed several evolution models following the merger of two equal mass helium white dwarfs for different masses from 0.25 to $0.4\,M_{\odot}$ and three modes of merging, including slow and fast mergers, as well as a combination of both. A sketch of the three processes is shown in Figure 20.

In the slow merger model the less massive and, hence, larger white dwarf fills its Roche lobe and its entire mass is transferred to form a disk around the more massive one in a few minutes. The material remains cold and can be accreted slowly onto the primary surface at a rate comparable to the Eddington accretion rate, which could last for several million years. Angular momentum is dissipated toward the disk circumference (Zhang & Jeffery 2012a).

In the fast merger model, on the other hand, no disk forms, but the entire mass of the less massive white dwarf directly falls onto the primary's surface. Because the material is strongly heated to 10^8 K it expands to form a hot corona within a few minutes.

The third model considered by Zhang & Jeffery (2012a), based partly on the results of 3D hydro simulations by Lorén-Aguilar et al. (2009), and others, combines both slow and fast merging to a composite merger model. One part of the disrupted companion forms a hot corona (30%–50% of its mass) while the rest forms a cold disk from which the surviving white dwarf accretes at half the Eddington rate, i.e., $10^{-5}\,M_{\odot}\,\mathrm{yr}^{-1}$.

Zhang & Jeffery (2012a) simulated the post-merger evolution. In the slow (cold) case the accreted material in the envelope of the survivor is that of the former companion and, therefore, nitrogen rich and carbon poor, whereas in the fast (hot) case carbon is predicted to be produced via the triple-α process and could be dredged-up to the surface by an opacity-driven convection zone that occurs when the material is heated up. The surface composition predicted by the composite model depends on the final mass of the merger. For low-mass mergers ($M < 0.65\,M_{\odot}$) the surface remains nitrogen-rich because no carbon-rich material is mixed into freshly accreted nitrogen-

rich material. For higher masses, however, strong convection zones are predicted, which mix N-rich with C-rich material. Accordingly the N-rich He-sdOs should be less massive than the C-rich ones.

The post-merger evolutionary tracks all end up evolving toward the helium main sequence through those regions of the $T_{\rm eff}$–log g diagram where the helium-rich hot subdwarf stars are found (see Figure 21).

3.4.2. Single sdBs

The existence of single sdB stars remains a conundrum. The merger of helium white dwarfs is an attractive option, although the predicted broad mass distribution does not seem to be consistent with the narrow mass distribution of sdB stars determined from asteroseismic analysis. Other merger processes are also conceivable. A low mass star or brown dwarf may merge with a red-giant core (Soker 1998; Politano et al. 2008) to form an sdB star. The population synthesis calculations of Politano et al. (2008) predicted that this would lead to rapidly rotating horizontal branch stars with a core mass distribution strongly peaked between 0.47 and 0.54 $M_{\odot}$, some of which may be single sdB stars if centrifugally enhanced mass loss driven by the fast rotation removed a sufficient amount of the envelope.

Clausen & Wade (2011) suggest that the coalescence of a helium white dwarf with a low-mass, hydrogen-burning star would create a star with a helium core and a thick hydrogen envelope that evolves into an sdB star in a few Gyr, which would also naturally explain the sdBs' slow rotation rates. Candidate systems might exist among low mass white dwarfs with dM companions in short-period systems (Parsons et al. 2013).

However, we cannot exclude that apparently single sdBs do have companions that have not been detected yet. First, compact massive companions such as white dwarfs could have escaped detection because their orbital planes are orthogonal to the line of sight. Second, low mass main sequence stars and brown dwarfs on wide orbits would have very small RV amplitudes, hard to detect. Such a population of binaries, however, is not predicted to exist by binary population synthesis models. *Gaia* observations are eagerly awaited.

4. Hot Subluminous Stars in Clusters

Stars in a cluster are expected to have common properties and are thought to have formed at the same time from the same interstellar cloud. Moreover, they are at almost the same distance from us, and, therefore, provide an important benchmark for stellar evolution theory allowing us to determine fundamental parameters, such as stellar mass, metallicity, distance, and age.

Hot subdwarfs stars have been found as EHB stars in several globular clusters as well as in the old, metal-rich open clusters NGC 6791 and NGC 188.

4.1. The Horizontal Branch Morphology of Globular Clusters and the Second Parameter Problem

The widely different morphology of the horizontal branches of globular clusters still awaits an explanation. Metallicity has been recognized as the main parameter, because metal-rich clusters have red horizontal branches, whereas metal-poor ones show blue HBs. However, the presence of clusters with the same metallicity but different horizontal branch morphologies requires one or more additional parameters. The list of candidate second parameters is long and includes properties of the globular clusters: age (e.g., Lee et al. 1994), mass (e.g., Recio-Blanco et al. 2006), core density/concentration (e.g., Fusi Pecci et al. 1993), as well as internal rotation and helium mixing of (post-)red giant branch stars (Sweigart 1997b), helium self-enrichment (e.g., D'Antona et al. 2002), the presence of planets (e.g., Soker 1998) among others. The age has been favored for a long time (Lee et al. 1994; Dotter et al. 2010; Gratton et al. 2010), but the helium content may play a role if a significant fraction of helium-enriched stars exist (for reviews see Catelan 2009; Gratton et al. 2010).

It is now well established that globular clusters (e.g., the massive ω Cen and NGC 2808) host multiple stellar populations, because their color–magnitude diagrams display two or more continuous sequences of stars from the main sequence to the red giant branch (for a review see Gratton et al. 2012) and the list of multi-population globular clusters is growing steadily, both for the Galaxy (e.g., Piotto et al. 2012; Milone et al. 2015a) as well as for others (Fornax dSph, Larsen et al. 2014). The ongoing *HST* UV legacy survey (Piotto et al. 2015) will allow the populations to be disentangled and improve our understanding of globular cluster formation and evolution. The differences *among* the stellar population with respect to their content of helium and light elements point toward two or more episodes of star formation. This scenario assumes that the second generation of stars formed from material polluted by the first one (see, e.g., D'Ercole et al. 2008; Milone 2015 and references therein).

The helium content has been identified as a viable second parameter. However, it is difficult to test because helium lines can be observed in early-type stars, only. BHB stars are the best choice for a direct determination of the helium abundance from its spectral lines. However, for stars hotter than 11,500 K the atmospheric composition is affected by the same diffusion processes that govern the atmospheres of sdB stars and the information on the original surface abundance has been erased (Behr 2003a; Michaud et al. 2008). Hence, the technique can be applied to horizontal branch stars in a limited temperature

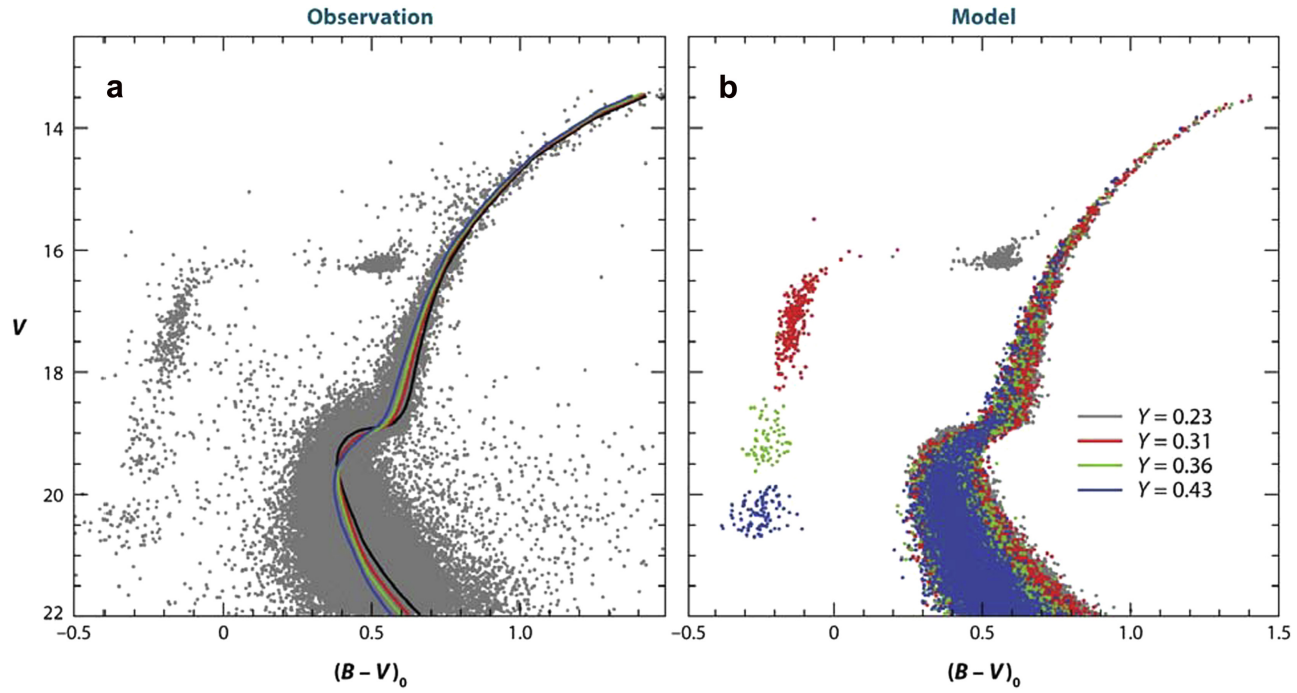

Figure 22. The observed and modeled color–magnitude diagrams of the globular cluster NGC 2808 (Yi 2008). Left-hand panel: observed color–magnitude diagram, showing an exceptionally wide distribution of horizontal branch stars. Right-hand panel: theoretical color–magnitude derived from evolutionary calculations for four different helium compositions. The observations can be reproduced if a large range of helium abundance is assumed. From Heber (2009); Copyright ARA&A; reproduced with permission. (A color version of this figure is available in the online journal.)

range (≈8500–11,500 K), where atmospheric convection impedes diffusion, so that the helium abundance should be the same as that from which the star was formed. Indeed, Marino et al. (2014) found an enrichment of helium with respect to the original value in BHB stars with $T_{\rm eff} < 11{,}500$ K in the massive globular cluster NGC 2808. It has, therefore, been suggested that the evolution, stellar and atmospheric properties of hot subdwarf stars may also depend on the helium content of the cluster population(s) (D'Antona et al. 2002, 2010).

Yi (2008) computed stellar evolution sequences for different helium contents to model the color–magnitude diagram of NGC 2808. Using four sub-population having different helium enrichments, they succeeded to reproduce the observed horizontal branch morphology well. Accordingly, the bluest HB stars are the most helium-rich ones (see Figure 22).

4.2. The Formation of EHB and Blue Hook Star in Globular Clusters

The color–magnitude diagrams of several globular clusters show blue tails and blue hooks to their horizontal branches, which are supposed to consist of hot subdwarf stars (see Moehler 1999, 2001, 2010, for reviews). Blue hook stars are on the HB but with fainter luminosity than the normal EHB stars (Whitney et al. 1998; D'Cruz et al. 2000) and populate the very blue end ($T_{\rm eff} > 32{,}000$ K, Moni Bidin et al. 2012), for a detailed discussion of the occurrence of blue hook stars see Moehler (2010).

We have discussed the formation and evolution of sdB stars and compared them with observations of field stars extensively in Section 3. Briefly, the frequency of binary sdB stars is so large, 50% of the single-lined systems have periods of less than 30 days, that common envelope ejection is considered the only viable process to form such systems. Double-lined systems may form as wide binaries through stable RLOF and periods of about 1000 days. Single sdB stars may result form mergers of double He-core white dwarfs. For single stars the most popular scenario rivalling the close binary scenario is the late hot flasher scenario that explains the reduction of the hydrogen envelope of the progenitor star through internal mixing and burning.

Do these scenarios also apply to EHB and blue hook stars in globular clusters? The low frequency of close binary sdB stars in globular clusters (Moni Bidin et al. 2009, 2011) argues against the presences of a large populations of close binary sdB stars. The recent discovery of a unique close binary consisting of a K-type main sequence star and an sdB star in a 1, 6 day orbit (Moni Bidin et al. 2015) comes much to our surprise, because no counterpart is known in the field. Wide binaries with periods of 1000 days or more may be disrupted by

dynamical interaction in the dense cluster environment. Therefore, the hot flasher scenario is often favored to explain the formation of EHB and blue hook stars in globular clusters.

An alternative scenario explains the EHB and blue hook stars by the presence of a second generation of helium-enriched stars. Recently, three additional scenarios were added: (i) He white dwarf mergers (Han 2008), (ii) enhanced mass loss by rapid rotation (Tailo et al. 2015), and (iii) tidally enhanced mass loss in binaries (Lei et al. 2013a, 2013b, 2015).

4.2.1. Late Hot-flasher

Many studies of EHB and blue hook stars in globular clusters explain their formation via the flasher scenario (e.g., Miller Bertolami et al. 2008) although they cannot explain the range of colors observed in such stars, in particular for the most metal-rich clusters (Brown et al. 2010a). The consequences for their location in the $T_{\rm eff}$–$\log g$ plane and the chemical compositions has already been discussed in Section 3.3.

4.2.2. Helium-enriched Second-generation Stars

The enhanced helium enrichment model assumes that the second generation stars are enriched in helium up to a mass fraction of $Y \approx 0.4$. Otherwise, the evolution is considered canonical. The resulting horizontal branches are blue and more luminous than those for normal He content.

4.2.3. Double Helium White Dwarf Mergers

The low fraction of close sdB binaries in globular clusters may result from a high fraction of mergers. Binary population synthesis calculations by Han (2008) suggest that the merger rate for double white dwarfs increases with age and after only about 8 Gyr the merger channel dominates over all others. Accordingly, the fraction of close binaries with short orbital periods for a stellar population age of 10 Gyr is only ≈2.5% in the standard model and ranges between 0% and 20% depending on the choice of common envelope ejection efficiency parameter α. Hence, this scenario provides a straightforward explanation for the scarcity of short-period sdB binaries in globular clusters. The predicted location of the stars in the $T_{\rm eff}$–$\log g$ plane and the chemical composition should be similar to that discussed in Section 3.4.1.

4.2.4. Enhanced Mass Loss by Rapid Stellar Rotation

Because a late hot flasher is supposedly a rare event it is surprising to find such a high fraction of EHB stars in ω Cen and other massive clusters. Therefore, Tailo et al. (2015) revisited the RGB helium-mixing scenario of Sweigart (1997a, 1997b), in which rapid rotation of a red giant might lead to a dredge-up of helium from the hydrogen-burning shell into the envelope. Tailo et al. (2015) suggest that rapid rotation of second generation stars may result from the star-forming history and the early dynamics of very massive clusters, such as ω Cen (see Section 4). Hydrodynamical models of the gas dynamics combined with N-body simulation (D'Ercole et al. 2008) showed that second generation stars that formed from material ejected from super-AGB and AGB stars of the first generation, are located in a centrally more concentrated subcluster. Hence, the second generation main sequence stars are born in very dense stellar environment and rotate faster because their disks are destroyed early-on. Core rotation is assumed to persist during RGB evolution, because angular momentum transport is considered to be slow. However, asteroseismology of red giants showed that angular momentum transfer is a lot faster than previously assumed (Aerts 2015), which may challenge this scenario.

4.2.5. Tidally Enhanced Mass Loss in Binaries

Lei et al. (2013a, 2013b, 2015) investigated the role of binary evolution for the formation of sdB stars in globular clusters by considering a tidally enhanced wind of a red giant star to cause the required huge mass loss. The model binary was chosen to consist of $0.85\,M_{\odot}$ star and a $0.53\,M_{\odot}$ companion. For initial orbital period longer than 2200 days, no effect was found and the evolution of the primary would be canonical. For initial periods between 2200 and 2000 days, the primary star would experience an early hot flash and become a canonical EHB star. However, the primary undergoes a late hot flash on the white dwarf cooling curve and ends up as a blue hook star if the initial period is between 1600 and 2000 days. For even shorter periods helium is not ignited and the red giant evolves into a helium white dwarf. These results are similar to those presented by Siess et al. (2014) to explain the long-period low-mass WD & K0 III/IV binary IP Eri (see Section 8.2). However, such wide binaries may be disrupted well before the primary evolves into a red giant. Moreover, the results may be difficult to reconcile with the observed orbital properties of wide sdB + F/G/K binaries in the field (see Vos et al. 2015).

4.3. Observational Tests: Spectroscopic Analyses of EHB and Blue Hook Stars in Globular Clusters

In order to clarify the formation of EHB and blue hook stars in globular clusters quantitative spectral analyses are important to place the stars in the $T_{\rm eff}$–$\log g$ plane, derive their chemical composition, and compare them to those of the field stars.

4.3.1. Classical Globular Clusters Hosting EHB Stars

Because of its very blue HB morphology and its proximity, NGC 6752 has been targeted for quantitative spectral analyses of hot subdwarf stars for a long time (Heber et al. 1986; Moehler et al. 1997; Moni Bidin et al. 2007). More recently, these studies have been extended to the similar clusters M80 and NGC 5986 (Moni Bidin et al. 2009). Salgado et al. (2013)

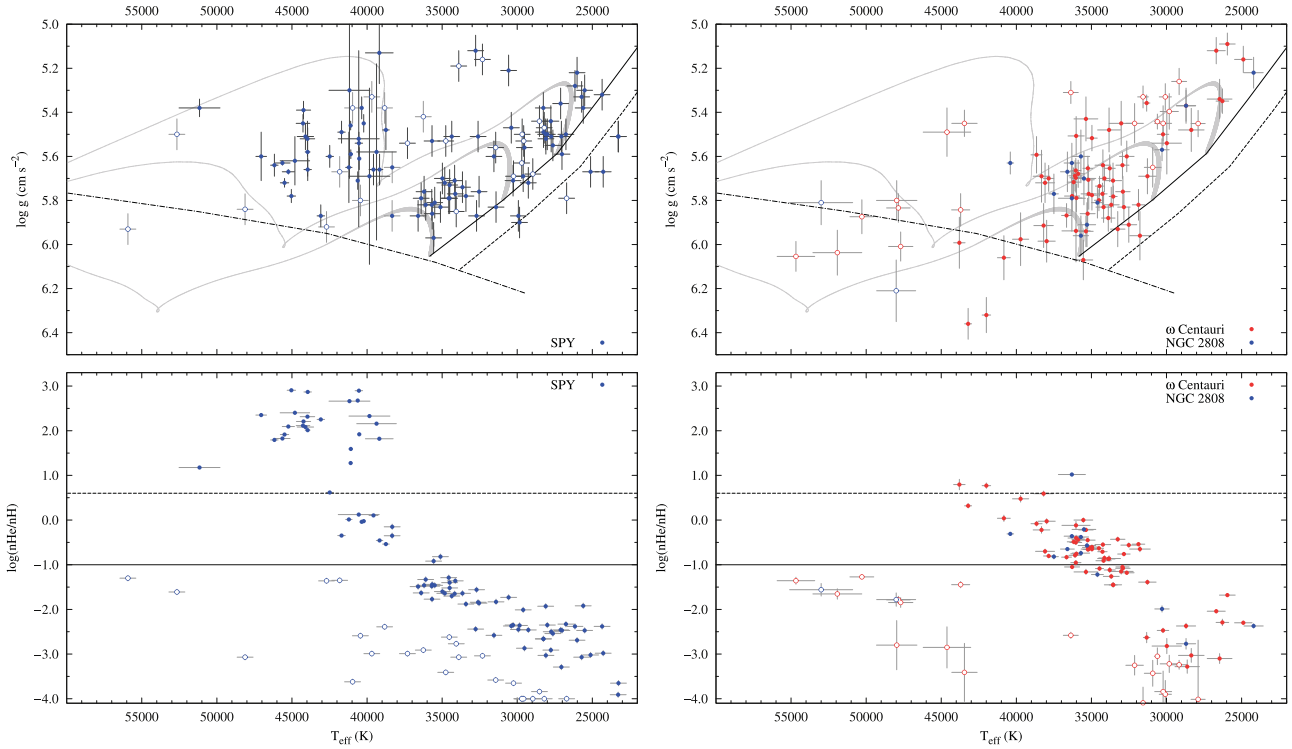

Figure 23. Upper, left hand panel: distribution of hot subwarf stars in the $T_{\rm eff}$–log g plane from the ESO-SPY project. Lower, left hand panel: same for the helium abundance vs. $T_{\rm eff}$ distribution. Upper, right hand panel: distribution of hot subwarf stars in the $T_{\rm eff}$–log g plane from different samples of stars in the globular cluster ω Cen (red symbols) and NGC 2808 (blue symbols). Lower panels: same for the helium abundance vs. $T_{\rm eff}$ distribution. From P. Németh (2016, private communication). (A color version of this figure is available in the online journal.)

present the spectroscopic analyses of BHB stars in M22, an in-depth comparison with NGC 6752, M80 and NGC 5986, and conclude that the gravities and masses of HB stars in M22 with $T_{\rm eff}$ = 7000–25,000 K match those for NGC 6752, M80, and NGC 5986. For all four clusters both the location of the HB band in the $T_{\rm eff}$–log g plane, their helium abundances as well as their masses agree with theoretical expectations (see Salgado et al. 2013 for details). Information on the chemical composition beyond helium remains scarce for EHB stars in globular clusters, while there is more detailed information for BHB stars (e.g., Behr 2003a; Fabbian et al. 2005; Pace et al. 2006; Hubrig et al. 2009).

Chayer & Dixon (2014) carried out an analysis of far-UV spectra obtained with the *FUSE* satellite of three hot subdwarf stars in NGC 6752 and derived NLTE abundances for the C, N, and O elements as well as for Si, P, and S. The abundance patterns for all three stars turned out to be very similar to those of the field stars (Geier 2013), nitrogen being slightly subsolar, while all other elements are depleted by more than one order of magnitude with respect to the Sun. Although the number of stars studied in metal-poor clusters is small, the similarity of their chemical abundance pattern may hint that the outcome of atmospheric diffusion does not depend on metallicity.

4.4. The Enigmatic Globular Clusters NGC 2808 and ω Cen and their Blue Hook Stars

The massive globular clusters NGC 2808 and ω Cen have caught a lot of attention in recent years because they are the most extreme cases of globular clusters with multiple stellar populations and host large populations of BHB stars. In addition their horizontal branches show a so-called blue hook at the blue end in UV color–magnitude diagrams, that cannot be explained by canonical stellar evolution theory. Moehler et al. (2004) pointed out that the frequency of blue hook stars is related to the clusters' total mass rather than to the population of the EHB. NGC 6752 for instance shows a well populated EHB, but not a single blue hook star has been found, whereas there are roughly as many blue hook stars as EHB stars in NGC 2808 (Brown et al. 2001), which is a hundred times more luminous than NGC 6752.

No less than five populations of main sequence and red giant stars have been identified from *HST* multi-wavelength photometry of NGC 2808, four of which might be enriched in helium

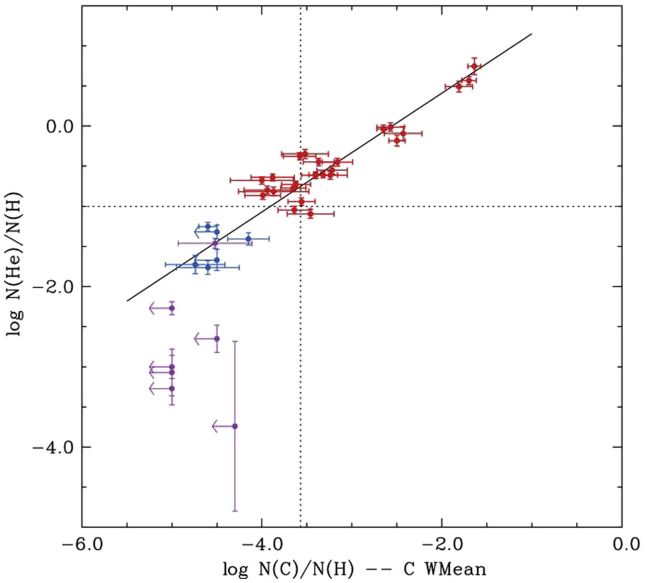

Figure 24. Helium abundance vs. the mean carbon abundance for ω Cen stars (Latour et al. 2014c). The "cool," helium-poor EHB stars are shown in magenta, the intermediate temperature, helium-rich ones in red, and the hottest, helium-poor ones in blue. The upper limits on the carbon abundance inferred for eight stars are indicated by arrows instead of error bars. This diagram shows an obvious relation between the abundances of the two elements, which is illustrated by the linear regression (black solid line). Dotted lines indicate the solar helium and carbon abundances. From Latour et al. (2014c); copyright ApJ; reproduced with permission.
(A color version of this figure is available in the online journal.)

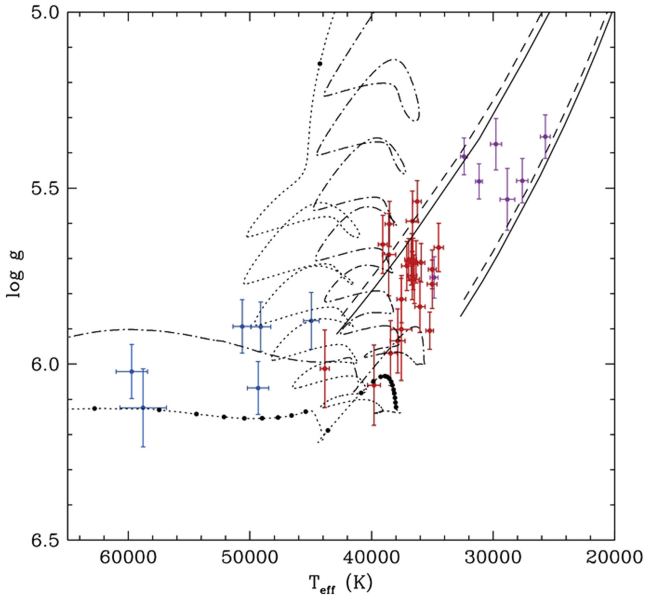

Figure 25. Comparison of the sample of hot subdwarf stars of Latour et al. (2014c) in the globular cluster ω Cen with late-flasher evolutionary tracks by Miller Bertolami et al. (2008). The tracks are for a metallicity of $Z = 0.001$ and refer to a deep mixing event ($M = 0.48150\,M_{\odot}$; dotted line) and a shallow mixing event ($M = 0.49145\,M_{\odot}$; dashed–dotted line), respectively. Points at 5 Myr intervals are shown on the first track, to give an idea of the evolutionary timescale in the different regions. From Latour et al. (2014c); copyright ApJ; reproduced with permission.
(A color version of this figure is available in the online journal.)

by $\delta Y = 0.03$ to 0.13 (Milone et al. 2015b). Many EHB and blue hook stars have been identified from UV photometry. Likewise, ω Cen shows complex multiple stellar population patterns and hosts blue hook stars (Whitney et al. 1998; D'Cruz et al. 2000).

Both clusters have recently been targeted in several spectroscopic studies of BHB stars (NGC 2808, Moehler et al. 2004 and ω Cen, Moehler et al. 2011; Moni Bidin et al. 2012; Latour et al. 2014c). Multi-object spectroscopy is the most efficient way to obtain spectra in crowded fields such as in globular clusters. Therefore, Moehler et al. (2004) and Latour et al. (2014c) used the multi-object mode of FORS at the ESO-VLT to secure optical spectra of EHB and blue hook stars in NGC 2808 and ω Cen, respectively. Spectra of stars in ω Cen were also obtained by Moehler et al. (2011) using the multi-fiber instrument FLAMES + GIRAFFE at the ESO-VLT, which provides higher spectral resolution ($R = 6400$) than FORS. Moehler et al. (2004) derived atmospheric parameters for 19 members of NGC 2808 using NLTE models of H/He composition for the hotter stars and Kurucz LTE models for the cooler ones, while Moehler et al. (2011) and Latour et al. (2014c) determined atmospheric parameters and abundances of EHB and blue hook stars in ω Cen using different sets of NLTE and LTE models.

The helium-poor hot subdwarfs form two groups, one on the EHB at typical sdB temperatures and another one at higher temperatures exceeding 40,000 K, typical for post-EHB stars (see Figure 23). At intermediate effective temperatures the majority of targets are He-rich ($\log N(\mathrm{He})/N(\mathrm{H}) \gtrsim -1.0$) and cluster in the temperature range from 32,000 to 43,000 K along the bluest part of the EHB band (see Figure 23). However, the enhancement of helium is moderate, i.e., the He/H ratio does not exceed unity except for a handful of stars with He/H < 10. In comparison to the field stars, two striking differences become apparent from Figure 23. First, the helium-rich hot subdwarfs in the field are hotter than the cluster stars and lie beyond the EHB and second the helium enrichment is higher in many field stars than that of the most strongly enriched star in NGC 2808 and ω Cen.

Latour et al. (2014c) concluded that "these differences point toward fundamental differences between the helium-enriched EHB star population in the field and in ω Cen and are likely *to be* related to the fact that sdB and sdO stars in globular cluster have older (12–13 Gyr) and typically metal-poorer progenitors than their field counterparts."

Both studies find a strong positive correlation between the carbon and helium abundances (see Figure 24). The carbon abundance ranges from 1/10 solar for the cool, helium-poor stars to almost a hundred times solar for the most helium-rich

stars of intermediate temperature. Almost the same positive correlation of carbon (and nitrogen) with helium abundance, has been found for the hot subdwarfs in the *GALEX* sample (see Figure 9 of Németh et al. 2012, see also Section 2). In this respect metal-poor and metal-rich populations do not differ.

In order to understand the formation of the blue hook stars in ω Cen, Moehler et al. (2011) and Latour et al. (2014c) compared their results to the predictions of the He-enhanced scenario as well as to the hot flasher scenario (see Figure 25).

The enhanced helium scenario can readily be dismissed, because the helium mass fraction should not exceed ≈0.4 and no enrichment of carbon is expected, nor for any other chemical element.

If the hot flasher scenario were correct, the burning and mixing in a typical hot flasher event should enrich the atmosphere not only with helium but also with carbon, and to a lesser extent, nitrogen (Cassisi et al. 2003). The observed correlation between helium and carbon enrichments, therefore, is in qualitative agreement with the hot flasher scenario. At the quantitative level, however, Moehler et al. (2011) and Latour et al. (2014c) noted some inconsistencies, in particular they find that the predicted helium (96% by mass) and carbon content (3%–4% by mass) is too high, that is only the three most helium-rich stars in the sample come close to the prediction. The helium and carbon abundances of all other *stars* are a lot lower than predicted. Another inconsistency becomes apparent when comparing the observed locations of the stars in the $T_{\rm eff}$–$\log g$ plane to the prediction for the hot flasher evolutions of both a deep and a shallow mixing event (Figure 25). The observed He-rich stars are cooler than predicted by both tracks, even for the case of shallow mixing only. This discrepancy was already noted by Moehler et al. (2002) who considered that up to 10% of hydrogen may survive the hot flasher evolution and calculated the position of stars in the $T_{\rm eff}$–$\log g$ diagram by adding hydrogen layers of different thickness to post-flasher models. Indeed, the models predict the stars to be somewhat cooler and, hence, closer to the observed position of blue hook stars.

4.5. Post-EHB Stars in Globular Clusters: The UV-bright Stars

For more than a hundred years it is known that some globular clusters host extremely blue stars of high luminosities (Barnard 1900; Kustner 1921) that stand out against the large population of red stars. These so-called UV-bright stars are rare; de Boer (1987) lists 45 UV-bright stars in 36 globular clusters. Quantitative spectral analyses have been presented by e.g., by Heber & Kudritzki (1986), Moehler et al. (1998a, 1998b), Rauch et al. (2002), Thompson et al. (2007), and Chayer et al. (2015). The most striking object is the helium-rich sdO star ZNG-1 in the globular cluster M 5 because it rotates so fast (170 km s^{-1}). Dixon et al. (2004) favor a "born-again" origin but previous binary interaction may offer a straightforward explanation for the rapid rotation of the star. The UV-bright stars represent a mixed bag of post-AGB stars, including four central stars of planetary nebulae (Pease 1928; Gillett et al. 1989; Harrington & Paltoglou 1993; Jacoby et al. 1997), post-early AGB stars and post-EHB stars, among them also stars of relatively low temperatures (<10,000 K) (e.g., Ambika et al. 2004; Jasniewicz et al. 2004). Optically selected UV-bright stars tend to be mostly post-AGB and post-EAGB stars, whereas UV-selected stars turn out to be less luminous ("supra-HB" stars) and are mostly identified as post-EHB stars (Moehler et al. 1998b), which share the helium deficiency with their counterparts of the field populations (for reviews see van Winckel 2003; Moehler 2010).

4.6. Hot Subdwarf Stars in Open Clusters

The concept that globular clusters host single populations of coeval stars of the same chemical composition has recently been challenged by the detection of multiple populations of stars with different properties in several massive clusters. Therefore, Salaris (2015) argues that open clusters probably remain the only example of simple single population environments and provide the best laboratory available to test stellar evolution. However, EHB stars have been found in two open clusters only, i.e., in the near-by old metal-rich clusters, NGC 6791 (Kaluzny & Udalski 1992; Liebert et al. 1994), one of the richest open clusters known, and NGC 188 (Green et al. 1997, 2004). While NGC 188 hosts only one sdB star (a binary with an 2.15 days orbital period), NGC 6791 harbors 5 (perhaps 6) sdB stars (Schindler et al. 2015). NGC 6791 has received great attention in recent years, because it is one of only two open clusters in the *Kepler* field. The presence of EHB stars make this cluster an important laboratory to study their evolution.

Schindler et al. (2015) used NGC 6791 and NGC 188 as template clusters to understand the formation of the EHB stars by investigating 15 open clusters that come close to NGC 6791 and NGC 188 with respect to age and metallicity. Four of them have similar ages but lower metallicities, three are of similar metallicity but slightly younger age, and eight clusters are of slightly lower metallicity and age. Combining the color–magnitude diagrams of all 15 clusters yields four times as many red giant clump stars as NGC 6791 but not a single EHB star. Schindler et al. (2015) conclude that older stellar populations (6–9 Gyr, turn-off masses of ≈1.1–1.3 $M_{\odot}$) of very high metallicity produce a much larger fraction of EHB stars than younger ones. Accordingly red giant progenitors are preferentially of lower mass.

However, it should be noted that NGC 6791 may be a rather unusual cluster and not suitable as the cluster of reference. Green et al. (2001) point out that both NGC 6791 and NGC 188 have enormously high fractions of blue stragglers with respect to horizontal branch stars. NGC 6791 also *hosts* a

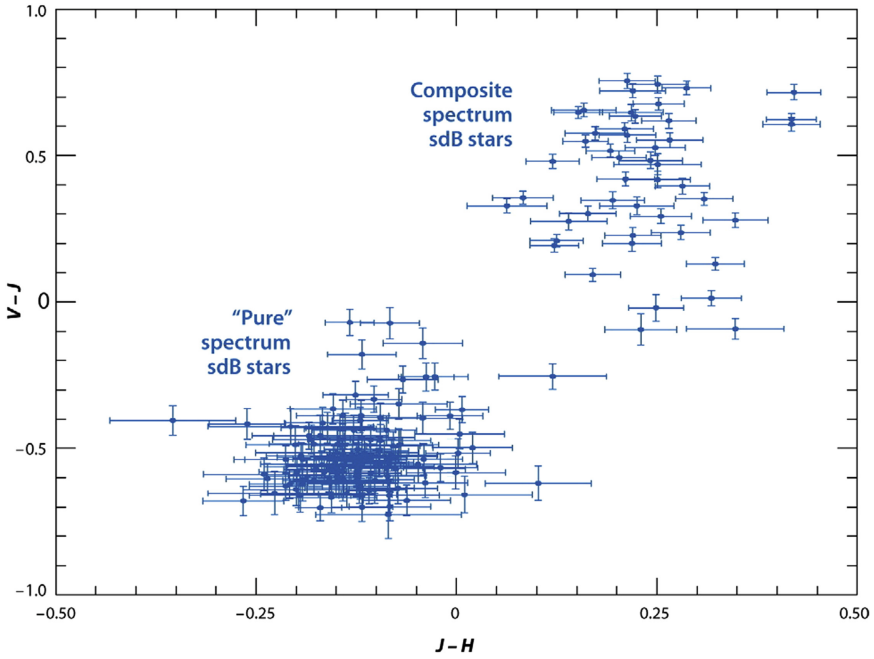

Figure 26. Two-color plot of $V - J$ vs. $J - H$ of sdB stars from the sample of Green et al. (2008). The composite-spectrum sdB-stars are in the upper right and the stars with "pure" sdB spectra at the lower left. The latter group includes both the "apparently single" sdBs that have no detectable radial velocity (RV) variations above a level of a few km s^{-1} over periods of many months, as well as sdB binaries with invisible secondaries, either degenerate objects or dwarf M companions too faint to affect the $V - J$ or $J - H$ colors. All known binaries that fall at the lower left are post-common-envelope systems with periods of a few hours to several days, while all of the composite-spectrum binaries at the upper right appear to have much longer periods (Green et al. 2008). From Heber (2009); copyright ARA&A; reproduced with permission.
(A color version of this figure is available in the online journal.)

large number of interacting binaires (cataclysmic variables and contact binaries, de Marchi et al. 2007).

Hundreds of white dwarfs have been identified on deep *HST* images of NGC 6791 (Bedin et al. 2005, 2008a), reaching the very faint end of its white dwarf cooling sequence. Two bumps in the white dwarf luminosity function pointed to a cluster age of only 6 or 4 Gyr, respectively, in strong conflict with the turn-off age of 8.3 Gyr (Brogaard et al. 2012). Kalirai et al. (2007) derived spectroscopic masses and find a substantial fraction of the white dwarfs to be undermassive and, therefore, to be of helium composition. The two peaks in the white dwarf luminosity function may, therefore, result from two populations of white dwarfs, the brighter one being caused by helium-core white dwarfs (Hansen 2005; Bedin et al. 2008a). However, this conclusion was found to be at odds with evolution theory. Bedin et al. (2008b) revisited the problem and found that the bumps in the luminosity function can be naturally accounted for if ≈34% of the white dwarfs are actually double degenerate systems. Such a large fraction is plausible in view of the many interacting binaries. Bedin et al. (2008b) conjectured that the high binary fraction may be related to the other peculiarities of this cluster, including the existence of the EHB. In fact, the sdB in NGC 188 and NGC6791/B4 are close binaries of 2.15 and 0.3985 days period, respectively (Green et al. 2004; Pablo et al. 2011).

Whether NGC 6791 and NGC 188 are just peculiar cases among the open clusters or represent a standard stellar population suitable as a reference for the field population and UV-upturn galaxies, remains an open-ended question.

More information on the sdB stars in NGC 6791 has been gathered recently from the analysis of *Kepler* light curves that led to the discovery of multi-periodic oscillations in three of them, including the binary B4 (Pablo et al. 2011; Reed et al. 2012). Hence B4, as well as B3 and B5, which are apparently non-binary sdBVs, are of extra-ordinary interest, because cluster membership provides a stringent constraint on age, metallicity, and progenitor mass, which must be close to the turnoff mass of 1.1–1.2 $M_{\odot}$ (Pablo et al. 2011). The analysis of the g-mode pulsations of B4 as well as its binary properties allows models of the interior structure and evolution of sdB stars to be constrained as will be discussed in more detail in Sections 5 and 7.

5. Binaries

In the course of the PG survey (Green et al. 1986) it became clear that a significant fraction of sdB stars (at least 20%, Ferguson et al. 1984) have composite colors and spectra. In particular companions of F, G, or K type can easily be detected. The 2MASS survey led to a better estimate of the fraction of

about 30% in an approximately volume-limited sample (Stark & Wade 2003).

Since the year 2000 evidence is growing that many more hot subdwarfs reside in close binaries with invisible companions. About half of the single-lined sdB stars have invisible companions orbiting with periods of 30 days or less (Maxted et al. 2001; Morales-Rueda et al. 2003; Napiwotzki et al. 2004; Copperwheat et al. 2011). The invisible companions are either low mass main sequence stars or white dwarfs.

The composite-color systems are well separated from the "pure spectrum" sdBs, whether RV variable or not, in two color diagrams (see Figure 26), which points to a bimodal mass distribution for main-sequence companions.

While many RV studies have provided orbit information for more than 140 sdB binaries, such information for composite-color sdB binaries have become available only recently and is still scarce. We shall begin with a discussion of the short-period single-lined systems in Section 5.1, highlighting the HW Vir stars, which are eclipsing sdB systems hosting low mass stars and substellar objects (brown dwarfs), in Section 5.2. The *Kepler* mission (Koch et al. 2010) has provided light curves of unprecedented precision, which allowed the detection of low-amplitude effects, such as Doppler boosting and self-lensing (Section 5.3). Evidence for massive compact companions comes from X-ray studies that will be summarized in Sections 5.4.1 and 5.4.3. Hot subdwarf binaries with massive white dwarf companions are considered as viable progenitor systems for SNe Ia as shall be discussed in Section 5.5. An outlook on the options to measure the orbital decay due to gravitational wave radiation follows in Section 5.6. We turn to the composite-color binaries in Section 5.7, report evidence for the existence of triple or quadruple systems (Section 5.8), and end this section with a glimpse at the zoo of giant and massive companions to hot subdwarf stars (Section 5.9).

5.1. Single-lined sdB Binaries

The first sdB/O binaries were discovered from their light variability caused by eclipses, reflection effects or ellipsoidal deformations, such as the short-period sdB/O+dM binaries AA Dor (Kilkenny 1978), HW Vir (Menzies & Marang 1986) and PG 1336−018 (Kilkenny et al. 1998) and in sdB+white dwarf binaries that show ellipsoidal variability, e.g., KPD 0422 +5421 (Koen et al. 1998) and KPD 1930+2752 (Maxted et al. 2000b).

HD 49798 was the first sdO+WD system discovered from RV measurements (Thackeray 1970). Indeed, surveys for RV variations among apparently single hot subdwarf stars turned out to be very efficient in discovering short-period sdB+WD and sdB+dM systems. The early exploitation of the PG catalog (Green et al. 1986) uncovered seven sdB+WD systems with periods between 0.25 and 2.5 day (Saffer et al. 1998; Moran et al. 1999), but the number of systems grew quickly as the survey proceeded (Maxted et al. 2001; Morales-Rueda et al. 2003; Napiwotzki et al. 2004). Other surveys, e.g., the ESO/SPY and the SDSS based MUCHFUSS projects followed, which extended the sample of short-period sdB binaries to well above one hundred.

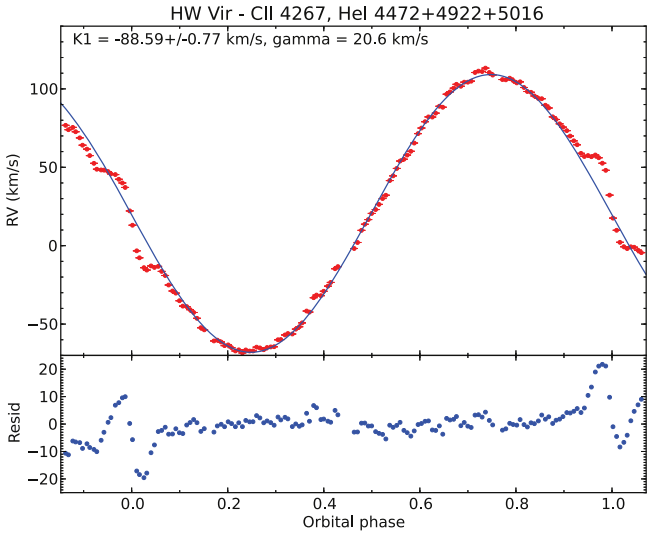

Figure 27. Radial velocity curve (upper panel) of HW Vir. Red symbols represent the observation. Note the Rossiter–McLaughlin effect at phase 0 and 1 which is caused by the rotation of the star. The blue sinusoid is not a fit to the data. Therefore, the residuals (lower panel) near phase 0.0 and 1.0 seem to be different, which is actually not the case as can be seen from the radial velocity curve (upper panel). From Vučković et al. (2014); copyright ASP; reproduced with permission.

(A color version of this figure is available in the online journal.)

5.1.1. The ESO/SPY Project

The ESO/SPY project was a large project to search for double degenerate systems and targeted mostly white dwarfs (Napiwotzki et al. 2005), but also a significant number of hot subdwarf stars (see Section 2). While the frequency of RV variable double white dwarfs was found to be low (5.7%, Koester et al. 2009) that fraction for sdB binaries was found to be 48% (Napiwotzki et al. 2004). Follow-up spectroscopy allowed the orbits of twelve sdB+WD binaries to be measured (Napiwotzki et al. 2001b; Karl et al. 2005, 2006; Geier et al. 2008b, 2010a, 2011b). Spin-off studies from SPY included the quantitative spectral analyses of sdB and sdO stars (Lisker et al. 2005; Stroeer et al. 2007, see Section 2).

5.1.2. The MUCHFUSS Project

A treasure chest for RV studies of hot subdwarfs stars is the the SDSS because its data base provides spectra for a large selection of faint hot subdwarfs. At least three individual spectra are available for each star, which provides a valuable starting point to search for RV variations and to detect unseen

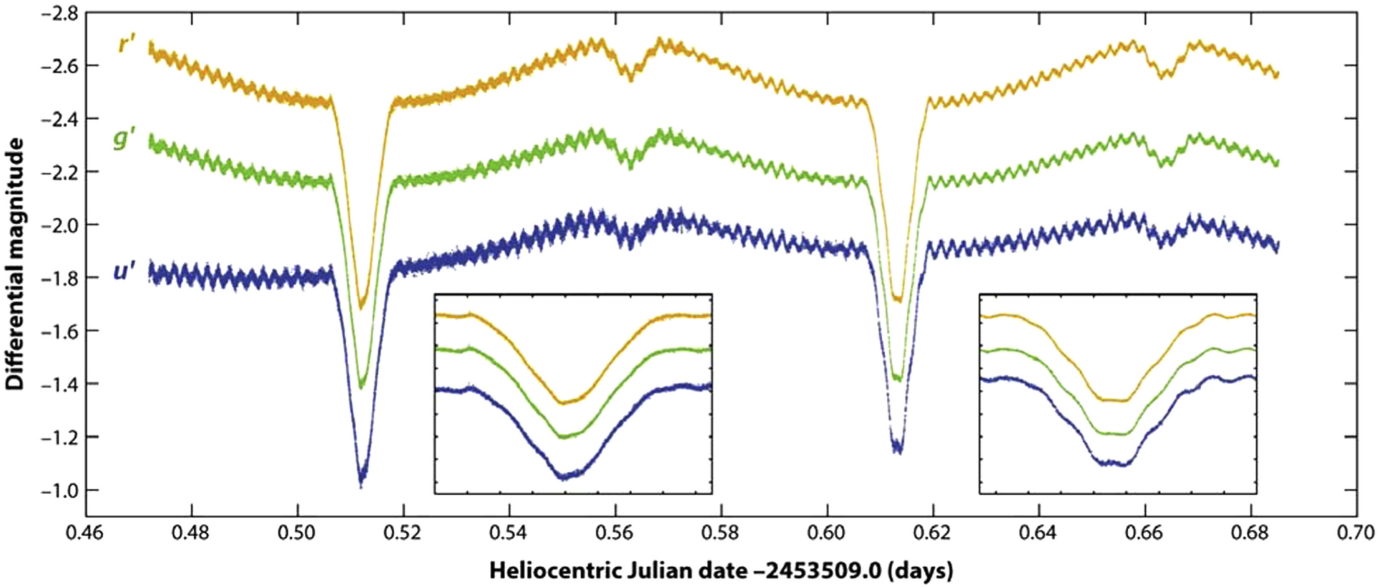

Figure 28. ULTRACAM/VLT r (upper), g (middle), and u (bottom) light curves of the eclipsing sdB star NY Vir (Vučković et al. 2007). Light variations are due to reflection effect and eclipses as well as to multi-periodic pulsations. The insets show enlarged sections of the two primary eclipses, where pulsations are clearly visible. The differences between the two consecutive primary eclipses are due to the beating of the modes and different phases covered during the eclipse. This object provides an excellent opportunity to derive the stellar mass in two independent ways: from light and radial velocity curve as well as from asteroseismology. Both results are in excellent agreement. From Heber (2009); copyright ARA&A; reproduced with permission.
(A color version of this figure is available in the online journal.)

companions via the Doppler reflex motion of the primary. Therefore, a collaboration, the MUCHFUSS, was established to explore the SDSS data base and in the first step ≈1400 hot subdwarf stars were selected by color and visual inspection of the spectra from Data Release 7 (Abazajian et al. 2009). Finally a priority list was established for follow-up observations (see Geier et al. 2011b, 2015b). The main aim of the project is to search for the most extreme close hot subdwarf binaries; that is, those with (i) the shortest periods, (ii) the most massive as well as (iii) the least massive companions. Because such systems are rare, an observing strategy was developed to select targets with the highest RV variations as well as the most rapid changes in RV in order to suppress the typical sdB binaries with orbital periods of more than half a day and RV half-amplitudes of less than 100 km s^{-1}. A detailed description of the selection procedure can be found in Geier et al. (2011b). Atmospheric parameters have been determined for 190 hot subdwarf stars (Geier et al. 2015b) and results for additional sdO stars were reported by Hirsch et al. (2008).

5.1.3. Single-lined sdB Binaries

The sample of short-period sdB binaries that have known orbits has grown to more than 140 (Kawka et al. 2015; Kupfer et al. 2015). All systems are single-lined; that is, have unseen companions. The RV curve of HW Vir is shown in Figure 27 as an illustrative example. Companion masses have been

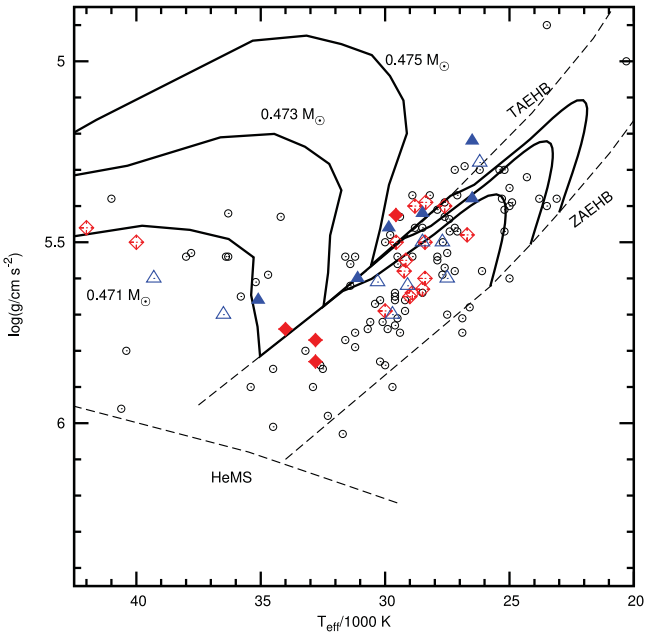

Figure 29. Distribution of sdB stars in close binaries (Kupfer et al. 2015) in the $T_{\rm eff}$–log g plane. Reflection effect systems are highlighted in color, eclipsing (HW Vir types) as red squares, non-eclipsing ones as blue triangles. Filled symbols mark pulsators. This is a modified version of Figure 5 from Schaffenroth et al. (2014a); V. Schaffenroth (2016, private communication).
(A color version of this figure is available in the online journal.)

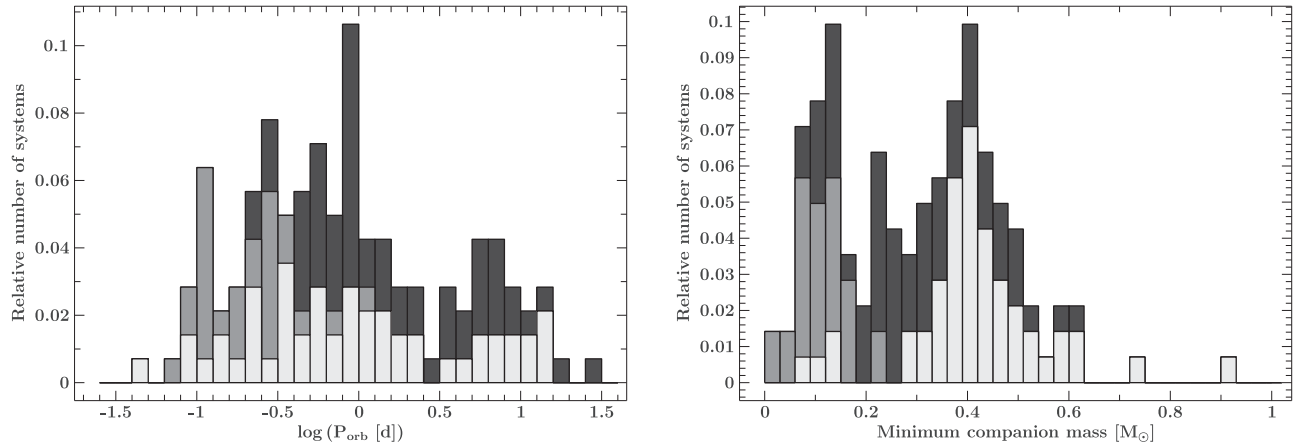

Figure 30. Distribution of periods and minimum companion masses. Light gray: WD companions, gray: dM companion, dark gray: unknown companion type. Left hand panel: period histogram of the full sample. Right hand panel: histogram of minimum companion masses. At least two separated populations are present. The first one peaks at around 0.1 $M_{\odot}$ and consists mainly of systems with low-mass main-sequence companions. The second population peaks at around 0.4 $M_{\odot}$ and consists of WD companions if the nature of the companion has been revealed at all. Only two WD companions have masses exceeding 0.65 $M_{\odot}$. From Kupfer et al. (2015); copyright A&A; reproduced with permission.

determined for eclipsing systems only, which comprise a little more than 10% of the sample. For all others minimum companion masses were derived from the mass functions by adopting the canonical mass for the sdB component (Kawka et al. 2015; Kupfer et al. 2015).

As to the nature of the unseen companion, important information comes from photometry. A low-mass star or brown dwarf companion would reflect a significant amount of light, that varies with orbital phase (Figure 28).

A white dwarf would be too small and the reflection effect is expected to be very small. The absence of a reflection effect may be a hint that the companion is not a main sequence star but a white dwarf (see, e.g., Maxted et al. 2002, 2004; Shimanskii et al. 2008a). However, tidal forces would distort the hot subdwarf star and produce ellipsoidal light variation with a period of half the orbital one (see Figure 39 for an example). An infrared excess could hint at the presence of a cool, low mass companion as well.

Spectroscopically a main-sequence nature can be excluded, if the companion is more massive than $\approx$0.45 $M_{\odot}$ because otherwise spectral feature would be detectable in optical spectra (Lisker et al. 2005).

The distribution of the sdB binaries of Kupfer et al. (2015) in the $T_{\rm eff}$–log g plane is shown in Figure 29. Most of the stars populate the EHB band all the way down to the helium main sequence while about 10% of the sdB sample has already evolved off the EHB. Such a homogeneous coverage is indeed expected from evolutionary models, which show a linear time–luminosity-relation while the star is in the EHB strip until close to central helium exhaustion. Thereafter, the evolution speeds up by a factor of ten consistent with the $\approx$10% of post-EHB stars observed. Hence the observations are consistent with canonical evolution.

5.1.4. Distribution of Orbital Periods and Minimum Companion Masses

The nature of the companion has been established for more than half of the sample only. In 30 systems low-mass stellar or substellar companions have been identified, while in another 52 cases the companion is a white dwarf (Kupfer et al. 2015). In a few systems the companion mass may exceed the Chandrasekhar limit (Geier et al. 2010b); that is, the companion could be a neutron star or black hole.

The distribution of orbital periods of the single-lined sdB binaries is bimodal (Figure 30). A wide peak around $P_{\rm orb} = 0.3$ days is found. The majority of systems in this group host dM companions detected from reflection effects in their light curves. Beyond half a day the contribution from the confirmed dM companions decreases significantly, because the probability for eclipses decreases as the separation of the stars increases and the reflection effect weakens and becomes harder to detect. Another peak occurs at $P = 0.8$–0.9 days. The companions turn out to be white dwarfs although the nature of many companions in this period range is still unknown. At longer periods the number of systems drops, but selection bias increases. White dwarf companions are found over the full period range, although a gap near 3 days might occur in Figure 30, whether real or not.

The distribution of the minimum masses of the companions is also bimodal (Figure 30). At the low mass end (0.1 $M_{\odot}$; that is, close to the hydrogen burning limit) most companions were identified as dwarf M stars. Another four stars have masses

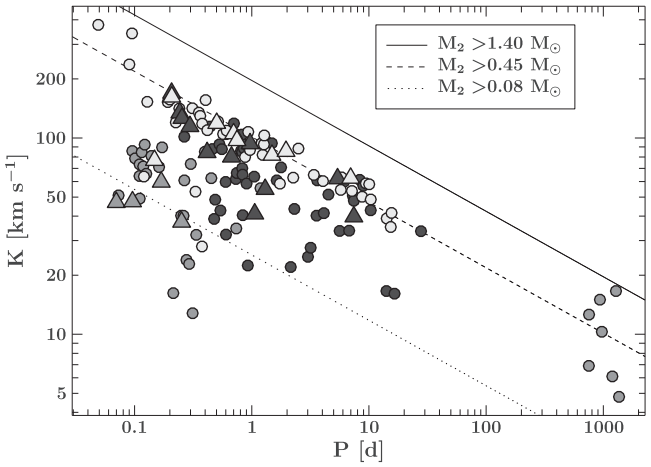

Figure 31. The RV semi-amplitudes of all known sdB binaries (single-lined systems from Kupfer et al. (2015), double-lined from Figure 43) with spectroscopic solutions plotted against their orbital periods (light gray: WD companions, gray: M-dwarf companion, dark gray: unknown companion type). The lines mark the regions to the right where the minimum companion masses derived from the binary mass function (assuming 0.47 $M_\odot$ for the sdBs) exceed the hydrogen burning limit (dotted), the canonical core helium flash mass (dashed) and the Chandrasekhar mass (full drawn). From T. Kupfer (2016, private communication).

lower than the hydrogen-burning limit and therefore are brown dwarfs (see Section 5.2). Only four white dwarf companions have been found in this group, which could belong to the class of extremely low mass (ELM) white dwarfs ($M < 0.3\,M_\odot$, see Section 8.2) if the inclination of the orbit is sufficiently high.

At higher minimum masses ($>0.2\,M_\odot$) most of the companions are white dwarfs with minimum masses near $0.4\,M_\odot$. The minimum masses of all confirmed white dwarf companions (except for the massive KPD 1930+2752 and CD $-30°$ 11223) are lower than the average mass of single C/O white dwarfs and might indicate that the white dwarfs need to lose a significant amount of mass during the evolution either during the first phase of mass transfer when the white dwarf is formed or during the common envelope phase when the sdB is formed.

A proper discussion of the mass distribution for the companions, however, would require knowledge of the system inclinations, which is available for few stars only. Therefore, Kupfer et al. (2015) preferred to discuss the RV half amplitude K as a function of orbital periods (Figure 31). The distribution of the stars in this diagram is truncated near the $0.45\,M_\odot$ limit, which would indicate the masses of the white dwarf companions are below the average mass of a C/O white dwarf.

Kawka et al. (2015) took a different approach by assuming that no inclination bias exists and therefore a statistical average may be applicable for the sample. The resulting mass distribution is shown in Figure 32. Besides the peak at $\sim 0.1\,M_\odot$ a second peak occurs at $\sim 0.6\,M_\odot$, which would be consistent with the companions being C/O white dwarfs (Liebert et al. 2005). Kawka et al. (2015) point that a third peak occurs at $\sim 0.25\,M_\odot$ in Figures 30 and 32, which might be helium white dwarfs.

Kupfer et al. (2015), however, argue that the average inclination is likely to be larger than the statistical one because of selection biases. The sample under study is an inhomogeneous collection of results from the literature. This means that targets were pre-selected either from spectroscopy (RV variations) or from light variations (reflection effect, ellipsoidal variation and/or eclipses) and, therefore, the sample is biased toward high inclinations, both for RV variables (large amplitudes preferred) and light variables (reflection effect and/or eclipses detected). Hence the minimum companion masses will be preferentially below the statistical mean, close to their actual masses in many cases.

Whether the companion white dwarf is of helium or C/O composition is of utmost importance for understanding the evolution of hot subdwarf stars, because the primary (now the white dwarf) had to fill its Roche lobe on the RGB in the first case or the AGB in the second (cf. panel (a) of Figure 19).

White dwarfs with masses of $\sim 0.4\,M_\odot$ are usually considered to be of helium composition and a significant fraction of the white dwarf companions in the WD peak in Figure 32 might be of helium- rather than of C/O composition.

5.2. *Reflection Effects in sdB/O+dM Binaries: The HW Vir Stars*

Close low-mass companions to hot subdwarf stars may be identified via the reflection effect. In a typical system a cool low-mass main-sequence star orbits a hot subdwarf at a distance of about one solar radius and is irradiated by an intense radiation field, which heats the facing hemisphere and leads to reemission of light. This effect is misleadingly called "reflection" effect and in most light curve modeling tools (e.g., MORO (Drechsel et al. 1995) or PHOEBE (Prša & Zwitter 2005) based on the Wilson–Divinney approach (Wilson & Devinney 1971) treated simply by albedos or allow for some kind of energy redistribution. The physics of an irradiated atmosphere, however, is far more complicated but difficult to model (Barman et al. 2004; Shimanskii et al. 2012; Hoyer et al. 2015; Vučković et al. 2016). Although this approach reproduces observed light curves in the pre-*Kepler* era reasonably well, it is challenged by the high-precision *Kepler* light curves of reflection-effect binaries. Since the temperature stratification of an irradiated atmosphere is inverted, emission lines are expect to occur along with the continuum emission and are actually observed for HW Vir and AA Dor.

Eclipsing binary stars are important for deriving stellar masses and radii. Very few eclipsing sdB+WD binaries are known (see Section 8.2). However, there is a growing number

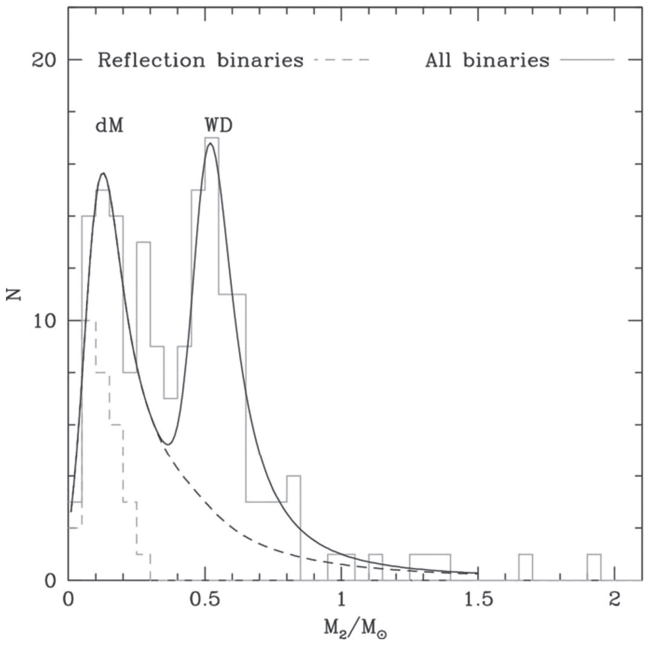

Figure 32. Mass distribution of all known binaries with a hot subdwarf primary star as a function of the secondary mass, assuming an average inclination of 57° (full histogram). The peak distribution of low-mass stars is marked dM and that of white dwarfs, WD. Binaries showing the reflection effect in their light curves are shown with a dashed histogram. The full lines show synthetic distributions smoothed to two-bins width for a combination of late-type stars and white dwarfs (double-peaked full line), and that excluding white dwarfs (dashed line). From Kawka et al. (2015); copyright MNRAS; reproduced with permission.

of sdB/O+dM systems, that do show eclipses accompanied by a strong reflection effect, which is characteristic for such so-called HW Vir systems (see Figure 28 for an illustrative example). An example of a RV curve is shown in Figure 27. Because the sdB stars in close binaries are spun up by tidal force, the Rossiter–McLaughlin effect is seen and can be used to determine the rotation velocity and the orbital obliquity.

Seventeen systems (see Jeffery & Ramsay 2014; Schaffenroth et al. 2015, for an overview) and about an equal number of non-eclipsing sdB+dM binaries are known, which according to Jeffery & Ramsay (2014) should be named XY Sex stars after the prototype. A spectacular addition to the sample is 2M1938 +4603 which was discovered by Østensen et al. (2010a) from an early *Kepler* light curve to be a sdB binary with a dM companion in the *Kepler* field showing strong reflection and shallow eclipses. The orbital period turned out to be relatively long (181.1 minutes) and the RV amplitude of the sdB star in 2M1938+4603 to be $K_1 = 65.7 \pm 0.6$ km s^{-1}. Extended *Kepler* light curves showed pulsations and hint at the presence of a circumbinary substellar object (see Section 7.5).

Actually, in three HW Vir systems, AA Dor (Kudritzki et al. 1982), V1828 Aql (Almeida et al. 2012), and Konkoly J064029.1+385652.2 (Derekas et al. 2015), the primary is an sdO star and, hence, has evolved beyond the EHB already. Nevertheless, we count these systems in the HW Vir class.[10] The distribution of the HW Vir systems as well as that of other non-eclipsing reflection effect systems in the $T_{\rm eff}$–log g plane is shown in Figure 29.

The prototype HW Vir and its hotter sibling, AA Dor, have been studied from light- and radial-velocity curves. Their atmospheric parameters and chemical composition have been derived from high-resolution spectra (see Section 2.4). Most importantly, in both cases the RV curve of the companion has been measured from emission lines (see Figure 33) arising from the heated hemisphere of the dM companion (Vučković et al. 2008, 2014, 2016; Derekas et al. 2015; Hoyer et al. 2015). Recently, attempts to model the spectral and light variations were successful to reproduce the spectrum of the irradiated hemisphere of AA Dor (Hoyer et al. 2015; Vučković et al. 2016, see Figure 34) allowing tight constraints on their masses and radii to be derived. Hoyer et al. (2015) used UVES and XSHOOTER spectra to determine the masses for AA Dor and its companion to unprecedented precision and obtain the mass of the primary to $M_{\rm pri} = 0.470^{+0.0975}_{-0.0354}\,M_{\odot}$, in perfect agreement with the canonical mass from evolution theory. The mass of the companion of $M_{\rm sec} = 0.0811^{+0.0184}_{-0.0102}\,M_{\odot}$ places it right at the hydrogen-burning limit. An independent analysis of the same UVES spectra by Vučković et al. (2016) confirmed those numbers.

All-sky photometric surveys such as the "All Sky Automated Survey" (ASAS, Pojmanski 1997), e.g., ASAS102322-3737.0 (Schaffenroth et al. 2013), SuperWASP (Pollacco et al. 2006) and NSVS (Woźniak et al. 2004), e.g., NSVS 14256825 (Almeida et al. 2012), provided new discoveries of HW Vir stars, almost as bright as the prototype, and suitable for high resolution spectroscopy. All transient surveys are bound to find such objects at fainter magnitudes. For example the latest study (Schindewolf et al. 2015) deals with an HW Vir system discovered by the Palomar Transient Facility (Law et al. 2009). Recently, Pietrukowicz et al. (2013) and Soszyński et al. (2015) announced the discovery of three dozen HW Vir stars from the OGLE experiment. A detailed spectroscopic and photometric analysis by the recently formed EREBOS collaboration[11] of these systems will triple the sample and will allow solid conclusions about the formation of HW Vir stars and sdB stars in general to be drawn.

Figure 35 displays the companion masses in HW Vir systems as a function of orbital period (Schaffenroth et al. 2014b, 2015).

[10] HW Vir stars form a subgroup of pre-cataclysmic variables, which include very hot sdO and DAO white dwarf binaries (e.g., Sing et al. 2004; Aungwerojwit et al. 2007), some of which are associated with planetary nebulae (e.g., BE UMa, Ferguson et al. 1999; Shimanskii et al. 2008b). Many of them show very strong reflection effects with amplitudes exceeding one magnitude and emission line dominated spectra (see Shimansky et al. 2006 for an overview). A compilation of pre-cataclysmic variables can be found in Ritter & Kolb (2003). The primaries are probably very hot (~100 kK) post-AGB stars (Shimansky et al. 2008) rather than post- EHB objects and are, hence, not considered here in more detail.

[11] "Eclipsing Reflection Effect Binaries from the OGLE Survey," a large project at the ESO VLT led by V. Schaffenroth.

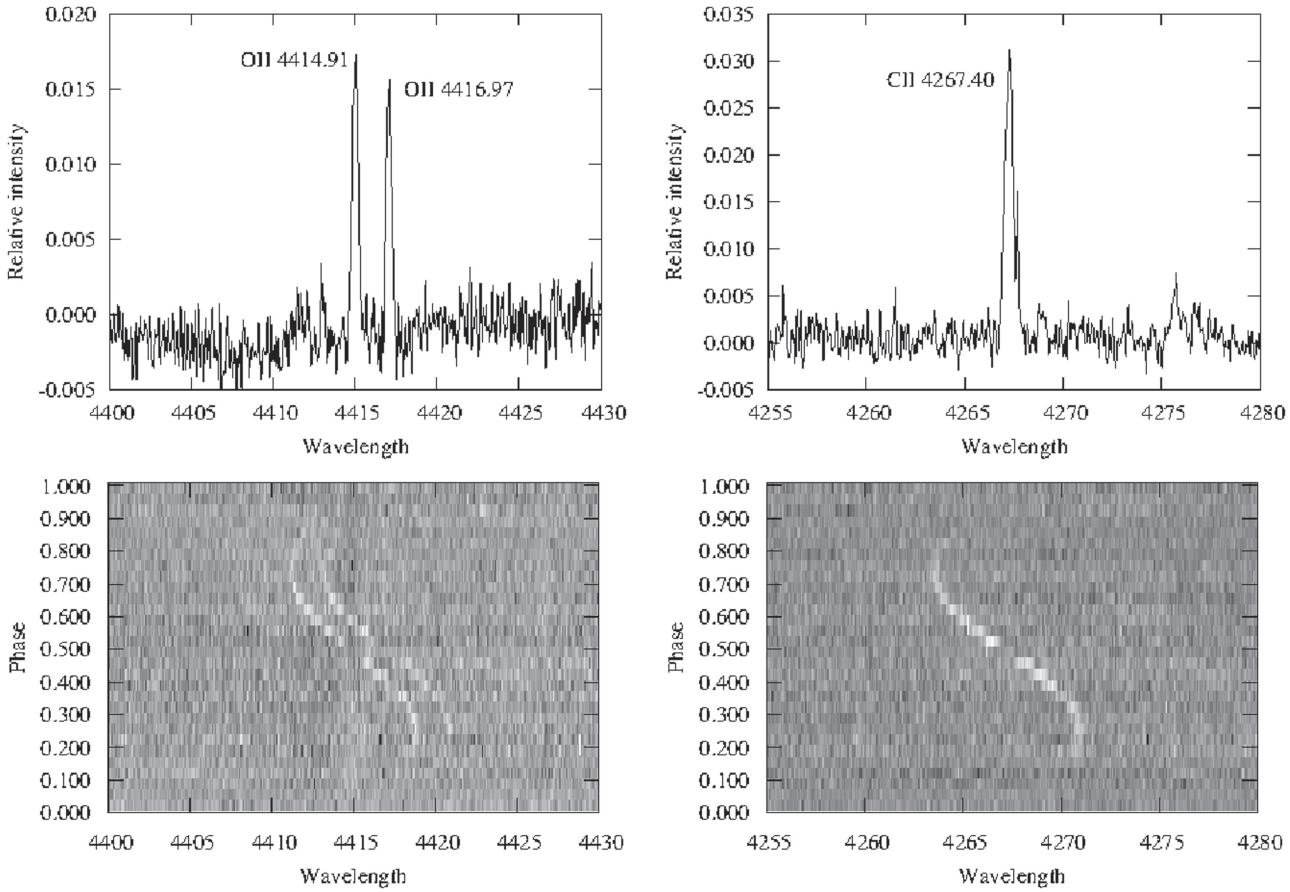

Figure 33. Emission lines originating from the heated atmosphere of the companion of AA Dor. Top: the residual spectrum in the rest frame of the secondary after the contribution of the primary has been removed. The O II (left) and C II (right) lines are clearly visible. Bottom: trailed and phase-binned residual spectra in the rest frame of the primary. From Vučković et al. (2008); copyright ASP; reproduced with permission.

While most companions are late M-dwarfs with masses between 0.1 $M_{\odot}$ and 0.16 $M_{\odot}$, there is no sharp drop below the hydrogen-burning limit. AA Dor and HS 2231+2441 (Østensen et al. 2007) have companion masses of 0.08 $M_{\odot}$, which is on the hydrogen-burning limit. Of particular interest are the binaries SDSS J082053.53+000843.4 (Geier et al. 2011c), SDSS J162256.66+473051.1 (Schaffenroth et al. 2014b), and V2008-1753 (Schaffenroth et al. 2015), because their companion masses are likely to be below that limit and, accordingly, they would be brown dwarfs. The primary is pulsating which makes V2008-1753 a particularly interesting system.

Figure 36 compares the HW Vir stars with their non-eclipsing siblings, which show a reflection effect only. As orbital inclinations of the latter are unknown, the RV half-amplitudes are shown rather than the masses. There are four non-eclipsing systems[12] with periods between ~0.2 and ~0.4 days and $K < 30$ km s^{-1}, which corresponds to masses less than the hydrogen-burning limit if the inclination is sufficiently high. Schaffenroth et al. (2014b) calculate that the probability, that the companion in all four cases is of stellar type, is just 2%. Hence it is likely that at least one of them is a brown dwarf. This suggests that a substantial fraction of the reflection effect binaries host a brown dwarf. A lack of binaries with even shorter periods (<0.2 days) and $K < 54$ km s^{-1} is obvious from Figure 36, which corresponds to companion masses of less than ~0.06 $M_{\odot}$. Schaffenroth et al. (2014b) suggest that such companions cannot exist because they are of too low mass to survive the common envelope phase but evaporate or merge with the red giant core; that is, those systems have evolved into single sdB stars.

5.3. *Low-amplitude Signals in Binary Light Curves: Doppler Boosting, Gravitational Lensing, and Rømer Delay*

Although only a few dozen of hot subdwarfs were discovered in the field monitored by the *Kepler* satellite, the high precision light curves turned out to be a treasure

[12] One of them, PHL 457, is of particular interest, because it is a slow pulsator (Kilkenny & Koen 2016).

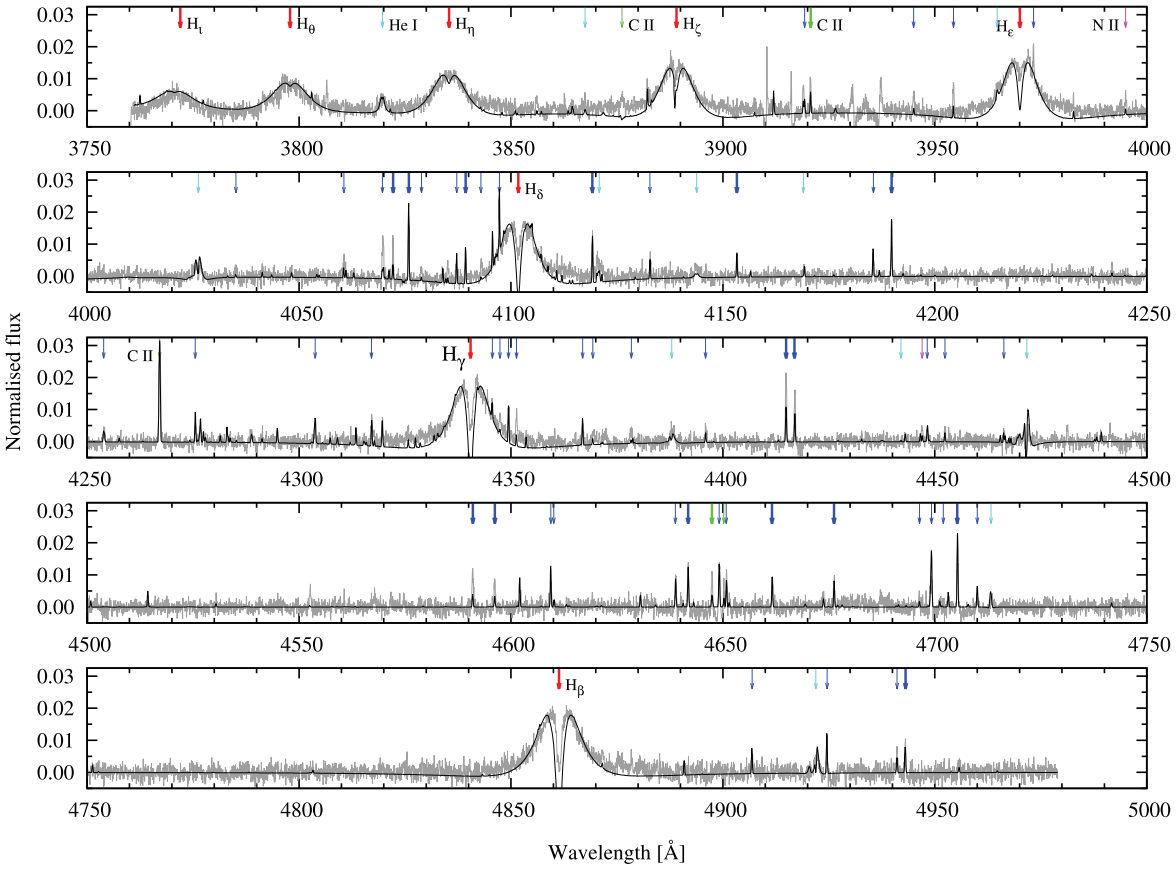

Figure 34. Synthetic emission line spectrum of the dM secondary in AA Dor compared to residual high-resolution spectrum after subtraction of the sdOB component (Vučković et al. 2016). Species are identified by the color coding of the arrows; Balmer lines: red, O II: blue, C II and C III: green, He I: cyan, N II: purple). From Vučković et al. (2016); copyright A&A; reproduced with permission.
(A color version of this figure is available in the online journal.)

chest for sdB asteroseismology (see Section 7) and binary research. Subtle effects such as Doppler boosting, Rømer delay, and gravitational microlensing were detected and used for analysis for the first time. These low-amplitude signals allow physical information to be derived without the need for spectroscopy. A review is presented by Bloemen et al. (2013).

5.3.1. Doppler Beaming (Doppler Boosting)

Doppler beaming, which means light gets beamed toward the direction of motion making the star appear brighter when it moves toward the observer, is a relativistic effect. However, non-relativistic effects add to the low-amplitude flux variations and can provide the dominant contributions to the flux variations observed. First the photon arrival rate is enhanced/decreased and the star appears brighter/fainter when it moves on its orbit toward/away from the observer. Second, the Doppler shift of the stellar spectrum with respect to the photometric bandpass leads to a change of the observed flux unless the spectrum is flat (Shakura & Postnov 1987). The beaming factor, therefore, depends on the shape of the spectrum. Since all three effects act at the same time the term "Doppler boosting" is often used instead of Doppler beaming, as we shall do in this paper. Because the combined effect scales linearly with the ratio of the orbital velocity to the speed of light the changes to the light curves are minute. However, it allows the RV curve to be measured photometrically without any spectroscopic measurements (see, e.g., van Kerkwijk et al. 2010 and Section 8.2).

Doppler boosting was first discovered in the light curve of KPD 1930+2752 (Maxted et al. 2000b), an sdB+WD binary, showing strong ellipsoidal variations. More recently the effect was found in ground-based light curves of CD−30°11223 (see Section 5.5), and the eclipsing white dwarf binaries NLTT 11748 (Shporer et al. 2010) and SDSS J0651+38 (Brown et al. 2011b).

The *Kepler* satellite has provided light curves of sdB binaries of unprecedented precision, which allowed the Doppler

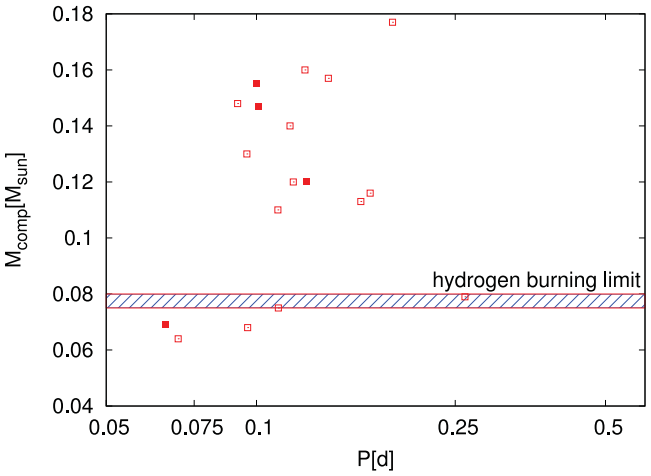

Figure 35. Masses vs. orbital period of all known HW Vir. Filled symbols mark pulsating stars. The hydrogen-burning limit is shown as a hatched band (V. Schaffenroth 2016, private communication).
(A color version of this figure is available in the online journal.)

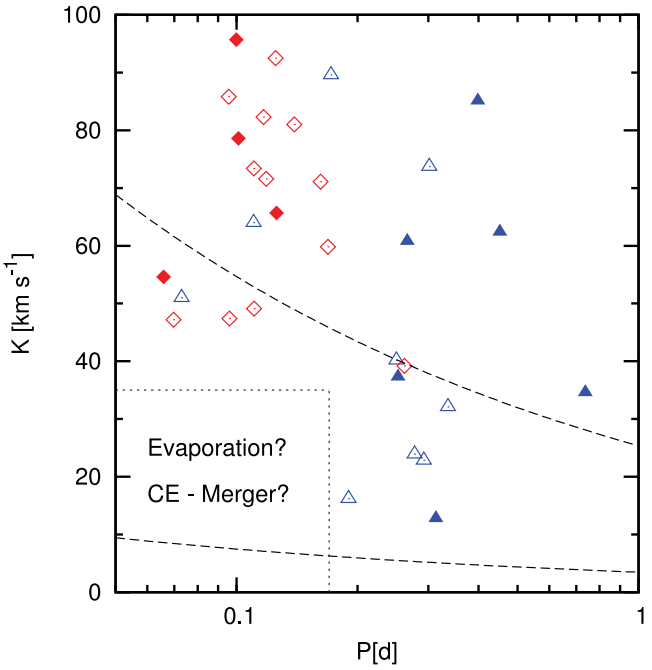

Figure 36. The RV semiamplitudes of all known sdB binaries with reflection effect and RV curve solutions plotted against their orbital periods. The dashed lines mark the regions to the right where the minimum companion masses derived from the binary mass function exceed 0.01 $M_{\odot}$ (lower curve) and 0.08 $M_{\odot}$ (upper curve). Filled symbols are pulsators. Eclipsing binaries are shown as red diamonds (HW Vir). Blue triangles mark non-eclipsing reflection effect binaries. This is a modified version of Figure 4 from Schaffenroth et al. (2014b); V. Schaffenroth (2016, private communication).
(A color version of this figure is available in the online journal.)

boosting effect at lower amplitudes to be studied. Three sdB+WD binaries were of particular interest.[13]

The first one is the pulsating sdB binary KIC 11558725, for which Telting et al. (2012) detected light variations at the 238 ppm level with a clear signal of Doppler boosting, consistent with the observed spectroscopic orbital RV amplitude of the subdwarf, despite its rather long orbital period ($P = 10.05$ days). Because the star is pulsating a third consistent estimate of the orbital RV amplitude was derived from the orbital light-travel time delay of 53.6 s, which causes aliasing and lowers the amplitudes of the shortest-period pulsation modes. In the same way Telting et al. (2014b) analyzed the pulsating sdB+WD binary KIC 7668647 whose orbital period is even longer (14.2 days). Again its RV amplitude of 39 km s^{-1} was consistently derived from the orbital Doppler beaming of 163 ppm in the *Kepler* light curve, the spectroscopic RV curve and the orbital light-travel time delay of 27 s from timing of pulsation modes.

Another Doppler-beaming system, KIC 10553698B, was found by Østensen et al. (2014b) to host a normal white dwarf with a mass close to 0.6 $M_{\odot}$ if the pulsation axis is aligned with the orbital axis, because the inclination of the former can be derived from the shape of the rotationally split multiplets. The star is pulsating, slowly rotating ($P_{\rm rot} = 41$ days, see Section 7.5), and, most interestingly shows trapped pulsation modes as will be discussed in Section 7.3.1.

Another effect of even lower amplitude may become detectable for rotating stars. Groot (2012) suggested that Doppler boosting due to rotation, the photometric analog of the spectroscopic Rossiter–McLaughlin effect (see Figure 27), might become detectable in systems such as NLTT 11748 and SDSS J0651+38, which would provide information about the sky-projected spin–orbit angle from gravity darkening of the rotating star (Barnes et al. 2013).

[13] Two other interesting Doppler boosting cases are KOI-74 and KOI-81, which are binaries consisting of early type main-sequence stars orbited by helium-core objects to be discussed in Section 8.2.

5.3.2. Gravitational Lensing

Transiting compact objects can gravitationally magnify their companions, as predicted by Maeder (1973). Marsh (2001) investigated the effect for white dwarf binaries. The high quality of the *Kepler* photometry allowed the detection a "self-lensing" system (KOI 3278, Kruse & Agol 2014), a Sun-like star and a white dwarf in a 88.18 day orbit. A 5 hr pulse of 0.1% amplitude occurs every orbital period. The pulse is due to magnification by microlensing, which allowed Kruse & Agol (2014) to derive the mass of the white dwarf as 0.63 $M_{\odot}$, typical for a C/O white dwarf (Liebert et al. 2005).

A combination of ellipsoidal variations, Doppler boosting and self-lensing has been found in the *Kepler* light curve of the sdB binary KPD 1946+4340 (Bloemen et al. 2011) (see. Figure 37). The former leads to unequal amplitudes of the light maxima caused by ellipsoidal deformation of the sdB, the latter weakens the eclipse depth. The photometric RV from Doppler boosting is consistent with the spectroscopic one,

demonstrating the reliability of photometric radial velocities from Doppler boosting.

5.3.3. Rømer Delay from Eclipse Timing

The lightcurve of a binary on a perfectly circular orbit should show primary and secondary eclipses separated by half the period. Due to the finite speed of light, however, a travel time delay occurs, when the masses of the binary components are unequal. This so-called Rømer delay depends on the size of the orbit and allows the mass ratio of the binary to be constrained (see Kaplan 2010).

However, a slight ellipticity of the orbit would also shift the secondary minimum from phase 0.5. The two effects can be disentangled, because the Rømer delay always shifts the eclipse to a larger phase, whereas the eccentricity can shift it either way. Hence, the observed shift of the minimum can be a superposition of both effects.

While the Rømer effect is familiar in radio pulsar timing, such light travel time effects have been found in the light curves of pulsating sdB stars (Silvotti et al. 2007; Telting et al. 2012) (see Sections 6 and 7). From eclipse timings the Rømer delay has been discovered in the light curve of an eclipsing binary white dwarf for the first time by Kaplan et al. (2014a) who also constrained the eccentricity of the orbit to be as small as $e \cdot \cos\omega = (-4 \pm 5) \cdot 10^{-5}$.

Detection of the Rømer delay from eclipse timing in an sdB binary was first claimed for 2M1938+4603 from the analysis of its *Kepler* lightcurve (Barlow et al. 2012a) based on the delay of the secondary eclipse of 2.06 ± 0.12 s. However, the analysis of a more extended *Kepler* light curve called this conclusion into question. Baran et al. (2015c) demonstrated that even the larger data set is insufficient to disentangle the Rømer delay signal from ellipticity. Instead evidence for a circumbinary substellar companion was found (see also Section 6.1).

5.4. X-Rays from Hot Subdwarf Stars

Main-sequence O stars emit X-rays originating from turbulence and shocks in their strong winds (Lucy & White 1980; Owocki et al. 1988). The mass-loss of hot subdwarf stars is much lower and, therefore, they are not expected to be X-ray sources. However, X-ray emission from the sdO star HD 49798 was discovered with the *ROSAT* satellite (Israel et al. 1997). It turned out that the X-rays do not originate from the sdO star but from accretion onto a compact companion, either a neutron star or a massive white dwarf. Recently additional X-ray emitting sdO stars have been discovered from *Chandra* and *XMM-Newton* observations and limits on the mass loss rates of sdB stars have been derived (for a recent review see Mereghetti & La Palombara 2015).

5.4.1. X-Rays from Wind Accretion in Hot Subdwarf Binaries

The compact companions of hot subluminous stars are difficult to detect in optical/UV data. However, they might give rise to detectable X-ray emission if the subdwarf can provide an adequate accretion rate. In this respect, luminous sdO stars offer the best prospects for X-ray detections because of their relatively high mass loss rates ($\dot{M} \sim 10^{-7}$ $-10^{-10}\,M_{\odot}\,\mathrm{yr}^{-1}$, Jeffery & Hamann 2010). This is well demonstrated by the case of the luminous sdO HD 49798, a single-lined spectroscopic binary ($P = 1.5$ days), which was discovered as a soft X-ray source by the *ROSAT* satellite. Remarkably, the X-ray flux shows a strong periodic modulation at 13.2 s (Israel et al. 1997), indicating the presence of a compact object. X-ray eclipses (which constrain the system's inclination, see Figure 38) allowed a dynamical measurement of the masses of the two binary components. This showed that the companion of HD 49798 is a very massive ($1.28 \pm 0.05\,M_{\odot}$) white dwarf (Mereghetti et al. 2009, 2011b, 2013), making this binary a potential progenitor of a SN Ia (see Section 5.5). Prompted by the case of HD 49798, a search for X-ray emission from other hot subdwarf binaries was launched. While searches with the *Swift*/XRT of a dozen sdB binaries hosting compact companions gave negative results (Mereghetti et al. 2011a), pulsed X-ray emission in the luminous, hydrogen-deficient sdO BD+37°442 was discovered (La Palombara et al. 2012). The observed X-rays have a soft spectrum (a blackbody with temperature ~45 eV plus a weak power-law component), and show a significant modulation at a period of 19.2 s. Hence it is tempting to assume that BD+37° 442 is an X-ray binary very similar to HD 49798. However, no RV variations could be found despite of intense spectroscopic monitoring (Heber et al. 2014). Therefore, the nature of the pulsing X-ray source remains a mystery.

Because sdB stars are less luminous than the sdO stars discussed and, therefore, have much lower mass loss rates, X-ray fluxes from wind accretion onto a compact companion are expected to be lower and may occur in the most favorable cases; that is, the shortest period sdB binaries with the most massive companions. CD−30°11223 and PG 1232−136 are considered the best targets and were observed by Mereghetti et al. (2014) with *XMM-Newton*. However, no X-ray photons were detected, which constrained their mass loss rates to lower than $\sim 10^{-13}\,M_{\odot}\,\mathrm{yr}^{-1}$, which would be consistent with predictions from models of radiatively driven winds (Vink & Cassisi 2002) if the metallicities were low, but too low for solar metallicity.

5.4.2. X-Rays from the Winds of Hot Subdwarfs?

A continued X-ray search with *Chandra* (La Palombara et al. 2014) and *XMM-Newton* (La Palombara et al. 2015) resulted in the discovery of an additional X-ray emitting luminous sdO star, BD+37°1977 (a spectroscopic twin to BD+37°442), for which no RV curve has been measured yet. It is, therefore,

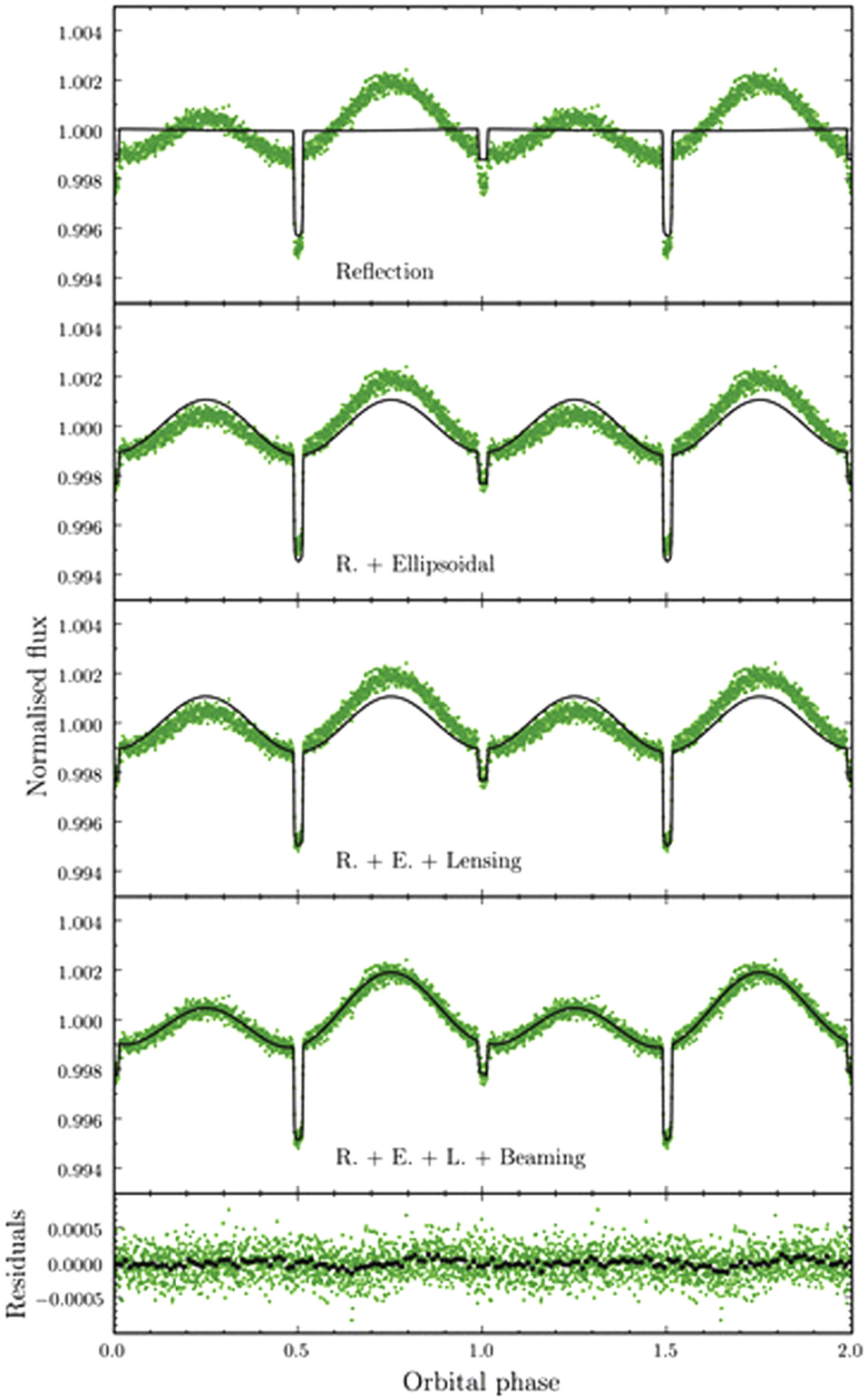

Figure 37. Phase-folded light curve of KPD 1946+4340 (green, data points grouped by 30) from *Kepler* data and the best-fitting model (black) of Bloemen et al. (2011). In the top panel, only the eclipses and reflection effects are modeled. In the second panel, ellipsoidal modulation is added. In the third panel, gravitational lensing is taken into account as well, which affects the depth of the eclipse at orbital phase 0.5. The bottom panels show the full model, taking into account Doppler beaming, and the residuals (grouped by 30 in green and grouped by 600 in black). From Bloemen et al. (2011); copyright MNRAS; reproduced with permission. (A color version of this figure is available in the online journal.)

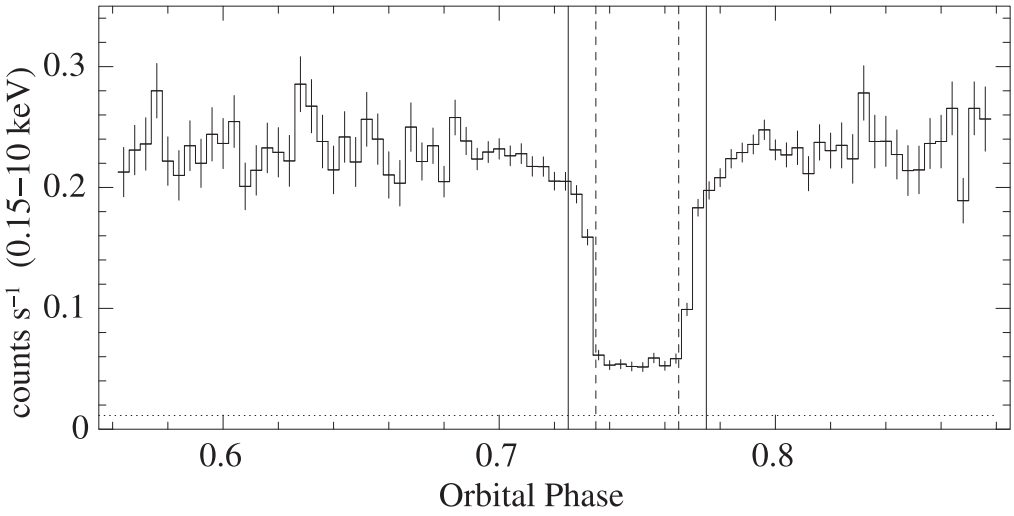

Figure 38. Light curve of HD 49798 in the 0.15–10 keV energy range folded at the orbital period in bins of 535 s. The eclipse is clearly visible with totality lasting 4311 s and gradual ingress and egress lasting ≈500 s, each. The horizontal line indicates the background level. Note that there is residual X-ray flux at totality which might arise from light from the companion scattered in the wind of the sdO star or from HD 49798 itself, due to shocks and instabilities in the wind. The vertical lines delimit the phase intervals used for the spectral analysis. From Mereghetti et al. (2013); copyright A&A; reproduced with permission.

unknown whether the star hosts a compact companion or not. La Palombara et al. (2015) were able to match the observed X-ray spectrum with the sum of two thermal plasma components, as in normal early-type stars, and conclude that the X-ray emission is intrinsic to the star and arises from shocks in the stellar wind.

La Palombara et al. (2014) detected X-rays from the very hot compact sdO stars Feige 34 and BD+28°4211. There is no evidence for a compact companion in either case; no RV variations, neither on short nor on long timescales have been found for both BD+28°4211 (Latour et al. 2015) and BD+37°442 (Heber et al. 2014). If there are compact companions orbiting BD+37°442 and BD+28°4211 and accreting from their winds, they would need to be on orbits seen almost pole-on. *Gaia* observation will be tale telling. Therefore, the X-ray emission is more likely to be intrinsic to the sdO star.

La Palombara et al. (2015) and Mereghetti & La Palombara (2015) find that X-ray spectra and the X-ray to bolometric luminosities L_X/L_{bol} of intrinsic emission of all the sdOs are well-fitted by a multi-temperature plasma, once the proper elemental abundances are used. Despite their lower mass-loss rates, the estimated L_X/L_{bol} ratios of the sdO stars are consistent with those of the massive early-type stars and Mereghetti & La Palombara (2015) conclude that X-ray emission is caused by the same mechanism as for the massive stars; that is, by turbulence and shocks in their winds.

5.4.3. Radio-emission from Hot Subdwarf Stars

If the most massive companions of sdB binaries were in fact neutron stars, they could be pulsars. This idea has been tested by Coenen et al. (2011) who searched for radio pulsations from the potential neutron star binary companions to the subdwarf B stars HE 0532–4503, HE 0929–0424, TONS 183 and PG 1232–136 proposed by Geier et al. (2010b) using the Green Bank Telescope. No pulsed emission was found to mean flux densities as low as 0.2 mJy.

5.5. Progenitors of SNe Ia

Hot subdwarf stars with white dwarf companions are viable progenitor systems for SNe Ia (Maxted et al. 2000b). Because recent observations show that the class of SNe Ia is more diverse than previously thought, a diversity of progenitor systems is expected too, which reinforced the search for progenitors of SNe Ia. The various observational evidence on the nature of SN Ia as well as the rivalling progenitor and explosion models are reviewed by Hillebrandt et al. (2013), Maoz et al. (2014), Postnov & Yungelson (2014), and Ruiz-Lapuente (2014).

A SN Ia is caused by the thermonuclear explosion of a white dwarf in a close binary either with another white dwarf (double degenerate scenario, DD) or with a non-degenerate companion, either a normal star or a helium star (single degenerate scenario, SD). In a double degenerate system the merger of two C/O white dwarfs driven by gravitational wave radiation might lead to a SN Ia if the total mass is larger than a critical mass, which is mostly assumed to be the Chandrasekhar mass. If the orbital period of a DD system is shorter than about half a day, the system will merge within a Hubble time.

A sdB+WD system will evolve into a DD system within $\approx 10^8$ years, which is shorter than the merger time for most known systems. If the system is sufficiently massive, it would qualify as a SN Ia progenitor system. However, a sdB+WD

system may also become a SD progenitor system, if the sdB transfers parts of its helium envelope to the white dwarf companion before having reached the white dwarf cooling sequence.

The sdB+WD binary KPD 1930+2752 was the first DD system discovered to be a good candidate for the progenitor of a SN Ia (Maxted et al. 2000b), because the white dwarf is sufficiently massive ($>0.9\,M_{\odot}$) so that the total mass will exceed the Chandrasekhar limit when the system will merge in $\approx 10^8$ years. Geier et al. (2007) revisited KPD 1930+2752 by analyzing time-resolved high-resolution spectra and derived the masses of both components by assuming tidally locked rotation (see Sections 2.7.1 and 7.6). The resulting masses sum up to almost exactly the Chandrasekhar mass. Hence, the analyses confirmed that KPD 1930+2752 is a viable SN Ia progenitor candidate.

Several studies, notably from the SPY survey, have provided periods and masses for a couple of DD systems, mostly double white dwarfs but also several sdB+WD systems. Although no system has yet been found to exceed the Chandrasekhar limit beyond any doubt, several have been found close to that limit (see Figure 19 of Postnov & Yungelson 2014). The resulting DD mass distribution implies that super-Chandrasekhar systems must exist and that the DD scenario is viable.

More recently, the sdO+WD system HD 49798 has been proposed as a candidate SN Ia progenitor system because it hosts a white dwarf of very high mass (Wang & Han 2010).

The double detonation scenario predicts that an (underluminous) supernova may result from accretion of helium by a C/O white dwarf. A detonation of the accreted helium shell can occur once a sufficient amount of helium ($\approx 0.1\,M_{\odot}$) accumulated (Livne & Glasner 1990). The explosion of the He-shell triggers a subsequent detonation in the C/O core which might produce SNe Ia explosions depending on its mass (Fink et al. 2007, 2010). The most favorable accretor mass is $\approx 1.0\,M_{\odot}$ which is predicted to launch a normal SN Ia (Sim et al. 2010), but minimum mass models of $0.8\,M_{\odot}$ predict double detonation SN Ia, though underluminous (Fink et al. 2010).

CD−30°11223 is the best candidate for a binary evolving into a double detonation supernova. The system was discovered independently by Vennes et al. (2012) and Geier et al. (2013c) to be an eclipsing binary sdB in a 70 minutes orbit. The light curve displays ellipsoidal variations, eclipses of both companions, and the Doppler boosting effect. The companion must be a white dwarf because strong ellipsoidal variations are seen in the light curve (see Figure 39). Shallow secondary eclipses demonstrate that the white dwarf must be hot and relatively luminous. The Doppler boosting effect can be used to measure the RV from photometry and agrees well with the spectroscopic RV curve. Geier et al. (2013d) constrain the masses to $0.47\,M_{\odot}$ or $0.54\,M_{\odot}$ for the sdB, and to $0.76\,M_{\odot}$ or $0.79\,M_{\odot}$ for the white dwarf by assuming tidally locked rotation or making use of the mass–radius relation for the white dwarf, respectively. The derived mass indicates that the white dwarf is of C/O composition. Its future evolution strongly depends on the stability of the mass transfer of helium to the white dwarf and the companion's mass. Geier et al. (2013d) investigated the future evolution of the system and find that stable mass transfer will occur once the sdB star fills its Roche lobe. The detonation in the accreted helium layer is sufficiently strong to trigger the explosion of the core. The helium star will then be ejected at such high velocity that it will escape the Galaxy. Such a so-called hyper-velocity star (HVS) has, indeed, been discovered, the He-sdO US 708, which will be discussed in Section 9.

5.6. Orbital Decay by Gravitational Wave Radiation

Because the binaries emit gravitational wave radiation, their orbital periods have to decrease. The rate of period change strongly depends on the orbital period (Peters & Mathews 1963), and therefore will be easiest to detect for the shortest period systems. Hermes et al. (2012a) reported the detection of orbital decay in the 12.75 minute, detached binary white dwarf SDSS J065133.338+284423.37 at a rate of $-0.31 \pm 0.09\,\mathrm{ms\,yr^{-1}}$, consistent with the prediction from General Relativity for the orbital decay due to gravitational wave radiation ($-0.26 \pm 0.05\,\mathrm{ms\,yr^{-1}}$).

2M1938+4603 is the only sdB binary for which the period decrease has been derived (Baran et al. 2015c) to be $\dot{P} = 4.13(2) \cdot 10^{-11}\,\mathrm{s\,s^{-1}}$ using *Kepler* data. The shortest period sdB+WD systems KPD 1930+2752 and CPD−31° 11223 are the most promising candidates *for measuring the* period decay due to gravitational wave radiation.

5.7. Composite Color Hot Subdwarf Binaries

Previously most sdB stars were discovered as very blue objects in surveys for UV-excess objects. Because of color-cuts usually applied, such surveys are biased against sdB binaries with cool companions, because their colors are reddish and their composite spectra are flat. Hence, a large number of sdB stars may have been missing from current samples. An sdB star shines as bright as the Sun in the visual band. An F-type companion would dominate the optical spectrum while an A-type dwarf (or earlier) would outshine a hot subdwarf completely (but see Section 5.9).

Nevertheless, a large number of systems with F- to K-type companions are known, but quantitative spectral analyses remained scarce (e.g., Aznar Cuadrado & Jeffery 2002) because of the difficulties of disentangling the composite spectrum.

Recent large-area ultraviolet (*GALEX*), optical (SDSS and several others) and infrared (2MASS, UKIDSS) photometric surveys offer a less biased option to search for new composite systems comprising subdwarfs plus MS star companions of mid-M-type and earlier. By combining the photometric measurements the spectral energy distribution (SED) can be constructed in a broad wavelength range. Cuts in color–color

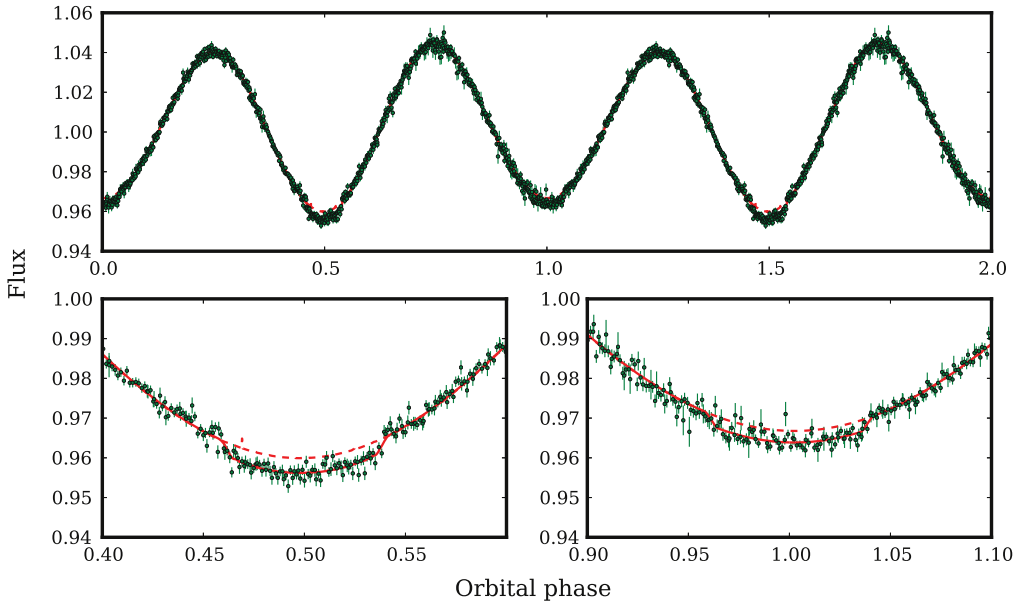

Figure 39. Upper panel: V-band light curve of the eclipsing sdB+WD system CD−30°11223 (green) with superimposed model (red) plotted twice against the orbital phase for better visualization. The dashed red curve marks the same model without transits and eclipses. The sinusoidal variation is caused by the ellipsoidal deformation of the hot subdwarf as a result of the tidal influence of the compact white dwarf. The difference in the maxima between phase 0.25 and 0.75 originates from the Doppler boosting effect (see Section 5.3), Lower panels: close-up on the transit of the WD in front of the sdB (left) and the eclipse of the WD by the sdB (right). From Geier et al. (2013d); copyright A&A; reproduced with permission.
(A color version of this figure is available in the online journal.)

space have to be employed to separate these objects from possible contaminants.

Girven et al. (2012) constructed two complementary samples of composite sdB candidates by applying color cuts to the aforementioned photometric catalogs. A large but shallow one, and a smaller, but deeper sample, led to the discovery of a large number of composite subdwarf binaries. Their SEDs were matched with synthetic spectra using grids of appropriate model spectra for the sdB and the companion star, respectively. Effective temperatures of both stars as well as the distance were derived for all systems. The subdwarf effective temperatures primarily lie in the cooler part of the EHB (20,000–30,000 K), with 5%–10% at even lower temperatures. The companions are mostly of spectral type F0 to K0, while subdwarfs with M-type companions appear much rarer. This is consistent with population synthesis models predicting a very efficient first stable RLOF channel.

5.7.1. Double Lined sdB Binaries: Orbital Periods Found at Last

SEDs are a very efficient tool to characterize binary systems. More information can be obtained from quantitative spectral analyses of the composite spectra, which however, require broad wavelength coverage and accurate flux calibration. From the spectra the atmospheric parameters of both components can be derived as well as their RV curves.

Atmospheric Parameters. It is more difficult to derive atmospheric parameters of sdB binaries from composite spectra or SEDs. Substantial progress in spectral disentangling has been reported by Németh et al. (2012) who analyzed composite spectrum sdBs from the *GALEX* sample based on NLTE model atmospheres and carefully selected template spectra for the cool companions (see Figure 40).

The companions turned out to be dwarfs with spectral types between G1V and F2V. One giant G3.5III companion to an sdO star was found as well as subgiant companions to two sdB stars. The distribution of the hot subdwarf primaries in the $T_{\rm eff}$–log g plane (see Figure 41) shows that they predominantly populate the hot end of the EHB unlike the sample studied by Girven et al. (2012) from SEDs. They appear to cluster in the instability strip of rapid p-mode pulsators (28,000–36,000 K, see Section 7). In fact, the first four p-mode pulsators discovered were sdB+F/G dwarfs (Kilkenny et al. 1997; Koen et al. 1997; Stobie et al. 1997a; O'Donoghue et al. 1997).

Radial velocity curves. Binary population synthesis models (Han et al. 2003) predicted that the orbital periods of such systems should be in the range 10–500 days. Early long-term RV monitoring at low spectral resolution did not find any variations indicating that the orbital periods must be larger than predicted and accordingly the amplitudes of the RV-curves below the detection limits of low resolution spectroscopy. This called for high spectral resolution observations, which were initiated at the Hobby–Eberly telescope (Barlow et al. 2012b;

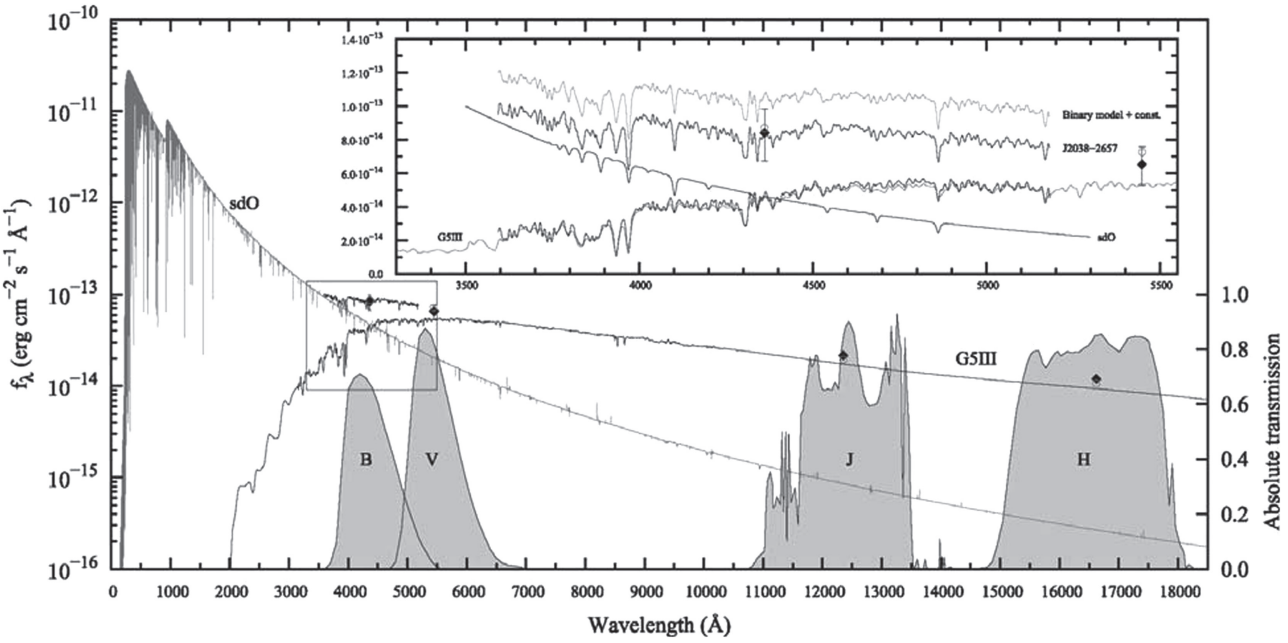

Figure 40. Disentangling the composite spectrum of an sdO binary. The synthetic SED from an NLTE model for the sdO star (gray) and a G5III template are marked. Bessell B, V and 2MASS J and H filter transmission curves cut out the contribution of each star to the synthetic photometry. Inset: magnified part of the spectrum where decomposition was performed. The G5III templates and the sdO spectra add up nicely and this binary model fits the observation. The binary model is shifted up for clarity. Photometry measurements are plotted with black diamonds. Gray circles show the synthetic photometry. From Németh et al. (2012); copyright MNRAS; reproduced with permission.

Wade et al. 2014) as well as the Mercator telescope (Vos et al. 2012, 2014). Deca et al. (2012) were the first to derive the orbit of such a composite sdB system (PG 1018−047) and found the orbital period to be, indeed, longer (753 days) than predicted by the binary population models available at that time. Additional discoveries followed quickly.

Vos et al. (2013) derived orbits for BD+29°3070 (1283 days), BD+34°1543 (972 days), and Feige 87 (936 days). The RV curves for those stars are displayed in Figure 42. Note that the system velocities seem to be different for the primary and secondary in all three cases, which is caused by the difference in gravitational redshift. Although well known in white dwarf systems (Adams 1925) this is the first discovery of the gravitational redshift in a sdB star and allowed Vos et al. (2013) to determine the surface gravities of the sdB stars. At about the same time long-term spectroscopic monitoring with the Hobby–Eberly telescope was successful and allowed orbits for PG 1449+653 ($P = 909$ days) and PG 1701+359 (734 days, Barlow et al. 2013) to be determined.

By now, the orbits of nine composite spectrum sdB binaries have been solved, the periods of which range from 707 to ≈1370 days, exceeding the predicted upper limit of 500 days considerably. This triggered improved binary population studies, that, indeed, succeeded in producing systems of similarly long periods as observed (see also Section 3.4).

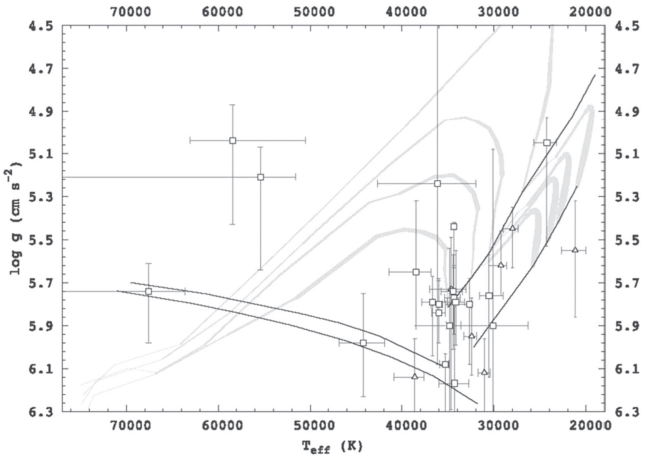

Figure 41. $T_{\rm eff}$–log g diagram of sdB star composite spectrum binaries. A crowding of composites can be observed near the location of possible rapid pulsators at $T_{\rm eff} = 33{,}500$ K, log $g = 5.8$. Németh et al. (2012); copyright MNRAS; reproduced with permission.

5.7.2. The Eccentricity Puzzle

It came much as a surprise that the orbits turned out not to be circular as expected, because tidal interaction should lead to circularization of the orbit before RLOF occurs. The observed

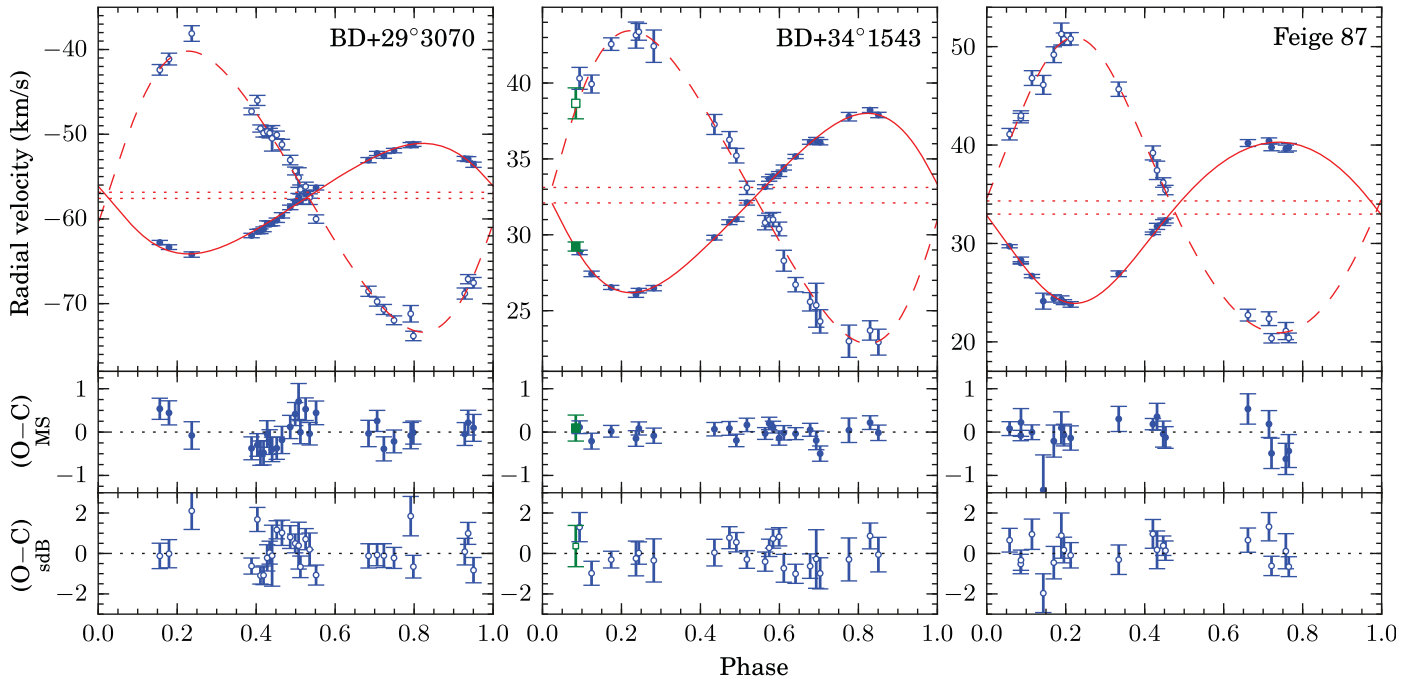

Figure 42. Radial velocity curves for BD+29°3070 (left), BD+34°1543 (center), and Feige 87 (right). Top: spectroscopic orbital solution (solid line: MS, dashed line: sdB), and the observed radial velocities (filled symbols: MS component, open symbols: sdB component). The measured system velocities of both components are shown by a dotted line. The offset between the two lines results from gravitational redshift. Middle: residuals of the MS component. Bottom: residuals of the sdB component. From Vos et al. (2013); copyright A&A; reproduced with permission.
(A color version of this figure is available in the online journal.)

RV curves, however, indicated eccentricities as large as 0.25 and a trend of the eccentricity to increase with increasing orbital period (see Figure 43, Vos et al. 2015).

A similarly puzzling binary is IP Eri, a system consisting of a giant K0 and a He WD with a period of 1071 days and an eccentricity of 0.23 (Merle et al. 2014, see also Section 8.2). In order to explain the formation of such a system Siess et al. (2014) suggested that the sdB progenitor avoided RLOF but ejected its envelope on the RGB due to a tidally enhanced stellar wind. According to this scenario the eccentricity is preserved or can even be increased if the orbital period is long enough. Vos et al. (2015) performed similar calculations for the long-period sdB binaries, but found that they are insufficient to explain the high eccentricities, because the red giant would need to loose so much mass that it would not ignite helium and could not evolve into an sdB star. Therefore, Vos et al. (2015) investigated two additional eccentricity pumping mechanisms; that is, phase-dependent RLOF on eccentric orbits and the interaction between a circumbinary disk and the binary. Assuming a certain minimal eccentricity, phase-dependent RLOF can reintroduce eccentricity and could produce binaries at the short period regime with eccentricities up to 0.15. When adding a circumbinary disk, higher eccentricities could be reached due to resonances between the binary and the disk.[14] Because such a disk would exist during the mass-loss era and then dissipate quickly thereafter it would hardly be observable. However, the models predict that the eccentricities should decrease with increasing period, while the observed systems show the opposite trend. However, the models of Vos et al. (2015) are of exploratory nature as many model parameters are poorly constrained yet.

5.8. *Multiple Systems*

More than 20% of all binary stars are in fact members of triple systems (Rappaport et al. 2013) and stay bound on long timescales if they have a hierarchical structure; that is, consist of a close binary accompanied by a relatively distant third star.

Some sdB binaries may actually be hierarchical triples, such as PG 1253+284, a composite-spectrum sdB with a dwarf companion. The components were resolved by *HST* imaging (Heber et al. 2002), which indicated that the dwarf companion is on a wide orbit. Nevertheless, RV variations of the sdB star were observed, which must stem from another unresolved companion on a short-period orbit. Hence PG 1253+284 is a

[14] A similar scenario has been recently proposed by Antoniadis (2014) to explain eccentric orbits of milli-second pulsars with helium white dwarf companions.

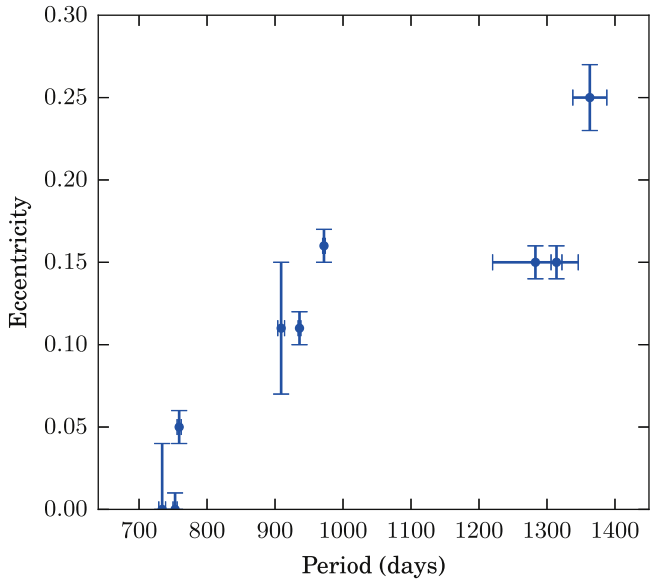

Figure 43. The observed period–eccentricity diagram of all known long-period sdB binaries. There is a clear trend for higher eccentricities visible at higher orbital periods. From Vos et al. (2015); copyright A&A; reproduced with permission.

(A color version of this figure is available in the online journal.)

triple system. Additional evidence of multiplicity (triples, quadruples) among sdB systems has recently been reported by Barlow et al. (2014). New observations from the MUCHFUSS project have identified another candidate triple system (J09510 +03475, Kupfer et al. 2015).

5.9. Giant and Massive Companions to Hot Subdwarf Stars

Most cool companions to sdB stars are main-sequence stars. A giant companion has been found to BD–7°5477 on a wide orbit (orbital period $P = 1195 \pm 30$ days, Vos et al. 2014) resulting from stable RLOF (see Section 5.7.1). In addition subgiant or giant companions were found for the sdO star FF Aqr (K0 III, Dworetsky et al. 1977; Etzel et al. 1977; Vaccaro & Wilson 2003; Shimanskaya et al. 2011) and the sdB HD 185510 (K III–IV, Jeffery et al. 1992; Fekel et al. 1993; Frasca et al. 1998) on short orbits ($P = 9.2$ and 20.7 days, respectively), but still detached.[15] The systems are photometrically variable, caused by the reflection effect, chromospheric activity and spots. Németh et al. (2012) discovered a third such system, GALEX J2038−2657, which hosts a G8III companion. Its variability was discovered only recently by Kawka et al. (2015). Howarth & Heber (1990) and Rauch (1993) showed that the sdO+G giant binary HD 128220 (orbital period $P = 871.78$ days) formed via case C mass transfer; that is, the sdO progenitor filled its Roche lobe while ascending the asymptotic giant branch. Accordingly the sdO component is a post-AGB star of 0.55 $M_{\odot}$.

Three sdO stars are known as companions to Be stars: 59 Cyg (Peters et al. 2008), FY CMa (Peters et al. 2013), and ϕ Per (Gies et al. 1998).[16] Such sdO stars were predicted by Pols et al. (1991) to form when the donor star begins mass transfer during its shell-hydrogen burning phase and evolves into an sdO star. The less-massive gainer is spun-up and evolves into a Be star.

6. Substellar and Planetary Companions to sdB Stars

Most extra-solar planets known today have been discovered by either the RV method or the transit method. In the case of hot subluminous stars, both methods have not yet been successful (Jacobs et al. 2011; Norris et al. 2011), although brown dwarf companions have been found.

However, a scientific breakthrough came with the discovery of sinusoidal variations of the pulsation frequencies of the sdB pulsator V391 Peg (=HS 2201+2610), which are due to the light travel time effect. Accordingly, the sdB star is orbited by a $M \sin i = 3.2\, M_{\rm Jupiter}$ planetary companion at about 1.7 au in 3.2 years and implies that a planet may survive the expansion of the red giant host star at distances of less than 2 au (Silvotti et al. 2007).

Light curves from the *Kepler* mission provided evidence for Earth-sized planets around two pulsating sdB stars. The analysis of the *Kepler* light curves from quarters Q5 to Q8 of KIC 05807616 revealed a rich pulsation spectrum (Charpinet et al. 2011a). The frequency spectrum shows gravity modes as well as acoustic modes but no clear multiplet structures. Most importantly, Charpinet et al. (2011a) detected two weak modulations at frequencies below the cut-off frequencies, which limits pulsational periods. Excluding other effects Charpinet et al. (2011a) arrived at the conclusion that the signals are due to the reflection effect of two Earth-size planets orbiting with periods of 5.7 and 8.2 hr, respectively. Krzesinski (2015) analyzed all available *Kepler* photometry from Q4 to Q17 and confirm the presence of both frequencies. Moreover, they found evidence that both amplitudes and frequencies are unstable, with amplitudes varying between non-detection (signal-to-noise $S/N < 4$) to $S/N = 6$–8. These variations can hardly be due to planetary reflection effects and Krzesinski (2015) *conjectures* that both frequencies are some sort of damped pulsation frequencies beyond the pulsational cut-off.

Similar low-frequency modulations were found for KIC 10001893 in all available *Kepler* photometry (993.8 days of short and 147.9 days of long cadence) data and interpreted as caused by planetary reflection effects suggesting the

[15] The hot subdwarf in HD 185510 is possibly a low-mass helium-core object (Jeffery & Simon 1997) (see Section 8.2).

[16] The Be star HR 7409 (7 Vul) may be a related object (Vennes et al. 2011a), but the nature of the companion needs to be clarified.

presence of three planets with orbital periods of $P1 = 5.273$, $P2 = 7.807$, and $P3 = 19.48$ hr, respectively (Silvotti et al. 2014a). Interestingly, the period ratios $P2/P1 = 1.481$ and $P3/P2 = 2.495$ are very close to the 3:2 and 5:2 resonances, respectively. One of the main pulsation modes of the star at 210.68 μHz corresponds to the third harmonic of the orbital frequency of the inner planet, suggesting that *g*-mode pulsations of an sdB star are tidally excited by a planetary companion. This interpretation, though, should be taken with a grain of salt in view of the results for KIC 05807616. However, phase and amplitude variations such as seen in the light curve of the latter have not been reported by Silvotti et al. (2014a).

If confirmed such systems would be interesting *for* studying the survivability of planets during red giant evolution (see, e.g., Villaver & Livio 2007, 2009; Nordhaus et al. 2010; Nordhaus & Spiegel 2013; Villaver et al. 2014).[17] Those planets must have lost a large amount of their initial few Jupiter masses during the CE phase. Passy et al. (2012b) investigated whether such planets could have been stripped of significant amounts of mass during the CE phase and concluded that the Earth-mass planets of KIC 05807616 could well be the remnants of one or two Jovian-mass planets that were stripped of their envelope when they orbited in the envelope of the red giant. Bear & Soker (2012) suggested an alternative scenario, which assumes a single massive planet of 5 Jupiter masses, that loses its entire gaseous envelope during spiral-in in the CE phase, its metallic core is then disrupted into two or more surviving Earth-size fragments that migrate to resonant orbits.

However, independent confirmations of those discoveries are still lacking (see Schuh et al. 2014; Silvotti et al. 2014b for discussions). Hence, all substellar companions reported in this section should be regarded as candidates, only. The more so, because recent deep SPHERE@ ESO-VLT observations of the white dwarf plus brown dwarf candidate V471 Tau ruled out that the observed eclipse timing variation are caused by a proposed circumbinary brown dwarf at the expected position (Hardy et al. 2015).

6.1. Circumbinary Planets and Brown Dwarfs

Circumbinary planets have been discovered around unevolved binaries such as the dG+dM system Kepler 47 (Orosz et al. 2012) or Kepler 16 (Doyle et al. 2011). To find out whether such planetary systems can survive stellar evolution, it is important to search for planets around evolved binaries. Eclipsing sdB binaries provide a useful playground, because mid-eclipse timings would allow a search for period changes. HW Vir stars are well suited for such an exercise, because their periods are short and some, in particular the prototype, have already been observed for decades. HW Vir was discovered by Menzies & Marang (1986) and the first orbital period change was found nine years later (Kilkenny et al. 1994).[18]

Moreover, the brightest HW Vir systems have been covered by automatic all-sky surveys such as SuperWASP (Lohr et al. 2014) that provide plenty of eclipse epochs.

While AA Dor did not show any evidence for period variations for decades (Kilkenny 2014), almost all HW Vir systems, that have been monitored for a sufficiently long time show period changes. Lee et al. (2009) announced the detection of two giant planets orbiting the prototype HW Vir from systematic variations in the timing of eclipses. This finding, however, was questioned, because the planetary orbits were found to be mutually crossing. Strong gravitational interactions have to be expected so that the system would be unstable on the required long timescales.

Horner et al. (2012) performed a detailed stability analysis of the proposed HW Vir planetary system and confirmed that, indeed, the system is unstable with a mean lifetime of less than a thousand years. Hence, it was concluded that the exoplanets do not exist.

The picture changed again, when new eclipse timings became available (Beuermann et al. 2012) as demonstrated in Figure 44. The new timings deviate strongly from the model of Lee et al. (2009). Including observations up to 2012, Beuermann et al. (2012) presented a new secularly stable solution with two companions (see Figure 45). The inner one is a giant planet of $M_3 \sin i_3 = 14\,M_{\rm Jup}$ orbiting HW Vir in 12.7 years. The outer one is a brown dwarf or low-mass main-sequence star of $M_4 \sin i_4 = 30$–$120\,M_{\rm Jup}$ on a 55 years orbit. The uncertainty of the orbital period of the latter is large (± 15 years) because the observational time base is still too short. Beuermann et al. (2012) find that such a system would be stable over more than 10^7 years, in spite of the sizeable interaction. Since no process other than the light-travel time variations had to be invoked, the planetary hypothesis of the eclipse-time variations has been revived.

The Beuermann team announced the detection of third bodies to the sdB binaries NSVS 14256825 and HS 0705 +6700 from cyclic variations in their measured orbital period. The third object in NSVS 14256825 is a giant planet with a mass of roughly $12\,M_{\rm Jup}$, whereas, in the case of HS 0705 +6700, it is a brown dwarf of $31\,M_{\rm Jup}$ if the orbit is coplanar with the binary (Qian et al. 2009). An extended series of eclipse timings is consistent with the presences of a third body to the HS 0705+6700 system and hints at the possible presence of a fourth (Pulley et al. 2015).

[17] See also the proceedings of the conference "Planetary systems beyond the main sequence" (Schuh et al. 2011).

[18] The history ("saga") of HW Vir observations is nicely summarized by Vučković et al. (2014).

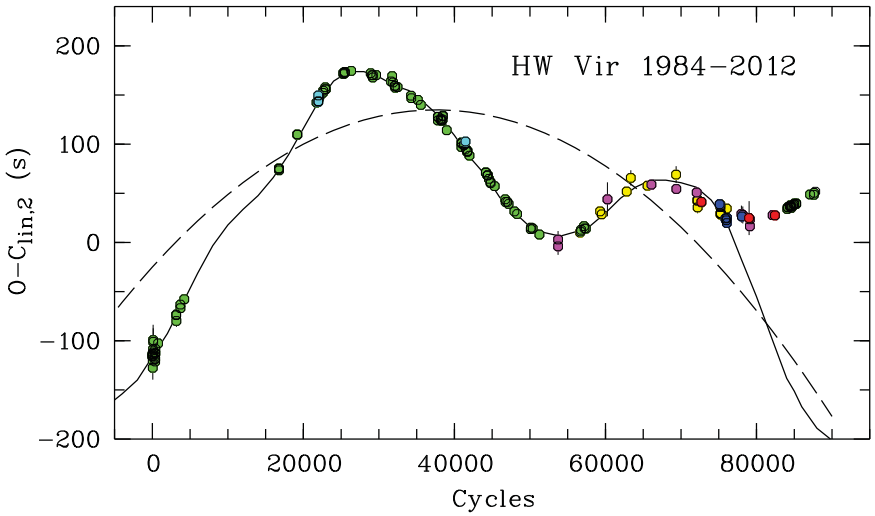

Figure 44. O–C diagram residuals of the mid-eclipse times from the linear ephemeris used by Lee et al. (2009) along with their model curves for the two-companion model (solid) and the underlying quadratic ephemeris (dashed). Note that the new 2008–2012 epochs from Beuermann et al. (2012) strongly deviate from the Lee et al. (2009) model. From Beuermann et al. (2012); copyright A&A; reproduced with permission.
(A color version of this figure is available in the online journal.)

For NSVS 14256825, the existence of a fourth body was proposed (Almeida et al. 2013). However, the orbital stability analysis by Wittenmyer et al. (2013) suggested that proposed orbits for the two planets are extremely unstable on timescales of less than a thousand years, regardless of the mutual inclination between the planetary orbits. Hinse et al. (2014) reanalyzed the photometric data and find no evidence for the existence of a second planet. The one-companion model is shown to be poorly constrained by the existing data set, because various models result in substantially different orbits despite similar statistical significance. The baseline of timing data needs to be extended to nail down the orbit of the third body.

Finally, NY Vir is a pulsating sdB binary harboring a circumbinary planet (Qian et al. 2012). The issue of stability arose in this case also when Lee et al. (2014) presented a new model based on historical eclipse times combined with their long-term CCD data and found that the periodic variations are most likely caused by a pair of light-travel-time effects due to the presence of two planets of $M_3 \sin i_3 = 2.8\,M_{\rm Jup}$, and $M_4 \sin i_4 = 4.5_{\rm Jup}$, respectively. However, their dynamical analysis suggests that long-term stability requires the outer companion to orbit on a moderately eccentric orbit. Further monitoring is required to corroborate this issue. The most recent discovery is a low mass circumbinary companion to the pulsating sdB+dM system 2M1938+4603 (Baran et al. 2015c, see also Section 7.5).

However, the travel time variation could be due to other non-circumbinary mechanisms. The Applegate mechanism (Applegate 1992), which is caused by gravitational coupling of the orbit to changes of oblateness of a magnetically active star, is often considered, but the luminosity of the convective secondaries is mostly found to be insufficient to drive the Applegate mechanism (e.g., for HS 0705+6700, Pulley et al. 2015).

The lesson learned from the HW Vir case is that one has to be patient and never stop observing. Despite of the problems described, evidence is accumulating that, indeed, sdB binaries of the HW Vir type are orbited by additional substellar companions that may have survived the giant-phase evolution of their host binary.

6.2. Planet Formation: First or Second Generation

Substellar circumbinary objects have also been discovered in other post common envelope binary (PCEB) systems, hosting white dwarfs instead of sdB stars (e.g., Beuermann et al. 2013).

Among the ten well studied systems all but AA Dor show period changes calling for the presence of circumbinary planets (Zorotovic & Schreiber 2013). This frequency (90%) of substellar-mass circumbinary companions to PCEB systems is surprisingly high when compared to that of close main-sequence binaries, for which Welsh et al. (2012) found from the *Kepler* sample that more than 1% of such binaries have giant planets on nearly coplanar orbits.

In order to test the hypothesis that the PCEB companions could indeed be of first generation, Zorotovic & Schreiber (2013) compared binary population models with observational and theoretical results for the formation of circumbinary giant planets and concluded that only 10% of the PCEBs could have first generation giant planets.

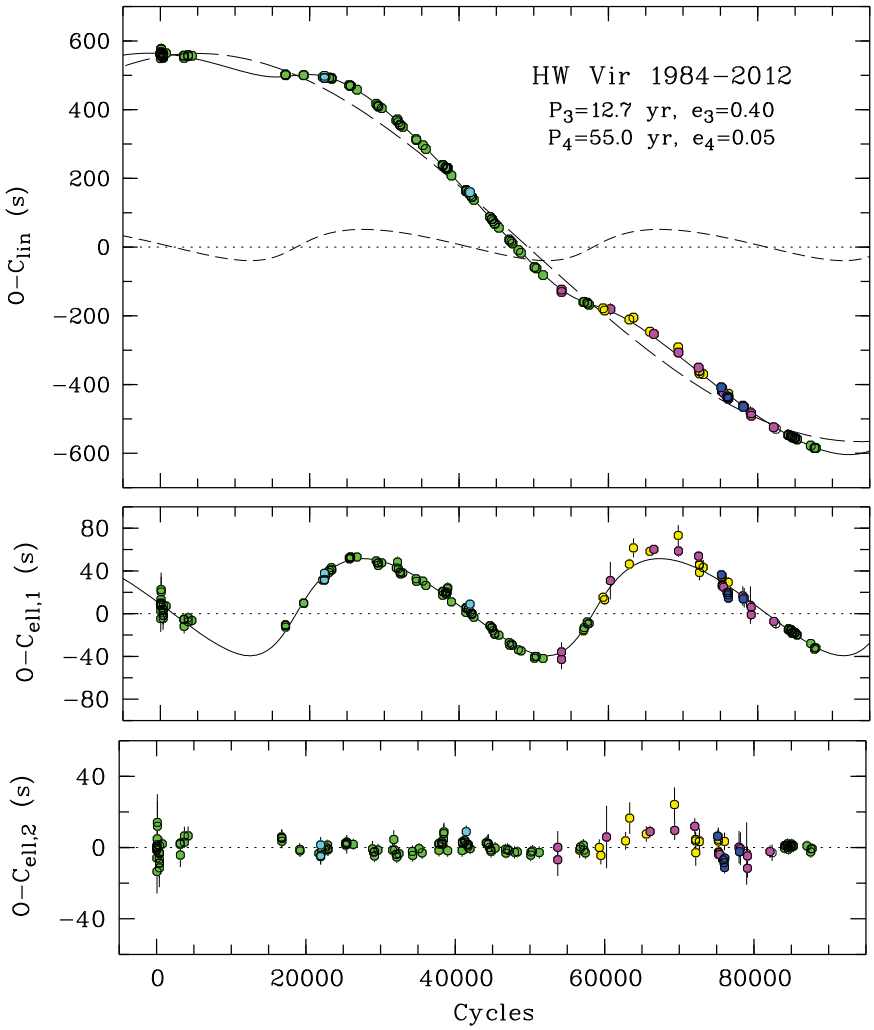

Figure 45. Fit of two Keplerian orbits to the eclipse-time variations of HW Vir. Top: data of Figure 44 relative to the linear ephemeris of Beuermann et al. (2012). The curves denote the model light travel time effect (solid) and the contributions by the outer companion (long dashes) and the inner planet (short dashes). Center: data with the contribution by the outer companion subtracted and model for the inner planet (solid curve). Bottom: residuals after the subtraction of the contributions by both companions. From Beuermann et al. (2012); copyright A&A; reproduced with permission.
(A color version of this figure is available in the online journal.)

The circumbinary planets may not have existed before the CE phase, but may have formed from the material of the common envelope (Bear & Soker 2014).

Recent simulations of common envelope evolution showed that some fraction (≈10%) of the ejected material may remain bound to the PCEB (Schleicher & Dreizler 2014) and is likely to form a circumbinary disk, sufficiently massive for gravitational instabilities to occur and form giant planets. However, the process has to be sufficiently fast to explain systems as young as NN Ser (1 Myr), a white dwarf binary with two circumbinary massive planets similar to HW Vir (Beuermann et al. 2013). A detailed discussion can be found in Zorotovic & Schreiber (2013).

Second-generation planets might form more efficiently if remnants of lower mass planets survived the common envelope phase and provided seeds to accrete material quickly to form giant planets (hybrid first- and second-generation scenario, Zorotovic & Schreiber 2013; Schleicher & Dreizler 2014).

Schleicher & Dreizler (2014) and Schleicher et al. (2015) modeled the case of NN Ser, and find that the current data cannot be explained by pure first generation models, whereas the second generation scenario naturally explains the observed masses of the two circumbinary planets. Bear & Soker (2014) carried out similar calculations, compared them to twelve PCEB systems that host planets and concluded from angular

momentum considerations that they are more likely to be of first generation. However, Schleicher & Dreizler (2014) point out that there are probably two populations, where some systems form primordially with the progenitor star and some are of second generation.

Zorotovic & Schreiber (2013) suggested that the eclipse timing variations may not be caused by the existence of third and fourth bodies at all, but by the secondary being magnetically active. They suggest that this could be tested because the period variations should not occur in close WD binaries with a second WD component as the secondary is not likely to be active. Hence the formation of circumbinary planets to PCEBs remains an open question.

7. Pulsating Hot Subdwarf Stars

Multi-periodic light variations of low amplitudes (few milli-mag) and periods of a few minutes were discovered in sdB stars (now termed V361 Hya stars, Kilkenny et al. 1997) at almost the same time at which they were predicted by theory to be caused by non-radial pulsations (Charpinet et al. 1996). The driving mechanism was readily identified as being due to an iron opacity bump (Charpinet et al. 1997). The V361 Hya stars are found among the hotter sdB stars with $28{,}000 < T_{\rm eff} < 35{,}000$ K and $5.2 < \log g < 6.1$ (see Figure 46). The periods suggest that the stars are p-mode pulsators, offering the opportunity of using oscillations to probe the interior of sdB stars. Asteroseismology of sdB stars received another boost when pulsations with periods of 45 minutes–2 hr were discovered (Green et al. 2003, now termed V1093 Her stars). Typical light curves are shown in Figure 47. The much longer period pulsations found in these stars indicate that they are gravity modes. The stars are typically cooler than the p-mode pulsators (see Figure 46). The pulsations in both groups are driven by an opacity bump due to iron ionization (and other iron-group elements, see Charpinet et al. 1997; Fontaine et al. 2003, 2008a). However, iron must be enhanced by diffusion processes in the sub-photospheric layers in order to drive the pulsations ("Z-bump").

Of great importance for the development of asteroseismology are the so-called hybrid pulsators which show both short period p-mode pulsations as well as long-period g-mode pulsations (e.g., Schuh et al. 2006) and which lie at the temperature boundary (≈28,000 K) between both classes of pulsating stars (see Figure 46). Acoustic waves (p-modes) propagate in the outer regions of the star, whereas g-modes do in the deep interior (see Figure 48 for an illustration). Hence, the internal structure of the star can be probed if both types of pulsations are detected in a star.

Dedicated surveys that targeted sdB stars in the predicted instability strip were partially successful at finding new sdB pulsators. For example a survey at the Nordic Optical Telescope (Østensen et al. 2010b) monitored more than 300 sdBs predicted to lie in the instability strip but discovered only twenty new short-period pulsators which means that only about 10% of the stars in the V361 Hya instability strip are actually pulsating with amplitudes of a few mmag, detectable from ground.[19]

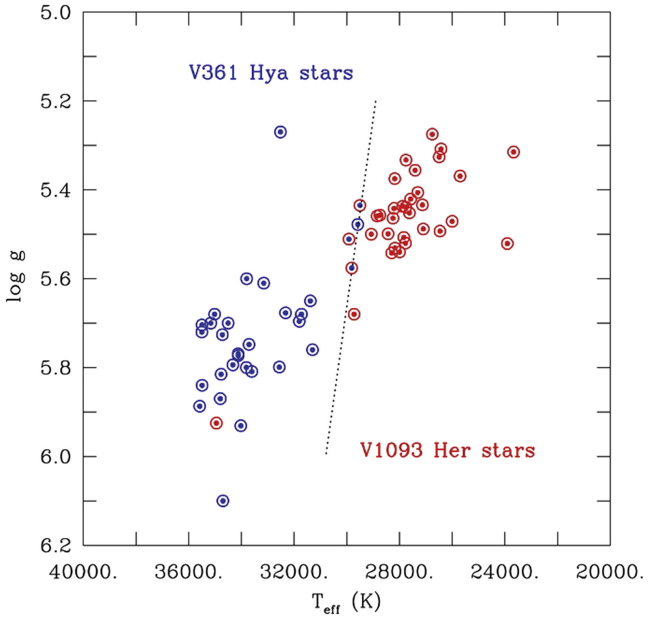

Figure 46. Distribution of pulsating sdB stars in the effective temperature–surface gravity plane. The locations of 28 short-period p-mode pulsators of the V361 Hya type are indicated in blue, while those of 30 long-period g-mode variables of the V1093 Her type are shown in red. Three hybrid pulsators, showing simultaneously both p-modes and g-modes, are shown in red and blue, lying at the common boundary between the two distinct domains, defined approximately by the dotted line. LS IV−14°116 finds itself (the red symbol in the V361 Hya domain) totally out of place. From Green et al. (2011); copyright ApJ; reproduced with permission.
(A color version of this figure is available in the online journal.)

Searches for long-period pulsations require a lot more observing time and photometric precision. New discoveries have, for instance, been reported from ground-based studies, e.g., two pulsators of V1093 Her type (GALEX J0321+4747 and GALEX J2349+3844, Kawka et al. 2012). The companion to the sdB in GALEX J0321+4747 is a low mass dwarf, whereas in the case of GALEX J2349+3844 it is probably a white dwarf. Another important discovery from the MUCHFUSS project was FBS 0117+396, a hybrid pulsator in an sdB +dM system (Østensen et al. 2013, see Section 7.6). The *Kepler* mission provided a much better option to search for long-period sdB pulsators and, indeed, discovered more than a dozen of them (Østensen et al. 2010c, 2011).

[19] Østensen et al. (2010b) also provide limits on the pulsation amplitudes for 285 objects with no obvious variations at the expected timescales.

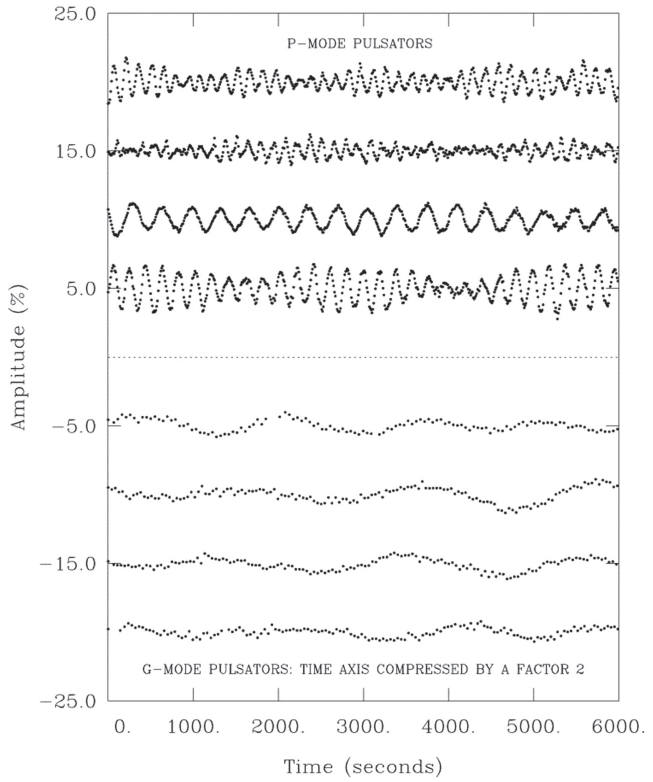

Figure 47. Representative light curves of four short-period (top) and four long-period (bottom) pulsating sdB stars. The short-period *p*-mode pulsators (V361 Hya stars) are, from top to bottom, PG 1047+003, PG 0014+067, Feige 48, and KPD 2109+4401. These curves are "white-light" light curves expressed in terms of percentage of residual amplitude relative to the mean brightness of the star. The curves have been shifted by arbitrary amounts in the vertical direction away from the zero point for visualization purposes. The long-period *g*-mode pulsators (V1093 Her stars) have been observed through different bandpasses. The pulsators are, from top to bottom, PG 1716+426 (R), PG 0850+170 (R), PG 1338+481 (B), and PG 1739+489 (V). Note that the time axis refers to the top half of the figure; the light curves in the bottom half have been compressed by a factor of 2. From Fontaine et al. (2003); copyright ApJ; reproduced with permission.

Pulsation modes can be described by three quantized numbers, n, ℓ, and m, where n is the number of radial nodes between center and surface, ℓ that of surface nodes perpendicular to the pulsation axis, and m the number of surface nodes passing through the pulsation axis. The radial fundamental mode is assigned 0,0,0 and negative n denote gravity (g) and positive n pressure (p) modes.

Ground-based observations did not reach sufficient precision and resolution to pin down those numbers unambiguously, leaving the theorists with the so-called forward modeling technique of quite incomplete frequency spectra (e.g., Charpinet et al. 2007, 2008b). The breakthrough came with the *Kepler* satellite mission that achieved just that goal. It is not exaggerating to say that *Kepler* data have revolutionized asteroseismology of pulsating stars in general and of pulsating sdB stars in particular.

However, before exploring the *Kepler* era, we shall first discuss fundamental issues and techniques such as the location of the instability strips for *p*-mode and *g*-mode pulsators, respectively (Section 7.1). The *Kepler* satellite provided broad-band photometry of unprecedented precision and frequency resolution, whereas ground-based telescopes offer complementary techniques such as multi-band photometry and time-series spectroscopy, which will be discussed in Section 7.2. We shall turn to the sdB pulsators in the *Kepler* field (Section 7.3), review the perspective to probe the stellar interior and determine stellar ages (Section 7.4), visit the pulsating sdBs in eclipsing binaries (Section 7.5), revisit the rotation characteristics derived from multiplet splittings and discuss the impact on synchronization timescales (Section 7.6). New classes of pulsating hot subdwarf star have also been discovered, e.g., in the globular cluster ω Cen (Section 7.7), as well as the unique pulsating He-sdB star LS IV−14°116 (Section 7.8). Finally we take a glance at the ongoing *Kepler K2* mission.

7.1. The Instability Strips

The location of the instability strip in the $T_{\rm eff}$–log g plane is of foremost interest. For the V361 Hya pulsators the prediction from models provide an excellent match to the observations (see Charpinet et al. 2007), as the excited modes have periods very similar to those observed in these stars.

However, the predicted instability strip is wider than observed and pulsators and non-pulsators coexist in the same region of the $T_{\rm eff}$–log g diagram, i.e., only one out of ten stars pulsates. Because ground-based observations may have missed low-amplitude pulsators, this might be just an observational selection effect. High-precision *Kepler* photometry, however, has confirmed the scarcity of *p*-mode pulstors[20] indicating that the *V361 Hya* instability strip is by no means pure (Østensen et al. 2011).

The long-period, low-amplitude oscillations of the V1093 Her stars are much harder to detect from the ground. *Kepler* photometry has revealed that almost all sdB stars which have effective temperatures in the predicted instability strip in the *Kepler* field are indeed pulsating.

The theoretical blue edge of the V1093 Her stars posed a problem to modelers. Early models predicted the blue edge at about 5000 K cooler than observed (see Charpinet et al. 2007). However, Jeffery & Saio (2006, 2007) found that adding Ni and using opacities from the Opacity Project (rather than OPAL) shifts the *g*-mode instability strip by 5000 K to the blue. Artificial abundance enhancements of Fe and Ni were introduced in the pulsation driving layers. Therefore, a more detailed investigation of the driving mechanism is required

[20] Østensen et al. (2011) surveyed 32 sdB pulsator candidates hotter than 28,000 K and found only one pulsator of V361 Hya type, a transient one and one hybrid pulsator.

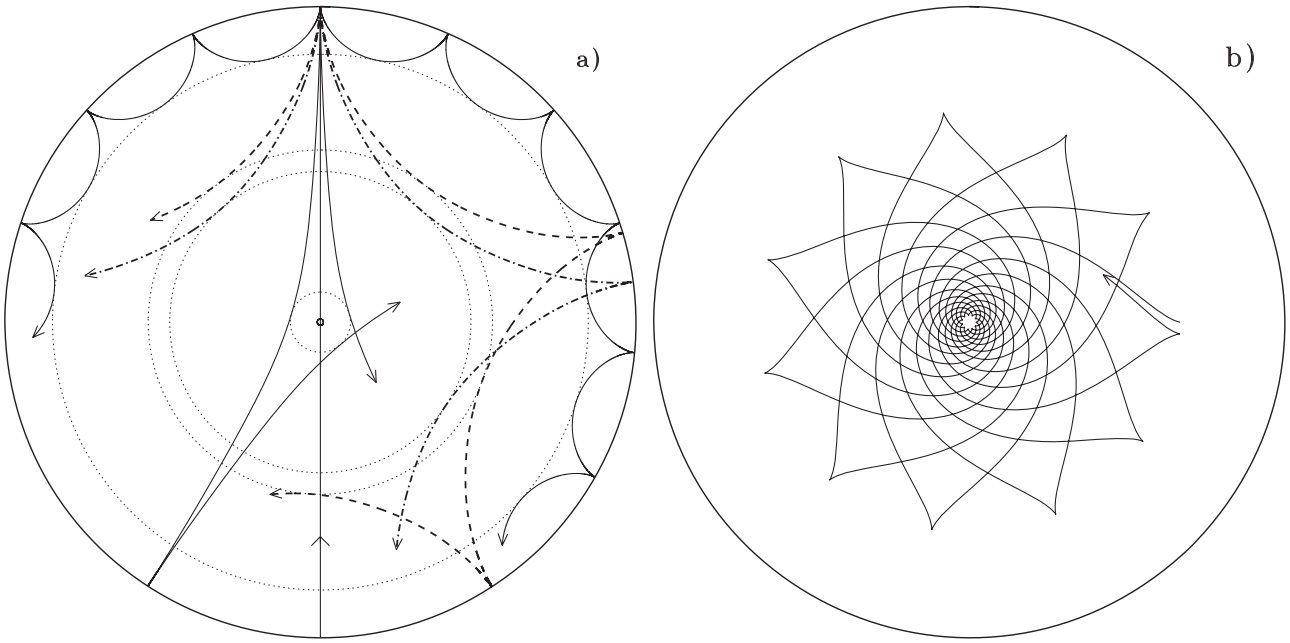

Figure 48. Illustration of the propagation of sound and gravity waves in a cross-section of the solar interior. The acoustic ray paths (panel (a)) are bent by the increase in sound speed with depth until they reach the inner turning point (indicated by the dotted circles) where they undergo total internal refraction. At the surface the acoustic waves are reflected by the rapid decrease in density. Rays show corresponding modes with frequency 3000 μHz and degrees (in order of increasing penetration depth) $l = 75$, 25, 20 and 2; the line passing through the center schematically illustrates the behavior of a radial mode. The gravity-mode ray path (panel (b)) corresponds to a mode of frequency 190 μHz and degree 5. From Cunha et al. (2007); copyright A&ARv; reproduced with permission.

accounting for Ni and other iron-group elements with abundance stratifications shaped by diffusion. Self-consistent calculations that account for an enrichment of iron group elements in the driving regions resolved the issue (Bloemen et al. 2014). In fact, Bloemen et al. (2014) found that the abundance enhancements of Fe and Ni were actually previously underestimated. The new models predict the instability strip of observed *g*-mode pulsators very well for masses close to 0.47 $M_{\odot}$, which solved the blue edge problem of the sdB *g*-mode instability strip.

7.2. Multi-color Light Curves and Time-series Spectroscopy

Monochromatic light curves are typically used to study the pulsations of hot subdwarf stars, with the *Kepler* space mission being the flagship tool that provided enormous progress in the field (see Section 7.3). Often observations are done in white light; that is, no filters are employed, in order to improve throughput and, hence, the S/N. However, multi-color photometry provides another important tool to study the properties of pulsating stars. The three-channel imager ULTRACAM (Dhillon et al. 2007) has provided excellent light curves in three filters (e.g., Jeffery et al. 2004, 2005; Aerts et al. 2006; Østensen et al. 2013). An illustrative example is the light curve of the HW Vir binary NY Vir (Vučković et al. 2007), which shows the pulsations in addition to the reflection effect and the eclipses (see Figure 28). Also the four-channel imager BUSCA at Calar Alto observatory (Reif et al. 1999) has provided multi-color observation of pulsating sdB stars (e.g., Falter et al. 2003). The degree index ℓ can be inferred from multi-color lightcurves and spectrophotometry by making use of the frequency dependence of the amplitude of an oscillation and its phase, and synthesizing the brightness variation expected from temperature, radius, and surface gravity perturbations across the stellar disk from model atmospheres. The optical UV band is of particular importance because of the much higher photospheric opacities in this wavelength range compared to filters transmitting light redder than the Balmer edge. Randall et al. (2005) developed the theoretical framework and showed that non-adiabatic effects are significant. Temperature and radius changes turned out to dominate the brightness variations, while surface gravity perturbations play a minor role only.

7.2.1. Mode Identification from Multi-color and Spectro-photometry

Tremblay et al. (2006) reviewed the state-of-the-art from a homogeneous analysis of multi-color data sets of six V361 Hya pulsators available at that time using the models of Randall et al. (2005). Their results suggested that a majority of the modes must have l-values of 0, 1, and 2 and predicted that $\ell = 4$ modes in rapidly pulsating B subdwarfs have a better visibility than $\ell = 3$

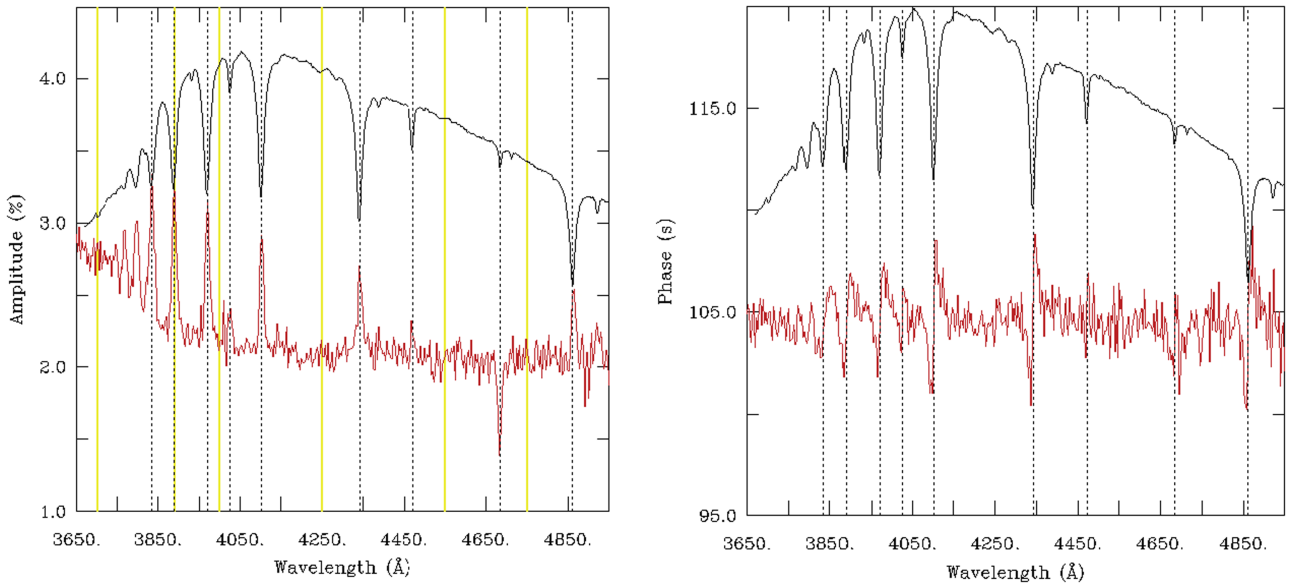

Figure 49. Left panel: observed amplitude of flux variations of EC 20338–1925 as a function of wavelength for the dominant pulsation mode f_1 (red). The averaged spectrum (black) is plotted on an arbitrary y-axis scale and also the central wavelengths of the Balmer and prominent He lines are marked by dotted vertical lines. Right panel: the same as the left panel, but for the observed phase. Increasing amplitudes of the flux variations correspond to increasing opacities e.g., in the Balmer line cores and the Paschen continuum. From Randall et al. (2010); copyright A&A; reproduced with permission.
(A color version of this figure is available in the online journal.)

ones. Charpinet et al. (2008a) used high-precision *UBV* photometry of Balloon 090100001 to show that its dominant pulsation mode is a radial one, while eight other modes have $\ell = 1$ or 2. The rapid pulsator HS 2201+261 (=V391 Peg) is a high priority target to asteroseismology because it hosts a Jupiter-mass planet (Silvotti et al. 2007). Subsequent WHT/ULTRACAM photometry allowed the dominant mode to be identified as a radial one and the second-highest amplitude mode as an $\ell = 1$ mode (Silvotti et al. 2010).

Spectrophotometric studies of EC 20338–1925 and EC 01541–1409 using ESO VLT/FORS were presented by Randall et al. (2010) and Randall et al. (2014b). Again the dominant modes turned out to be radial modes, while the much lower amplitude mode is an $\ell = 2$ pulsation (see Figure 49).

7.2.2. Mode-identification from Time-series Spectroscopy

Time-series spectroscopy allow stellar surface motions to be traced. This method was pioneered for sdB stars by, e.g., O'Toole et al. (2000, 2005a) who were successful in detecting many modes in velocity that were also seen in the light curves. Line profile variations caused by pulsations can be monitored (see, e.g., Figure 50; Telting et al. 2010) and allow the identification of pulsation modes (e.g., Vučković et al. 2007; Baran et al. 2008; Telting 2008; Telting et al. 2010).

A beautiful example is the bright high-amplitude pulsating subdwarf B star Balloon 090100001, for which Telting et al. (2008) presented an analysis of time-resolved high-resolution spectroscopy using 56 narrow absorption lines to compute cross-correlation functions that for each individual pulsation phase represent the average line-profile shape. The line profile variations with phase are displayed in Figure 51 and the RV curve in Figure 52. The pulsation amplitude of the main mode decreased from 19 km s^{-1} in the first epoch of observations (2004) to 14.5 km s^{-1} about two years later. The main pulsation mode is identified as $\ell = 1$ in accordance with the results of the light curve analysis by Charpinet et al. (2008a). In addition to RV variations, radial and non-radial pulsations lead to changing physical conditions (temperature and density variations) when parts of the stellar surface expand or contract. This is witnessed by variations *in* the shape of the line profile in the disk-integrate spectrum. Therefore, time-series spectroscopy can also be used to deduce temperature and gravity variations of pulsating stars, which will then allow mode identifications from fits of observed line shape variations to synthetic profiles calculated from appropriate model atmospheres (e.g., Tillich et al. 2007). Despite the stars' faintness, such analyses have recently been carried out for V361 Hya stars (e.g., Telting & Østensen 2004; Tillich et al. 2007; Telting et al. 2008; Vučković et al. 2009; Østensen et al. 2010d). As an illustrative example the temperature and gravity variations from the main pulsation mode in PG 1605+072 are shown in Figure 53 (Tillich et al. 2007). A cleaning procedure for phase binned spectra has been devised by Tillich et al. (2007) which allowed $T_{\rm eff}$ and $\log g$ variations as small as 100 K and 0.01 dex, respectively, to be measured.

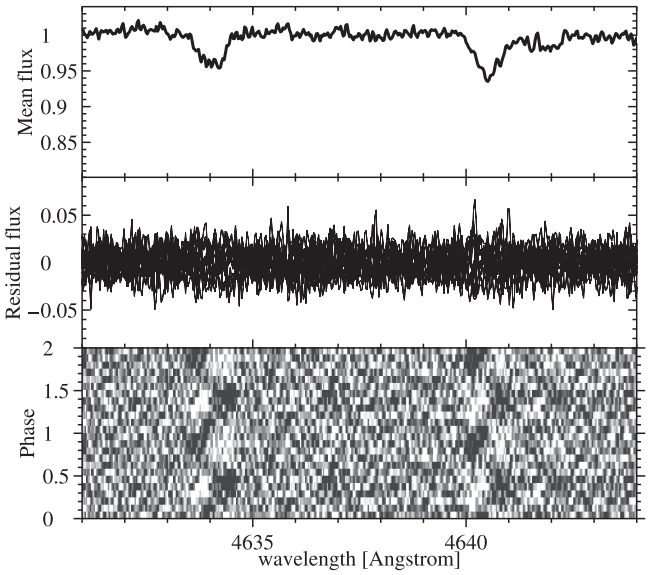

Figure 50. Line-profile variability in the strongest N III lines (4634.2 and 4640.6 Å) in the spectrum of the pulsating sdB star QQ Vir. The top panel shows the mean spectrum and the middle one twelve phase-binned spectra, after subtraction of the mean spectrum. These residual spectra are displayed as a function of pulsational phase in the gray-scale representation at the bottom. From Telting et al. (2010); copyright Ap&SS; reproduced with permission.

In most cases, the strongest mode is a radial one. Often the power spectrum is dominated by a single high-amplitude mode which renders the analysis of fainter modes difficult.

In summary, both multi-color lightcurves and time-series spectroscopy demonstrate that rapidly pulsating sdB stars, indeed, follow the expected amplitude hierarchy and the dominant pulsations correspond to radial modes.

7.3. The Kepler Legacy of Pulsating sdB Stars

Ground-based observations of pulsating stars suffer from many aliasing problems and the limited photometric accuracy and duration. Space missions such as *CoRoT* (Auvergne et al. 2009) and *Kepler* (Koch et al. 2010) largely overcome those limitations by providing long-term, uninterrupted, high-precision photometry. *Kepler* used two sampling rates (30 or 1 minute, respectively), and achieved very high precision (some tens of ppm, typically, see Figure 54 for an example, Reed et al. 2014), interrupted only every quarter of a year for reorientation of the spacecraft and monthly interruptions for data downlink during four years of operation.

A survey of the *Kepler* field for pulsating sdB stars by Østensen et al. (2010c, 2011) resulted in 13 *g*-mode V1093 Her pulsators and two multi-periodic V361 Hya *pulsators*.[21] The number of known sdB pulsators increased to 18 when another

[21] Four He-sdOB stars were also found in the *Kepler* field, none of which pulsates but two show irregular light variations (Østensen et al. 2010c; Jeffery et al. 2013).

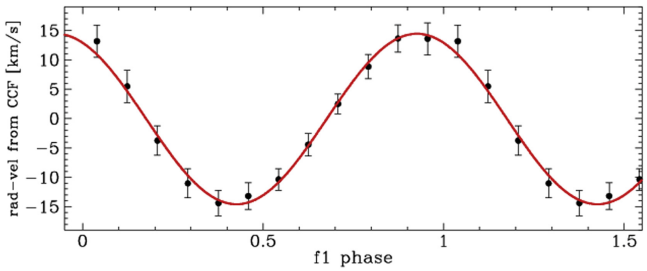

Figure 51. Main pulsation mode radial velocity variation of Balloon 090100001 as obtained from the cross-correlation analysis. From Telting et al. (2008); copyright A&A; reproduced with permission.
(A color version of this figure is available in the online journal.)

three V1093 Her pulsators were found in the open cluster NGC 6791 (Pablo et al. 2011; Reed et al. 2012).

The results from the analyses of *Kepler* light curves had an enormous impact on our understanding of pulsating sdB stars, the long-period V1093 Her pulsators in particular. Already the analysis of data from the first year of the *Kepler* mission revealed very rich frequency spectra of most sdB pulsators. Their analysis led to important discoveries, especially the *g*-mode periods turned out to be evenly spaced (e.g., Reed et al. 2011) and frequency multiplets became apparent (Baran 2012; Baran & Winans 2012; Pablo et al. 2012; Telting et al. 2012). Both patterns allowed pulsational and rotational periods to be assigned. Recently, the first analyses of the full *Kepler* data sets revealed stunning results, which we shall discuss in a bit more detail highlighting the detection of trapped modes, which pave the way to probe the internal structure and age of the stars (see Section 7.4), slow rotation and stochastic variations discovered for the first time.

7.3.1. Mode Identification of g-mode Pulsations

Even period spacings as predicted for the asymptotic limit have been found in the *Kepler* light curves of many sdB pulsators indicating high radial order modes. An example is NGC 6971-B3 (see Figure 55), for which Reed et al. (2012) derived period spacings near 245 s as appropriate for $\ell = 1$ modes.

For most of the *Kepler* sdB pulsators the mode spectrum is much more complex than that of NGC 6791-B3 with more than hundred oscillation frequencies detected. A Kolmogorov–Smirnov test is then applied to identify the most frequently observed spacing in a dataset. Østensen et al. (2014b) studied the light curve of KIC 10553698A (see Figure 56). Two minima are seen around $\Delta P = 260$ s and $\Delta P = 150$ s which can be readily identified as high-order ($n = 10$–35) modes with $\ell = 1$ or $\ell = 2$, respectively, because the ΔP relation between the two peaks matches the value of $\frac{1}{\sqrt{3}}$ expected from the asymptotic approximation. When only the high-amplitude modes (>1000 ppm) are considered the peak at $\Delta P = 150$ s disappears, indicating that they are $\ell = 1$ modes.

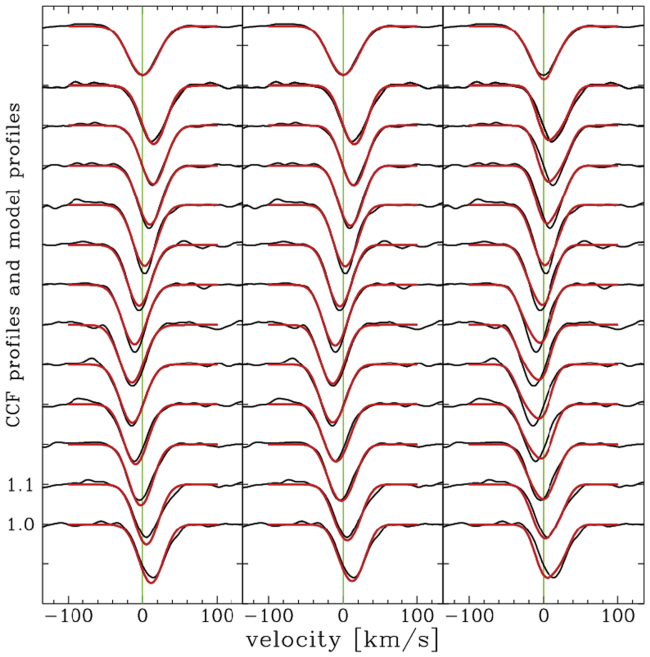

Figure 52. Observed cross-correlation functions (CCFs), offset as a function of pulsation phase by 0.1 continuum units (phase is increasing upwards), with the mean of all CCFs at the top. Overplotted are model predictions (in red): Left panel: model profile variations for a radial pulsation mode: $\ell = 0$, $i = 70°$, surface velocity amplitude 22 km s^{-1}. Middle panel: profile variations expected for a non-radial pulsation with $\ell = 1$, $m = -1$, $i = 50°$, surface velocity amplitude 35 km s^{-1}. Right panel: profile variations expected for a non-radial pulsation with $\ell = 2$, $m = -1$, $i = 40°$, surface velocity amplitude 38 km s^{-1}, which is the best-fit $\ell = 2$ mode. Both the radial and $\ell = 1$ mode fit better than any $\ell = 2$ mode. From Telting et al. (2008); copyright A&A; reproduced with permission.
(A color version of this figure is available in the online journal.)

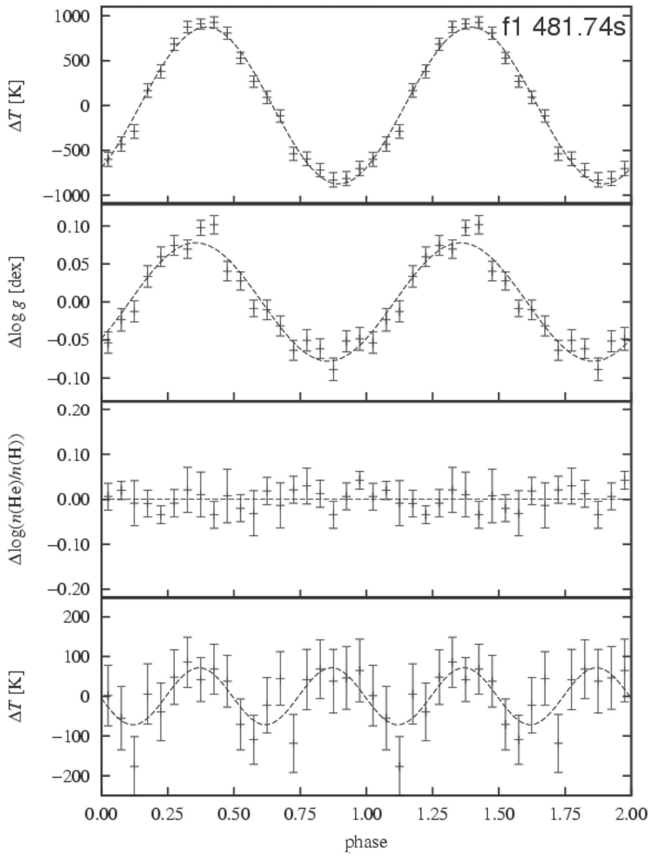

Figure 53. The variations of the atmospheric parameters of PG 1605+072 with pulsation phase derived from a quantitative spectral analysis of optical spectra (statistical error bars and sine fit are also shown). Upper panels: temperature and surface gravity variations. Lower panels: He/H abundance and the temperature residuals (with a sine fit for the first harmonic). From Tillich et al. (2007); copyright A&A; reproduced with permission.

KIC 10553698A: trapped modes. By sequencing the observed periods, Østensen et al. (2014b) noted that six modes were missing from the sequences, indicating that they are trapped modes. The trapping signature can be demonstrated in a diagram, where the period difference between consecutive modes are plotted against reduced period ($\frac{P}{\sqrt{l(l+1)}}$, see, e.g., Figure 3 of Charpinet et al. 2002). For KIC 10553698A drop-offs in both the $\ell = 1$ and $\ell = 2$ sequences were found by Østensen et al. (2014b) to occur for radial order $n = 20,26,27$ and for the $\ell = 1$ sequence at $n = 13$ (see Figure 57). These are g-modes trapped by transition zones such as the boundary of the convective core and the transition layers of changing chemical composition inside the star (conf. Section 7.4).

7.3.2. Rotation of Pulsating sdB Stars

From equidistant splitting of multiplets it became possible to determine the rotation of many *Kepler* sdB pulsators. A particularly striking example is KIC 10670103. Reed et al. (2014) detected as many as 278 pulsation frequencies in the 2.75 years of *Kepler* data with periods ranging 0.4–11.8 hr and amplitudes between 0.1 and 14 ppt. Splitting into frequency multiplets is obvious (see Figure 58), which translates into a rotation period of 88 ± 8 days. Such a slow rotation was unexpected but has also been seen in other *Kepler* pulsators, with rotation periods between ≈7 and ≈100 days (see Table 2 of Reed et al. 2014), irrespective of whether the star is single or in a binary. Surprisingly, no mode splitting could be found from the *Kepler* lightcurve of KIC 8302197, which implies that either the star is rotating very slowly with a period exceeding 1000 days or the rotation axis is seen pole-on (Baran et al. 2015b).

7.3.3. KIC 2991276: Stochastic Variations of a p-mode Pulsator

It is remarkable that some short-period pulsators (V361 Hya stars) show coherent pulsations that are stable in phase over many years. The most important case is HS 2201+261 (Silvotti et al. 2007), which showed periodic phase variations

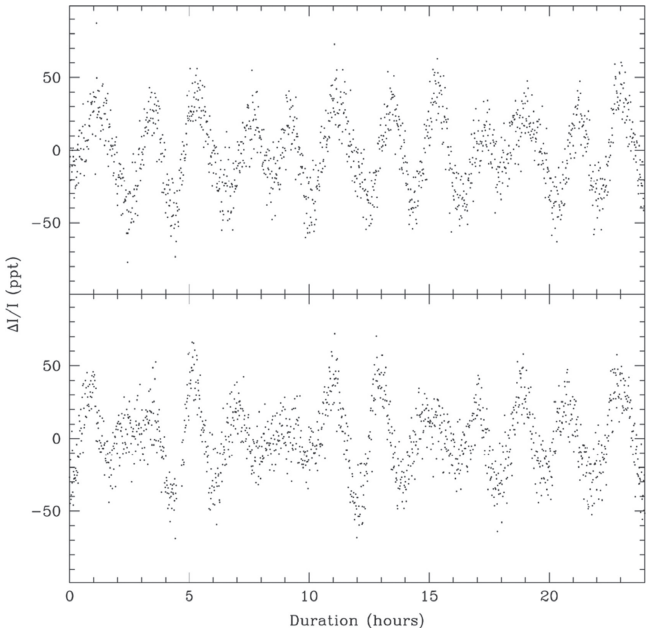

Figure 54. Sample *Kepler* light curve of KIC 10670103, showing 24 hr of data near the beginning (top) and end (bottom) of the 33 months long run with an impressive duty cycle of 93.8%. From Reed et al. (2014); copyright MNRAS; reproduced with permission.

($P = 3.2$ years) caused by an orbiting planet (see Section 6). On the other hand, amplitude variations seem to be quite common among V361 Hya stars, and recently, even evidence for stochastic pulsations in the sdB star KIC 2991276 was presented by Østensen et al. (2014a). Their analysis of the *Kepler* light curve which spans no less than 1051.5 days revealed that the pulsations in KIC 2991276 lose coherence on timescales of ≈60 days or more and are therefore stochastic in nature. Such stochastic oscillations are normal for solar-like pulsations and have already been suggested for the high-amplitude sdB pulsator PG 1605+072 (Pereira & Lopes 2005), but KIC 2991276 is the first sdB pulsator for which stochasticity has been established beyond doubt (see Figure 59). Because the oscillations are driven by the *Z*-bump, it is not obvious what causes the stochastic behavior. External influence by an unseen close compact companion would be an option. However, the star does not show RV variations and is therefore likely a single star unless a potential companion orbits on a highly inclined orbit. Østensen et al. (2014a), therefore, favor thermohaline convection in the driving zone which may temporarily stall the driving by changing the chemical composition.

Evidence is growing that KIC 2991276 may not be a unique case but several sdB pulsators observed with the *Kepler* satellite show some degree of stochasticity (Østensen, 7th meeting on hot subdwarfs and related objects[22]), which may be related to the question of why oscillation were found only for about 10% of rapidly pulsating sdB stars in the instability strip (Østensen et al. 2010b).

7.3.4. Pulsating sdB Stars in Binaries

Kepler data have also revealed that four pulsating sdB stars are actually in binaries, including one eclipsing binary (KIC 9472174 = 2M1938+4603, Østensen et al. 2010a), showing light variations due to the reflection effect in addition to oscillations. The three non-eclipsing sdB+dM binaries, host *g*-mode sdB pulsators which have rather long orbital periods of 0.443, 0.395 and 0.399 days (Kawaler et al. 2010b, 2010a; Pablo et al. 2011), respectively, difficult to discover from ground. Radial velocity monitoring of the *Kepler* sdB pulsators has confirmed binarity and led to the discovery of three additional ones. Hence, at least eight of the 18 pulsating sdB stars in the *Kepler* field are binaries (Telting et al. 2014a; Baran et al. 2016). Three of them have been used to investigate tidal synchronization timescales by comparing rotation periods measured from rotational splittings of pulsation frequency multiplets to the binaries' orbital periods (Pablo et al. 2012, see Section 7.6).

7.4. Internal Structure and Stellar Age from Asteroseismology

One of the first great achievements from asteroseismology of *CoRoT* and *Kepler* light curves was the determination of the internal structure of the stellar core and the age of sdB pulsators. A general review *of* stellar age determinations via asteroseismology is given by Aerts (2015). Because the *g*-modes are sensitive to the deep interior of the star, the structure of the helium-burning core, e.g., its size and composition, can be studied. The mixed convective core is bound by the chemical transition from He/C/O to He composition.

The first successful case study targeted KPD 0629-0016, which was discovered by Koen & Green (2007) to be a slowly pulsating sdB star. Charpinet et al. (2010) detected many *g*-mode pulsations in its *CoRoT* light curve, carried out the first detailed asteroseismic analysis, and found the total mass of $M_{\rm tot} = 0.471 \pm 0.002\,M_{\odot}$ to be in excellent agreement with the canonical mass. The age of the star with respect to the ZAEHB was derived to be 42.6 ± 1.0 Myr. In two subsequent studies, Van Grootel et al. (2010) and Charpinet et al. (2011b) used the same technique to analyze *Kepler* light curves of KPD 1943+4058 and KIC 2697388, respectively, which are also *g*-mode pulsators. KPD 1943+4058 was found to be slightly more massive ($M_{\rm tot} = 0.496 \pm 0.002\,M_{\odot}$) and younger ($18.4 \pm 0.1$ Myr) than KPD 0629-0016. Their hydrogen-rich envelopes turned out to be thicker than for the hotter short-period sdB pulsators, which is expected from models. For KIC 2697388 no unique set of parameters could be found, but two families of solution were identified which matched the

[22] http://www-astro.physics.ox.ac.uk/~aelg/SDOB7/booklet.pdf

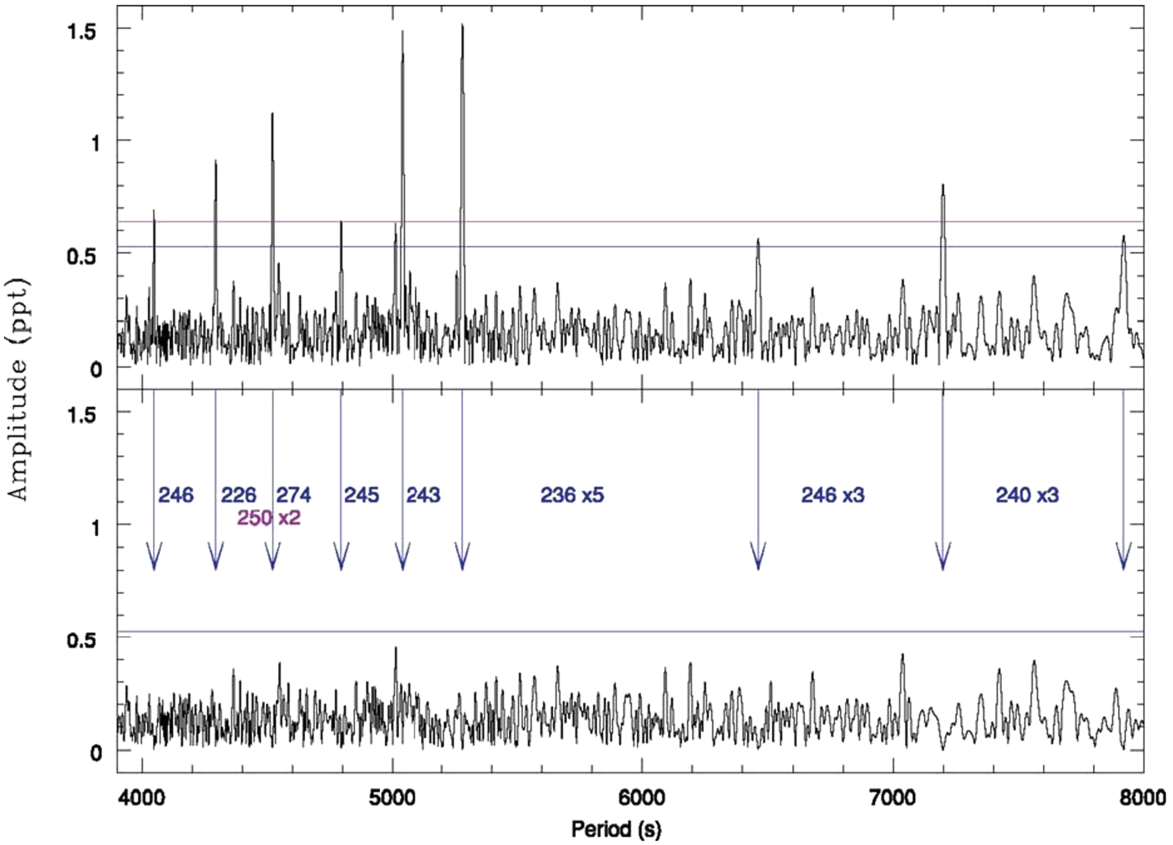

Figure 55. Temporal spectra of NGC 6791-B3. The top panel shows the original Fourier transform (FT) with the 4σ detection threshold and the false alarm probability = 99.9% limit. The bottom panel shows the pre-whitened FT. The fitted periods are indicated by arrows and the period spacings between them are given as integer numbers. Note the nearly constant period spacing as predicted by theory for the asymptotic limit. From Reed et al. (2012); copyright MNRAS; reproduced with permission.

(A color version of this figure is available in the online journal.)

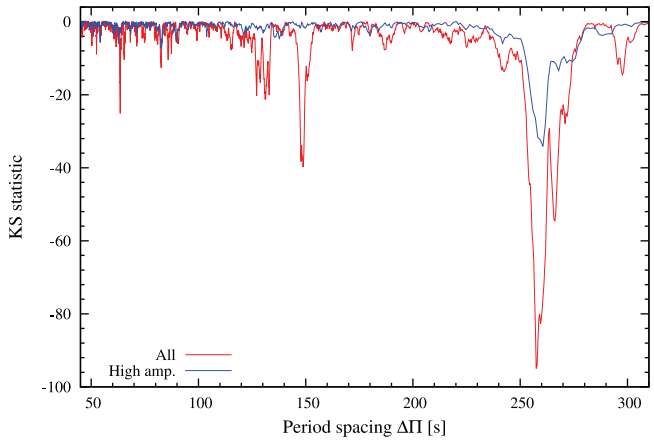

Figure 56. The g-mode pulsator KIC 10553698: Kolmogorov–Smirnov test statistic for the full frequency list (red) and high-amplitude ($A > 1000$ ppm) modes (red) respectively. From Østensen et al. (2014b); copyright A&A; reproduced with permission.

(A color version of this figure is available in the online journal.)

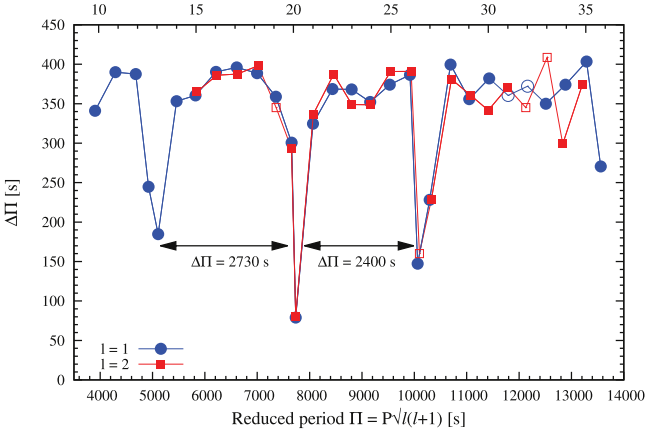

Figure 57. The g-mode pulsator KIC 10553698: Period difference (ΔPi) between consecutive modes of the $\ell = 1$ and $\ell = 2$ sequences, after converting to reduced periods. The asymptotic order of the modes, n, is indicated on the upper axis. From Østensen et al. (2014b); copyright A&A; reproduced with permission.

(A color version of this figure is available in the online journal.)

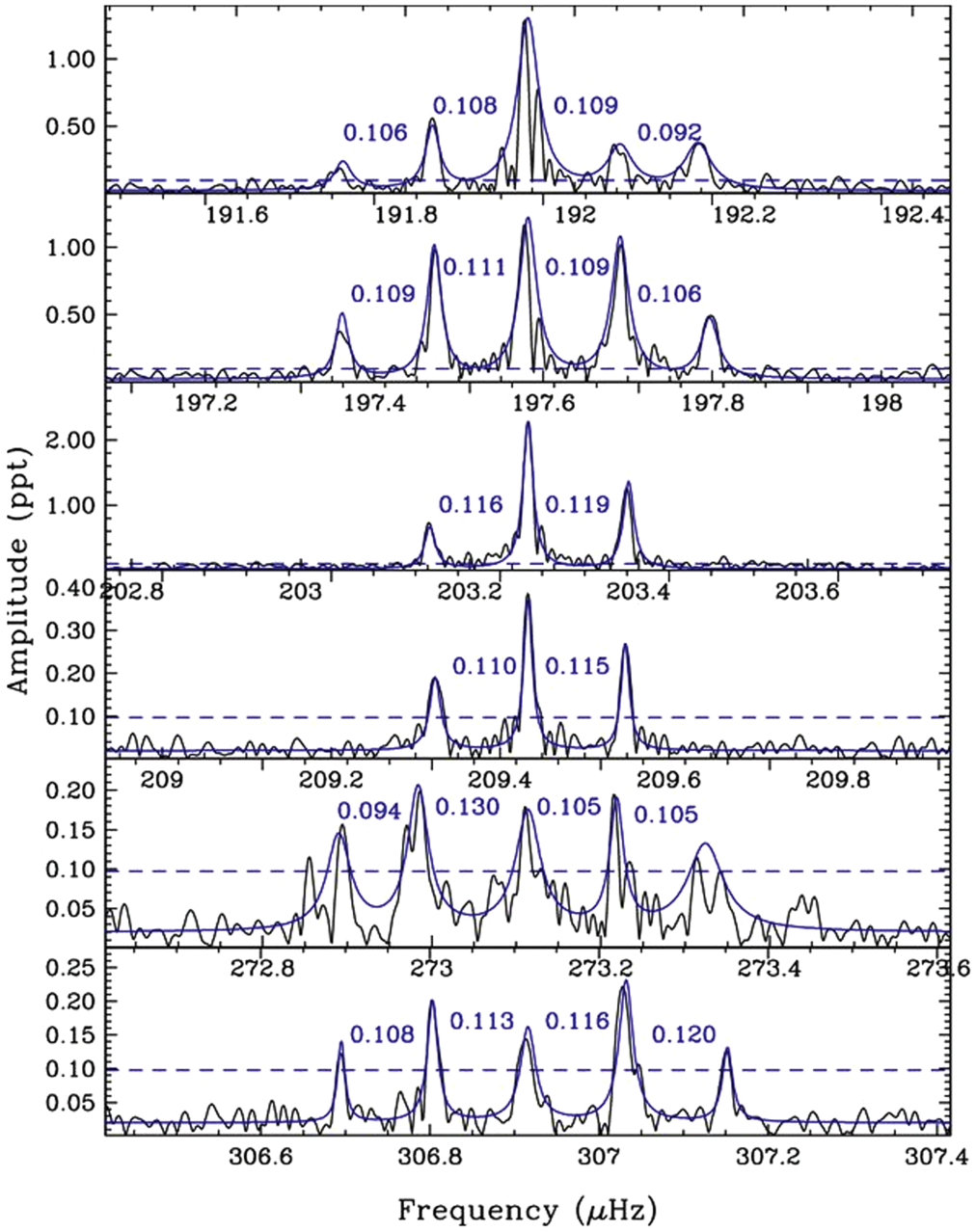

Figure 58. KIC 10670103: Fourier transform spectrum: $\ell = 2$ multiplets with splittings of roughly 0.11 μHz. From Reed et al. (2014); copyright A&A; reproduced with permission.
(A color version of this figure is available in the online journal.)

observation equally well. Nevertheless an upper limit for the age of 55 Myr (since the zero-age EHB) was derived.

All three studies concluded that the mixed convective cores are more massive than expected from evolutionary tracks. In the case of KPD 1943+4058, for instance, more than half (57%) of the total mass of the star is in the convective core, while only 25% of its helium nuclear fuel was burned. Therefore, it was concluded that extra mixing has to occur early-on in the evolution of the helium cores of sdB stars, caused, for example, by core overshooting, semi-convection and/or differential rotation. In order to remedy this discrepancy, Constantino et al. (2015) carried out an extensive investigation of the pulsation properties of core helium burning stars considering four different modes of mixing (no overshooting, standard-overshoot, semi-convection, and a new maximum-overshoot scheme) as well as varying the input

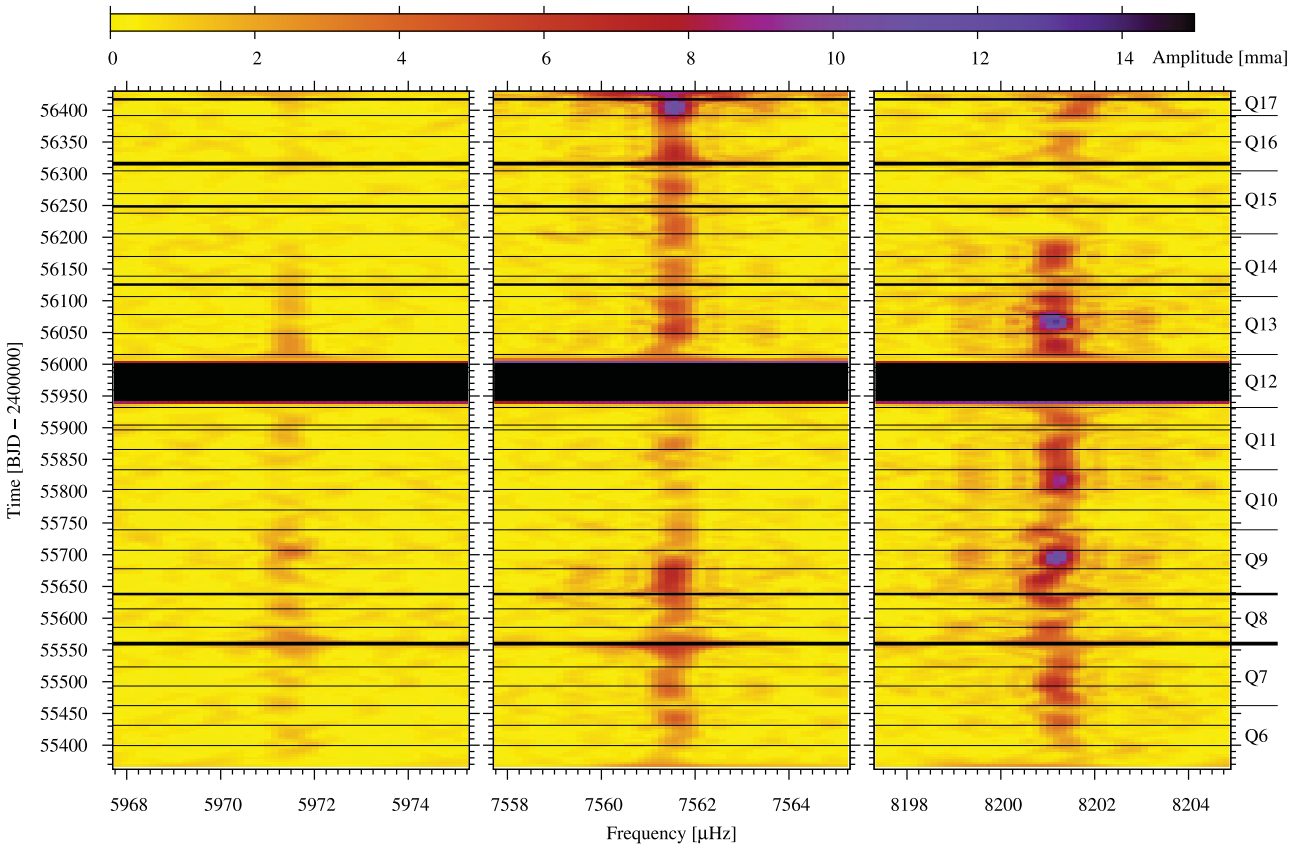

Figure 59. Stochastic variations of the strongest pulsations in KIC 2991276. Sliding Fourier transforms are computed for 20 day chunks of data. Amplitudes of up to 1.4% are reached in individual months, but vary substantially in amplitude as well as phase on timescales of about a month and occasionally disappear completely. The horizontal lines reflect data gaps. From Østensen et al. (2014a); copyright A&A; reproduced with permission.
(A color version of this figure is available in the online journal.)

physics (stellar composition and the He-burning reaction rates). The latter as well as three of the mixing schemes failed to increase the mixed-convective core to the size required to match the observations. The only successful models invoked a maximal-overshoot scheme proposed by Constantino et al. (2015), which, however, is an ad hoc scheme to ensure a maximum size of the core but lacks a physical explanation. Schindler et al. (2015) added atomic diffusion processes and confirmed this result by calculations with the MESA code. Because sufficiently large convective core masses resulted only for extreme overshooting, Schindler et al. (2015) called for realistic 3D hydrodynamical modeling of the convective core boundary (Viallet et al. 2013).

7.5. Stellar Mass and Radius: Asteroseismology versus Eclipsing Binaries

Mass and radius are the most fundamental parameters of a star, which can be derived by studying double-lined, eclipsing binaries by making use of Kepler's 3rd law. Asteroseismology provides an important alternative, already demonstrated convincingly for about a dozen of sdB pulsators (Fontaine et al. 2012; Van Grootel et al. 2014b). Hence it is obvious that pulsating stars in eclipsing binary systems are important benchmarks to understand structure and evolution of hot subdwarf stars because they allow cross-checking of results from asteroseismology with dynamical estimates (Huber 2014).[23] In 2009 only one such system, NY Vir was known, which Charpinet et al. (2008b) termed a "Rosetta stone" for the field. The asteroseismic modeling combined with a full orbital solution allowed mass and radius of the sdB star to be determined to an unprecedented precision (Vučković et al. 2007; Van Grootel et al. 2013a).

NY Vir remains the benchmark because it is a bright and well studied eclipsing sdB+dM system, which hosts a V361 Hya pulsator. Interest in this system increased when two circumbinary planets were discovered (Qian et al. 2012; Lee et al. 2014) making NY Vir one of the 18 known systems to host a circumbinary planet (Chavez et al. 2015; Baran et al. 2015a). Hence, the light variations of NY Vir are

[23] A general review of asteroseismology of eclipsing binary stars in the *Kepler* era (Huber 2014) includes sdB binaries.

regularly monitored (e.g., Kilkenny 2014), also by making use of robotic telescopes (see, e.g., Chote et al. 2014).

As already pointed out, siblings to NY Vir have been discovered recently by the MUCHFUSS survey, and by other studies. The *Kepler* satellite also discovered pulsating sdB stars in eclipsing binaries, which have their light curves measured to very high quality and length. Arguably the most important discovery is 2M1938+4603 = KIC 9472174 which is even brighter than NY Vir (Østensen et al. 2010a).

An unusually large number of oscillation frequencies were identified in the *Kepler* light curve of 2M1938+4603 at amplitudes too low to be detectable from the ground. Fifty five pulsation frequencies between 50 and 4500 μHz, were attributed to both *p*-mode and *g*-mode pulsations making 2M1938+4603 a hybrid pulsator (Østensen et al. 2010a). Combined with the RV semi-amplitude (see Section 5) and spectroscopic gravity, a mass of $M = 0.48 \pm 0.03\,M_{\odot}$ was derived, making the star a prime target for an asteroseismology analysis.

7.6. Rotation and Tidal Synchronization

For a pulsating star the rotation rate can be derived from the characteristic even splitting of the oscillation frequency multiplets (if $\ell \geqslant 1$). From ground-based light curves the explicit identification is difficult. However, the *Kepler* mission provided light curves for several sdB pulsators that allowed rotational splittings to be identified and rotation rates derived.

From ground-based observations the *p*-mode pulsations of NY Vir and Feige 48 have successfully been modeled and the rotation profile determined. Charpinet et al. (2008b) found that the rotation of the sdB star in the HW Vir binary NY Vir (orbital period $P = 0.101$ days) is synchronized to its orbit and that the sdB rotates as a solid body for at least the outer half of the star. The second case is Feige 48, a non-eclipsing sdB+dM binary (Latour et al. 2014a) of relatively long orbital period, for which Van Grootel et al. (2008) found tidally locked rotation and solid body rotation of the outer part of the star. However, this conclusion was called into question when Latour et al. (2014a) revised the orbital period downwards to $P = 8.25$ hr.

Synchronization timescales are predicted to strongly depend on the orbital period. Therefore it is important to study binaries of different orbital periods and ages. We might expect that the systems of shortest orbital periods are more likely to have reached synchronization (see Section 2.7.1).

Kepler light curves of sdB pulsators are very important in this respect. 2M1938+4603 has a short orbital period of about 1/8 days. The analysis of the rich pulsation spectrum of its primary derived from the *Kepler* light curve led Østensen et al. (2010a) to conclude that the sdB primary is rotating with a period close to the orbital one demonstrating that the sdB's rotation is indeed synchronized. However, for binaries with longer periods, this was found not to be the case. Pablo et al. (2011), for example, were able to infer a rotation period of 9.63 days for the sdB binary NGC 6791/B4. Because its orbital period is much shorter (0.399 days) this demonstrates that the rotation of the primary is not tidally locked to the orbit. The same is true for both of the *g*-mode pulsators of Kawaler et al. (2010a), which have orbital periods similar to that of NGC 6791/B4 but longer than that of 2M1938+4603.

From these results Østensen et al. (2013) concluded that tidal synchronization of the primary in sdB+dM binaries is efficient at periods of 1/8 days but not at 2/5 days. A new sdB pulsator, FBS 0117+396, was found in an 1/4 days orbit with a dM companion. Two short (337 and 379 s), as well as eight long periods (45 minutes to 2.5 hr) were discovered, making FBS 0117+396 a hybrid pulsator in an sdB+dM binary.

Because of its intermediate orbital period, Østensen et al. (2013) suggested that FBS 0117+396, would be important to investigate at which point the tidal forces become sufficiently strong to enforce synchronization in sdB+dM systems. However, the rotational period splittings have not yet been determined.

7.6.1. Radial Differential Rotation

Recently, radial differential rotation has been detected in red giants and HB clump stars as well as in a white dwarf binary from *Kepler* data. In red giants the rotational splitting of mixed modes showed that in several cases the stellar cores rotate at least five times faster than the stars' envelopes (e.g., Beck et al. 2012). In the white dwarf binary SDSS J1136+0409, the core rotates at a period of $P = 2.49 \pm 0.53$ hr considerably faster than the orbital period ($P \approx 6.9$ hr, Hermes et al. 2015), indicating that the core rotation is not tidally locked to the orbit. Mosser et al. (2012) studied a large sample of red giants and conclude from the observed rotational splittings that the mean core rotation significantly slows down during the last stages of the red giant branch, more quickly than expected. Aerts (2015) concludes: "Core-to-envelope rotation rates during the red-giant stage are far lower than theoretical predictions, pointing toward the need to include new physical ingredients that allow strong and efficient coupling between the core and the envelope in the models of low-mass stars in the evolutionary phase prior to core helium burning."

In the light of these discoveries, it would be very interesting to search for radial differential rotation in sdB pulsators that show *p*- and *g*-modes at the same time. The number of such hybrid pulsators keeps growing thanks not only to the *Kepler* mission but also through ground-based discoveries (e.g., Baran et al. 2011). Because *p*- and *g*-mode pulsations probe different regions inside the star, the combination of both allows the rotation of the interior with depth to be traced. A first result was presented by Foster et al. (2015) who analyzed the *Kepler* light curve of the hybrid-pulsator KIC 3527751 and found that the rotation period derived from the *p*-mode splitting ($P = 15.3 \pm 0.7$ days), which trace the outer envelope, is

smaller than that from the splitting of the g-modes ($P = 42.6 \pm 3.4$ days) which probe deep layers of the star. They conclude that the core rotates more slowly than the outer regions of the star. If confirmed, this finding would be the first discovery of radial differential rotation of an sdB and in fact very surprising, because it is the opposite to what is expected from the results for the rotation of RGB stars and the white dwarf binary discussed above.

7.7. A New Class of sdO Pulsators in Globular Clusters

Also among the sdO stars, a rapid pulsator was discovered (Woudt et al. 2006), which exhibits very rapid p-mode pulsations with periods of 60–120 s. Fontaine et al. (2008b) readily explained the pulsation as driven by an iron group opacity bump. However, despite a lot of observational effort, searches for pulsating subluminous O stars met with little success (e.g., Rodríguez-López et al. 2007; Johnson et al. 2014). The only new discovery is the reclassification of EO Ceti (=PB 8783), the second sdB star found to pulsate (Koen et al. 1997), which turns out to be of spectral type sdO (≈50,000 K or hotter), with an F-type companion (Østensen 2012; Van Grootel et al. 2014c). However, irregular yet unexplained variations in light or RV were found for some He-sdO stars (Green et al. 2014; Geier et al. 2015b).

Randall et al. (2011) carried out a search for sdO pulsators in the globular cluster ω Cen similar to the field star SDSS J160043.6+074802.9 (V499 Ser, Woudt et al. 2006), which is a very hot, helium-enhanced star (68,500 K, log (He/H) = 0.64, Latour et al. 2011).

The five pulsators that were discovered by Randall et al. (2011) appear to form a homogeneous class in terms of pulsation properties and atmospheric parameters. Like for V499 Ser the pulsation periods are short (80–125 s), but ω Cen stars are considerably cooler (48,000–54,000 K) than the field sdO and helium-poor rather than helium-rich. Therefore, Randall et al. (2014a) argue that these stars do not exist among the field sdO population, because a dedicated monitoring of 36 sdO stars in the field (Johnson et al. 2014) failed to uncover a single pulsator. Randall et al. (2016) identified the same κ mechanism that excites the p-mode instability in the sdB variables to drive the rapid pulsations in the ω Cen variables. However, the models predict excited pulsation at somewhat higher temperatures and shorter periods than observed. This discrepancy may be resolved, when more heavy element opacities were included in the calculations.

Hence, globular clusters seem to be a more promising place to search for pulsating stars among O subdwarfs. Indeed, six pulsating subdwarfs were found among the blue hook stars in the massive globular cluster NGC 2808 (Brown et al. 2013a). Their pulsation periods range from 85 to 149 s and UV amplitudes of 2.0%–6.8%, similar to that of the ω Cen stars. However, their atmospheric parameters require a proper determination. They span a rather wide range of UV color which might indicate a much wider spread in temperature than for the ω Cen stars. Hence, besides the binary fraction and the atmospheric parameters the pulsational properties of field and cluster population differ markedly. However, if its effective temperature and helium content could be better constrained, EO Ceti (see above) may turn out to be the first field counterpart to the ω Cen variables.

7.8. The Enigmatic Intermediate He-sdB LS IV−14°116 (V0366 Aqr)

LS IV−14°116 (V0366 Aqr) is the only intermediate He-sdB showing multi-periodic light variations (Ahmad & Jeffery 2005), very likely caused by non-radial g-mode pulsations (Green et al. 2011) because of the long periods (1953 s for the dominant mode and 2620–55,084 s for others). Its effective temperature and gravity are inconsistent with domains known to be unstable to g-mode oscillations, that is LS IV−14°116 is out of place in the $T_{\rm eff}$–log g diagram (see Figure 46, according to which short-period p-mode pulsations were expected). Recently, Jeffery et al. (2015a) detected RV variations of $>5\,{\rm km\,s^{-1}}$ caused by the dominant oscillation mode.

Miller Bertolami et al. (2011) and Miller Bertolami et al. (2013) suggested that LS IV−14°116 might represent the first known case of ϵ-driven pulsation. Naslim et al. (2012) suggested that the He-sdB stars have not yet settled onto the helium main-sequence and are still evolving toward it. Driving by the ϵ-mechanism would be acting on helium-burning shells which occur sequentially when the star transits from the tip of the RGB to the EHB. Recently, Randall et al. (2015) derived a significantly higher surface gravity for LS IV−14°116, which places the star on the EHB; that is, in the core helium-burning phase, during which the ϵ mechanism is unlikely to work. The evolution of late flashers may reach high gravities as well for low mass progenitors just before settling on the EHB (Miller-Bertolami 2016, private communication). Hence, the evolutionary status of LS IV−14°116 and the driving of its pulsations remain issues to be solved.

7.9. The K2 Mission, Kepler Goes on

The two-wheel mission of the *Kepler* space telescope (*K2*) has already generated important results. Jeffery & Ramsay (2014) studied the *Kepler K2* light curve of the pulsating subdwarf B star EQ Psc. Besides the rich g-mode pulsation spectrum, light variation of 2% amplitude were discovered, probably caused by the reflection effect. This indicates that EQ PSc is a binary with a cool companion orbiting the sdB in 19.2 hr, the longest period found for a sdB+dM binary up to now. Reed et al. (2016) discovered another new g-mopde pulsator, PG 1142–037, from the first *K2* campaign (14 periodicities between 0.9 and 2.5 hr with amplitudes below

0.35 ppt). In addition variations caused by ellipsoidal deformation and Doppler boosting reveal that the sdB has a compact companion (most likely a white dwarf) in a 13 h orbit. Despite the close orbit no rotationally split pulsation multiplets were found, indicating that the rotation period is longer than 45 days and, therefore, PG 1142–037 is the first case for non-synchronized rotation in an ellipsoidal variable.

8. Low Mass White Dwarfs: The Close Relatives of sdB Stars

The formation of sdB stars through mass transfer in close binaries requires some fine tuning, because mass transfer must start close to the tip of the red giant branch, that is the core must have grown close to the canonical mass to ignite helium burning when the red giant progenitor fills its Roche lobe. Hence binaries must exist which result from envelope stripping of a red giant star well before core helium burning ignites (see Figure 60). The remnant of such an event would be a helium white dwarf. As in the case of the sdB stars, the companion is expected to be a either a normal dwarf star or a white dwarf.

The mass distribution of DA white dwarfs revealed the existence of low mass white dwarfs (Bergeron et al. 1992) with masses below the canonical mass for helium ignition (0.47 $M_{\odot}$) which were, therefore, considered as helium core white dwarfs. Later studies of larger samples (e.g., Liebert et al. 2005, see Figure 61) confirmed the existence of a population of white dwarfs with a mean mass of 0.4 $M_{\odot}$. Since the evolutionary time for a single star to evolve into a helium-core white dwarf would exceed the age of the universe by far, Bergeron et al. (1992) concluded that they must be in close binaries, which was, indeed, confirmed *in* many cases by observations (Marsh et al. 1995, and others) thereafter.

8.1. Low Mass White Dwarfs (0.3 to 0.5 $M_{\odot}$)

About 10% of the white dwarfs have masses below the 0.5 $M_{\odot}$ limit and are often referred to as helium white dwarfs. However, it is premature to assume that white dwarfs with masses below the canonical mass for core helium burning are of helium composition, because intermediate mass ($\geqslant$2.3 $M_{\odot}$) red giants may ignite helium in non-degenerate conditions at core masses as low as 0.33 $M_{\odot}$ (Han et al. 2002; Hu et al. 2008; Prada Moroni & Straniero 2009). Hence, a bona-fide helium-core object has to be less massive than 0.33 $M_{\odot}$. We shall address such stars in see Section 8.2.

8.1.1. Low Mass White Dwarf in Single Degenerate Systems: WD+dM

Because of their similar absolute visual magnitudes, dM stars can be detected as companions to hot white dwarfs. Their SED is unique, with the white dwarf dominating the blue, the dM the red part of the spectrum. Hence, they are easy to detect and have, indeed, been discovered in large numbers (Rebassa-Mansergas et al. 2013), and a significant fraction of them are hosting white dwarfs of low mass (<0.5 $M_{\odot}$, Rebassa-Mansergas et al. 2011). Compact WD+dM binaries may be the product of CE evolution and, therefore, we might expect that the properties of those binaries are similar to that of the sdB+dM binaries. Many of the WD+dM systems are RV variable and orbits have be determined for several *dozen* with periods ranging from 0.08 to almost 10 days (Nebot Gómez-Morán et al. 2011; Rebassa-Mansergas et al. 2012).

Kupfer et al. (2015) compared the period distributions of the WD+dM and sdB+dM systems and find the former to be much wider than the latter. Hot subdwarfs with dM companions have very short periods (less than 0.3 days). However, this difference is likely *to be* due to observational bias, because the WD+dM systems are identified spectroscopically, while most sdB+dM systems were identified photometrically via the reflection effect, the amplitude of which decreases with increasing period, making it difficult to find long period systems.

Rebassa-Mansergas et al. (2011) found that 1%–20% of the low mass white dwarfs in their sample are not RV variable on timescales of weeks or longer. Hence they must be wide binaries not formed by common envelope evolution, similar to IP Eri, a K0 (sub)giant + He-WD system (Vennes et al. 1995), with an eccentric orbit (e = 0.25) and a long period of P = 1071 days (Merle et al. 2014). It is interesting to note that the orbit of IP Eri is very similar to those of the long-period sdB & F/G/K binaries discussed in Section 5.7.1.

For an extensive discussion on the origin of low-mass white dwarfs see Rebassa-Mansergas et al. (2011), who also discussed several evolutionary scenarios that may lead to wide binaries and single low mass white dwarfs, including triple mergers, similar to that put forward by Clausen & Wade (2011) to explain wide sdB & F/G/K binaries.[24]

8.1.2. Low Mass White Dwarfs in Double Degenerate Systems

The SPY survey of DA white dwarfs has found 39 double degenerates among 679 observed white dwarfs which corresponds to a binary frequency of 5.7% (Koester et al. 2009). The binary frequency for low mass white dwarfs is much higher (>70%, Brown et al. 2011a), even larger than that of sdB stars. The number of double degenerates has been boosted recently, by the discovery of dozens of ELM white dwarfs, for which the binary frequency is close to 100% (see Section 8.2).

A spectacular recent addition is WD 1242−105 in the solar neighborhood, at a distance of only 39 pc. It is a double-lined

[24] More exotic scenarios for the formation of He-WDs have also been proposed that do not involve binary evolution, e.g., stellar collisions in the dense cores of globular clusters (Knigge et al. 2008) or tidal stripping of a red giant star by a supermassive black hole (Bogdanović et al. 2014).

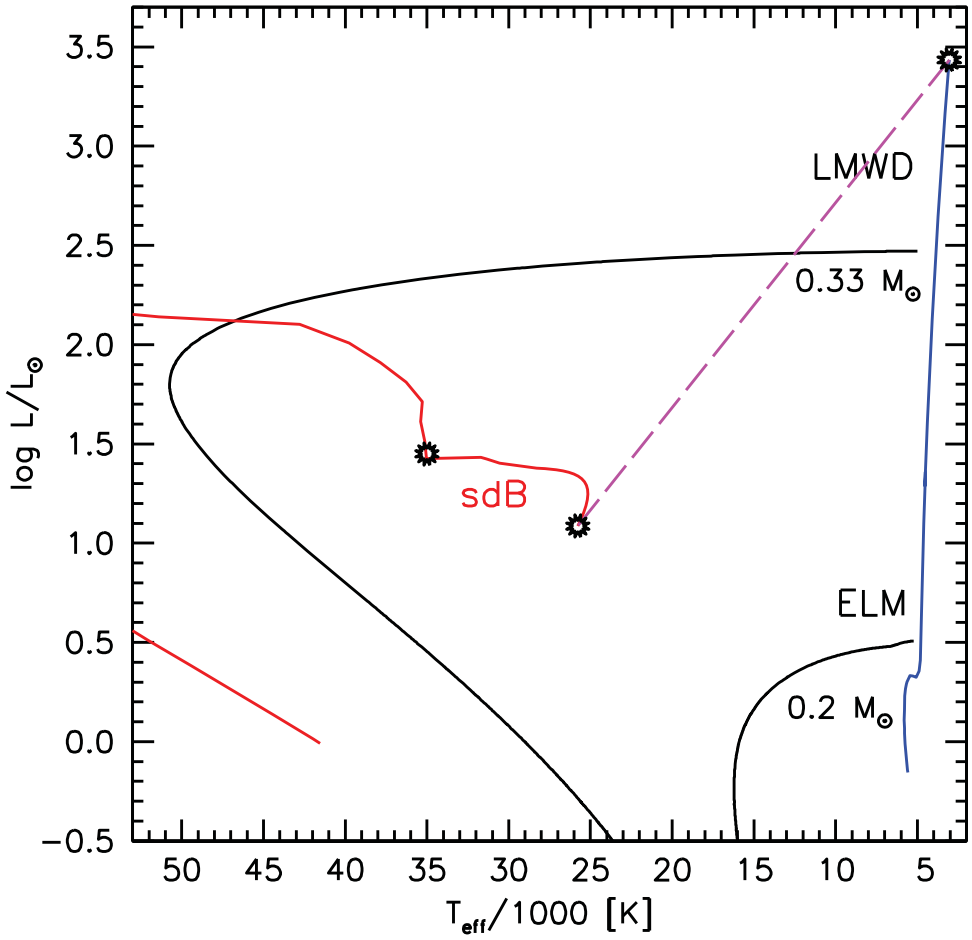

Figure 60. Sketch of the evolution of an 1 $M_{\odot}$ star (blue) from the zero age main sequence to the tip of the red giant branch, stripped at a core mass of ≈0.2 $M_{\odot}$ to form an extremely low mass (ELM) white dwarf; stripped at ≈0.33 $M_{\odot}$ to form a low mass white dwarf (LMWD), and at the onset of the helium flash to form an sdB star (dashed line). The beginning and the end of the core helium burning of the sdB evolution (red line) is also marked.
(A color version of this figure is available in the online journal.)

spectroscopic binary consisting of two white dwarfs of 0.56 $M_{\odot}$ and a 0.39 $M_{\odot}$, respectively, in an 0.1188 day orbit (Debes et al. 2015).

8.1.3. Single Low Mass White Dwarfs

However, not all low-mass WDs are found in binary systems (Maxted et al. 2000a; Napiwotzki et al. 2007). Brown et al. (2011a) estimate that the fraction of apparently single low-mass white dwarfs is less than 30%. The origin of these stars remains a puzzle just like the origin of the singleton sdB stars. Similar scenarios as for the formation of sdB singles have been advocated (Justham et al. 2009; Rebassa-Mansergas et al. 2011).

8.2. Thermally Bloated Hot White Dwarfs, Proto-helium White Dwarfs, or Extremely Low Mass White Dwarfs

Even the largest sample of white dwarfs (Kepler et al. 2015) did not find white dwarfs with masses below 0.3 $M_{\odot}$. Only recently several dozen of these extremely low-mass (ELM) white dwarfs have been found. White dwarfs are usually thought to have surface gravities exceeding $\log g = 7$ and correspondingly show strongly Stark broadened spectral lines. The newly discovered white dwarfs of very low mass (≈0.15 to 0.3 $M_{\odot}$) have lower gravities ranging from $\log g = 4.5$ to 7. Therefore, their colors and spectra are quite different from classical white dwarfs. Actually, very-low mass white dwarfs have been found by a survey that *was* primarily aimed at finding hypervelocity stars of late B-type (Brown et al. 2006) by exploring a sparsely populated region in a two-color diagram (Brown et al. 2010b, 2013b; Kilic et al. 2011, 2012). The low gravities indicate that the stars are bloated, that is they have not yet reached the cooling sequence. When such a star is formed by detaching from its binary Roche lobe it retains a rather thick envelope (≈0.01 $M_{\odot}$) which sustains hydrogen burning resulting in transition times to the cooling sequence up to several billion years (depending on the stellar mass, Istrate

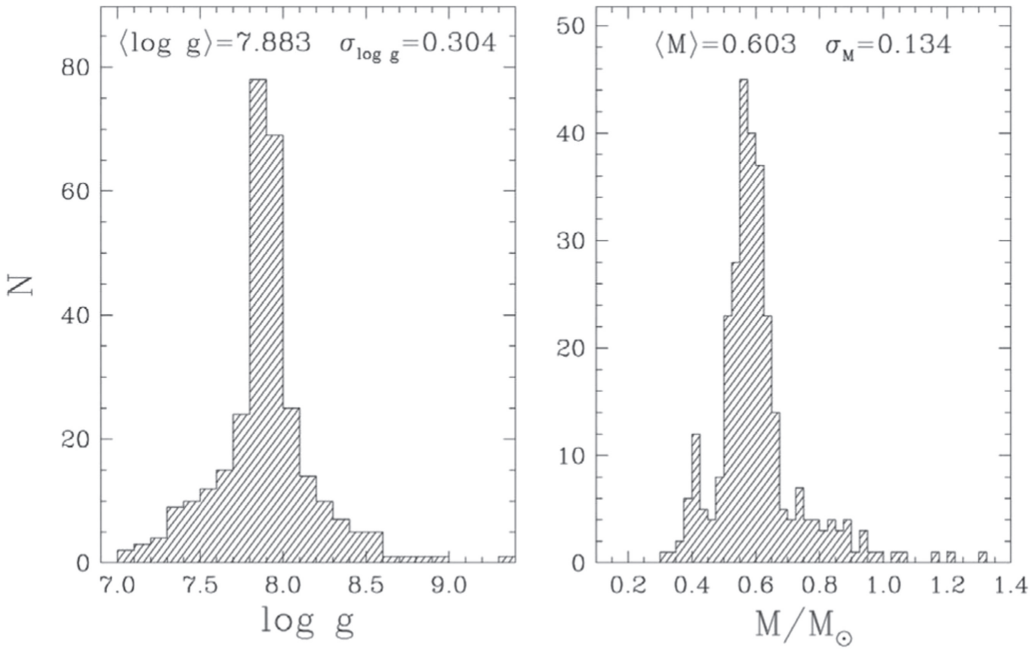

Figure 61. Gravity and mass distribution of DA white dwarfs. Note the presence of a low-mass population at M ≈ 0.4 $M_{\odot}$. From Liebert et al. (2005); copyright ApJ; reproduced with permission.

et al. 2014). These very-low mass objects were termed "helium core white dwarf progenitors" (Heber et al. 2003), "proto-helium white dwarfs" (Istrate et al. 2014),"thermally bloated, hot white dwarf" (Carter et al. 2011), "pre-He-WD" (Maxted et al. 2013), or "ELM white dwarfs" (Brown et al. 2010b), which we regard as synonymous.

Interest in low mass white dwarfs arose when such objects were discovered as companions to millisecond pulsars. van Kerkwijk et al. (1996) showed that the companion of a neutron star in the millisecond pulsar PSR J1012+5307 is a low-mass helium-core object, for which Driebe et al. (1998) determined a mass of $M = 0.19 \pm 0.02\,M_{\odot}$ and a cooling age of 6 ± 1 Gyr. Istrate et al. (2014) list another eight milli-second pulsars in short period binaries with a low-mass ($<0.21\,M_{\odot}$) proto-helium white dwarf. Further discoveries unrelated to pulsar binaries followed (Heber et al. 2003; Liebert et al. 2004; Kawka et al. 2006, 2010; O'Toole et al. 2006; Kilic et al. 2007), but the number of such stars remained small until a dedicated search was initiated using the SDSS data base (Brown et al. 2010b, 2013b; Kilic et al. 2011, 2012). Because these stars are expected to result from close binary evolution, they were monitored for RV variations with a very high success rate. The majority of them is, indeed, found to have orbital periods shorter than one day, the companions being white dwarfs as well.

An ELM white dwarf in a triple system. Ransom et al. (2014) reported the discovery of PSR J0337+1715, a triple system of a neutron star orbited by *two* white dwarfs. PSR J0337+1715 contains a $1.438\,M_{\odot}$ radio millisecond pulsar and two low mass WDs. The inner WD companion is an ELM with $0.197\,M_{\odot}$ on a 1.63 days circular orbit. The system is highly hierarchical because the outer white dwarf is distant orbiting in 327 days (Ransom et al. 2014). The system must have survived *three* phases of mass transfer and, in addition, has managed to survive a supernova explosion. Tauris & van den Heuvel (2014) presented a model to explain the evolution of this fascinating triple and find the two white dwarf companions to match the theoretical expectations from the mass–orbital period relation of WDs (e.g., Tauris & Savonije 1999).

Kaplan et al. (2014b) discovered the optical counterpart of the radio source and identified it with the inner white dwarf companion. Their spectroscopic analysis resulted in the mass and radius of the inner WD which are fully consistent with predictions for a young ELM WD. Its high effective temperature (15,800 K) implies that the inner white dwarf is relatively young and formed last, as expected from models (Tauris & van den Heuvel 2014).

Eclipsing ELM white dwarfs. Eclipsing binaries are of great importance, because their masses and radii can be tightly constrained. Hallakoun et al. (2016) found an eclipsing binary consisting of two low mass white dwarfs of 0.38 and $0.23\,M_{\odot}$, respectively. Now six eclipsing systems are known, with CSS 41177 being the only double-lined eclipsing WD system known (Bours et al. 2014, 2015), for which mass and radius could be determined to unprecedented precision.

8.2.1. Confusion with Other Types of Star

The transition track of a proto-helium white dwarf from the red giant branch to the cooling sequence leads through a wide area of the ($T_{\rm eff}$, log g) plane and across the main sequence and the (extreme) horizontal branch, and therefore, proto-helium white dwarfs may be confused with normal stars. In fact a few such cases are known. The most extreme case, HZ 22, even mimics an early type main-sequence star, while the sdB stars HD 188112, KIC 06614501, SDSS J0815+2309, SDSS J1625 +3632 and GALEX J0805−1058 mimic sdB stars, albeit at a somewhat higher gravity (see Figure 62).

HZ 22 (UX CVn)—imitating a massive B star HZ 22 (UX CVn, Young et al. 1972; Greenstein 1973), is star No. 22 in the very first survey for faint blue stars at high Galactic latitudes (Humason & Zwicky 1947). The object was discussed at the first conference on faint blues stars (Luyten 1965) because its spectrum mimics that of an early-type main-sequence star, which would place the star very far from the Galactic plane, where no young star had been found at that time. Light and RV variation showed that it must be a single-lined binary. The orbital period turned out to be about half a day (Young et al. 1972), which is too short to accommodate a massive B star. Hence HZ 22 must be a subluminous B star (Smak 1969). The strong ellipsoidal light variations indicate that the companion must be a white dwarf (Young & Wentworth 1982). Using evolutionary models Trimble (1973) found that HZ 22 is a helium-core object of 0.3–0.4 $M_{\odot}$. Schönberner (1978) carried out similar calculations and derived a mass of 0.39 $M_{\odot}$ confirming the identification of HZ 22 as a proto-helium core white dwarf. The star remained unique, when Greenstein & Sargent (1974) completed their seminal work on faint blue stars. Shimanskii (2002) revisited the star and derived atmospheric parameters and metal abundances from a detailed quantitative spectral analysis of medium-resolution (2.6 Å) optical spectra obtained at the 6 m telescope of the Special Astrophysical Observatory. The helium, carbon and iron deficiency are consistent with an old evolved star, i.e., support the interpretation as a proto-helium core white dwarf. In the light of these results Shimansky et al. (2002) reconsider the evolutionary status of the system and confirm the previous interpretation of the system. Shimanskii (2002) noted that their spectrum of HZ 22 taken in 1999 differed from that published by Greenstein (1973), in particular with respect to the He II 4686 Å line which is present in their spectrum but absent in the early one. This led to the conjecture that the star has increased its temperature by 2000 K within 40 years and, hence, must be in phase of rapid evolution. This conjecture, however, needs confirmation, because of the respective uncertainties of the temperature determinations. Although HZ 22 remains a unique and fascinating object, it has not gotten the attention in recent years that it deserves.

Proto-helium white dwarfs imitating sdB stars. Heber et al. (2003) found the sdB star HD 188112 to be of somewhat higher gravity than a core-helium burning EHB star from a quantitative spectral analysis. Its *Hipparcos* parallax combined with the spectroscopic gravity allowed the mass to be determined to be 0.23 $M_{\odot}$, consistent with evolutionary model predictions for stripped RGB stars by Driebe et al. (1998) (see also Latour et al. 2016). The star turned out to be a short period binary with a white dwarf companion of at least 0.7 $M_{\odot}$. Two very similar sdB binaries were discovered recently in the *Kepler* field (KIC 6614501, Silvotti et al. 2012) and in the *GALEX* survey (GALEX J080510.90−105834.00, Kawka et al. 2015), respectively. A star of similar temperature but somewhat higher gravity was found by Kilic et al. (2011).

8.2.2. Evolution of ELM White Dwarfs

Thermal instabilities in the hydrogen burning shell are expected to occur during the post-RGB evolution (Gautschy 2013), but theoretical models (Driebe et al. 1999; Sarna et al. 2000; Nelson et al. 2004; Panei et al. 2007; Althaus et al. 2013; Gautschy 2013; Istrate et al. 2014) disagree about the thickness of the hydrogen envelope and the range of helium core masses for which shell flashes occur. Because hydrogen is being burnt efficiently during a flash, the evolutionary lifetime is shortened considerably, if such a flash occurs. Many of these differences may be due to differences in the treatment of the physical processes within the donor star and the secular evolution of the binary itself (Nelson et al. 2004). The least massive stars are predicted not to suffer from flashes and therefore, quiescent hydrogen burning guarantees a long evolutionary timescale (up to a few Gyr). Althaus et al. (2013) showed that gravitational settling has an important effect on the occurrence and strength of flashes which reduce the hydrogen envelope.

8.3. Abundance Pattern of ELM White Dwarfs

Few ELM white dwarfs are sufficiently bright for detailed quantitative abundance analyses. Nevertheless, Gianninas et al. (2014a) were able to determine abundances (or upper limits thereof) of He, Ca, and Mg in their sample of 61 stars. Calcium lines were found in all stars with log $g < 6.0$.

Detailed abundance studies are available for four objects, only. Latour et al. (2016) analyzed very high resolution ultraviolet spectra of HD 188112 taken with the Hubble Space telescope's STIS spectrograph and derived abundances of 14 metals and upper limits for C, N, and O, which turn out to be all subsolar (with the exception of lead that is solar, see upper panel of Figure 63). A comparison with predictions from

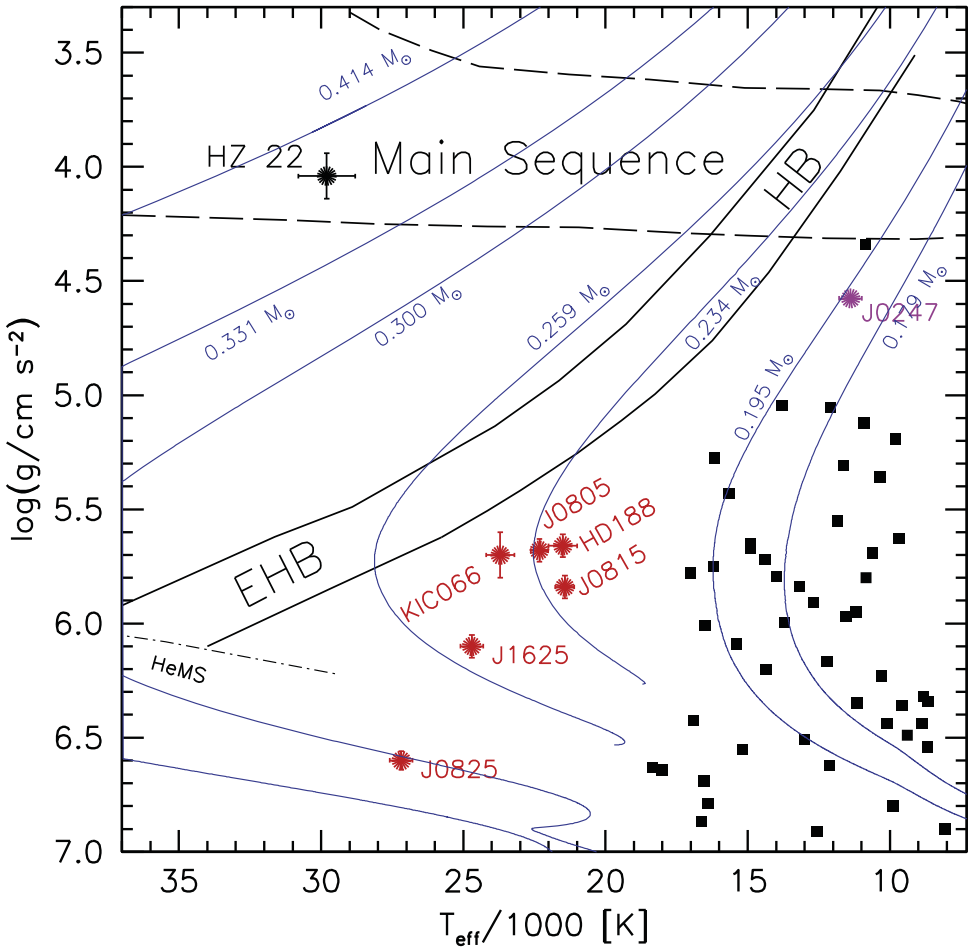

Figure 62. Distribution of proto-helium white dwarfs in the $T_{\rm eff}$–log g diagram from the list compiled by Althaus et al. (2013). Tracks for the evolution of proto-helium white dwarfs are from Driebe et al. (1998) and labelled with their mass. The main sequence band is shown (dashed lines) as well as the HB and EHB band. Note that the tracks cross both bands leading to confusion for objects in the overlapping regions. The values for WASP J0247−25B are from Maxted et al. (2013), for HZ 22 from Saffer et al. (1997), for GALEX J0805−1058 (G0805) from Kawka et al. (2015), for SDSS J1625+3632 (J1625), SDSS J0815+2309 (J0815) and SDSS J0825+1152 (J0825) are from Gianninas et al. (2014a). Other abbreviations: KIC066 = KIC 06614501, HD188 = HD188112
(A color version of this figure is available in the online journal.)

diffusion models was disappointing. While the Fe abundance is quite close to the prediction, the derived abundances of all other elements were either well below the predicted ones (C, Al, Si, S, Fe) or much higher (Ca by 1.5 dex, for Mg no radiative support at all is expected).

GALEX J1717+6757 (discovered by Vennes et al. 2011c) has a surface gravity of $\log g = 5.67$, almost identical to that of HD 188112, but is significantly cooler ($T_{\rm eff} = 14{,}900$ K) and of lower mass ($0.19\,M_{\odot}$). Hermes et al. (2014) derived abundances for nine metals, all of them being higher (by roughly 0.5 to 2.0 dex) than in HD 188112. Unlike for HD 188112, radiative levitation for N, O, Si, P, and Fe gives predictions in line with the star's abundance pattern (Hermes et al. 2014).

Two *metal-rich* ELM white dwarfs are also known: the companion of a massive millisecond pulsar PSR J1816+4510 ($T_{\rm eff} = 16{,}000$ K, $\log g = 4.9$, Kaplan et al. 2013), and SDSS J0745+1949 ($T_{\rm eff} = 8380$ K, $\log g = 6.2$), a tidally distorted star (Gianninas et al. 2014b). The analyses of their optical spectra allowed for the abundance determination of Mg, Ca, Ti, Cr, and Fe, which turned out to be close to solar in the case of SDSS J0745+1949, while He, Mg, Ca, Si and Fe are about 10 times solar in PSR J1816+4510.

It seems that the diverse abundance pattern of the four stars can neither be explained by diffusion models nor by mixing during repeated shell flashes.

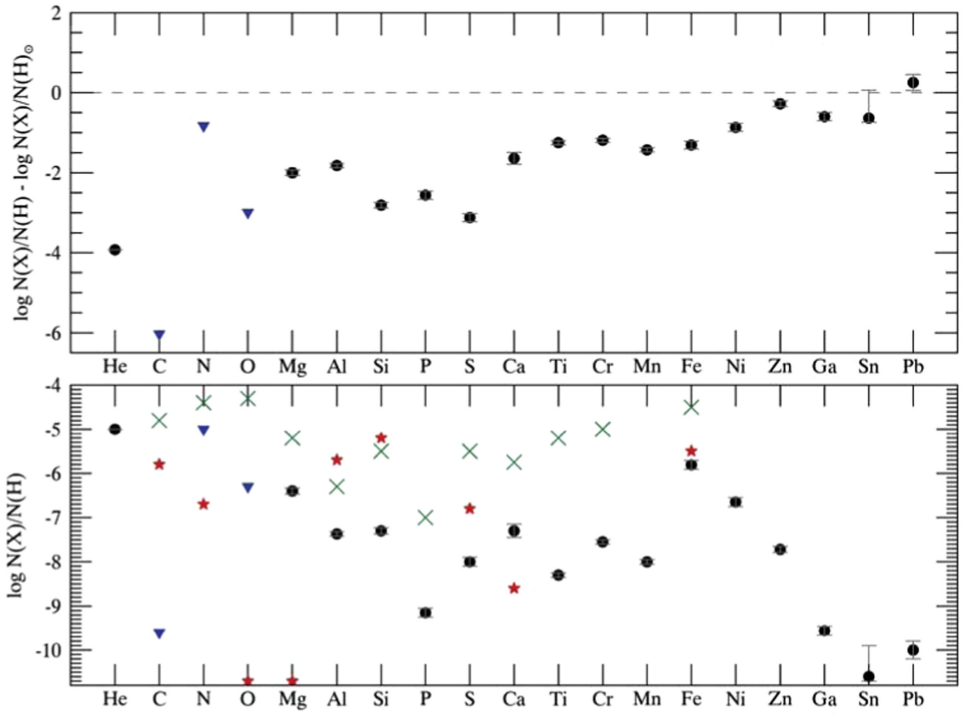

Figure 63. Summary of the determined chemical composition of HD 188112 (Latour et al. 2016). The top panel shows the abundances relative to the solar ones (Asplund et al. 2009) and the bottom panel the absolute ones. Downward triangles indicate upper limits determined for C, N, and O. The asterisks on the bottom panel indicate abundances predicted by radiative levitation (P. Chayer 2016, private communication). No radiative support is expected for oxygen and magnesium (asterisks at the bottom of the panel). The green crosses indicate the average abundances for sdB stars. The diffusion model fails to reproduce the observed abundances of oxygen and Mg, dramatically, while it matches those of silicon and iron. From Latour et al. (2016); copyright A&A; reproduced with permission.
(A color version of this figure is available in the online journal.)

8.4. Pulsations of ELM White Dwarfs

Photometric monitoring of ELM white dwarfs led to the discovery of pulsations. The first object, SDSS J1840+6423 (Hermes et al. 2012b) is in a 4.59 hr orbit with another white dwarf and shows multiperiodic light variations with a dominant period of about 4698 s. Four additional pulsating ELM white dwarfs were found soon thereafter (Hermes et al. 2013a, 2013b), and a sixth member of this new class of pulsating white dwarfs has been reported recently (Bell et al. 2015). All stars have effective temperatures between 7800 and 9500 K, gravities between $\log g = 6.0$ and 6.8. The light curves are multiperiodic, with a handful of periodicities between 1300 and 7000 s. The detected periodicities of the light curves are caused by *g*-mode pulsations (Hermes et al. 2012b), thus, opening a new opportunity and challenge for asteroseismology.

These observations triggered several investigations to model pulsations of ELM white dwarfs and to identify the driving mechanism (e.g., Steinfadt et al. 2010; Córsico et al. 2012; Van Grootel et al. 2013b; Córsico & Althaus 2015), which led to the conclusion that the pulsating ELM white dwarfs form an extension of the ZZ Ceti instability strip (Van Grootel et al. 2013b) albeit at lower temperature.

8.5. ELM White Dwarf and sdB+WD Binaries in Comparison

At the time of writing the ELM survey has identified 88 ELM white dwarfs (Brown et al. 2016), of which one dozen appear to be non-RV-variable. From a "clean" subsample[25] of 65 ELM WD binaries (Brown et al. 2016) found that the orbital periods have a lognormal distribution with a median period of 5.4 hr, which is consistent with predictions from binary population synthesis models (Han 1998). The distribution of companion mass is best described by a normal distribution with a mean of $0.76\,M_{\odot}$. Typically the systems' total masses of about one solar mass, with a mass ratio of $\approx$1:4.

Kupfer et al. (2015) compared the distributions of orbital periods and minimum companion masses of 55 ELM white dwarf binaries from Gianninas et al. (2014a) to their sdB+WD sample (Figures 64 and 65). No ELM white dwarf with an

[25] The subsample contains only binaries with RV semi-amplitudes larger than 75 km s^{-1}. for which the catalog should be 95% complete.

orbital period significantly longer than one day has been found yet, which, however, is likely to be a selection effect. For orbital periods between a quarter of a day and one day both distributions are very similar. However, for the shortest periods (<0.25 days) ELM white dwarfs are more numerous compared to the sdB+WD systems (Figure 64), that is ELM white dwarfs are formed preferentially with shorter periods than sdB+WD systems, which may be expected, because the progenitor of an ELM white dwarf may fill its Roche lobe early-on during its red giant evolution.

ELM-WD companions cover a wider range of minimum masses than that of sdB+WD (Figure 65); that is, masses extend to low as well as to high masses in comparison to the sdB companions. There is no apparent preferred mass which compares with the peak at 0.4 $M_{\odot}$ for the WD companions to sdB stars.

The white dwarf nature of the companion to most ELM-WDs and many sdB stars is inferred from the mass function which only allows a lower limit to be derived. Additional information, such as ellipsoidal light variations or the lack of a reflection effect and of X-ray emission (Kilic et al. 2011, 2014; Mereghetti et al. 2011a), help to identify the companion as a white dwarf. However, more massive companions may exist. The existence of neutron *star* companions to ELM white dwarfs is obvious from the systems hosting millisecond pulsars, but no pulsar companion has as yet been detected to accompany a hot subdwarf star, although such systems are predicted by theory (Pfahl et al. 2003). However, the pulsar signal can only be detected if the orientation of the beam is appropriate. Hence, other ELM and sdB binaries may host neutron stars as well but do not appear as radio sources. In order to estimate the neutron star fraction in the ELM survey sample Andrews et al. (2014) developed a statistical model to infer the companion mass distribution. Applying it to 55 ELM white dwarfs they find the distribution to be consistent with no neutron star companion in the sample and derive an upper limit to the neutron star fraction of 16% (within 1σ limit).

The orbital periods of the ELM-WD binaries are short and, therefore, many are expected to start transferring mass within a Hubble time (see Figure 66). The nature of the mass transfer phase depends on the mass ratio q of the two components. If mass transfer is stable a disk will form around the more massive white dwarf resulting in an AM CVn system. If the mass is accreted directly, the orbit may be destabilized and a merger occurs (Marsh et al. 2004). The stability criteria for different binaries are shown in Figure 67 and compared to the observed ELM-WD mass distribution. Four ELM-WD systems lie in the stable mass transfer regime and, therefore, should end up as AM CVn systems. Most ELM-WD binaries, however, lie between the stable and unstable regions and the final merger products remain uncertain.

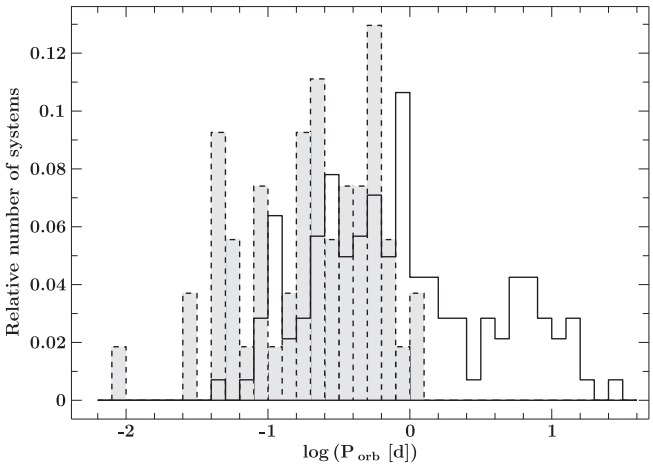

Figure 64. Comparison of orbital periods of sdB binaries with confirmed WD companions to the known ELM-WD binaries with orbital solutions (gray shaded area) taken from Gianninas et al. (2014a). From Kupfer et al. (2015); copyright A&A; with permission.

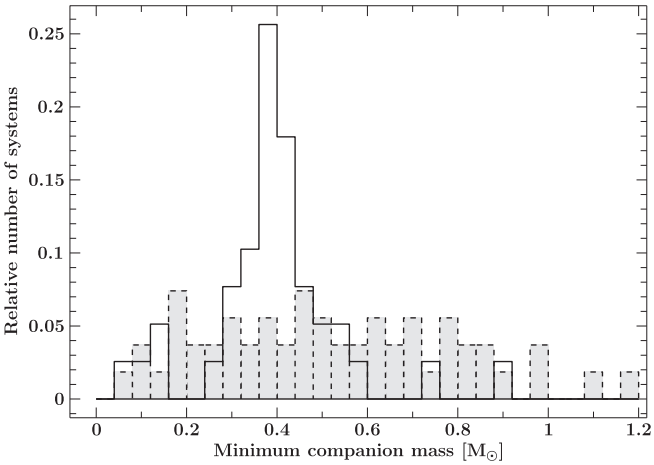

Figure 65. Comparison of minimum companion masses of sdB binaries to the ELM-WD binaries (gray shaded area) taken from Gianninas et al. (2014a). From Kupfer et al. (2015); copyright A&A; reproduced with permission.

8.6. Low-mass Proto-helium White Dwarfs with Main-sequence Companions

We also expect extremely low-mass helium-core objects with main-sequence companions to exist, which result when the more massive star starts to fill its Roche lobe when it is still a subgiant or very early on the first giant branch. This may result in either a stable RLOF or in a common envelope ejection event.

Among the *Kepler* Objects of Interest (KOI) two early-type stars, KOI-74 (spectral type A, orbital period $P = 5.2$ days) and KOI-81 (late B-type, $P = 23.9$ days), show transits of planet-size objects. However, the minima of their light curves were shallower during the transit than during occultation of the

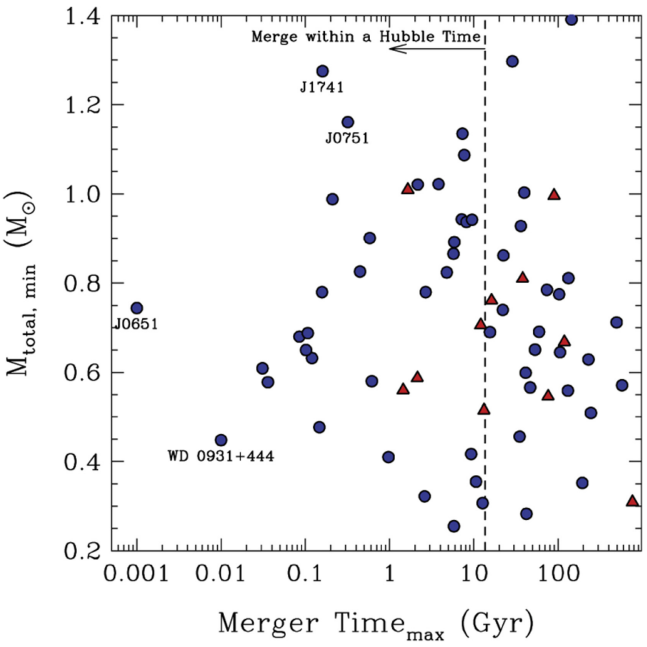

Figure 66. Minimum total mass as a function of the maximum merger time for the entire ELM Survey sample (blue circles and red triangles). From Gianninas et al. (2015); copyright ApJ; reproduced with permission.
(A color version of this figure is available in the online journal.)

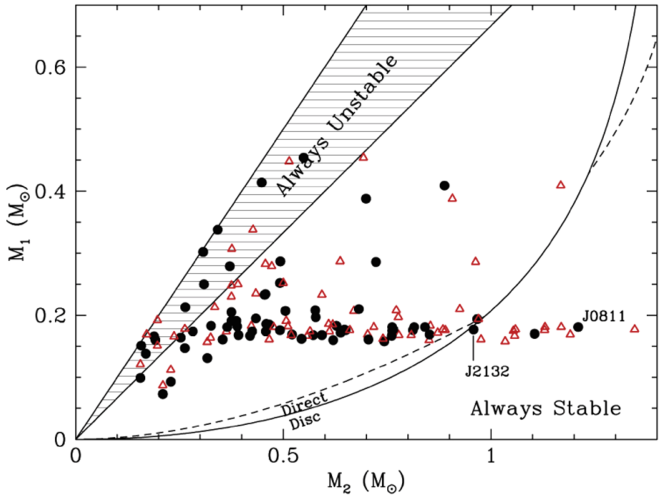

Figure 67. Plot of M_1 vs. M_2 for the entire ELM-WD sample. The companion masses are shown for inclinations of 90° (black dots) and 60° (red triangles). The majority of the ELM-WD binaries lie in the region between the regions of stable and unstable mass transfer. From Gianninas et al. (2015); copyright ApJ; reproduced with permission.
(A color version of this figure is available in the online journal.)

companion (Rowe et al. 2010). Hence the companion must be hotter than its host star. Rowe et al. (2010) and van Kerkwijk et al. (2010) concluded that the companions must be low mass white dwarfs. Doppler boosting present in the *Kepler* light curve allowed van Kerkwijk et al. (2010) to determine the companion mass to KOI-74 to be 0.22 $M_\odot$. Using *HST*/COS spectra, Matson et al. (2015) were able to reconstruct the UV spectrum of the companion to KOI-81 and to measure the companion's RV curve resulting in a mass of $M = 0.194 \pm 0.02\,M_\odot$ and a radius of $0.0911 \pm 0.0025\,R_\odot$. The UV Spectrum resembled that of the sdB star CD−64°481, and the effective temperature was constrained to >19,000 K. Hence the star is very similar to the helium core subdwarf HD 188112.

Further discoveries of similar objects of a low mass white dwarf with an A-dwarf secondary from *Kepler* light curves followed KIC 10657664 (Carter et al. 2011) as well as KIC 9164561 and KIC 10727668 (Rappaport et al. 2015) with periods between 1.3 and 5.2 days and masses determined from Doppler boosting. In addition a F-type secondary was found in KOI-1224 (Breton et al. 2012). Recently, Faigler et al. (2015) added another four *Kepler* systems consisting of A type stars hosting ELM white dwarf companions with orbital periods between 1.17 and 3.82 days and companion masses from 0.19 to 0.22 $M_\odot$

Such eclipsing binaries have also been discovered from ground-based (SuperWASP) lightcurves (Maxted et al. 2011, 2014a). The host stars are of spectral type A and orbital periods range from 0.7 to 2.2 days. The class was named "EL CVn" stars after the prototype.[26]

Perhaps not surprisingly, the low mass helium-core objects in KOI-71, KOI-81, and 1SWASP J024743.37−251549.2 (J0247-25B) were found to be pulsating (Rowe et al. 2010; Maxted et al. 2013). The oscillations of J0247-25B are mixed non-radial modes (Maxted et al. 2013), that is they behave like g-modes near the stellar core and like p-modes in the outer layers. This paves the way to probe its interior structure and to measure its internal rotation profile (Aerts 2015). The pulsations are probably driven by the κ-mechanism, i.e., by the change in opacity in the second partial ionization zone of helium. Hence, Maxted et al. (2013) conjecture that other ELM white dwarfs with effective temperatures similar to J0247-25B may also show pulsations. Indeed Maxted et al. (2014b) found a second candidate pulsator (WASP 1628+10B, $T_{\rm eff} \approx 9200$ K) as a companion to an A2V star which itself is a δ Scuti pulsator.

Jeffery & Saio (2013) explored the boundaries of the instabilities of low- to high-order radial oscillations in ELM WDs and found them to depend strongly on chemical composition and radial order number. For J0247-25B they conclude that the envelope must be hydrogen deficient ($0.2 < X < 0.3$), in agreement with expectations from evolution models, but still lacks observational confirmation.

[26] It is interesting to note that Regulus A (a bright B7 star) has a low mass white dwarf companion in a 40 day orbit (Gies et al. 2008). Making use of the white dwarf period–mass relation Rappaport et al. (2009) showed that the white dwarf companion must be of low mass ($0.28 \pm 0.05\,M_\odot$). Hence, the inner binary of Regulus qualifies as a EL CVn system.

9. Kinematics, Population Membership and a Unique Hyper-velocity Star

Hot subdwarf stars are found in all stellar populations. Globular cluster hot subdwarfs are population II stars, while the members of open clusters belong to the disk population. Most of the hot subdwarfs in the field belong to an old disk population (de Boer et al. 1997; Thejll et al. 1997; Altmann et al. 2004; Kawka et al. 2015). Finally, hot subdwarfs have been discovered in the Galactic bulge (Busso et al. 2005). However, some high-velocity hot subdwarf stars may have been ejected from their place of birth (Tillich et al. 2011), that is they may be run-away stars. An extreme such case is US 708, a hyper-velocity star (HVS), that travels so fast that it will escape from the Galaxy (Hirsch et al. 2005).

9.1. Population Membership

For normal stars chemical tagging allows the identification of stellar population membership. However, this is not possible for hot subdwarf stars, because atmospheric diffusion has altered the abundance pattern and washed out any information on the original metallicity. Therefore, we are left with the Galactic kinematics of the hot subdwarf stars to assign an individual hot subdwarf to a stellar population. To do this the full 6D phase space information needs to be available. Distances are usually derived from the atmospheric parameters by assuming a canonical sdB mass. Proper motions can be drawn from large astrometric catalogs but typically have substantial uncertainties. Although straightforward the RV measurement requires a considerable effort. Because the frequency of RV variables among the sdB stars is very large (about 50% with periods less than 30 days), multi-epoch observations are needed to rule out RV variability or derive the systemic velocity from the RV curve of a close binary system.

Systemic radial velocities are now available for 142 sdB binaries (Kupfer et al. 2015) and have recently been used to determine their population membership from kinematic diagnostic diagrams such as the v_ϕ–v_r and the e–J_z diagrams (Eichie et al. 2016, in preparation; see Figure 68) where v_ϕ is the velocity component in the direction of Galactic rotation, v_r the component in Galactic radial direction,[27] J_z the component of the angular momentum of the star's Galactic orbit perpendicular to the Galactic disk and e the eccentricity of the Galactic orbit.

Accordingly, the vast majority of binaries belongs to the thin disk, with a few thick disk stars and a single halo object, SDSS J002323-002953. Most of the stars in the sample are nearby, and therefore it is not surprising that they belong to the thin disk population.

However, the MUCHFUSS survey, which includes much fainter and, therefore, distant hot subdwarfs, has identified a couple of high-velocity stars that may belong to the halo population.[28]

9.1.1. High Velocity Hot Subdwarfs Stars: Run-away Stars or Genuine Halo Stars

Tillich et al. (2011) analyzed the kinematics of ten high-velocity hot subdwarfs, starting from their own proper motion measurements. Using spectroscopic distances and radial velocities Galactic trajectories were calculated (see Irrgang et al. 2013, for details). Accordingly, nine sdB stars were found to belong to the halo and one to the thick disk. Two distinctive kinematic groups emerged from their analysis (see Figure 68): the normal halo subdwarfs (G1) with low Galactic rotation and the extreme halo subdwarfs (G2) on highly eccentric retrograde orbits. Tillich et al. (2011) also considered that the objects are actually run-away disk stars ejected from their place of birth in the Galactic plane. A close inspection of their Galactic trajectories showed that the members of class G2 stars would come from the outer disk excluding an origin in the Galactic center. The members of the G1 class, however, would originate from the inner Galactic disk or bulge, including the Galactic center, and might have been ejected by a super-massive black hole slingshot mechanism (Hills 1988; see Section 9.2). Some sdB stars of the sample of Tillich et al. (2011) that are approaching the Earth, J1644+4523 in particular, have to be bound to the Galaxy and therefore might provide constraints on the mass of the dark matter halo.

9.1.2. J1211+1437—An Extremely Fast Halo Hot Subdwarf Star in a Wide Binary System

The most interesting star in the sample, however, turned out to be J1211+1437, because recent spectroscopic follow-up (Németh et al. 2016) revealed a metal-weak K-type main-sequence companion in a wide orbit (see Figure 69 for the spectral energy distribution (SED)). Whether this binary with a Galactic rest frame velocity of 570 km s^{-1} is bound or unbound to the Galaxy depends on the Galactic mass model preferred. Its Galactic kinematic rules out an origin in the Galactic center, but essentially all other acceleration mechanisms discussed for HVS and runaway stars can be excluded as well. The binary is too fragile to survive dynamical interaction in a dense stellar population or the kick of a core-collapse supernova. Hence, Németh et al. (2016) concluded that J1211+1437 is either a bound extreme halo object or was accreted from the a former satellite galaxy torn to shreds by the tidal forces of the Milky

[27] v_ϕ and v_r often referred to as V and U, but may be confused with the cartesian velocities v_x and v_y (Johnson & Soderblom 1987), see also Randall et al. (2015).

[28] Halo and thick disk stars have also been identified among the ELM white dwarfs (Gianninas et al. 2015) and the EL CVn binaries (Maxted et al. 2014a) discussed in Section 8.

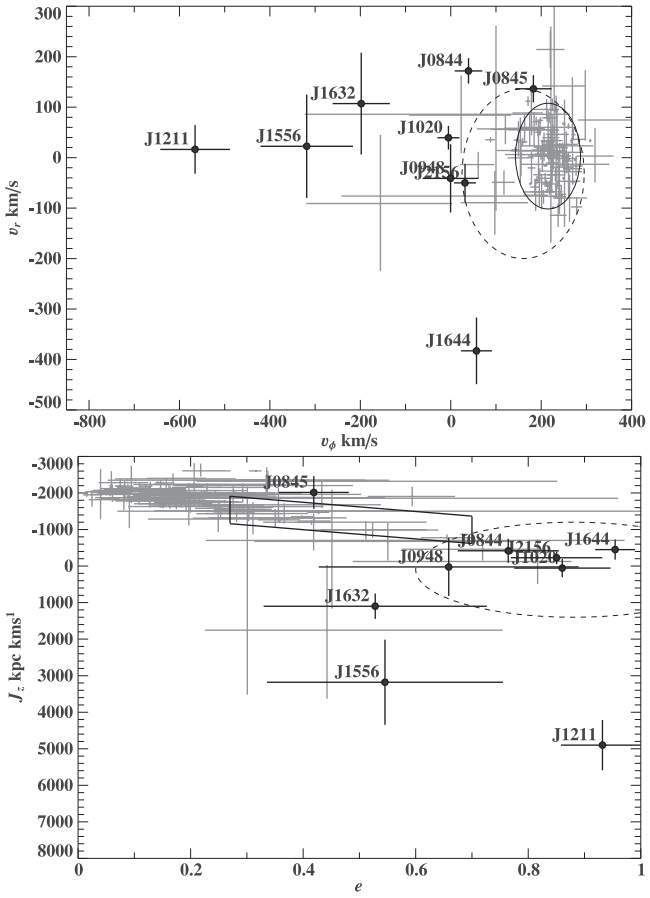

Figure 68. v_ϕ–v_r diagram (upper panel) and e–J_z diagram (lower panel) for nine high-velocity sdB stars (Tillich et al. 2011) labelled by their abbreviated name (see Tillich et al. 2011). The sample of binary sdBs from Kupfer et al. (2015) and analyzed from PPXML proper motions by Eichie et al. (2016, in preparation, gray error bars) serves as a comparison. The solid ellipses render the 3σ-thin (solid) and thick disk contours (dashed) in the v_ϕ–v_r diagram (upper panel), while the solid box in the e–J_z diagram (lower panel) marks the thick disk region as specified by Pauli et al. (2006). The values for J1211+1437 are taken from Németh et al. (2016) using model II of Irrgang et al. (2013). Accordingly, eight stars would be assigned halo membership (J0845 is considered a thick disk star). Tillich et al. (2011) identify two groups, one (G1) lying inside the dashed ellipse in the e–J_z diagram (lower panel), while those with positive J_z form their group G2. From E. Ziegerer (2016, private communication).

Way (Abadi et al. 2009). However, kinematically J1211+143 could not be associated to any stellar stream in the halo that might represent the debris of a destroyed satellite galaxy.

9.2. The Unique Hyper-velocity Star US 708—A Remnant Donor of an SN Ia Explosion

Hirsch et al. (2005) discovered that the sdO star US 708 shows an exceptionally high RV of $+708 \pm 15\,\mathrm{km\,s^{-1}}$. Accordingly, its Galactic rest frame velocity ($>757\,\mathrm{km\,s^{-1}}$) exceeds the local Galactic escape velocity. At the time of discovery US 708 was only the second HVS known to be unbound to the Galaxy.[29] A quantitative non-LTE model atmosphere analysis of optical spectra obtained with the Keck I telescope by Hirsch et al. (2005) showed that US 708 is a normal *helium-rich* sdO at a distance of 19 kpc.

It has been suggested by Hills (1988) that such HVSs can be formed by the tidal disruption of a binary through interaction with a super-massive black hole. It is plausible that US 708 might have originated from the Galactic center, because this is the only place in the Galaxy known to host a super-massive black hole, and the time of flight from the Galactic center to its present position is sufficiently short (36 Myr, Figure 70(a)). Whether or not the star originated in the Galactic center can only be answered from very high precision proper-motion measurements.

Geier et al. (2015a) revisited US 708 by obtaining new spectra at better resolution at the Keck telescope to improve the RV measurement. In addition, they were able to determine the star's proper motion by combining position measurements from astrometric photographic plates with modern CCD measurements (SDSS, PANSTARRS). By calculating Galactic trajectories in the Galactic potential the place of origin was found in the Galactic disk, but far from the Galactic center, which was excluded at a 5σ confidence level.

The proper motion has also been determined recently from *HST* astrometry (Brown et al. 2015). The conclusion is the same as from the ground-based measurements of Geier et al. (2015a), i.e., the Galactic center is excluded as the place of origin (see Figure 70(b)). Accordingly, the Galactic rest-frame velocity of US 708 is $1082 \pm 19\,\mathrm{km\,s^{-1}}$ and the ejection velocity from the disk $894 \pm 13\,\mathrm{km\,s^{-1}}$ (Ziegerer 2016, private communication), which makes US 708 the fasted HVS star known.

9.2.1. A Link to SNe Ia

Justham et al. (2009) suggested a link to SNe Ia by considering single low-mass (hyper-velocity) white dwarfs and He-sdO stars as the donor remnants to the exploding white dwarfs. Justham et al. (2010, 2011) investigated the case of the hypervelocity sdO US 708. Geier et al. (2015a) investigated the evolution of a progenitor system consisting of an sdB star and a massive C/O white dwarf. The evolution is depicted in Figure 71. Accordingly, the donor was released at the moment of explosion and traveled away at approximately the orbital velocity. In order to gain a space velocity as high as that of US 708 the progenitor binary must have been extra-ordinarily tight and the white dwarf companion rather massive. Geier et al. (2015a) assumed that the system consisted of a compact helium star of $\sim 0.3\,M_\odot$ and a massive carbon-oxygen WD

[29] An HVS survey has increased the number of known HVSs to about two dozen (Brown et al. 2014). A comprehensive review is presented by Brown (2015).

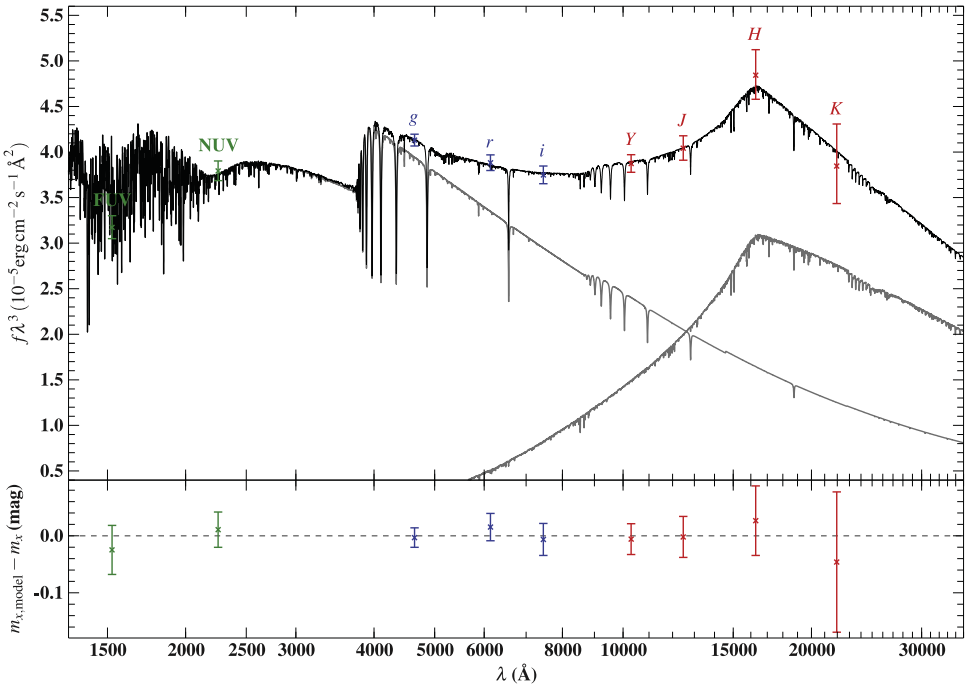

Figure 69. Comparison of synthetic and observed photometry of the fast sdB+K binary J1211+1437 (Németh et al. 2016). Top panel: the spectral energy distribution. The colored data points are fluxes, which are converted from observed magnitudes, and the solid gray line is the composite (sdB+K) model. The individual contributions are plotted in light gray. Bottom panel: the residuals show the differences between synthetic and observed magnitudes. The photometric systems have the following color code: *GALEX* (green), SDSS (blue), UKIDSS (red). This is a modified version of Figure 2 of Németh et al. (2016), from A. Irrgang (2016, private communication).

(A color version of this figure is available in the online journal.)

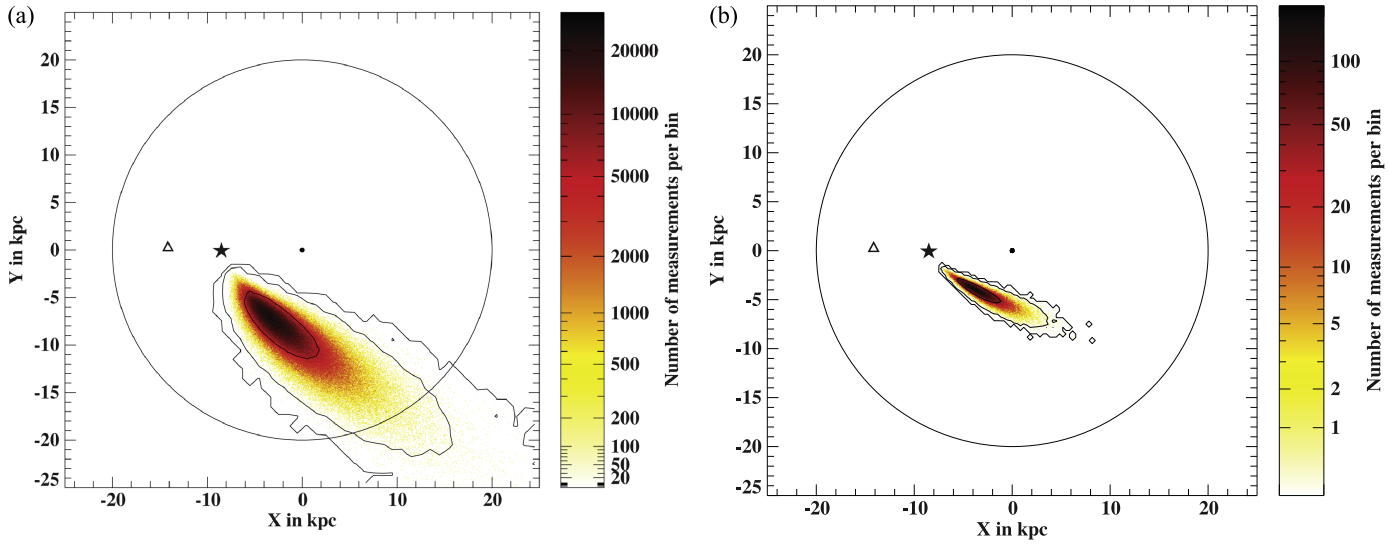

Figure 70. Origin of US 708. Monte Carlo simulation of the past trajectory of US 708. The color-coded bins mark the positions, where the star crossed the Galactic disc, which is shown pole-on. The position of the Galactic center is marked by the black dot, the position of the Sun as asterisk. The current position of US 708 is marked by a triangle. (a) Based on ground-based astrometry. The contours correspond to the 1σ, 3σ, and 5σ limits. From Geier et al. (2015a); copyright Science; reproduced with permission. (b) Based on the *HST* proper motion of US 708 (Brown et al. 2015). The contours correspond to the 1σ and 3σ limits. From E. Zieger (2016, private communication).

(A color version of this figure is available in the online journal.)

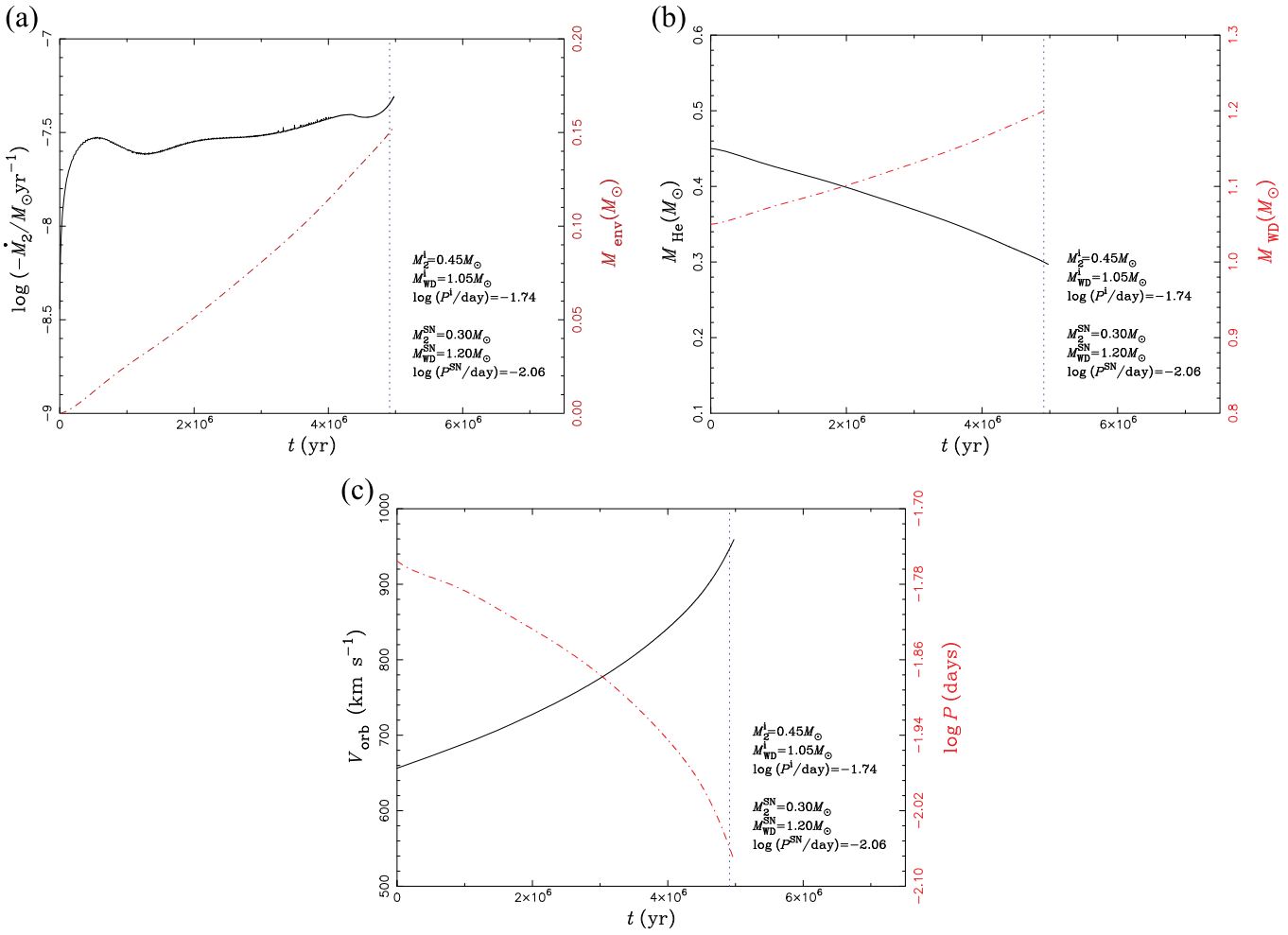

Figure 71. (a) Evolution of the progenitor after the He star fills its Roche lobe. The dotted vertical lines indicate the position where the double-detonation may happen (the mass of the He shell increases to ∼0.15 $M_\odot$). The initial binary parameters and the parameters at the moment of the SN explosion are also given. (a) Mass transfer rate (full drawn) and the mass of the WD envelope (dashed-dotted) are varying with time. (b) Same as (a) but for the mass of the He-star (solid line) and of the WD (dashed–dotted line). (c) Same as (a), but for the radial velocity semiamplitude (solid line) and the orbital period (dashed–dotted line) of the binary. From Geier et al. (2015a); copyright Science; reproduced with permission.
(A color version of this figure is available in the online journal.)

(1.0–1.2 $M_\odot$) with an orbital period of about 10 minutes[30] at the time of explosion.

The rotation of the components in such ultra-short binaries are assumed to be tidally locked to the orbit. Hence, the surviving remnant is expected to be rapidly rotating. Geier et al. (2015a) derived the rotational is expected velocity from their Keck spectra, which turned out to be $v_{rot} \sin i = 115 \pm 8\,km\,s^{-1}$ much higher than observed for single He-sdO stars (Hirsch & Heber 2009), but smaller than the expected rotation velocity at the time of ejection (≈350 km s^{-1}). Accounting for the evolution of the sdO star, which led to an expansion of the star (Pan et al. 2013), and assuming conservation of angular momentum, Geier et al. (2015a) estimate $v_{rot} \sin i \approx 120\,km\,s^{-1}$ in perfect agreement with the observed rotation rate. This lends strong support to the SN Ia donor remnant scenario.

Another imprint of a thermonuclear explosion of the original white dwarf primary would be the debris deposited on the surface of the surviving donor (Liu et al. 2013) which could possibly be traced by UV spectroscopy. The scenario also predicts a low mass for the He-sdO star because of the transfer of a significant fraction of the helium envelope prior to the explosion and additional few percent by ablation during the explosion (Liu et al. 2013).

Up to now, US 708 remained unique; the only known hypervelocity hot subdwarf star. This, however, is expected to change, when the *Gaia* measurements become available.

[30] Such tight binaries do exist as witnessed by the eclipsing He-WD+CO-WD binary SDSS J065133+284423 (orbital period of only 12 minutes, Brown et al. 2011b).

10. Conclusion

This review updates and extends that of Heber (2009) and includes a section about the new classes of extremely low mass (ELM) white dwarfs, which are the stripped helium cores of red giant stars similar to many subluminous B (sdB) stars in binaries. The latter, however, managed to ignite core helium burning and therefore populate the extreme horizontal branch (EHB), while the ELM white dwarfs evolve toward the fully degenerate configuration, eventually experiencing hydrogen shell flashes. Many sdB stars reside in binaries accompanied by either white dwarfs on close orbits (periods of 0.1–30 days), main sequence stars of M-type on even closer orbits, or F/G/K type on wide orbits (periods of 700–1200 days). Similarly, almost all ELM white dwarfs are found in close binaries with another white dwarf or with an A- or F-type main sequence star ("EL CVn"). Since the orbital separations in the short period sdB binaries are only a few solar radii, much smaller than the size of the red-giant progenitor, their orbit must have shrunk considerably with respect to the original one. Therefore, the progenitor system must have undergone a common envelope (CE) phase, during which the companion was engulfed in the red giant's envelope leading to a spiral-in due to friction and eventually to the ejection of the envelope.

Progress in the field has been enormous over the last seven years. Many of the new discoveries, however, cannot be easily explained and pose new questions:

1. Quantitative spectral analyses of high-resolution optical and ultraviolet spectra have established a coarse abundance pattern of sdB stars. On average the abundances of the lighter elements (helium to sulfur) are subsolar, while those of heavier elements (Ca to Pb) are enriched with respect to the Sun reaching factors larger than one hundred, in a few cases up to ten thousand (e.g., for Pb). Notable exceptions are nitrogen and iron which are close to solar with remarkably small star-to-star scatter. On the other hand, very large star-to-star scatter is obvious for carbon and silicon. There is no doubt, that these patterns result from atmospheric diffusion processes. Diffusion theory has advanced considerably and included turbulence, but is still limited by the lack of atomic data for many heavy elements.
2. Many of the compact companions in close binaries are white dwarfs. With respect to our understanding of binary evolution, it would be important to find out how many of them are of helium composition, hence, originate from the first giant branch, or of C/O composition, hence from the second giant branch. Neutron-star or black hole companions to sdB stars are predicted but have not yet been discovered, while ELM white dwarfs have been found as partners to milli-second pulsars already. Binary sdB stars with massive white dwarf companions are candidate supernova Ia progenitors both in the double degenerate scenario (e.g., KPD 1930+2752) and the single degenerate scenario as helium donors for double detonation supernovae (e.g., CD−30°11223). For a long time the candidate SN Ia progenitor HD 49798 was the only known X-ray source among hot subdwarf stars. Modern X-ray satellites have now identified a handful of X-ray sources among the hottest subluminous O (sdO) stars, including two non-binaries.
3. The wide orbits of sdB binaries with main-sequence companions of spectral type F/G/K result from stable RLOF. Only recently, their periods have been determined to lie between 700 and 1200 days. Because the sdB star will evolve directly into a white dwarf, we expect a population of F/G/K stars with unseen white dwarf companions to exist (Parsons et al. 2016) with similar orbital periods. Such systems will be easily detectable by *Gaia* as astrometric binaries.
4. Substellar companions to sdB stars have also been found. For HW Vir systems the companion mass distribution extends from 0.2 $M_{\odot}$ to below the stellar mass limit; that is, into the brown dwarf regime. A giant planet companion to the *p*-mode pulsator V391 Peg marked the first discovery of a planet that survived the red giant evolution of its host star. Evidence for Earth-size planets to two pulsating sdB stars has been reported and circumbinary giant planets or brown dwarfs have been found around HW Vir systems by the eclipse timing technique. The high incidence of circumbinary substellar objects favors a second generation nature; that is, the planets are formed from remaining CE material. However, none of the candidates have been confirmed by an independent method. Therefore, it remains unclear whether those substellar companions are real.
5. Thanks to *Kepler* light curves, asteroseismology advanced to determine the rotation rates of a handful of pulsating sdB stars from the splittings of frequency multiplets. The stars are found to rotate much more slowly (tens of days) than expected. What causes efficient angular momentum transport and loss, probably early-on on the red giant branch? Does radial differential rotation occur? Asteroseismology of gravity-mode pulsators allowed the internal structure of some sdB stars to be probed. The size of the convective cores are larger than the models imply indicating that convection is more efficient than assumed by today's standard physical models.
6. Almost half of the sdB population is apparently single, which may be explained in the context of binary evolution, if they result from binary mergers of helium white dwarfs, or *result* from the disruption of a companion; that is, massive enough to initiate CE ejection but of too low mass to survive. However, an sdB star may form in isolation by internal processes that

allow the helium core of a red giant to grow beyond the canonical size and cause delayed helium flashes, when the star has already departed from red giant branch. Could rapid core rotation be the clue?

7. What is the origin of the helium subdwarf O (He-sdO) stars? The binary frequency of He-sdO stars is much lower than that of the sdB stars, indicating that they arise from a different evolutionary path than the latter. The merger of two helium white dwarfs is the most popular scenario for the origin of He-sdO, rivaled by the late hot flasher scenarios. The merger scenario may explain the observed carbon and nitrogen abundance pattern at least qualitatively, whereas the very late flasher may be able to match the nitrogen-rich stars. However, the predicted location of the He-sdOs in the $T_{\rm eff}$–$\log g$ diagram does not match the spectroscopic one. It is, though, notoriously difficult to determine the surface gravity of He-sdO stars from optical spectra. Independent gravity estimates, would be needed. The origin of erratic RV variations and strong magnetic fields also awaits an explanation.
8. The small class of intermediate He-sdB stars contains chemically very peculiar members, in particular the halo star LS IV-14°116. Large enrichment of heavy elements such as zirconium, yttrium, and lead are common to those stars. In addition, LS IV-14°116 is a unique pulsator. What causes those pulsations? Are the intermediate He-sdBs objects in transition; that is, evolving onto the EHB as suggested by Jeffery et al. (2012)?
9. The hot subdwarf population in globular clusters appears to be different from that of the field. Counterparts to the blue hook stars have not yet been found in the field population, whereas the extremely helium rich sdO stars, which are frequent in the field, seem to be lacking in globular clusters. Similarly, the counterparts to the pulsating sdO stars in ω Cen have not yet been found in the field population.
10. The discovery of the extremely low-mass white dwarfs filled a gap in the mosaic of binary stellar evolution. As for the hot subdwarfs the binary frequency is high, actually even higher than that of the sdB stars. Companions are either white dwarfs, neutron stars (pulsars) or main sequence stars ("EL CVn" stars). Multi-periodic oscillations were also discovered and shown to be related to the ZZ Ceti strip of pulsating white dwarfs.

In order to tackle the newly revealed shortcomings improvement to models of the stellar interior, envelope, and atmosphere as well as additional observations and facilities are needed. Atomic data for heavy elements are required to improve diffusion calculations, which are crucial for our understanding of pulsation driving, radiative levitation, atmospheric abundance pattern and stratification of O/B subdwarfs as well as ELM white dwarfs. The lack of atomic data (opacities and line broadening) still limits the accuracy for atmospheric parameter determination and chemical abundances.

The treatment of convection in stellar interiors remains a challenge despite of decade-long efforts. Asteroseismology of hot subdwarfs adds new constraints to improve interior models, because it allows the size of the convective core to be constrained. The *MESA* code provides new options to tackle the problems. Asteroseismology of red giants and hot subdwarf stars revealed that additional physical mechanisms are required to understand their evolution, in particular the angular momentum transport, tidal synchronization and the origin of turbulence remain to be clarified. In order to understand the evolution of close binaries the physics of the common envelope ejection as well as of stellar mergers need to be understood. The hot subdwarf stars and ELM white dwarf will provide ideal laboratories to this end.

On the observational side the *Kepler* mission is going on and we can expect surprises from the *K2* campaign both for asteroseismology and binary research. The massive ground-based photometric surveys, such as the Palomar Transient facility, will be upgraded (Smith et al. 2014) and new projects will start culminating in the *LSST* (LSST Science Collaboration et al. 2009). They will increase the inventory of binary hot subdwarfs, low mass white dwarfs an EL CVn systems significantly and may even lead to the detection of optical transients caused by white dwarf mergers to form hot subdwarf stars. New spectroscopic surveys such as *LAMOST* already discovered and characterized hot subdwarf stars (Luo et al. 2016) and will go on to do so.

The masses of hot subwarf stars, both single or in binaries, are the key to understand their evolution. The tools available are the analysis of eclipsing binary orbits and asteroseismology. Therefore, NY Vir, a pulsating sdB star in an eclipsing binary was considered the "Rosetta stone" by Charpinet et al. (2008b) because it allows both techniques to be applied and cross-checked and was unique at the time of writing. In the mean time a few similar systems have been found. Combining dynamical and seismic analyses of eclipsing binaries with pulsating components will put stringent constraints on evolutionary models (see Tkachenko et al. 2014, for an example).

The ability to derive masses is also impeded by the poor knowledge of the stars' distances. In most cases spectroscopic distances are used, which rest on an adopted subdwarf mass and the atmospheric parameters determined by quantitative analyses. The largest contribution to the error budget usually comes from the surface gravity. This will soon be remedied by the *Gaia* astrometric mission (Perryman et al. 2001), which will provide parallaxes to 10 μas precision in the most favorable cases. Parallax measurements for the near-by hot subdwarfs will provide a benchmark to test atmospheric models (surface gravity) and/or the mass distribution of

binary as well as single hot subdwarf stars. Already the first data release, expected in 2016, will provide parallaxes and proper motions for many of the 2.5 million stars from the Tycho-2 catalog (Michalik et al. 2015) to sub-mas precision. This catalog contains about 180 hot subdwarfs of all types and will provide a first benchmark, although not yet full-fledged. *Gaia* will be very efficient to study astrometric binaries with periods from a few weeks to years, which makes it complementary to many RV studies which are biased toward short periods (<30 days).

Gaia will provide proper motions for a huge number of hot subdwarf stars that will allow the different stellar populations to be disentangled. The halo members will be particularly interesting, because they allow a meaningful comparison with the population of globular cluster hot subdwarfs.

The *Gaia* survey will be complemented by large spectroscopic surveys using multi-object spectrographs like 4*MOST* (de Jong et al. 2014) and *WEAVE* (Dalton et al. 2012). They will allow large samples of faint blue stars to be studied in detail, including new types of hot subluminous stars. The fastest hot subdwarfs will allow the mass of the dark matter halo to be constrained further and other unbound HVSs similar to the sdO HVS US 708 will be discovered.

I thank the editor, Dr. Jeff Mangum, for the invitation and his patience with the slow progress of my work. I thank the organizers of the "7th meeting on hot subdwarf stars and related objects," Tony Lynas-Gray and Philipp Podsiadlowski, for offering such a lively environment to discuss with many colleagues. Financial support for publication costs by the Deutsche Forschungsgemeinschaft (grant He1356/45-2) is gratefully acknowledged. I thank Andreas Irrgang, Peter Németh, and Eva Ziegerer for providing me with their figures prior to publication, and to Stephan Geier, Simon Jeffery, and Thomas Kupfer for providing updated versions of their figures and John Telting for his original figures. My sincere thanks go to Warren Brown, Stefan Dreizler, Stephan Geier, Andreas Irrgang, Simon Jeffery, Thomas Kupfer, Marilyn Latour, Tony Lynas-Gray, Sandro Merreghetti, Marcello Miller-Bertolami, Sabine Moehler, Peter Németh, Roy Østensen, Nicole Reindl, Veronika Schaffenroth, and Markus Schindewolf for their most helpful comments, corrections and suggestions.

Appendix
Atmospheric Parameters and Abundances of He-sdO Stars

The atmospheric parameters and helium, carbon, and nitrogen abundances of He-sdO stars from Hirsch (2009) are listed in Table 1 (available in the online journal) as plotted in Figures 4, 5, 12, 13, and 21.

References

Abadi, M. G., Navarro, J. F., & Steinmetz, M. 2009, ApJL, 691, L63
Abazajian, K. N., Adelman-McCarthy, J. K., Agüeros, M. A., et al. 2009, ApJS, 182, 543
Adams, W. S. 1925, PNAS, 11, 382
Aerts, C. 2015, AN, 336, 477
Aerts, C., Jeffery, C. S., Fontaine, G., et al. 2006, MNRAS, 367, 1317
Ahmad, A., & Jeffery, C. S. 2005, A&A, 437, L51
Almeida, L. A., Jablonski, F., & Rodrigues, C. V. 2013, ApJ, 766, 11
Almeida, L. A., Jablonski, F., Tello, J., & Rodrigues, C. V. 2012, MNRAS, 423, 478
Althaus, L. G., Miller Bertolami, M. M., & Córsico, A. H. 2013, A&A, 557, A19
Altmann, M., Edelmann, H., & de Boer, K. S. 2004, A&A, 414, 181
Ambika, S., Parthasarathy, M., Aoki, W., et al. 2004, A&A, 417, 293
Andrews, J. J., Price-Whelan, A. M., & Agüeros, M. A. 2014, ApJL, 797, L32
Antoniadis, J. 2014, ApJL, 797, L24
Applegate, J. H. 1992, ApJ, 385, 621
Asplund, M., Grevesse, N., Sauval, A. J., & Scott, P. 2009, ARA&A, 47, 481
Auer, L. H., & Mihalas, D. 1969, ApJ, 158, 641
Aungwerojwit, A., Gänsicke, B. T., Rodríguez-Gil, P., et al. 2007, A&A, 469, 297
Auvergne, M., Bodin, P., Boisnard, L., et al. 2009, A&A, 506, 411
Aznar Cuadrado, R., & Jeffery, C. S. 2002, A&A, 385, 131
Baran, A., Pigulski, A., & O'Toole, S. J. 2008, MNRAS, 385, 255
Baran, A. S. 2012, AcA, 62, 179
Baran, A. S., Gilker, J. T., Reed, M. D., et al. 2011, MNRAS, 413, 2838
Baran, A. S., Koen, C., & Pokrzywka, B. 2015a, MNRAS, 448, L16
Baran, A. S., Telting, J. H., Németh, P., et al. 2016, A&A, 585, A66
Baran, A. S., Telting, J. H., Németh, P., Bachulski, S., & Krzesiński, J. 2015b, A&A, 573, A52
Baran, A. S., & Winans, A. 2012, AcA, 62, 343
Baran, A. S., Zola, S., Blokesz, A., Østensen, R. H., & Silvotti, R. 2015c, A&A, 577, A146
Barlow, B., Wade, R., Liss, S., & Stark, M. 2014, in ASP Conf. Ser. 481, 6th Meeting on Hot Subdwarf Stars and Related Objects, ed. V. van Grootel et al. (San Francisco, CA: ASP), 301
Barlow, B. N., Liss, S. E., Wade, R. A., & Green, E. M. 2013, ApJ, 771, 23
Barlow, B. N., Wade, R. A., & Liss, S. E. 2012a, ApJ, 753, 101
Barlow, B. N., Wade, R. A., Liss, S. E., Østensen, R. H., & Van Winckel, H. 2012b, ApJ, 758, 58
Barman, T. S., Hauschildt, P. H., & Allard, F. 2004, ApJ, 614, 338
Barnard, E. E. 1900, ApJ, 12, 176
Barnes, J. W., van Eyken, J. C., Jackson, B. K., Ciardi, D. R., & Fortney, J. J. 2013, ApJ, 774, 53
Baschek, B., & Norris, J. 1970, ApJS, 19, 327
Bear, E., & Soker, N. 2012, ApJL, 749, L14
Bear, E., & Soker, N. 2014, MNRAS, 444, 1698
Beauchamp, A., Wesemael, F., & Bergeron, P. 1997, ApJS, 108, 559
Beck, P. G., Montalban, J., Kallinger, T., et al. 2012, Natur, 481, 55
Bedin, L. R., King, I. R., Anderson, J., et al. 2008a, ApJ, 678, 1279
Bedin, L. R., Salaris, M., Piotto, G., et al. 2005, ApJL, 624, L45
Bedin, L. R., Salaris, M., Piotto, G., et al. 2008b, ApJL, 679, L29
Behara, N. T., & Jeffery, C. S. 2006, A&A, 451, 643
Behr, B. B. 2003a, ApJS, 149, 67
Behr, B. B. 2003b, ApJS, 149, 101
Bell, K. J., Kepler, S. O., Montgomery, M. H., et al. 2015, in ASP Conf. Ser. 493, 19th European Workshop on White Dwarfs, ed. P. Dufour, P. Bergeron, & G. Fontaine (San Francisco, CA: ASP), 217
Bergeron, P., Saffer, R. A., & Liebert, J. 1992, ApJ, 394, 228
Beuermann, K., Dreizler, S., & Hessman, F. V. 2013, A&A, 555, A133
Beuermann, K., Dreizler, S., Hessman, F. V., & Deller, J. 2012, A&A, 543, A138
Blanchette, J.-P., Chayer, P., Wesemael, F., et al. 2008, ApJ, 678, 1329
Bloecker, T. 1995, A&A, 299, 755
Bloemen, S., Degroote, P., Conroy, K., et al. 2013, in EAS Publications Ser. 64, Setting a New Standard in the Analysis of Binary Stars, ed. K. Pavlovski, A. Tkachenko, & G. Torres (Les Ulis: EDP Sciences), 269
Bloemen, S., Hu, H., Aerts, C., et al. 2014, A&A, 569, A123

Bloemen, S., Marsh, T. R., Østensen, R. H., et al. 2011, MNRAS, 410, 1787
Bluhm, H., Marggraf, O., de Boer, K. S., Richter, P., & Heber, U. 1999, A&A, 352, 287
Bogdanović, T., Cheng, R. M., & Amaro-Seoane, P. 2014, ApJ, 788, 99
Bours, M. C. P., Marsh, T. R., Gänsicke, B. T., & Parsons, S. G. 2015, MNRAS, 448, 601
Bours, M. C. P., Marsh, T. R., Parsons, S. G., et al. 2014, MNRAS, 438, 3399
Brassard, P., Fontaine, G., Chayer, P., & Green, E. M. 2010, in AIP Conf. Ser. 1273, 17th European White Dwarf Workshop, ed. K. Werner, & T. Rauch (Melville, NY: AIP), 259
Breton, R. P., Rappaport, S. A., van Kerkwijk, M. H., & Carter, J. A. 2012, ApJ, 748, 115
Brogaard, K., VandenBerg, D. A., Bruntt, H., et al. 2012, A&A, 543, A106
Brown, J. M., Kilic, M., Brown, W. R., & Kenyon, S. J. 2011a, ApJ, 730, 67
Brown, T. M., Landsman, W. B., Randall, S. K., Sweigart, A. V., & Lanz, T. 2013a, ApJL, 777, L22
Brown, T. M., Sweigart, A. V., Lanz, T., et al. 2010a, ApJ, 718, 1332
Brown, T. M., Sweigart, A. V., Lanz, T., Landsman, W. B., & Hubeny, I. 2001, ApJ, 562, 368
Brown, W. R. 2015, ARA&A, 53, 15
Brown, W. R., Anderson, J., Gnedin, O. Y., et al. 2015, ApJ, 804, 49
Brown, W. R., Geller, M. J., & Kenyon, S. J. 2014, ApJ, 787, 89
Brown, W. R., Geller, M. J., Kenyon, S. J., & Kurtz, M. J. 2006, ApJ, 647, 303
Brown, W. R., Gianninas, A., Kilic, M., Kenyon, S. J., & Allende Prieto, C. 2016, ApJ, 818, 155
Brown, W. R., Kilic, M., Allende Prieto, C., Gianninas, A., & Kenyon, S. J. 2013b, ApJ, 769, 66
Brown, W. R., Kilic, M., Allende Prieto, C., & Kenyon, S. J. 2010b, ApJ, 723, 1072
Brown, W. R., Kilic, M., Hermes, J. J., et al. 2011b, ApJL, 737, L23
Busso, G., Moehler, S., Zoccali, M., Heber, U., & Yi, S. K. 2005, ApJL, 633, L29
Carter, J. A., Rappaport, S., & Fabrycky, D. 2011, ApJ, 728, 139
Cassisi, S., Schlattl, H., Salaris, M., & Weiss, A. 2003, ApJL, 582, L43
Castellani, M., & Castellani, V. 1993, ApJ, 407, 649
Catelan, M. 2009, Ap&SS, 320, 261
Charpinet, S., Fontaine, G., Brassard, P., et al. 1997, ApJL, 483, L123
Charpinet, S., Fontaine, G., Brassard, P., et al. 2007, CoAst, 150, 241
Charpinet, S., Fontaine, G., Brassard, P., et al. 2008a, in ASP Conf. Ser. 392, Hot Subdwarf Stars and Related Objects, ed. U. Heber, C. S. Jeffery, & R. Napiwotzki (San Francisco, CA: ASP), 297
Charpinet, S., Fontaine, G., Brassard, P., et al. 2011a, Natur, 480, 496
Charpinet, S., Fontaine, G., Brassard, P., & Dorman, B. 1996, ApJL, 471, L103
Charpinet, S., Fontaine, G., Brassard, P., & Dorman, B. 2002, ApJS, 139, 487
Charpinet, S., Green, E. M., Baglin, A., et al. 2010, A&A, 516, L6
Charpinet, S., Van Grootel, V., Fontaine, G., et al. 2011b, A&A, 530, A3
Charpinet, S., Van Grootel, V., Reese, D., et al. 2008b, A&A, 489, 377
Chavez, C. E., Georgakarakos, N., Prodan, S., et al. 2015, MNRAS, 446, 1283
Chayer, P., & Dixon, W. 2014, in ASP Conf. Ser. 481, 6th Meeting on Hot Subdwarf Stars and Related Objects, ed. V. van Grootel et al. (San Francisco, CA: ASP), 59
Chayer, P., Dixon, W. V., Fullerton, A. W., Ooghe-Tabanou, B., & Reid, I. N. 2015, MNRAS, 452, 2292
Chayer, P., Fontaine, G., Wesemael, F., et al. 2009, in AIP Conf. Ser. 1135, Future Directions in Ultraviolet Spectroscopy: A Conference Inspired by the Accomplishments of the Far Ultraviolet Spectroscopic Explorer Mission, ed. M. E. van Steenberg et al. (Melville, NY: AIP), 148
Chayer, P., Fontaine, M., Fontaine, G., Wesemael, F., & Dupuis, J. 2006, BaltA, 15, 131
Chen, X., Han, Z., Deca, J., & Podsiadlowski, P. 2013, MNRAS, 434, 186
Chote, P., Sullivan, D. J., Brown, R., et al. 2014, MNRAS, 440, 1490
Clausen, D., & Wade, R. A. 2011, ApJL, 733, L42
Clausen, D., Wade, R. A., Kopparapu, R. K., & O'Shaughnessy, R. 2012, ApJ, 746, 186
Coenen, T., van Leeuwen, J., & Stairs, I. H. 2011, A&A, 531, A125
Constantino, T., Campbell, S. W., Christensen-Dalsgaard, J., Lattanzio, J. C., & Stello, D. 2015, MNRAS, 452, 123
Copperwheat, C. M., Morales-Rueda, L., Marsh, T. R., Maxted, P. F. L., & Heber, U. 2011, MNRAS, 415, 1381
Córsico, A. H., & Althaus, L. G. 2015, in ASP Conf. Ser. 493, 19th European Workshop on White Dwarfs, ed. P. Dufour, P. Bergeron, & G. Fontaine (San Francisco, CA: ASP), 221
Córsico, A. H., Romero, A. D., Althaus, L. G., & Hermes, J. J. 2012, A&A, 547, A96
Cunha, M. S., Aerts, C., Christensen-Dalsgaard, J., et al. 2007, A&ARv, 14, 217
Dalton, G., Trager, S. C., Abrams, D. C., et al. 2012, Proc. SPIE, 8446, 84460P
Dan, M., Rosswog, S., Brüggen, M., & Podsiadlowski, P. 2014, MNRAS, 438, 14
D'Antona, F., Caloi, V., Montalbán, J., Ventura, P., & Gratton, R. 2002, A&A, 395, 69
D'Antona, F., Caloi, V., & Ventura, P. 2010, MNRAS, 405, 2295
Davis, P. J., Kolb, U., & Willems, B. 2010, MNRAS, 403, 179
D'Cruz, N. L., Dorman, B., Rood, R. T., & O'Connell, R. W. 1996, ApJ, 466, 359
D'Cruz, N. L., O'Connell, R. W., Rood, R. T., et al. 2000, ApJ, 530, 352
de Boer, K. S. 1987, in IAU Coll. 95, Second Conf. Faint Blue Stars, ed. A. G. D. Philip, D. S. Hayes, & J. W. Liebert (Schenectady, NY: L. Davis), 95
de Boer, K. S., Aguilar Sanchez, Y., Altmann, M., et al. 1997, A&A, 327, 577
de Jong, R. S., Barden, S., Bellido-Tirado, O., et al. 2014, Proc. SPIE, 9147, 91470M
de Marchi, F., Poretti, E., Montalto, M., et al. 2007, A&A, 471, 515
Debes, J. H., Kilic, M., Tremblay, P.-E., et al. 2015, AJ, 149, 176
Deca, J., Marsh, T. R., Østensen, R. H., et al. 2012, MNRAS, 421, 2798
D'Ercole, A., Vesperini, E., D'Antona, F., McMillan, S. L. W., & Recchi, S. 2008, MNRAS, 391, 825
Derekas, A., Németh, P., Southworth, J., et al. 2015, ApJ, 808, 179
Dhillon, V. S., Marsh, T. R., Stevenson, M. J., et al. 2007, MNRAS, 378, 825
Dixon, W. V. D., Brown, T. M., & Landsman, W. B. 2004, ApJL, 600, L43
Dorman, B., Rood, R. T., & O'Connell, R. W. 1993, ApJ, 419, 596
Dotter, A., Sarajedini, A., Anderson, J., et al. 2010, ApJ, 708, 698
Downes, R. A. 1986, ApJS, 61, 569
Doyle, L. R., Carter, J. A., Fabrycky, D. C., et al. 2011, Sci, 333, 1602
Drechsel, H., Haas, S., Lorenz, R., & Gayler, S. 1995, A&A, 294, 723
Dreizler, S. 1993, A&A, 273, 212
Dreizler, S., Heber, U., Napiwotzki, R., & Hagen, H. J. 1995, A&A, 303, L53
Dreizler, S., Heber, U., Werner, K., Moehler, S., & de Boer, K. S. 1990, A&A, 235, 234
Dreizler, S., & Werner, K. 1993, A&A, 278, 199
Dreizler, S., Werner, K., Heber, U., & Engels, D. 1996, A&A, 309, 820
Dreizler, S., Werner, K., Jordan, S., & Hagen, H. 1994, A&A, 286, 463
Driebe, T., Blöcker, T., Schönberner, D., & Herwig, F. 1999, A&A, 350, 89
Driebe, T., Schoenberner, D., Bloecker, T., & Herwig, F. 1998, A&A, 339, 123
Drilling, J. S., Jeffery, C. S., Heber, U., Moehler, S., & Napiwotzki, R. 2013, A&A, 551, A31
Dworetsky, M. M., Lanning, H. H., Etzel, P. B., & Patenaude, D. J. 1977, MNRAS, 181, 13P
Edelmann, H., Heber, U., Hagen, H.-J., et al. 2003, A&A, 400, 939
Edelmann, H., Heber, U., & Napiwotzki, R. 2001, AN, 322, 401
Edelmann, H., Heber, U., & Napiwotzki, R. 2006, BaltA, 15, 103
Edelmann, H., Heber, U., Napiwotzki, R., Reid, I. N., & Saffer, R. A. 1999, in ASP Conf. Ser. 169, 11th European Workshop on White Dwarfs, ed. S.-E. Solheim, & E. G. Meistas (San Francisco, CA: ASP), 546
Etzel, P. B., Lanning, H. H., Patenaude, D. J., & Dworetsky, M. M. 1977, PASP, 89, 616
Fabbian, D., Recio-Blanco, A., Gratton, R. G., & Piotto, G. 2005, A&A, 434, 235
Faigler, S., Kull, I., Mazeh, T., et al. 2015, ApJ, 815, 26
Falter, S., Heber, U., Dreizler, S., et al. 2003, A&A, 401, 289
Fekel, F. C., Henry, G. W., Busby, M. R., & Eitter, J. J. 1993, AJ, 106, 2370
Ferguson, D. H., Green, R. F., & Liebert, J. 1984, ApJ, 287, 320
Ferguson, D. H., Liebert, J., Haas, S., Napiwotzki, R., & James, T. A. 1999, ApJ, 518, 866
Ferrario, L., de Martino, D., & Gänsicke, B. T. 2015, SSRv, 191, 111
Fink, M., Hillebrandt, W., & Röpke, F. K. 2007, A&A, 476, 1133

Fink, M., Röpke, F. K., Hillebrandt, W., et al. 2010, A&A, 514, A53
Fontaine, G., Brassard, P., Charpinet, S., et al. 2003, ApJ, 597, 518
Fontaine, G., Brassard, P., Charpinet, S, et al. 2008a, in ASP Conf. Ser. 392, Hot Subdwarf Stars and Related Objects, ed. U. Heber, C. S. Jeffery, & R. Napiwotzki (San Francisco, CA: ASP), 231
Fontaine, G., Brassard, P., Charpinet, S., et al. 2012, A&A, 539, A12
Fontaine, G., Brassard, P., Green, E. M., et al. 2008b, A&A, 486, L39
Fontaine, G., & Chayer, P. 1997, in The Third Conf. on Faint Blue Stars, ed. A. G. D. Philip et al. (Schenectady, NY: L. Davis), 169
Fontaine, G., Green, E., Brassard, P., Latour, M., & Chayer, P. 2014, in ASP Conf. Ser. 481, 6th Meeting on Hot Subdwarf Stars and Related Objects, ed. V. van Grootel et al. (San Francisco, CA: ASP), 83
Foster, H. M., Reed, M. D., Telting, J. H., Østensen, R. H., & Baran, A. S. 2015, ApJ, 805, 94
Frasca, A., Marilli, E., & Catalano, S. 1998, A&A, 333, 205
Frew, D. J., Madsen, G. J., O'Toole, S. J., & Parker, Q. A. 2010, PASA, 27, 203
Fusi Pecci, F., Ferraro, F. R., Bellazzini, M., et al. 1993, AJ, 105, 1145
Gautschy, A. 2013, arXiv:1303.6652
Geier, S. 2013, A&A, 549, A110
Geier, S., Classen, L., & Heber, U. 2011a, ApJL, 733, L13
Geier, S., Fürst, F., Ziegerer, E., et al. 2015a, Sci, 347, 1126
Geier, S., & Heber, U. 2012, A&A, 543, A149
Geier, S., Heber, U., Edelmann, H., et al. 2013a, A&A, 557, A122
Geier, S., Heber, U., Heuser, C., et al. 2013b, A&A, 551, L4
Geier, S., Heber, U., Kupfer, T., & Napiwotzki, R. 2010a, A&A, 515, A37
Geier, S., Heber, U., & Napiwotzki, R. 2008a, MmSAI, 79, 723
Geier, S., Heber, U., & Napiwotzki, R. 2008b, in ASP Conf. Ser. 392, Hot Subdwarf Stars and Related Objects, ed. U. Heber, C. S. Jeffery, & R. Napiwotzki (San Francisco, CA: ASP), 225
Geier, S., Heber, U., Podsiadlowski, P., et al. 2010b, A&A, 519, A25
Geier, S., Hirsch, H., Tillich, A., et al. 2011b, A&A, 530, A28
Geier, S., Kupfer, T., Heber, U., et al. 2015b, A&A, 577, A26
Geier, S., Marsh, T. R., Dunlap, B. H., et al. 2013c, in ASP Conf. Ser. 469, 18th European White Dwarf Workshop, ed. J. ski Krzesiń et al. (San Francisco, CA: ASP), 373
Geier, S., Marsh, T. R., Wang, B., et al. 2013d, A&A, 554, A54
Geier, S., Napiwotzki, R., Heber, U., & Nelemans, G. 2011b, A&A, 528, L16
Geier, S., Nesslinger, S., Heber, U., et al. 2007, A&A, 464, 299
Geier, S., Schaffenroth, V., Drechsel, H., et al. 2011c, ApJL, 731, L22
Gianninas, A., Bergeron, P., Dupuis, J., & Ruiz, M. T. 2010, ApJ, 720, 581
Gianninas, A., Dufour, P., Kilic, M., et al. 2014a, ApJ, 794, 35
Gianninas, A., Hermes, J. J., Brown, W. R., et al. 2014b, ApJ, 781, 104
Gianninas, A., Kilic, M., Brown, W. R., Canton, P., & Kenyon, S. J. 2015, ApJ, 812, 167
Giddings, J. R. 1981, PhD thesis, Univ. London
Gies, D. R., Bagnuolo, W. G., Jr., Ferrara, E. C., et al. 1998, ApJ, 493, 440
Gies, D. R., Dieterich, S., Richardson, N. D., et al. 2008, ApJL, 682, L117
Gillett, F. C., Jacoby, G. H., Joyce, R. R., et al. 1989, ApJ, 338, 862
Girven, J., Steeghs, D., Heber, U., et al. 2012, MNRAS, 425, 1013
Gratton, R. G., Carretta, E., & Bragaglia, A. 2012, A&ARv, 20, 50
Gratton, R. G., Carretta, E., Bragaglia, A., Lucatello, S., & D'Orazi, V. 2010, A&A, 517, A81
Green, E., Johnson, C., Wallace, S., et al. 2014, in ASP Conf. Ser. 481, 6th Meeting on Hot Subdwarf Stars and Related Objects, ed. V. van Grootel et al. (San Francisco, CA: ASP), 161
Green, E. M., Fontaine, G., Hyde, E. A., For, B.-Q., & Chayer, P. 2008, in ASP Conf. Ser. 392, Hot Subdwarf Stars and Related Objects, ed. U. Heber, C. S. Jeffery, & R. Napiwotzki (San Francisco, CA: ASP), 75
Green, E. M., Fontaine, G., Reed, M. D., et al. 2003, ApJL, 583, L31
Green, E. M., For, B., Hyde, E. A., et al. 2004, Ap&SS, 291, 267
Green, E. M., Guvenen, B., O'Malley, C. J., et al. 2011, ApJ, 734, 59
Green, E. M., Liebert, J., & Saffer, R. A. 2001, in ASP Conf. Ser. 226, 12th European Workshop on White Dwarfs, ed. J. L. Provencal et al. (San Francisco, CA: ASP), 192
Green, E. M., Liebert, J. W., Peterson, R. C., & Saffer, R. A. 1997, in The Third Conf. on Faint Blue Stars, ed. A. G. D. Philip et al. (Schenectady, NY: L. Davis), 271
Green, R. F., Schmidt, M., & Liebert, J. 1986, ApJS, 61, 305
Greenstein, G. S. 1967, Natur, 213, 871
Greenstein, J. L. 1952, PASP, 64, 256
Greenstein, J. L. 1956, in Third Berkeley Symp. on Mathematical Statistics and Probability, ed. J. Neyman (Berkeley, CA: Univ. California Press), 11
Greenstein, J. L. 1973, A&A, 23, 1
Greenstein, J. L. 1987, in IAU Coll. 95, Second Conference on Faint Blue Stars, ed. A. G. D. Philip, D. S. Hayes, & J. W. Liebert, 3
Greenstein, J. L., & Sargent, A. I. 1974, ApJS, 28, 157
Groot, P. J. 2012, ApJ, 745, 55
Hagen, H.-J., Groote, D., Engels, D., & Reimers, D. 1995, A&AS, 111, 195
Hall, P. D., Tout, C. A., Izzard, R. G., & Keller, D. 2013, MNRAS, 435, 2048
Hallakoun, N., Maoz, D., Kilic, M., et al. 2016, MNRAS, 458, 845
Han, Z. 1998, MNRAS, 296, 1019
Han, Z. 2008, A&A, 484, L31
Han, Z., Jeffery, S., Podsiadlowski, P., & Dopita, M. A. 2010a, Ap&SS, 329, 1
Han, Z., Podsiadlowski, P., & Lynas-Gray, A. 2010b, Ap&SS, 329, 41
Han, Z., Podsiadlowski, P., Maxted, P. F. L., & Marsh, T. R. 2003, MNRAS, 341, 669
Han, Z., Podsiadlowski, P., Maxted, P. F. L., Marsh, T. R., & Ivanova, N. 2002, MNRAS, 336, 449
Hansen, B. M. S. 2005, ApJ, 635, 522
Hardy, A., Schreiber, M. R., Parsons, S. G., et al. 2015, ApJL, 800, L24
Harrington, J. P., & Paltoglou, G. 1993, ApJL, 411, L103
Hartoog, M. R. 1979, ApJ, 231, 161
Heber, U. 1986, A&A, 155, 33
Heber, U. 1987, MitAG, 70, 79
Heber, U. 2009, ARA&A, 47, 211
Heber, U., Dreizler, S., & Hagen, H.-J. 1996, A&A, 311, L17
Heber, U., & Edelmann, H. 2004, Ap&SS, 291, 341
Heber, U., Edelmann, H., Lisker, T., & Napiwotzki, R. 2003, A&A, 411, L477
Heber, U., Geier, S., & Gaensicke, B. 2013, EPJWC, 43, 04002
Heber, U., Geier, S., Irrgang, A., et al. 2014, in ASP Conf. Ser. 481, 6th Meeting on Hot Subdwarf Stars and Related Objects, ed. V. van Grootel et al. (San Francisco, CA: ASP), 307
Heber, U., & Hirsch, H. 2010, in AIP Conf. Ser. 1314, International Conference on Binaries: In celebration of Ron Webbink's 65th Birthday, ed. V. Kalogera, & M. van der Sluys (Melville, NY: AIP), 79
Heber, U., & Hunger, K. 1987, Msngr, 47, 36
Heber, U., Jordan, S., & Weidemann, V. 1991, White Dwarfs, Proceedings of the 7th European Workshop, ed. G. Vauclair & E. Sion (Dordrecht: Kluwer), 109
Heber, U., & Kudritzki, R. P. 1986, A&A, 169, 244
Heber, U., Kudritzki, R. P., Caloi, V., Castellani, V., & Danziger, J. 1986, A&A, 162, 171
Heber, U., Moehler, S., Napiwotzki, R., Thejll, P., & Green, E. M. 2002, A&A, 383, 938
Heber, U., Reid, I. N., & Werner, K. 1999, A&A, 348, L25
Heber, U., Reid, I. N., & Werner, K. 2000, A&A, 363, 198
Herbig, G. H. 1999, PASP, 111, 1144
Hermes, J. J., Gänsicke, B. T., Bischoff-Kim, A., et al. 2015, MNRAS, 451, 1701
Hermes, J. J., Gänsicke, B. T., Koester, D., et al. 2014, MNRAS, 444, 1674
Hermes, J. J., Kilic, M., Brown, W. R., et al. 2012a, ApJL, 757, L21
Hermes, J. J., Montgomery, M. H., Gianninas, A., et al. 2013a, MNRAS, 436, 3573
Hermes, J. J., Montgomery, M. H., Winget, D. E., et al. 2012b, ApJL, 750, L28
Hermes, J. J., Montgomery, M. H., Winget, D. E., et al. 2013b, ApJ, 765, 102
Hernandez, A. K., Wakker, B. P., Benjamin, R. A., et al. 2013, ApJ, 777, 19
Hillebrandt, W., Kromer, M., Röpke, F. K., & Ruiter, A. J. 2013, FrPhy, 8, 116
Hills, J. G. 1988, Natur, 331, 687
Hinse, T. C., Lee, J. W., Goździewski, K., Horner, J., & Wittenmyer, R. A. 2014, MNRAS, 438, 307
Hirsch, H. 2009, PhD thesis, Univ. Erlangen-Nuremberg, http://www.sternwarte.uni-erlangen.de/Arbeiten/2009-07_Hirsch.pdf
Hirsch, H., & Heber, U. 2009, JPhCS, 172, 012015
Hirsch, H. A., Heber, U., & O'Toole, S. J. 2008, in ASP Conf. Ser. 392, Hot Subdwarf Stars and Related Objects, ed. U. Heber, C. S. Jeffery, & R. Napiwotzki (San Francisco, CA: ASP), 131
Hirsch, H. A., Heber, U., O'Toole, S. J., & Bresolin, F. 2005, A&A, 444, L61
Homeier, D., Koester, D., Hagen, H.-J., et al. 1998, A&A, 338, 563

Horner, J., Hinse, T. C., Wittenmyer, R. A., Marshall, J. P., & Tinney, C. G. 2012, MNRAS, 427, 2812
Howarth, I. D., & Heber, U. 1990, PASP, 102, 912
Hoyer, D., Rauch, T., Werner, K., Hauschildt, P. H., & Kruk, J. W. 2015, A&A, 578, A125
Hu, H., Dupret, M.-A., Aerts, C., et al. 2008, A&A, 490, 243
Hu, H., Tout, C. A., Glebbeek, E., & Dupret, M.-A. 2011, MNRAS, 418, 195
Hubeny, I. 1988, CoPhC, 52, 103
Hubeny, I., & Lanz, T. 1995, ApJ, 439, 875
Huber, D. 2014, arXiv:1404.7501
Hubrig, S., Castelli, F., de Silva, G., et al. 2009, A&A, 499, 865
Humason, M. L., & Zwicky, F. 1947, ApJ, 105, 85
Iben, I., Jr. 1984, ApJ, 277, 333
Irrgang, A., Wilcox, B., Tucker, E., & Schiefelbein, L. 2013, A&A, 549, A137
Israel, G. L., Stella, L., Angelini, L., et al. 1997, ApJL, 474, L53
Istrate, A. G., Tauris, T. M., Langer, N., & Antoniadis, J. 2014, A&A, 571, L3
Ivanova, N., Justham, S., Chen, X., et al. 2013, A&ARv, 21, 59
Jacobs, V. A., Østensen, R. H., van Winckel, H., et al. 2011, in AIP Conf. Ser. 1331, Planetary Systems Beyond the Main Sequence, ed. S. Schuh, H. Drechsel, & U. Heber (Melville, NY: AIP), 304
Jacoby, G. H., Morse, J. A., Fullton, L. K., Kwitter, K. B., & Henry, R. B. C. 1997, AJ, 114, 2611
Jasniewicz, G., de Laverny, P., Parthasarathy, M., Lèbre, A., & Thévenin, F. 2004, A&A, 423, 353
Jeffery, C. S., Aerts, C., Dhillon, V. S., Marsh, T. R., & Gänsicke, B. T. 2005, MNRAS, 362, 66
Jeffery, C. S., Ahmad, A., Naslim, N., & Kerzendorf, W. 2015a, MNRAS, 446, 1889
Jeffery, C. S., Dhillon, V. S., Marsh, T. R., & Ramachandran, B. 2004, MNRAS, 352, 699
Jeffery, C. S., & Hamann, W.-R. 2010, MNRAS, 404, 1698
Jeffery, C. S., Pereira, C., Naslim, N., & Behara, N. 2012, in ASP Conf. Ser. 452, Fifth Meeting on Hot Subdwarf Stars and Related Objects, ed. D. Kilkenny, C. S. Jeffery, & C. Koen (San Francisco, CA: ASP), 41
Jeffery, C. S., & Ramsay, G. 2014, MNRAS, 442, L61
Jeffery, C. S., Ramsay, G., Naslim, N., et al. 2013, MNRAS, 429, 3207
Jeffery, C. S., & Saio, H. 2006, MNRAS, 372, L48
Jeffery, C. S., & Saio, H. 2007, MNRAS, 378, 379
Jeffery, C. S., & Saio, H. 2013, MNRAS, 435, 885
Jeffery, C. S., & Simon, T. 1997, MNRAS, 286, 487
Jeffery, C. S., Simon, T., & Evans, T. L. 1992, MNRAS, 258, 64
Jeffery, S., Naslim, N., Behara, N., & Hibbert, A. 2015b, A&G, 56, 020002
Jenkins, E. B. 2013, ApJ, 764, 25
Johnson, C., Green, E., Wallace, S., et al. 2014, in ASP Conf. Ser. 481, 6th Meeting on Hot Subdwarf Stars and Related Objects, ed. V. van Grootel et al. (San Francisco, CA: ASP), 153
Johnson, D. R. H., & Soderblom, D. R. 1987, AJ, 93, 864
Justham, S., Podsiadlowski, P., & Han, Z. 2011, MNRAS, 410, 984
Justham, S., Podsiadlowski, P., Han, Z., & Wolf, C. 2010, Ap&SS, 329, 3
Justham, S., Wolf, C., Podsiadlowski, P., & Han, Z. 2009, A&A, 493, 1081
Kalirai, J. S., Bergeron, P., Hansen, B. M. S., et al. 2007, ApJ, 671, 748
Kaluzny, J., & Udalski, A. 1992, AcA, 42, 29
Kaplan, D. L. 2010, ApJL, 717, L108
Kaplan, D. L., Bhalerao, V. B., van Kerkwijk, M. H., et al. 2013, ApJ, 765, 158
Kaplan, D. L., Marsh, T. R., Walker, A. N., et al. 2014a, ApJ, 780, 167
Kaplan, D. L., van Kerkwijk, M. H., Koester, D., et al. 2014b, ApJL, 783, L23
Karl, C., Heber, U., Jeffery, S., Napiwotzki, R., & Geier, S. 2006, BaltA, 15, 151
Karl, C., Heber, U., & Napiwotzki, R. 2005, in ASP Conf. Ser. 334, 14th European Workshop on White Dwarfs, ed. D. Koester, & S. Moehler (San Francisco, CA: ASP), 369
Kawaler, S. D., Reed, M. D., Østensen, R. H., et al. 2010a, MNRAS, 409, 1509
Kawaler, S. D., Reed, M. D., Quint, A. C., et al. 2010b, MNRAS, 409, 1487
Kawka, A., Pigulski, A., O'Toole, S., et al. 2012, in ASP Conf. Ser. 452, Fifth Meeting on Hot Subdwarf Stars and Related Objects, ed. D. Kilkenny, C. S. Jeffery, & C. Koen (San Francisco, CA: ASP), 121
Kawka, A., Vennes, S., Oswalt, T. D., Smith, J. A., & Silvestri, N. M. 2006, ApJL, 643, L123
Kawka, A., Vennes, S., O'Toole, S., et al. 2015, MNRAS, 450, 3514
Kawka, A., Vennes, S., & Vaccaro, T. R. 2010, A&A, 516, L7
Kepler, S. O., Pelisoli, I., Koester, D., et al. 2015, MNRAS, 446, 4078
Kilic, M., Allende Prieto, C., Brown, W. R., & Koester, D. 2007, ApJ, 660, 1451
Kilic, M., Brown, W. R., Allende Prieto, C., et al. 2011, ApJ, 727, 3
Kilic, M., Brown, W. R., Allende Prieto, C., et al. 2012, ApJ, 751, 141
Kilic, M., Hermes, J. J., Gianninas, A., et al. 2014, MNRAS, 438, L26
Kilkenny, D. 1978, Obs, 98, 207
Kilkenny, D. 2014, MNRAS, 445, 4247
Kilkenny, D., Fontaine, G., Green, E. M., & Schuh, S. 2010, IBVS, 5927, 1
Kilkenny, D., & Koen, C. 2016, MNRAS, 457, 723
Kilkenny, D., Koen, C., O'Donoghue, D., & Stobie, R. S. 1997, MNRAS, 285, 640
Kilkenny, D., Marang, F., & Menzies, J. W. 1994, MNRAS, 267, 535
Kilkenny, D., O'Donoghue, D., Koen, C., Lynas-Gray, A. E., & van Wyk, F. 1998, MNRAS, 296, 329
Kilkenny, D., Jeffery, C. S., & Koen, C. (ed.) 2012, in ASP Conf. Ser. 452, Fifth Meeting on Hot Subdwarf Stars and Related Objects (San Francisco, CA: ASP)
Kinman, T., Castelli, F., Cacciari, C., et al. 2000, A&A, 364, 102
Klepp, S., & Rauch, T. 2011, A&A, 531, L7
Knigge, C., Dieball, A., Maíz Apellániz, J., et al. 2008, ApJ, 683, 1006
Koch, D. G., Borucki, W. J., Basri, G., et al. 2010, ApJL, 713, L79
Koen, C., & Green, E. M. 2007, MNRAS, 377, 1605
Koen, C., Kilkenny, D., O'Donoghue, D., van Wyk, F., & Stobie, R. S. 1997, MNRAS, 285, 645
Koen, C., Orosz, J. A., & Wade, R. A. 1998, MNRAS, 300, 695
Koester, D., Voss, B., Napiwotzki, R., et al. 2009, A&A, 505, 441
Kruse, E., & Agol, E. 2014, Sci, 344, 275
Krzesinski, J. 2015, A&A, 581, A7
Kuassivi Bonanno, A., & Ferlet, R. 2005, A&A, 442, 1015
Kudritzki, R. P. 1976, A&A, 52, 11
Kudritzki, R. P. 1979, in The Elements and their Isotopes in the Universe, ed. A. Boury, N. Grevesse, & L. Remy-Battiau (Cointe-Ougree: Univ. de Liege), 295
Kudritzki, R. P., & Simon, K. P. 1978, A&A, 70, 653
Kudritzki, R. P., Simon, K. P., Lynas-Gray, A. E., Kilkenny, D., & Hill, P. W. 1982, A&A, 106, 254
Kupfer, T., Geier, S., Heber, U., et al. 2015, A&A, 576, A44
Kustner, F. 1921, VeBon, 15, 1
La Palombara, N., Esposito, P., Mereghetti, S., Novara, G., & Tiengo, A. 2015, A&A, 580, A56
La Palombara, N., Esposito, P., Mereghetti, S., & Tiengo, A. 2014, A&A, 566, A4
La Palombara, N., Mereghetti, S., Tiengo, A., & Esposito, P. 2012, ApJL, 750, L34
Landstreet, J. D., Bagnulo, S., Fossati, L., Jordan, S., & O'Toole, S. J. 2012, A&A, 541, A100
Lanz, T., Brown, T. M., Sweigart, A. V., Hubeny, I., & Landsman, W. B. 2004, ApJ, 602, 342
Larsen, S. S., Brodie, J. P., Grundahl, F., & Strader, J. 2014, ApJ, 797, 15
Latour, M., Fontaine, G., Brassard, P., et al. 2011, ApJ, 733, 100
Latour, M., Fontaine, G., Chayer, P., & Brassard, P. 2013, ApJ, 773, 84
Latour, M., Fontaine, G., & Green, E. 2014a, in ASP Conf. Ser. 481, 6th Meeting on Hot Subdwarf Stars and Related Objects, ed. V. van Grootel et al. (San Francisco, CA: ASP), 91
Latour, M., Fontaine, G., Green, E. M., & Brassard, P. 2015, A&A, 579, A39
Latour, M., Fontaine, G., Green, E. M., Brassard, P., & Chayer, P. 2014b, ApJ, 788, 65
Latour, M., Heber, U., Irrgang, A., et al. 2016, A&A, 585, A115
Latour, M., Randall, S. K., Fontaine, G., et al. 2014c, ApJ, 795, 106
Law, N. M., Kulkarni, S. R., Dekany, R. G., et al. 2009, PASP, 121, 1395
Lee, J. W., Hinse, T. C., Youn, J.-H., & Han, W. 2014, MNRAS, 445, 2331
Lee, J. W., Kim, S.-L., Kim, C.-H., et al. 2009, AJ, 137, 3181
Lee, Y.-W., Demarque, P., & Zinn, R. 1994, ApJ, 423, 248
Lehner, N., & Howk, J. C. 2004, PASP, 116, 895
Lei, Z., Chen, X., Zhang, F., & Han, Z. 2015, MNRAS, 449, 2741
Lei, Z.-X., Chen, X.-F., Zhang, F.-H., & Han, Z. 2013a, A&A, 549, A145
Lei, Z.-X., Zhang, F.-H., Ge, H.-W., & Han, Z.-W. 2013b, A&A, 554, A130

Lemke, M., Heber, U., Napiwotzki, R., Dreizler, S., & Engels, D. 1997, in The Third Conf. on Faint Blue Stars, ed. A. G. D. Philip et al. (Schenectady, NY: L. Davis), 375
Liebert, J., Bergeron, P., Eisenstein, D., et al. 2004, ApJL, 606, L147
Liebert, J., Bergeron, P., & Holberg, J. B. 2005, ApJS, 156, 47
Liebert, J., Saffer, R. A., & Green, E. M. 1994, AJ, 107, 1408
Linsky, J. L., Draine, B. T., Moos, H. W., et al. 2006, ApJ, 647, 1106
Lisker, T., Heber, U., Napiwotzki, R., et al. 2005, A&A, 430, 223
Liu, Z.-W., Pakmor, R., Seitenzahl, I. R., et al. 2013, ApJ, 774, 37
Livne, E., & Glasner, A. S. 1990, ApJ, 361, 244
Lohr, M. E., Norton, A. J., Anderson, D. R., et al. 2014, A&A, 566, A128
Lorén-Aguilar, P., Isern, J., & García-Berro, E. 2009, A&A, 500, 1193
LSST Science Collaboration, Abell, P. A., Allison, J., et al. 2009, arXiv:0912.0201
Lucy, L. B., & White, R. L. 1980, ApJ, 241, 300
Luo, Y.-P., Németh, P., Liu, C., Deng, L.-C., & Han, Z.-W. 2016, ApJ, 818, 202
Luyten, W. J. 1953, AJ, 58, 75
Luyten, W. J. 1965, Proceedings of the 1st Conference on Faint Blue Stars (Minneapolis, MN: Univ. Minnesota)
Lynas-Gray, A. E. 2004, Ap&SS, 291, 197
Macrae, D. A., Fleischer, R., & Weston, E. B. 1951, ApJ, 113, 432
Maeder, A. 1973, A&A, 26, 215
Maoz, D., Mannucci, F., & Nelemans, G. 2014, ARA&A, 52, 107
Marino, A. F., Milone, A. P., Przybilla, N., et al. 2014, MNRAS, 437, 1609
Marsh, T. R. 2001, MNRAS, 324, 547
Marsh, T. R., Dhillon, V. S., & Duck, S. R. 1995, MNRAS, 275, 828
Marsh, T. R., Nelemans, G., & Steeghs, D. 2004, MNRAS, 350, 113
Matson, R. A., Gies, D. R., Guo, Z., et al. 2015, ApJ, 806, 155
Maxted, P. F. L., Anderson, D. R., Burleigh, M. R., et al. 2011, MNRAS, 418, 1156
Maxted, P. F. L., Bloemen, S., Heber, U., et al. 2014a, MNRAS, 437, 1681
Maxted, P. f. L., Heber, U., Marsh, T. R., & North, R. C. 2001, MNRAS, 326, 1391
Maxted, P. F. L., Marsh, T. R., Heber, U., et al. 2002, MNRAS, 333, 231
Maxted, P. F. L., Marsh, T. R., & Moran, C. K. J. 2000a, MNRAS, 319, 305
Maxted, P. F. L., Marsh, T. R., & North, R. C. 2000b, MNRAS, 317, L41
Maxted, P. F. L., Morales-Rueda, L., & Marsh, T. R. 2004, Ap&SS, 291, 307
Maxted, P. F. L., Serenelli, A. M., Marsh, T. R., et al. 2014b, MNRAS, 444, 208
Maxted, P. F. L., Serenelli, A. M., Miglio, A., et al. 2013, Natur, 498, 463
Maza, N. L., Nieva, M.-F., & Przybilla, N. 2014, A&A, 572, A112
Menzies, J. W., & Marang, F. 1986, in IAU Symp. 118, Instrumentation and Research Programmes for Small Telescopes, ed. J. B. Hearnshaw, & P. L. Cottrell (Dordrecht: D. Reidel), 305
Mereghetti, S., Campana, S., Esposito, P., La Palombara, N., & Tiengo, A. 2011a, A&A, 536, A69
Mereghetti, S., & La Palombara, N. 2015, arXiv:1510.04173
Mereghetti, S., La Palombara, N., Esposito, P., et al. 2014, MNRAS, 441, 2684
Mereghetti, S., La Palombara, N., Tiengo, A., et al. 2011b, ApJ, 737, 51
Mereghetti, S., La Palombara, N., Tiengo, A., et al. 2013, A&A, 553, A46
Mereghetti, S., Tiengo, A., Esposito, P., et al. 2009, Sci, 325, 1222
Merle, T., Jorissen, A., Masseron, T., et al. 2014, A&A, 567, A30
Michalik, D., Lindegren, L., & Hobbs, D. 2015, A&A, 574, A115
Michaud, G., Richer, J., & Richard, O. 2008, ApJ, 675, 1223
Michaud, G., Richer, J., & Richard, O. 2011, A&A, 529, A60
Mickaelian, A. M., Nesci, R., Rossi, C., et al. 2007, A&A, 464, 1177
Mihalas, D. 1965, ApJS, 9, 321
Miller Bertolami, M. M., Althaus, L. G., Unglaub, K., & Weiss, A. 2008, A&A, 491, 253
Miller Bertolami, M. M., Córsico, A. H., & Althaus, L. G. 2011, ApJL, 741, L3
Miller Bertolami, M. M., Córsico, A. H., Zhang, X., Althaus, L. G., & Jeffery, C. S. 2013, EPJWC, 43, 04004
Milone, A. P. 2015, MNRAS, 446, 1672
Milone, A. P., Marino, A. F., Piotto, G., et al. 2015a, MNRAS, 447, 927
Milone, A. P., Marino, A. F., Piotto, G., et al. 2015b, ApJ, 808, 51
Mocák, M., Müller, E., Weiss, A., & Kifonidis, K. 2008, A&A, 490, 265
Mocák, M., Müller, E., Weiss, A., & Kifonidis, K. 2009, A&A, 501, 659
Moehler, S. 1999, in Reviews in Modern Astronomy, Vol. 12, ed. R. E. Schielicke (Hamburg: Astronomische Gesellschaft), 281
Moehler, S. 2001, PASP, 113, 1162
Moehler, S. 2010, MmSAI, 81, 838
Moehler, S., Dreizler, S., Lanz, T., et al. 2011, A&A, 526, A136
Moehler, S., Heber, U., Lemke, M., & Napiwotzki, R. 1998a, A&A, 339, 537
Moehler, S., Heber, U., & Rupprecht, G. 1997, A&A, 319, 109
Moehler, S., Landsman, W., & Napiwotzki, R. 1998b, A&A, 335, 510
Moehler, S., Sweigart, A. V., Landsman, W. B., & Dreizler, S. 2002, A&A, 395, 37
Moehler, S., Sweigart, A. V., Landsman, W. B., Hammer, N. J., & Dreizler, S. 2004, A&A, 415, 313
Moni Bidin, C., Moehler, S., Piotto, G., Momany, Y., & Recio-Blanco, A. 2007, A&A, 474, 505
Moni Bidin, C., Moehler, S., Piotto, G., Momany, Y., & Recio-Blanco, A. 2009, A&A, 498, 737
Moni Bidin, C., Momany, Y., Montalto, M., et al. 2015, ApJL, 812, L31
Moni Bidin, C., Villanova, S., Piotto, G., & Momany, Y. 2011, A&A, 528, A127
Moni Bidin, C., Villanova, S., Piotto, G., et al. 2012, A&A, 547, A109
Morales-Rueda, L., Maxted, P. F. L., Marsh, T. R., North, R. C., & Heber, U. 2003, MNRAS, 338, 752
Moran, C., Maxted, P., Marsh, T. R., Saffer, R. A., & Livio, M. 1999, MNRAS, 304, 535
Morrissey, P., Conrow, T., Barlow, T. A., et al. 2007, ApJS, 173, 682
Mosser, B., Goupil, M. J., Belkacem, K., et al. 2012, A&A, 548, A10
Münch, G. 1958, ApJ, 127, 642
Napiwotzki, R. 1992, in The Atmospheres of Early-Type Stars, Vol. 401, ed. U. Heber, & C. S. Jeffery (Berlin: Springer), 310
Napiwotzki, R. 1993, AcA, 43, 343
Napiwotzki, R. 1999, A&A, 350, 101
Napiwotzki, R. 2008, in ASP Conf. Ser. 392, Hot Subdwarf Stars and Related Objects, ed. U. Heber, C. S. Jeffery, & R. Napiwotzki (San Francisco, CA: ASP), 139
Napiwotzki, R., Christlieb, N., Drechsel, H., et al. 2001a, AN, 322, 411
Napiwotzki, R., Edelmann, H., Heber, U., et al. 2001b, A&A, 378, L17
Napiwotzki, R., Karl, C. A., Lisker, T., et al. 2004, Ap&SS, 291, 321
Napiwotzki, R., Karl, C. A., Nelemans, G., et al. 2005, in ASP Conf. Ser. 334, 14th European Workshop on White Dwarfs, ed. D. Koester, & S. Moehler (San Francisco, CA: ASP), 375
Napiwotzki, R., Karl, C. A., Nelemans, G., et al. 2007, in ASP Conf. Ser. 372, 15th European Workshop on White Dwarfs, ed. R. Napiwotzki, & M. R. Burleigh (San Francisco, CA: ASP), 387
Napiwotzki, R., & Rauch, T. 1994, A&A, 285, 603
Naslim, N., Geier, S., Jeffery, C. S., et al. 2012, MNRAS, 423, 3031
Naslim, N., Jeffery, C. S., Ahmad, A., Behara, N. T., & Şahìn, T. 2010, MNRAS, 409, 582
Naslim, N., Jeffery, C. S., Behara, N. T., & Hibbert, A. 2011, MNRAS, 412, 363
Naslim, N., Jeffery, C. S., Hibbert, A., & Behara, N. T. 2013, MNRAS, 434, 1920
Nebot Gómez-Morán, A., Gänsicke, B. T., Schreiber, M. R., et al. 2011, A&A, 536, A43
Nelson, L. A., Dubeau, E., & MacCannell, K. A. 2004, ApJ, 616, 1124
Németh, P., Kawka, A., & Vennes, S. 2012, MNRAS, 427, 2180
Németh, P., Ziegerer, E., Irrgang, A., et al. 2016, ApJL, 821, L13
Nordhaus, J., & Spiegel, D. S. 2013, MNRAS, 432, 500
Nordhaus, J., Spiegel, D. S., Ibgui, L., Goodman, J., & Burrows, A. 2010, MNRAS, 408, 631
Norris, J. M., Wright, J. T., Wade, R. A., Mahadevan, S., & Gettel, S. 2011, ApJ, 743, 88
O'Donoghue, D., Lynas-Gray, A. E., Kilkenny, D., Stobie, R. S., & Koen, C. 1997, MNRAS, 285, 657
Orosz, J. A., Welsh, W. F., Carter, J. A., et al. 2012, Sci, 337, 1511
Østensen, R., Oreiro, R., Drechsel, H., et al. 2007, in ASP Conf. Ser. 372, 15th European Workshop on White Dwarfs, ed. R. Napiwotzki, & M. R. Burleigh (San Francisco, CA: ASP), 483
Østensen, R. H. 2012, in ASP Conf. Ser. 452, Fifth Meeting on Hot Subdwarf Stars and Related Objects, ed. D. Kilkennyx, C. S. Jeffery, & C. Koen (San Francisco, CA: ASP), 233
Østensen, R. H., Geier, S., Schaffenroth, V., et al. 2013, A&A, 559, A35
Østensen, R. H., Green, E. M., Bloemen, S., et al. 2010a, MNRAS, 408, L51

Østensen, R. H., Oreiro, R., Solheim, J.-E., et al. 2010b, A&A, 513, A6
Østensen, R. H., Reed, M. D., Baran, A. S., & Telting, J. H. 2014a, A&A, 564, L14
Østensen, R. H., Silvotti, R., Charpinet, S., et al. 2010c, MNRAS, 409, 1470
Østensen, R. H., Silvotti, R., Charpinet, S., et al. 2011, MNRAS, 414, 2860
Østensen, R. H., Telting, J. H., Oreiro, R., et al. 2010d, Ap&SS, 329, 167
Østensen, R. H., Telting, J. H., Reed, M. D., et al. 2014b, A&A, 569, A15
O'Toole, S. J. 2004, A&A, 423, L25
O'Toole, S. J. 2008, in ASP Conf. Ser. 392, Hot Subdwarf Stars and Related Objects, ed. U. Heber, C. S. Jeffery, & R. Napiwotzki (San Francisco, CA: ASP), 67
O'Toole, S. J., Bedding, T. R., Kjeldsen, H., et al. 2000, ApJL, 537, L53
O'Toole, S. J., & Heber, U. 2006, A&A, 452, 579
O'Toole, S. J., & Heber, U. 2007, in ASP Conf. Ser. 372, 15th European Workshop on White Dwarfs, ed. R. Napiwotzki, & M. R. Burleigh (San Francisco, CA: ASP), 209
O'Toole, S. J., Heber, U., Jeffery, C. S., et al. 2005a, A&A, 440, 667
O'Toole, S. J., Jordan, S., Friedrich, S., & Heber, U. 2005b, A&A, 437, 227
O'Toole, S. J., Napiwotzki, R., Heber, U., et al. 2006, BaltA, 15, 61
Owocki, S. P., Castor, J. I., & Rybicki, G. B. 1988, ApJ, 335, 914
Pablo, H., Kawaler, S. D., & Green, E. M. 2011, ApJL, 740, L47
Pablo, H., Kawaler, S. D., Reed, M. D., et al. 2012, MNRAS, 422, 1343
Pace, G., Recio-Blanco, A., Piotto, G., & Momany, Y. 2006, A&A, 452, 493
Paczynski, B. 1976, in IAU Symp. 73, Structure and Evolution of Close Binary Systems, ed. P. Eggleton, S. Mitton, & J. Whelan (Dordrecht: D. Reidel), 75
Pan, K.-C., Ricker, P. M., & Taam, R. E. 2013, ApJ, 773, 49
Panei, J. A., Althaus, L. G., Chen, X., & Han, Z. 2007, MNRAS, 382, 779
Parsons, S. G., Gänsicke, B. T., Marsh, T. R., et al. 2013, MNRAS, 429, 256
Parsons, S. G., Rebassa-Mansergas, A., Schreiber, M. R., et al. 2016, arXiv:1604.01613
Parthasarathy, M., Garcia-Lario, P., de Martino, D., et al. 1995, A&A, 300, L25
Passy, J.-C., De Marco, O., Fryer, C. L., et al. 2012a, ApJ, 744, 52
Passy, J.-C., Mac Low, M.-M., & De Marco, O. 2012b, ApJL, 759, L30
Pauli, E.-M., Napiwotzki, R., Heber, U., Altmann, M., & Odenkirchen, M. 2006, A&A, 447, 173
Paxton, B., Bildsten, L., Dotter, A., et al. 2011, ApJS, 192, 3
Pease, F. G. 1928, PASP, 40, 342
Pereira, T. M. D., & Lopes, I. P. 2005, ApJ, 622, 1068
Perryman, M. A. C., de Boer, K. S., Gilmore, G., et al. 2001, A&A, 369, 339
Peters, G. J., Gies, D. R., Grundstrom, E. D., & McSwain, M. V. 2008, ApJ, 686, 1280
Peters, G. J., Pewett, T. D., Gies, D. R., Touhami, Y. N., & Grundstrom, E. D. 2013, ApJ, 765, 2
Peters, P. C., & Mathews, J. 1963, PhRv, 131, 435
Peterson, R. C., Rood, R. T., & Crocker, D. A. 1995, ApJ, 453, 214
Petit, P., Van Grootel, V., Bagnulo, S., et al. 2012, in ASP Conf. Ser. 452, Fifth Meeting on Hot Subdwarf Stars and Related Objects, ed. D. Kilkenny, C. S. Jeffery, & C. Koen (San Francisco, CA: ASP), 87
Pfahl, E., Rappaport, S., & Podsiadlowski, P. 2003, ApJ, 597, 1036
Pietrukowicz, P., Mróz, P., Soszyński, I., et al. 2013, AcA, 63, 115
Piotto, G., Milone, A. P., Anderson, J., et al. 2012, ApJ, 760, 39
Piotto, G., Milone, A. P., Bedin, L. R., et al. 2015, AJ, 149, 91
Podsiadlowski, P., Han, Z., Lynas-Gray, A. E., & Brown, D. 2008, in ASP Conf. Ser. 392, Hot Subdwarf Stars and Related Objects, ed. U. Heber, C. S. Jeffery, & R. Napiwotzki (San Francisco, CA: ASP), 15
Pojmanski, G. 1997, AcA, 47, 467
Politano, M., Taam, R. E., van der Sluys, M., & Willems, B. 2008, ApJL, 687, L99
Pollacco, D. L., Skillen, I., Collier Cameron, A., et al. 2006, PASP, 118, 1407
Pols, O. R., Cote, J., Waters, L. B. F. M., & Heise, J. 1991, A&A, 241, 419
Postnov, K. A., & Yungelson, L. R. 2014, LRR, 17, 3
Prada Moroni, P. G., & Straniero, O. 2009, JPhCS, 172, 012011
Pretorius, M. L., Knigge, C., & Kolb, U. 2007, MNRAS, 374, 1495
Prša, A., & Zwitter, T. 2005, ApJ, 628, 426
Pulley, D., Faillace, G., Smith, D., & Owen, C. 2015, arXiv:1502.04366
Qian, S.-B., Zhu, L.-Y., Dai, Z.-B., et al. 2012, ApJL, 745, L23
Qian, S.-B., Zhu, L.-Y., Zola, S., et al. 2009, ApJL, 695, L163
Randall, S. K., Bagnulo, S., Ziegerer, E., Geier, S., & Fontaine, G. 2015, A&A, 576, A65
Randall, S. K., Calamida, A., Fontaine, G., Bono, G., & Brassard, P. 2011, ApJL, 737, L27
Randall, S. K., Calamida, A., Fontaine, G., et al. 2016, arXiv:1602.05470
Randall, S. K., Fontaine, G., Brassard, P., & Bergeron, P. 2005, ApJS, 161, 456
Randall, S. K., Fontaine, G., Brassard, P., & Van Grootel, V. 2010, A&A, 522, A48
Randall, S. K., Fontaine, G., Charpinet, S., Van Grootel, V., & Brassard, P. 2014a, in IAU Symp. 301, Precision Asteroseismology, ed. J. A. Guzik et al. (Cambridge: Cambridge Univ. Press), 289
Randall, S. K., Fontaine, G., Geier, S., Van Grootel, V., & Brassard, P. 2014b, A&A, 563, A79
Ransom, S. M., Stairs, I. H., Archibald, A. M., et al. 2014, Natur, 505, 520
Rappaport, S., Deck, K., Levine, A., et al. 2013, ApJ, 768, 33
Rappaport, S., Nelson, L., Levine, A., et al. 2015, ApJ, 803, 82
Rappaport, S., Podsiadlowski, P., & Horev, I. 2009, ApJ, 698, 666
Rauch, T. 1993, A&A, 276, 171
Rauch, T., & Deetjen, J. L. 2003, in ASP Conf. Ser. 288, Stellar Atmosphere Modeling, ed. I. Hubeny, D. Mihalas, & K. Werner (San Francisco, CA: ASP), 103
Rauch, T., Heber, U., & Werner, K. 2002, A&A, 381, 1007
Rauch, T., Rudkowski, A., Kampka, D., et al. 2014, A&A, 566, A3
Rauch, T., Werner, K., & Kruk, J. W. 2010, Ap&SS, 329, 133
Rauch, T., Ziegler, M., Werner, K., et al. 2007, A&A, 470, 317
Rebassa-Mansergas, A., Agurto-Gangas, C., Schreiber, M. R., Gänsicke, B. T., & Koester, D. 2013, MNRAS, 433, 3398
Rebassa-Mansergas, A., Nebot Gómez-Morán, A., Schreiber, M. R., et al. 2012, MNRAS, 419, 806
Rebassa-Mansergas, A., Nebot Gómez-Morán, A., Schreiber, M. R., Girven, J., & Gänsicke, B. T. 2011, MNRAS, 413, 1121
Recio-Blanco, A., Aparicio, A., Piotto, G., de Angeli, F., & Djorgovski, S. G. 2006, A&A, 452, 875
Recio-Blanco, A., Piotto, G., Aparicio, A., & Renzini, A. 2002, ApJL, 572, L71
Reed, M. D., Baran, A., Østensen, R. H., Telting, J., & O'Toole, S. J. 2012, MNRAS, 427, 1245
Reed, M. D., Baran, A., Quint, A. C., et al. 2011, MNRAS, 414, 2885
Reed, M. D., Baran, A. S., Østensen, R. H., et al. 2016, MNRAS, 458, 1417
Reed, M. D., Foster, H., Telting, J. H., et al. 2014, MNRAS, 440, 3809
Reif, K., Bagschik, K., de Boer, K. S., et al. 1999, Proc. SPIE, 3649, 109
Reindl, N., Rauch, T., Parthasarathy, M., et al. 2014, A&A, 565, A40
Richter, D. 1971, A&A, 14, 415
Ricker, P. M., & Taam, R. E. 2012, ApJ, 746, 74
Ritter, H., & Kolb, U. 2003, A&A, 404, 301
Rodríguez-López, C., Ulla, A., & Garrido, R. 2007, MNRAS, 379, 1123
Rowe, J. F., Borucki, W. J., Koch, D., et al. 2010, ApJL, 713, L150
Ruiz-Lapuente, P. 2014, NewAR, 62, 15
Saffer, R. A., Bergeron, P., Koester, D., & Liebert, J. 1994, ApJ, 432, 351
Saffer, R. A., Keenan, F. P., Hambly, N. C., Dufton, P. L., & Liebert, J. 1997, ApJ, 491, 172
Saffer, R. A., Livio, M., & Yungelson, L. R. 1998, ApJ, 502, 394
Salaris, M. 2015, ASSP, 39, 43
Salgado, C., Moni Bidin, C., Villanova, S., Geisler, D., & Catelan, M. 2013, A&A, 559, A101
Sargent, A. W. L. W., & Jugaku, J. 1961, ApJ, 134, 777
Sargent, W. L. W., & Searle, L. 1966, ApJ, 145, 652
Sarna, M. J., Ergma, E., & Gerškevitš-Antipova, J. 2000, MNRAS, 316, 84
Savanov, I. S., Romaniuk, I. I., Semenko, E. A., & Dmitrienko, E. S. 2013, ARep, 57, 751
Schaffenroth, V., Barlow, B. N., Drechsel, H., & Dunlap, B. H. 2015, A&A, 576, A123
Schaffenroth, V., Classen, L., Nagel, K., et al. 2014a, A&A, 570, A70
Schaffenroth, V., Geier, S., Drechsel, H., et al. 2013, A&A, 553, A18
Schaffenroth, V., Geier, S., Heber, U., et al. 2014b, A&A, 564, A98
Schindewolf, M., Levitan, D., Heber, U., et al. 2015, A&A, 580, A117
Schindler, J.-T., Green, E. M., & Arnett, W. D. 2015, ApJ, 806, 178
Schleicher, D. R. G., & Dreizler, S. 2014, A&A, 563, A61

Schleicher, D. R. G., Dreizler, S., Völschow, M., Banerjee, R., & Hessman, F. V. 2015, AN, 336, 458
Schönberner, D. 1978, A&A, 70, 451
Schuh, S., Drechsel, H., & Heber, U. (ed.) 2011, AIP Conf. Ser. 1331, Planetary Systems Beyond the Main Sequence (Melville, NY: AIP)
Schuh, S., Huber, J., Dreizler, S., et al. 2006, A&A, 445, L31
Schuh, S., Silvotti, R., Lutz, R., Kim, S.-L. & Exotime Collaboration 2014, in ASP Conf. Ser. 481, 6th Meeting on Hot Subdwarf Stars and Related Objects, ed. V. van Grootel et al. (San Francisco, CA: ASP), 3
Şener, H. T., & Jeffery, C. S. 2014, MNRAS, 440, 2676
Serenelli, A., & Weiss, A. 2005, A&A, 442, 1041
Shakura, N. I., & Postnov, K. A. 1987, A&A, 183, L21
Shimanskaya, N. N., Bikmaev, I. F., & Shimansky, V. V. 2011, AstBu, 66, 332
Shimanskii, V. V. 2002, ARep, 46, 127
Shimanskii, V. V., Bikmaev, I. F., Borisov, N. V., et al. 2008a, ARep, 52, 729
Shimanskii, V. V., Borisov, N. V., Pozdnyakova, S. A., et al. 2008b, ARep, 52, 558
Shimanskii, V. V., Yakin, D. G., Borisov, N. V., & Bikmaev, I. F. 2012, ARep, 56, 867
Shimansky, V., Sakhibullin, N. A., Bikmaev, I., et al. 2006, A&A, 456, 1069
Shimansky, V. V., Borisov, N. V., Sakhibullin, N. A., Suleimanov, V. F., & Stupalov, M. S. 2002, ARep, 46, 656
Shimansky, V. V., Pozdnyakova, S. A., Borisov, N. V., et al. 2008, AstL, 34, 423
Shporer, A., Kaplan, D. L., Steinfadt, J. D. R., et al. 2010, ApJL, 725, L200
Siess, L., Davis, P. J., & Jorissen, A. 2014, A&A, 565, A57
Silvotti, R., Charpinet, S., Green, E., et al. 2014a, A&A, 570, A130
Silvotti, R., Östensen, R., Telting, J., & Lovis, C. 2014b, in ASP Conf. Ser. 481, 6th Meeting on Hot Subdwarf Stars and Related Objects, ed. V. van Grootel et al. (San Francisco, CA: ASP), 13
Silvotti, R., Østensen, R. H., Bloemen, S., et al. 2012, MNRAS, 424, 1752
Silvotti, R., Randall, S. K., Dhillon, V. S., et al. 2010, AN, 331, 1034
Silvotti, R., Schuh, S., Janulis, R., et al. 2007, Natur, 449, 189
Sim, S. A., Röpke, F. K., Hillebrandt, W., et al. 2010, ApJL, 714, L52
Sing, D. K., Holberg, J. B., Burleigh, M. R., et al. 2004, AJ, 127, 2936
Smak, J. 1969, AcA, 19, 165
Smith, R. M., Dekany, R. G., Bebek, C., et al. 2014, Proc. SPIE, 9147, 914779
Smoker, J. V., Lynn, B. B., Rolleston, W. R. J., et al. 2004, MNRAS, 352, 1279
Sneden, C., Cowan, J. J., & Gallino, R. 2008, ARA&A, 46, 241
Soker, N. 1998, AJ, 116, 1308
Soszyński, I., Stępień, K., Pilecki, B., et al. 2015, AcA, 65, 39
Stark, M. A., & Wade, R. A. 2003, AJ, 126, 1455
Steinfadt, J. D. R., Bildsten, L., & Arras, P. 2010, ApJ, 718, 441
Stobie, R. S., Kawaler, S. D., Kilkenny, D., O'Donoghue, D., & Koen, C. 1997a, MNRAS, 285, 651
Stobie, R. S., Kilkenny, D., O'Donoghue, D., et al. 1997b, MNRAS, 287, 848
Stroeer, A. 2004, Master's thesis Diplomarbeit, Univ. Erlangen-Nuremberg
Stroeer, A., Heber, U., Lisker, T., et al. 2007, A&A, 462, 269
Sweigart, A. V. 1987, ApJS, 65, 95
Sweigart, A. V. 1997a, ApJL, 474, L23
Sweigart, A. V. 1997b, in The Third Conf. on Faint Blue Stars, ed. A. G. D. Philip et al. (Schenectady, NY: L. Davis), 3
Tailo, M., D'Antona, F., Vesperini, E., et al. 2015, Natur, 523, 318
Tassoul, J.-L., & Tassoul, M. 1992, ApJ, 395, 259
Tauris, T. M., & Savonije, G. J. 1999, A&A, 350, 928
Tauris, T. M., & van den Heuvel, E. P. J. 2014, ApJL, 781, L13
Telting, J., Østensen, R., Oreiro, R., et al. 2010, Ap&SS, 329, 163
Telting, J., Østensen, R., Reed, M., et al. 2014a, in ASP Conf. Ser. 481, 6th Meeting on Hot Subdwarf Stars and Related Objects, ed. V. van Grootel et al. (San Francisco, CA: ASP), 287
Telting, J. H. 2008, CoAst, 157, 112
Telting, J. H., Baran, A. S., Németh, P., et al. 2014b, A&A, 570, A129
Telting, J. H., Geier, S., Østensen, R. H., et al. 2008, A&A, 492, 815
Telting, J. H., & Østensen, R. H. 2004, A&A, 419, 685
Telting, J. H., Østensen, R. H., Baran, A. S., et al. 2012, A&A, 544, A1
Thackeray, A. D. 1970, MNRAS, 150, 215
Thejll, P., Flynn, C., Williamson, R., & Saffer, R. 1997, A&A, 317, 689
Thompson, H. M. A., Keenan, F. P., Dufton, P. L., et al. 2007, MNRAS, 378, 1619
Tillich, A., Heber, U., Geier, S., et al. 2011, A&A, 527, A137
Tillich, A., Heber, U., O'Toole, S. J., Østensen, R., & Schuh, S. 2007, A&A, 473, 219
Tkachenko, A., Aerts, C., Pavlovski, K., et al. 2014, MNRAS, 442, 616
Tomley, L. 1970, ApJ, 162, 239
Toonen, S., & Nelemans, G. 2013, A&A, 557, A87
Tremblay, P.-E., Fontaine, G., Brassard, P., Bergeron, P., & Randall, S. K. 2006, ApJS, 165, 551
Trimble, V. 1973, A&A, 23, 281
Tumlinson, J. 2006, in ASP Conf. Ser. 348, Astrophysics in the Far Ultraviolet: Five Years of Discovery with FUSE, ed. G. Sonneborn, H. W. Moos, & B.-G. Andersson (San Francisco, CA: ASP), 401
Unglaub, K. 2008, A&A, 486, 923
Unglaub, K., & Bues, I. 2001, A&A, 374, 570
Vaccaro, T. R., & Wilson, R. E. 2003, MNRAS, 342, 564
van Grootel, V. et al. (ed.) 2014a, ASP Conf. Ser. 481, 6th Meeting on Hot Subdwarf Stars and Related Objects (San Francisco, CA: ASP)
Van Grootel, V., Charpinet, S., Brassard, P., Fontaine, G., & Green, E. M. 2013a, A&A, 553, A97
Van Grootel, V., Charpinet, S., Fontaine, G., et al. 2010, ApJL, 718, L97
Van Grootel, V., Charpinet, S., Fontaine, G., & Brassard, P. 2008, A&A, 483, 875
Van Grootel, V., Charpinet, S., Fontaine, G., Brassard, P., & Green, E. 2014b, in ASP Conf. Ser. 481, 6th Meeting on Hot Subdwarf Stars and Related Objects, ed. V. van Grootel et al. (San Francisco, CA: ASP), 229
Van Grootel, V., Charpinet, S., Fontaine, G., Brassard, P., & Green, E. M. 2014c, in ASP Conf. Ser. 481, 6th Meeting on Hot Subdwarf Stars and Related Objects, ed. V. van Grootel et al. (San Francisco, CA: ASP), 115
Van Grootel, V., Fontaine, G., Brassard, P., & Dupret, M.-A. 2013b, ApJ, 762, 57
van Kerkwijk, M. H., Bergeron, P., & Kulkarni, S. R. 1996, ApJL, 467, L89
van Kerkwijk, M. H., Rappaport, S. A., Breton, R. P., et al. 2010, ApJ, 715, 51
van Winckel, H. 2003, ARA&A, 41, 391
Vennes, S., Kawka, A., Jonić, S., et al. 2011a, MNRAS, 413, 2760
Vennes, S., Kawka, A., & Németh, P. 2011b, MNRAS, 410, 2095
Vennes, S., Kawka, A., O'Toole, S. J., Németh, P., & Burton, D. 2012, ApJL, 759, L25
Vennes, S., Mathioudakis, M., Doyle, J. G., Thorstensen, J. R., & Byrne, P. B. 1995, A&A, 299, L29
Vennes, S., Thorstensen, J. R., Kawka, A., et al. 2011c, ApJL, 737, L16
Verbeek, K., Groot, P. J., Nelemans, G., et al. 2013, MNRAS, 434, 2727
Verbeek, K., Groot, P. J., Scaringi, S., et al. 2014, MNRAS, 438, 2
Viallet, M., Meakin, C., Arnett, D., & Mocák, M. 2013, ApJ, 769, 1
Villaver, E., & Livio, M. 2007, ApJ, 661, 1192
Villaver, E., & Livio, M. 2009, ApJL, 705, L81
Villaver, E., Livio, M., Mustill, A. J., & Siess, L. 2014, ApJ, 794, 3
Vink, J. S., & Cassisi, S. 2002, A&A, 392, 553
Vos, J., Østensen, R., & Van Winckel, H. 2014, in ASP Conf. Ser. 481, 6th Meeting on Hot Subdwarf Stars and Related Objects, ed. V. van Grootel et al. (San Francisco, CA: ASP), 265
Vos, J., Østensen, R. H., Degroote, P., et al. 2012, A&A, 548, A6
Vos, J., Østensen, R. H., Marchant, P., & Van Winckel, H. 2015, A&A, 579, A49
Vos, J., Østensen, R. H., Németh, P., et al. 2013, A&A, 559, A54
Vučković, M., Aerts, C., Østensen, R., et al. 2007, A&A, 471, 605
Vučković, M., Bloemen, S., & Østensen, R. 2014, in ASP Conf. Ser. 481, 6th Meeting on Hot Subdwarf Stars and Related Objects, ed. V. van Grootel et al. (San Francisco, CA: ASP), 259
Vučković, M., Østensen, R., Bloemen, S., Decoster, I., & Aerts, C. 2008, in ASP Conf. Ser. 392, Hot Subdwarf Stars and Related Objects, ed. U. Heber, C. S. Jeffery, & R. Napiwotzki (San Francisco, CA: ASP), 199
Vučković, M., Østensen, R. H., Aerts, C., et al. 2009, A&A, 505, 239
Vučković, M., Østensen, R. H., Németh, P., Bloemen, S., & Pápics, P. I. 2016, A&A, 586, A146
Wade, R., Barlow, B., Liss, S., & Stark, M. 2014, in ASP Conf. Ser. 481, 6th Meeting on Hot Subdwarf Stars and Related Objects, ed. V. van Grootel et al. (San Francisco, CA: ASP), 311
Wakker, B. P. 2001, ApJS, 136, 463
Wang, B., & Han, Z.-W. 2010, RAA, 10, 681
Webbink, R. F. 1984, ApJ, 277, 355
Welsh, W. F., Orosz, J. A., Carter, J. A., et al. 2012, Natur, 481, 475

Werner, K. 1986, A&A, 161, 177
Werner, K. 1996, ApJL, 457, L39
Werner, K., Deetjen, J. L., Dreizler, S., Rauch, T., & Kruk, J. W. 2003a, in IAU Symp. 209, Planetary Nebulae: Their Evolution and Role in the Universe, ed. S. Kwok, M. Dopita, & R. Sutherland (San Francisco, CA: ASP), 169
Werner, K., Deetjen, J. L., Dreizler, S., et al. 2003b, in ASP Conf. Ser. 288, Stellar Atmosphere Modeling, ed. I. Hubeny, D. Mihalas, & K. Werner (San Francisco, CA: ASP), 31
Werner, K., & Dreizler, S. 1999, JCoAM, 109, 65
Werner, K., & Husfeld, D. 1985, A&A, 148, 417
Whitney, J. H., Rood, R. T., O'Connell, R. W., et al. 1998, ApJ, 495, 284
Wilson, R. E., & Devinney, E. J. 1971, ApJ, 166, 605
Wisotzki, L., Koehler, T., Groote, D., & Reimers, D. 1996, A&AS, 115, 227
Wittenmyer, R. A., Horner, J., & Marshall, J. P. 2013, MNRAS, 431, 2150
Woudt, P. A., Kilkenny, D., Zietsman, E., et al. 2006, MNRAS, 371, 1497
Woźniak, P. R., Vestrand, W. T., Akerlof, C. W., et al. 2004, AJ, 127, 2436
Yi, S. K. 2008, in ASP Conf. Ser. 392, Hot Subdwarf Stars and Related Objects, ed. U. Heber, C. S. Jeffery, & R. Napiwotzki (San Francisco, CA: ASP), 3
Young, A., Nelson, B., & Mielbrecht, R. 1972, ApJ, 174, 27
Young, A., & Wentworth, S. T. 1982, PASP, 94, 815
Zahn, J.-P. 1977, A&A, 57, 383
Zhang, X., & Jeffery, C. S. 2012a, MNRAS, 419, 452
Zhang, X., & Jeffery, C. S. 2012b, in ASP Conf. Ser. 452, Fifth Meeting on Hot Subdwarf Stars and Related Objects, ed. D. Kilkenny, C. S. Jeffery, & C. Koen (San Francisco, CA: ASP), 13
Zorotovic, M., & Schreiber, M. R. 2013, A&A, 549, A95